N80-12818

NASA Contractor Report 159104

A Study of the Prediction of Cruise Noise and Laminar Flow Control Noise Criteria for Subsonic Air Transports

G. Swift and P. Mungur

LOCKHEED-GEORGIA COMPANY
Marietta, Georgia 30063

CONTRACT NAS1-14946
AUGUST 1979

NASA
National Aeronautics and Space Administration
Langley Research Center
Hampton, Virginia 23665

FOREWORD

This report is one of two prepared by the Lockheed-Georgia Company, Marietta, Georgia, for NASA-Langley Research Center under Contract NAS1-14946, "Study of the Prediction of Cruise Noise and Laminar Flow Control Noise Criteria for Subsonic Air Transports". D. L. Lansing was the NASA Langley Contract Monitor, and J. S. Gibson is the Lockheed-Georgia Project Manager.

This report documents the analytical studies of the program to (1) predict the acoustic environment over the surface of an airplane during cruise and (2) to understand and predict the mechanisms whereby noise can cause the premature transition of a laminar boundary layer. A companion report is NASA CR-159105 which is a cruise noise prediction methods manual. This completely separate document defines the methods developed in algorithm form for the prediction of the acoustic environment during cruise.

TABLE OF CONTENTS

FIGURE NUMBER

TABLE OF ILLUSTRATIONS (cont'd)

FIGURE NUMBER

LIST OF FIGURES

ILLUSTRATION TITLE

LIST OF FIGURES (CONT'D)

LIST OF FIGURES (CONT'D)

LIST OF FIGURES (CONT'D)

LIST OF FIGURES (CONT'D)

The overall objective of this study is to develop procedures for identifying exterior surfaces on laminar flow control (LFC) aircraft which are subject to noise levels high enough to adversely impact LFC design and operation. To accomplish this goal, four specific sub-objectives identified are to (1) develop general procedures for the prediction of the noise levels incident upon surfaces of future subsonic commercial air transports during cruise, (2) to summarize and explicitly define all the prediction methods in a Cruise Noise Prediction Methods Manual, (3) to define criteria for critical sound pressure levels which may cause acoustically induced premature transition of a laminar boundary layer, and (4) to make recommendations which would result in further improvements in the noise prediction methods and the acoustically induced transition criteria. A summary of these four tasks is given in the following paragraphs.

Cruise Noise Level Prediction Methods

The potential noise sources are divided into three groups, propulsion sources, airframe sources and laminar flow control sources. General requirements established for the noise prediction procedures are that 1) the levels are to be in spectral, one-third octave and overall form, 2) the frequency range are to be 45 to 11,000 Hz, and 3) source directionalities are to be from 0° (forward) to 180° (aft). Subsonic aircraft cruise Mach numbers and altitudes are variable. The propulsion and airframe technology are of the 1985-1990 time frame.

The propulsion noise sources covered are the fan, compressor, core, turbine and the jet. Noise control effects of inlet flow Mach number and acoustic treatment may be included in the turbomachinery noise predictions. Discharge nozzle configurations include two-flow (short to co-planar), with or without primary plug, or a completely mixed flow nozzle. The turbomachinery and core noise are treated as point noise sources located at their nacelle emission locations. The jet noise sources are treated as distributed noise sources.

These predictive techniques are recent state-of-the-art methods. Some development was required to cover the directionality and frequency ranges.

The airframe noise sources, for which prediction methods are developed, are the turbulent boundary layer (treated as a distributed area source) and the trailing edge (treated as a finite line source).

The laminar flow control system noise sources are separated into those which radiate externally to the airframe from suction unit inlets and discharge ducts and those generated internally by the suction unit and the ducting system. Since the suction units operate on gas turbine cycles the external noise radiation characteristics would be predicted using the methods defined in the propulsion noise prediction methods section. Internal noise is capable of introducing fluctuating disturbances into the boundary layer through the slot; the acoustic power generated by the suction compressor can be predicted using propulsion noise prediction methods and the noise generated by the typically low speed duct flow and its interaction with duct components appear to be low and controllable. Methods for the prediction of the latter item are not, therefore, derived.

The basic predictions are at static or low forward speed and at low altitude and were free-field. Conversion to the cruise condition of high forward speed and altitude was accomplished by the introduction of the following transformations as appropriate for each noise source: 1) cruise effects on acoustic strength, 2) forward speed effects on acoustic propagation and 3) airframe modifications to the sound field. These transformations are presented or derived.

Examples of these prediction procedures are presented.

Prediction Methods Manual

The prediction methods manual entitled "Near-Field Noise Prediction for Aircraft in Cruising Flight" is a completely separate document, NASA CR-159105. There all the noise prediction methods with their assumptions are summarized

and explicitly defined. The methods have been organized as computational algorithms - which may be readily converted into computer programs.

Laminar Flow Control Acoustic Criteria

The factors and concepts that led to the development of the X-21A LFC/Acoustic criteria are discussed.

Limitations in its inadequacy to account for frequency and directionality are overcome by a proposed semi-numerical method based on numerical solutions of the homogeneous stability equation. For a specific LFC wing with a specified suction distribution, critical SPL spectra are computed for different chord locations and directionalities of the sound field. An application example is shown. The more fundamental problem of how sound excites boundary layer disturbances is analyzed by deriving an inhomogeneous Orr-Sommerfeld equation in which the same terms consist of production and dissipation of sound induced fluctuating vorticity; numerical solutions are obtained for sound impinging at arbitrary angles of incidence on a semi-infinite flat plate and comparison with measurements are made.

Recommendations for Further Improvements

Specific technology gaps and problem areas relative to both cruise noise prediction and LFC noise criteria are identified.

The cruise noise prediction methodologies are based largely on acoustic source data acquired at sea level under static or low forward speed conditions. To confirm the validity and to increase the accuracy of the methods developed for application to transonic conditions requires that analytical and test programs be conducted covering the following subjects.

1) Validation of methods through acquisition of high quality airplane cruise noise data in the presence of a laminar boundary layer and comparison with predicted total noise data.

2) Measurement of near field jet shock associated broad band noise from model two flow nozzles at conditions representative of cruise and at simulated forward speeds as high as possible, together with an investigation on the possible occurrence of jet screech.

3)&4) Theoretical and experimental study of the noise radiated by (a) turbulent & layers and (b) trailing edges immersed in high speed flows.

5) Improved understanding of convective and dynamic effects on all noise sources and application of these concept to cruise noise predictions.

6) Influence of wing pressure fields, shock waves and wakes on acoustic propagation.

7) Feasibility of a transonic acoustic facility to study high speed effects on individual noise sources and cruise transformations.

8) Update the cruise noise prediction methods manual as improved prediction methods become available, and

9) Using the methods, determine cruise noise contours over candidate LFC airframe configurations and reference spectra. These should be updated and included in the methods manual.

The recommendations for further improvements in the LFC/Acoustic criteria are as follows.

1) An experimental program needs to be undertaken to improve the calibration of the critical SPL spectra generated by the semi-numerical method.

2) The sound induced amplification calculations achieved for the semi-infinite flat plate be extended to the sucked airfoil case.

3) The pure tone sound induced boundary layer calculation on the flat plate be extended to two and three pure tones with same and varying phases.

4) Numerical evaluation of boundary layer excitation by the sound scattered from one and a distribution of suction slots.

The impending long-term shortages of petroleum-based fuel have resulted in a growing urgency for improving the cruise efficiency of long-haul subsonic commercial transport aircraft. Also, several recent studies of possible future transport aircraft systems have highlighted the importance of aerodynamic drag reduction to aircraft efficiency. These studies further recognize that, of the variety of drag reduction concepts which have been seriously analyzed, laminar flow control (LFC) appears to offer the greatest potential for improvement.

Basic theory, engineering concepts, and design techniques relative to the application of LFC have been generally known for a number of years. The validity of this technology and the potential for LFC were partially evaluated in the 1960's by the X-21A aircraft laminar flow control demonstration program. That program was terminated before the operational practicability of LFC in a realistic environment could be determined. However, one of the significant problems of LFC design and operation was determined to be the adverse effect of the aircraft's own noise in causing premature laminar to turbulent flow transition.

The concern over noise effects in the X-21A program, Reference 1-1, and more recent LFC design systems studies, Reference 1-2, has resulted in this research effort. These studies pointed out the need for the development of better understanding and improved and more detailed prediction methods both for cruise noise prediction and for LFC acoustic criteria. The basic objective of this study is "to develop a procedure for identifying those exterior aircraft surface areas of an LFC aircraft which may be subjected to noise levels sufficiently high to adversely impact the design and operation of an LFC system."

This report consists of two main subject areas, which are self contained: 1) cruise noise prediction methods, and 2) LFC acoustic criteria. The report has a common recommendations section. The results of the noise prediction study are presented in the form of a methods manual, which is the completely separate "Near-Field Noise Prediction for Aircraft in Cruising Flight" NASA CR-159105 .

In the area of noise prediction, advantage is taken of the considerable progress made in the last 10 years regarding the understanding and prediction of propulsion system and airframe noise generation and propagation at low altitudes and low speed. This provide the latest state-of-the-art noise source prediction techniques considerably in advance of those available, for example, at the time of the X-21A program. Where prediction techniques are not directly applicable (because of the closeness of the distributed noise source to the prediction location, as in the case of turbulent boundary layer noise and trailing edge noise), limited data is available to formulate prediction schemes. A series of transformations are developed for conversion of these noise estimates to the cruise conditions of high altitude and high speed.

The proposed methods are aimed for application to airplanes introduced into service around 1995. Thus, the prediction techniques are applicable to advanced engine and airframe technology of the 1985-1990 time frame. The methods are generalized, e.g., wing mounted or aft-fuselage mounted engines may be considered.

In the area of LFC/Acoustic criteria, the only sets of data available from an engineering application point of view are those developed during the X-21A design, although a few ad hoc experiments on sound induced transition have been reported. Most of the X-21A LFC/Acoustic criteria data were derived from turbulence induced transition data and therefore do not account for the spectrum or directionality of the sound field. In this report LFC/Acoustic criteria have been developed based on two approaches. For immediate engineering application, the X-21A criteria have been extended using a semi-numerical method to include the sensitivity to the spectrum and directionality of the sound field. In the second approach, with view to acquiring a more fundamental understanding of the process of sound induced boundary layer excitation, an inhomogeneous Orr-Sommerfeld equation is derived in which the source term corresponds to production and dissipation of sound induced fluctuating vorticity. Numerical solutions for the boundary layer disturbances are then obtained for the case of a plane sound wave incident at an arbitrary angle of incidence on to a semi-infinite flat plate with a Blasius velocity profile, and some comparison is made with a corresponding set of measurements.

2.1 INTRODUCTION

In the area of aircraft noise prediction, many advances have been made in the last 10 years. In fact, some new noise sources have been recognized since the X-21 days! The recent emphasis in aeronautical acoustics has been on ensuring that commercial airplanes comply with the Federal Noise Certification Standards (FAR 36), which were introduced in 1969. In 1978, an amendment to FAR 36 created even more stringent standards for new airplanes. Because of the severe impact of these standards and because of the many uncertainities in noise source identification, a large effort has been made in recent years to identify, and define in great detail, the acoustic characteristics of airplane noise sources. In the area of propulsion noise sources improved ways of predicting turbomachinery noise (fan, compressor and turbine) have been developed and are available; core/combustion noise has been identified and has been quantified, and some of the jet noise components have been receiving more attention. Some of these prediction techniques provide one-third octave band noise level estimates (from 50 to 10,000 Hz) over a wide range of directional angles, however, of necessity, the angles of interest have been primarily in the vicinity of peak flyover noise. For this study, for the general prediction of noise incident upon an airframe, all angles from 0° (ahead) to 180° (aft) need to be covered. FAR 36 is applicable to takeoff and landing, with airplane Mach numbers of about 0.2 which has resulted in considerable interest concerning the influence of these lower Mach numbers on acoustic generation and radiation characteristics of the propulsion noise sources.

Another fallout of the FAR 36 requirements is that airframe noise, at low speeds, has become of concern as a significant contributor to airplane flyover noise - in addition to propulsion noise. The most important result for this study is the identification of one type of airframe noise, as an important cruise noise source.

For this study, noise predictions are required at airplane cruise Mach numbers between 0.7 and 0.9 and at an altitude of about 25,000 to 40,000 feet. Thus,

the expanding acoustic technology data base just described still requires considerable transformation in order to be applicable to the high speeds and altitudes of concern.

Statically, airplane acoustic environments are obviously controlled by propulsion system noise sources. For low speed (M = 0.2) and low altitude operations, measurement and analysis studies have shown that for the earlier jet powered airplanes, propulsion noise sources dominated both the terminal area noise levels (frequently referred to as the far-field) and the acoustic environment in the vicinity of the airplane structure (frequently referred to as the near-field). During cruise, airframe noise sources (roughly proportional to V_A^6) can dominate at certain locations and the propulsion sources can dominate at others, depending upon the airframe/propulsion system configuration. The requirement that more recent airplanes comply with FAR 36, Stage 2 noise limits on takeoff and approach has resulted in newer, larger airplanes being powered by acoustically treated turbofan engines, which are quieter than the older turbo-jets, reducing the propulsion noise components. For these quieter airplanes the flow noise generated by the airframe noise sources is much more critical. New airplanes must meet the more stringent FAR 36, Stage 3 limits and future airplanes of the 1995 time frame will probably have to meet even stricter takeoff and landing noise limits. It is considered that the propulsion system for this time frame will consist of turbofan engines (with single stage fans) contained in acoustically treated nacelles similar to those on many of the current Stage 2 and Stage 3 airplanes. Turbine treatment and an internal jet mixer nozzle might also be included. However, low takeoff-noise propulsion systems on takeoff do not necessarily mean a low cruise noise propulsion system since new noise sources can be present during cruise. These can be, for example, jet shock associated broadband noise and jet screech which can occur when nozzles operate at supercritical pressure ratios (which does not happen on takeoff, but can happen during cruise). Further, cruise spatial co-ordinate transformation and sound level convective effects change the low speed directionalities and enhance the radiated noise in preferred directions at cruise speeds. These acoustic aspects are evaluated in this study.

FIGURE NUMBER

ILLUSTRATION TITLE

Noise measurements on the surface of airplanes at cruise conditions have been made and are reported in the literature. The measured data, normally at fuselage locations, at some distance from the engines, generally indicate that at those locations the turbulent boundary layer immediately adjacent to the microphone dominate the microphone signal. Such data, in the past has been able to yield little information concerning the contribution of other, less noisy sources to the measured noise. Thus, the field of transonic (high altitude-high speed) acoustics is relatively unexplored.

FIGURE NUMBER

2.2 APPROACH

ILLUSTRATION TITLE

The noise incident upon LFC airplane surfaces during subsonic cruise may be conveniently treated as originating from three major source groups. These are the propulsion system noise sources - discussed in 2.3.3, the airframe noise sources - discussed in 2.3.4 and the laminar flow control system noise sources, both internal and external - discussed in 2.3.5. These major source groups and their sub-sources are listed in Figure 2-1. Cruise conditions, at which noise prediction methodologies for each of the component noise sources are to be made, are typically in the range for airplane Mach numbers of 0.7 to 0.9 at altitudes from 30,000 to 50,000 ft. Other disturbance sources, which although not strictly acoustic, but which can occur and which are reviewed in this report include the structural vibration of skins and panels - which is included in the airframe section, 2.3.4, and aerodynamic instabilities in the flow control system - which is included in the LFC section, 2.3.5.

In all cases, the noise receiving location moves with the aircraft. The methods are generalized so that any engine/airframe configuration may be evaluated. The general approach to noise prediction is described in the following three steps. All of these steps are defined in detail and form part of the overall prediction procedure.

a. Selection of Noise Component Prediction Methodologies. Each noise source was evaluated in context of 1985-1990 technology as to its being a significant noise fource. The significant noise sources are then individually treated as indicated in Figure 2-2. The first step was to review the available prediction methods and then to select the best method at the best data base, which might be static, or low forward speed, whichever is appropriate to that particular source. Where appropriate, the basic noise prediction methods are to be current state of the art. However, the method must be capable of predicting acoustic data over the desired directional and frequency ranges. If a satisfactory method was not available, then one was formulated, based upon existing data. Where possible, prediction methodologies are formulated for the more common noise suppression devices, e.g., high Mach inlets and duct acoustic treatment. All of the predictive techniques are empirical in nature.

AIRFRAME SOURCES

- TURBULENT BOUNDARY LAYERS
- TRAILING EDGES AND WAKES
- ATMOSPHERIC DISTURBANCES
- OSCILLATING SHOCKS
- SEPARATED FLOWS
- IMPINGING FLOWS
- CAVITIES
- PROJECTIONS
- PANEL VIBRATIONS

PROPULSION SOURCES

- FANS
- COMPRESSORS
- TURBINES
- CORE/COMBUSTION
- JET
  - MIXING
  - SHOCK ASSOCIATED
  - SCREECH

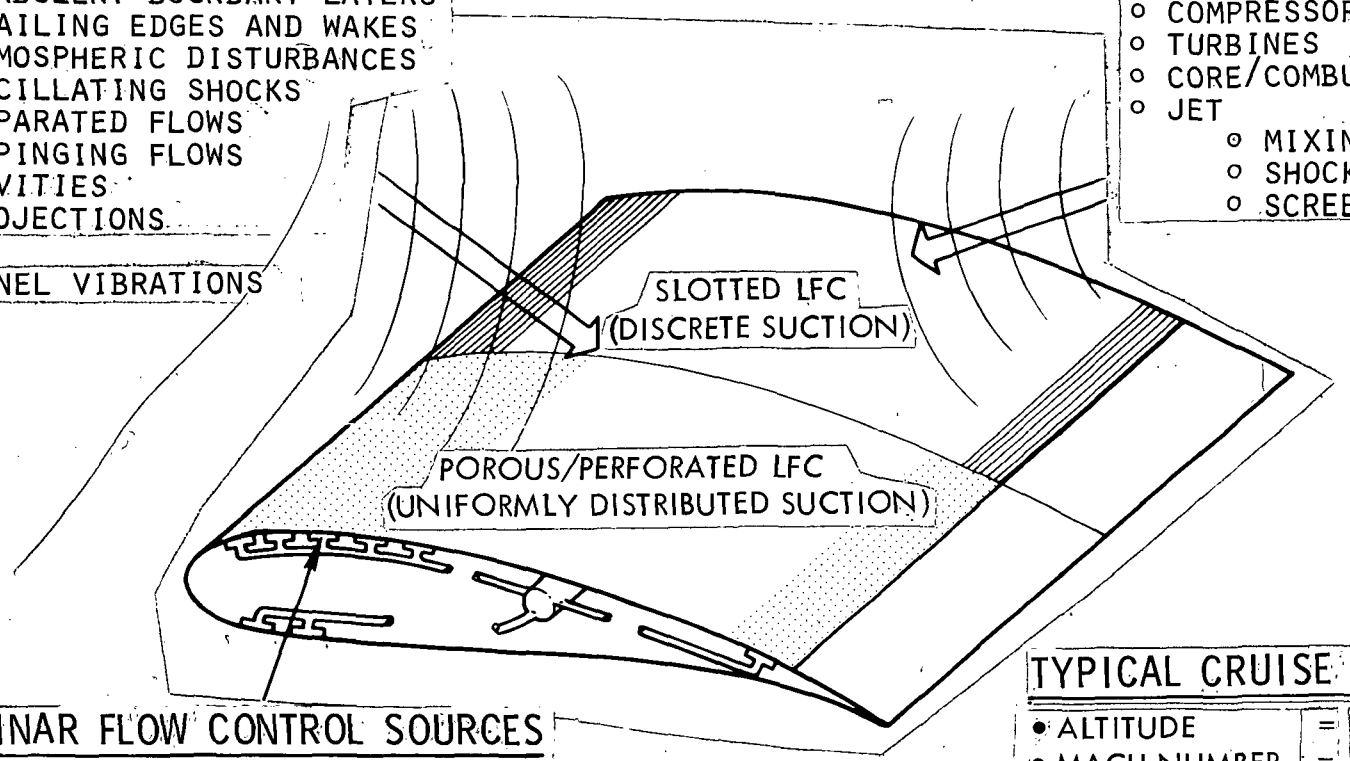

LAMINAR FLOW CONTROL SOURCES

- SUCTION UNIT-EXTERNAL
- SUCTION UNIT-INTERNAL
- DUCT FLOW DISTURBANCES
- DUCT FLOW RESONANCES
- SLOT WAKE OSCILLATIONS

TYPICAL CRUISE CONDITION

• ALTITUDE	=	38,000 FT
• MACH NUMBER	=	0.85

FIGURE 2-1. POTENTIAL CRUISE NOISE SOURCES

NOISE COMPONENT PREDICTION METHODOLOGY AT BEST DATA BASE	PREDICTIONS AT BEST DATA BASE	TRANSFORMATIONS			=	COMPONENT SPECTRAL NOISE
		CRUISE EFFECTS ON ACOUSTIC CHARACTERISTICS	FORWARD SPEED EFFECTS ON ACOUSTIC PROPAGATION	AIRCRAFT CONFIGURATION EFFECTS		
o Selection/Development	o Static/Low Speed o Airplane/Noise Source Geometry o Noise Component Parameters o Noise Receiver Location	o Cruise Operating Conditions o Cruise Noise Component Parameters o Relative Velocity Effects o Acoustic Impedance o Atmospheric Attenuation	o Coordinate Transformation o Doppler Effect o Convective Effect o Dynamic Effect	o Number & Location of Noise Sources o Suppression Devices o Airframe Flow Field Modifiers o Airframe Shielding o Airframe Reflection		o At Location o Broad Band Noise Discrete Tones 45 < Hz < 11,000

FIGURE 2-2. APPROACH TO CRUISE NOISE PREDICTION

b. Noise Prediction at the best data base - which might be static or low forward speed, whichever is appropriate to that particular source.

c. Transformations. The next step consists of a series of transformations which convert the initial predictions to those of high forward speed at altitude. This is accomplished through three sets of transformations. The first "cruise effects on acoustic characteristics" includes altitude effects which change the acoustic power of the field. The acoustic field predicted at this stage is an "equivalent static" at altitude. The second "forward speed effects on propagation" includes forward speed effects which change the directivity of the field. At this stage the acoustic field is for a single source at cruise altitude and Mach number and is free field. The third, "aircraft configuration effects" includes those features associated with the airplane design which modify the cruise free field levels to these in the presence of the airplane.

d. Noise Component Spectral Output at a Single Point. The final output, at any specified location is the spectral noise level (broadband and/or discrete) from the selected source at the specified cruise conditions.

Determination of the total sound pressure level requires first that all the component noise spectral levels be determined in the previously described manner with their own unique prediction and appropriate transformation and then combined to provide a total noise spectrum. This is the required format for the free field noise for evaluation in terms of laminar flow control acoustic criteria described in Section 3. Should spectral or overall noise contours over the structure be required, then multi-point evaluation of the sound field would be required.

2.3.1 Literature Review

Over the past 20 years a vast literature has been generated in the area of the acoustics of flight vehicles. The literature encompasses the range from noise measurements of total airplane noise and the noise of contributing sources to the development of understanding of noise generation and control and to the formulation of noise source prediction methods. Much of the earlier efforts were directed at the near field problem and was concerned with determining the external static and cruise noise environment (acoustic loading) over aircraft, missile and rocket structures in order to evaluate the problem of structural vibration, sonic fatigue and acoustic transmissability. The dominant noise sources were frequently turbojets, rockets and aero-acoustic loadings from airframe aerodynamic interactions.

Examples of prediction method summaries of this time era are presented in References 2-1 and 2-2. However, many of the proposed techniques dealt largely with a limited frequency range (in octave bands) and a limited directionality. Further developments and refinements of these approaches are presented for example in References 2-3 through 2-7.

The most recent comprehensive review of methods for estimating aeroacoustic loads on flight vehicle structures is that of Reference 2-7. The most important new contributions here are in the area of jet noise where methods are recommended for jet mixing noise from two flow engines and for jet screech.

Although these previously mentioned aspects remained an on-going problem, the emphasis changed in the late 1960's to the far-field noise problems, namely that of community noise and airplane compliance with noise certification regulation requirements which were introduced in 1969. Areas which then started to receive intensive attention included the noise source identification of high by-pass ratio engines (over a wider frequency range and directionality), the effect of low airplane speed on the contributing noise sources and the contribution of airframe noise to airplane flyover noise. Methods applicable to the prediction of current and advanced propulsion noise sources (turbo-

machinery, core, and jet) are summarized in References 2-8, 2-9 and 2-10. Although oriented towards far-field prediction, many of these methods are directly applicable to near field propulsion source estimation. Recently, these methods have been further refined as described in the body of this report. Further, flight effects on noise sources and airframe noise have recently been very active fields of acoustics research and are discussed in detail in this report.

For application to the current problem of developing methods for the estimation of the acoustic environment over an airframe surface during cruise, some of the methods are based largely on the older methods (for example, jet mixing and jet screech), but where there have been recent advancements (for example, turbomachinery, core and jet shock associated broad band noise and forward speed effects) the latest available state-of-the-art methods which have evolved are used. Some methods have been further developed in this report, (for example, turbulent boundary layer and trailing edge noise).

2.3.2 Near and Far Noise Fields

In the prediction of the cruise noise acoustic environment over an airframe, the locations of interest are frequently in close proximity to the noise source. Further, the noise source is often an extended source and not a point source. The acoustic field may be divided into three regions. Starting from locations far from the source, these regions may be described as follows:

a. Very Far-Field. Here at large distances from the source, a distributed source can be treated as a point source. This region is called the radiation field and consists of true sound, p, in which the inverse square law holds, e.g., $p \propto 1/r$, or $p^2 \propto 1/r^2$. In this region source to location distance, r, is greater than the source dimension. Further, over small distances the acoustic propagation may be regarded as plane wave propagation, hence, the acoustic pressure, p, and particle velocity, u, are in phase and are related by $p/u = \rho c$ where ρc is the characteristic impedance of the propagation medium.

In these prediction procedures, noise sources falling into this category are, the fan (forward and aft), compressor, combustion, turbine, and jet screech, from either the propulsion or suction unit systems.

b. Close-in Far Field. Here at smaller distances the size of the acoustic source is important and it can no longer be regarded as a point source. The acoustic radiation from each source element obeys the inverse square law, however, the distance from each element to the desired location is different. Consequently, the inverse square law does not hold for the total radiated noise. However, the total acoustic pressure may be computed knowing each element acoustic power, spectrum and directivity. Some examples are discussed in Reference 2-11, shown in Figure 2-3. The upper example shows that for a finite line source the noise increases at a reduced rate of 3 dB per doubling of distance at distances less than (source length)/π. The transition from the 6 to the 3 is actually a smooth, not a sudden transition. This example is applicable to the calculation of noise radiated away from a finite trailing edge, whose source strength is essentially constant along the edge span. Similarly for a uniform finite surface radiator (such as the distributed boundary layer over a surface) the transition also occurs at approximately a distance of (source length)/π and in this case the noise level becomes constant with reduced distance, until the acoustic near field is reached. The turbulent boundary layer is a noise source which could be approximately represented by this example. For fan noise radiated from the engine inlet, the $1/r^2$ field is obtained at distances greater than the (fan inlet diameter)/π, which in practice is greater than about 2 to 3 feet. Thus, for all locations, fan noise may be regarded as originating from a point source. Similar argument apply to aft fan, compressor, combustion, turbine and jet screech noise radiation.

Recent calculations of jet mixing noise propagation, Reference 2-12, show a similar effect. Far away from the jet ($r/D > 30$, where r is the distance and D is the nozzle diameter) the inverse-square-law is followed. At smaller distances the measured change of noise with

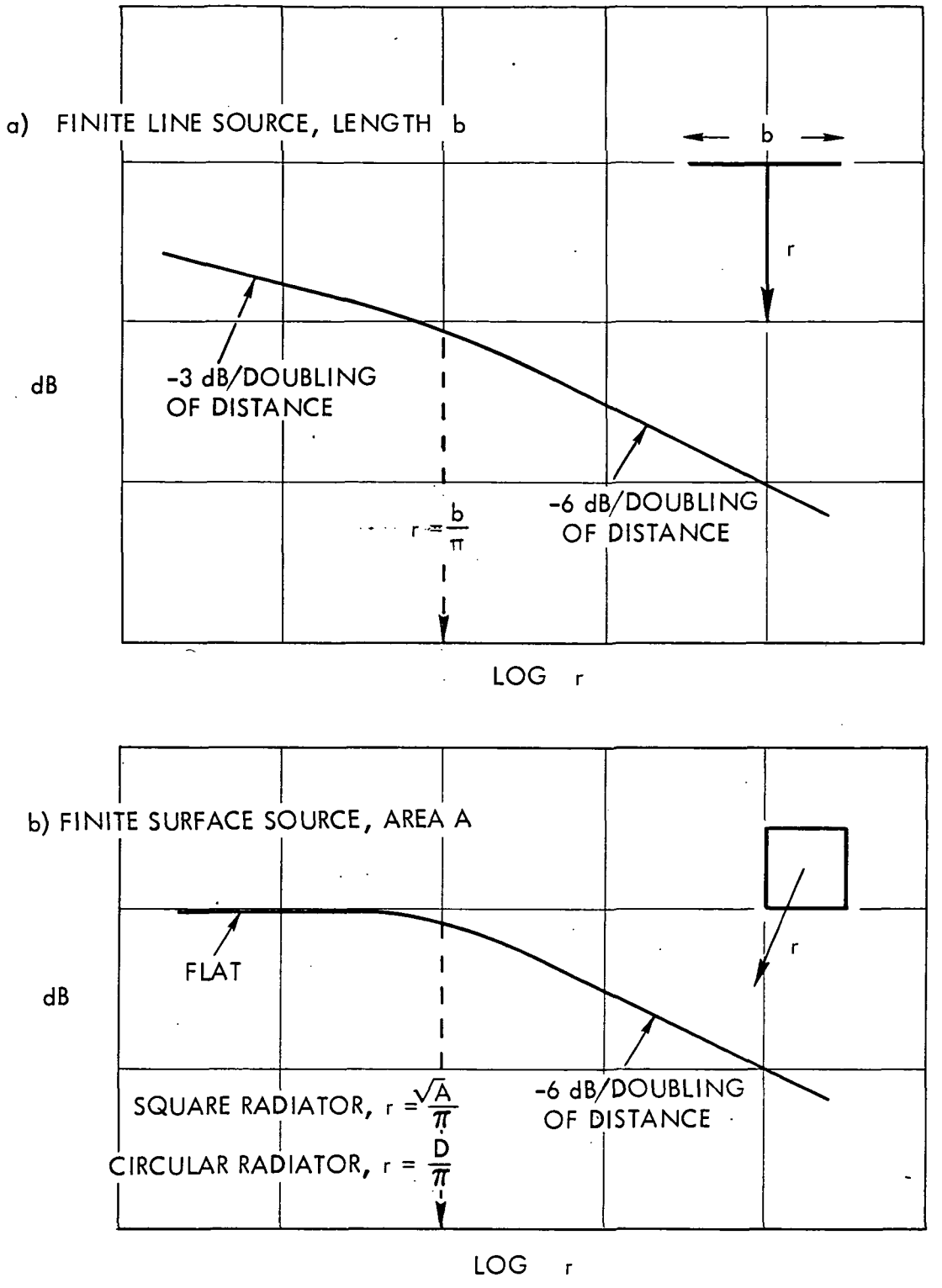

FIGURE 2-3. NOISE PROPAGATION FROM DISTRIBUTED SOURCES

distance diminishes. Calculated sound pressure (calculated from the estimated noise source distribution in the jet, its local frequency, its local $1/r^2$ and its local directionality) agree very closely with the measured noise. The method employed in the jet mixing noise prediction procedure in this report is basically a scaling method. This newer method requires more evaluation to determine if it is an improved prediction method.

c. Near Field. A completely different effect occurs very close to the source. Here, for small distances from the source, in the reactive part of the sound field, "pseudo-sound" exists. This is a pressure fluctuation associated with fluctuating mass flow movements of the air which falls off at least as the inverse square of distance, e.g., $p \propto 1/r^2$. Very close to the source, pseudo-sound dominates over the true sound. Where these effects start is a function of source type and frequency. For a simple source, or monopole, it can be considered to begin, for practical purposes when kr = 1 (where k, the wave number, = λ/c). For a dipole and a quadrupole the boundary is at kr = 2 and 3, respectively, see, for example, Reference 2-13. The relationships are presented in Figure 2-4 which defines, for practical purposes, the near and far-field regimes. The significance of this division is that where as in the far field all the acoustic pressures from all the source elements obey the 1/r relationship, in the near-field the pressures increase at different rates.

It can be seen from Figure 2-4, that the near-field extends for a greater region for a quadrupole than a monopole, and for lower frequencies than for higher frequencies. Further within this near field the fluctuating pressures associated with a quadrupole increase much more rapidly than for a monopole, Reference 2-14. Where this situation could be important is very close to a jet (considered as quadrupole radiation) or a turbulent boundary layer (dipoles and quadrupoles) especially at low frequencies. For example, at 500 Hz this effect becomes important at less than 1 foot from a quadrupole type source. For an LFC airplane, an area of concern for this effect of higher pressure fluctuation would probably be for locations

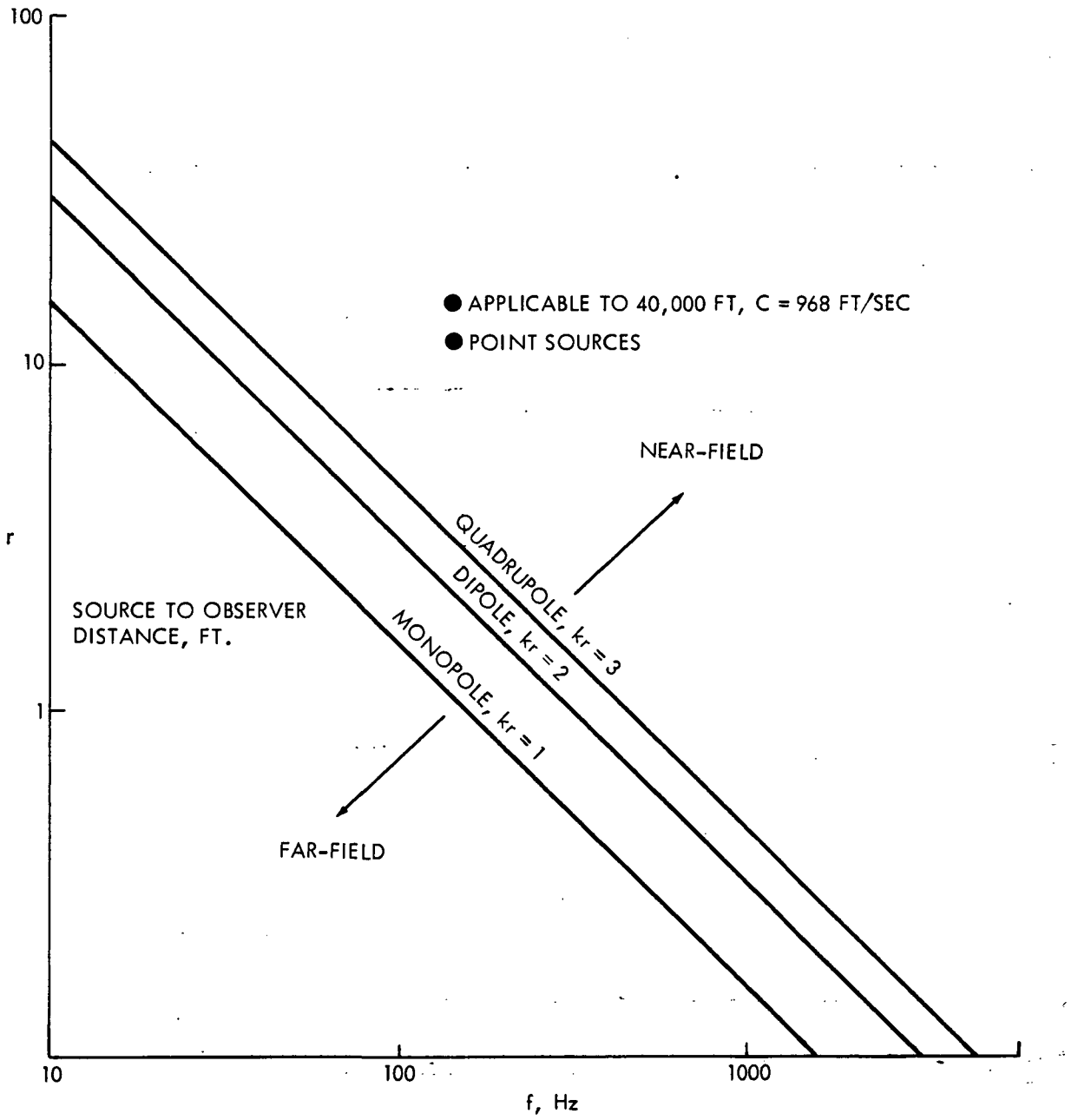

FIGURE 2-4. NEAR AND FAR ACOUSTIC FIELD DIVISION

very close to a fuselage turbulent boundary layer. However, this effect is not considered any further.

2.3.3 Propulsion Noise Sources

The propulsion system most probably anticipated for the 1985 - 1990 time frame is a high bypass ratio turbofan type, with a single stage fan, installed in an acoustically treated nacelle. The noise sources associated with such a propulsion system statically and at low forward speed have been studied extensively in recent years and are still undergoing research and evaluation. The use of an advanced design propeller is also a possibility. The contributing noise sources are expected to be:

- o Fan - forward and aft
- o Compressor
- o Turbine
- o Combustion
- o Nacelle case radiation
- o Jet
- o Advanced propellers

The above sources can give rise to discrete frequency and broad band noises all of which have their own directionalities and have different parameter dependancies. Therefore, each source requires its own prediction methodology.

The following sections describe these noise sources and methods available for their prediction are reviewed. These methods have been generally developed for the static case, which becomes the best data base. The influence of low forward speed on these noise sources is still being explored, but some preliminary trends and conclusions are available. However, basically, static prediction methods have been selected. The principal modification to these methods is to expand the directivity to cover the full forward and aft quadrants. It is anticipated that in the future these methods will be updated and revised as more knowledge and understanding become available.

At cruise, the propulsion system operates at different conditions than at takeoff, where the acoustics are best known. For example shock waves will probably occur in the jet exhaust, a condition which will not exist at takeoff, giving rise to jet shock noise. It is even possible that, especially at cruise, some new noise source may become evident.

Propulsion noise control features whose effect must be incorporated in a noise prediction include:

- o High Mach inlets
- o Acoustic liners

The first attenuates fan and compressor noise radiated from the inlet. The second can be applied to all engine internally generated noise sources. Currently, acoustic nacelles are designed for community noise control and FAR 36 noise certification compliance. However, if necessary, acoustic liners could be added or tuned for cruise noise control. Methods, based on available data in the literature, were formulated to estimate the source noise reductions (in directional and spectral terms) for both high Mach inlets and acoustic liner installation.

2.3.3.1 Fan and Compressor - Fan and compressor noise are generated within the engine by airflows interacting with the turbomachinery. Fan noise generally dominates over compressor noise. It radiates from both the engine inlet and the fan discharge duct. It has been shown, Reference 2-15 through 2-21, to consist of discrete tones, occurring in the mid to high frequencies, at the blade passage frequency and its harmonics and broad band noise centered around these frequencies. Should the fan blades be travelling supersonically at the tips, further discrete tones at blade passage subharmonics also exist, known as combination tones, which only radiate forward. The fan is noisier in the presence of unsteady flow, such as can exist statically. This can be an additional strong source of noise which diminishes as aircraft forward speed increases and which will not be present during cruise. Typically, at low forward speeds, forward radiated noise peaks at 60^{o} to the inlet and aft radiated noise peaks at 120^{o} to the inlet.

Over the last twenty years much research and development effort has been expended on the generation and control of fan noise. Summaries of some of the early work together with complex prediction procedures are presented by the work reported in Reference 2-15 through 2-17. The NASA Quiet Engine Program then served as a focal point for the application of this early low noise turbo-machinery technology. This engine has a large single stage fan. Some discussion and results of this program are presented in References 2-18 through 2-20. A fan noise prediction procedure, Reference 2-8, was developed by Boeing and is an empirical method based on the earlier formulations of References 2-15 through 2-17, and measured fan noise data from JT3D and JT9D engines.

A recent review made of fan and compressor noise was reported in Reference 2-21. There an interim prediction method was developed and recommended for use by the NASA ANOPP Office. The method is based on the Boeing method of Reference 2-8 and modified by results from the full-scale, static, single-stage fan tests of the NASA Quiet Engine Program, as reported in Reference 2-18 through 2-20, which encompassed high and low speed fans. It thus represents a broader data base. The method explicitly predicts inlet duct radiated and fan discharge duct radiated noise in terms of the discrete tone, broadband, and combination tone noise components. The 1/3 octave band and directivity variations of these sources are also specified. Thus, the total fan noise at any spatial location receives spectral contributions from five sub-component noise sources.

The method selected for the prediction of unsuppressed fan and compressor noise is the method presented in Reference 2-21. The method is a logical evolution of the earlier methods and is correlated with the kind of fans expected for the 1985-1995 time frame.

The method is directly applicably to single-stage fans and can also be used for two-stage fans and compressors. The basic prediction method consists of an expression for each of the five sub-noise sources giving the normalized peak 1/3 octave band sound pressure level as a function of rotor tip relative Mach number (operating and design). The normalization parameter is a function of the total temperature rise across the fan stage and the mass flow. Correc-

tions to the predicted levels are allowed for 1) presence of inlet guide vanes, 2) rotor stator spacing effects, 3) inlet flow distortion (assumed to be zero in flight operation) and 4) tone cut off.

The method is applicable to sea level static operation and to clean, relatively short, hardwall nacelle ducts, e.g., no noise amplification effects due to blown-in doors.

The only modification made to the method was to expand the directivity, for all five sub-sources, to cover angles from 0° to 180°. This expansion was made on a linear basis.

This fan noise prediction procedure is for far-field (community) noise application. Fan noise is a mid to high frequency noise. Since the source radiator dimensions (inlet or discharge duct) are similar to or greater than the radiated wavelength, the inverse square law will hold for distances greater than the source radiator dimension $\geq \pi$ - which is about 3 feet or less. Thus each of the noise subcomponents may be considered as radiating from point sources located at the inlet or fan discharge duct as appropriate.

For prediction of fan and compressor noise under cruise conditions the operating performance parameters appropriate to that flight condition must be employed, see Section 2.4.1. Since the noise is generated internally, airplane forward speed is not expected to otherwise directly influence the generated acoustic power. However, aircraft forward speed does effect the external propagation field, Section 2.4.2, and the coordinate transformation and convective effect are included in the cruise prediction method. The resulting acoustic free-field would of course be modified by airplane configuration features described in Section 2.4.3. Should fan inlet and discharge duct acoustic treatment be included in the nacelle design the noise reduction at cruise may be evaluated by use of the methods described in 2.3.3.7.

The prediction method and equation are summarized and defined in NASA CR-15905 "Cruise Noise Prediction Methods." A schematic of the fan/compressor cruise noise prediction methodology is shown in Figure 2-5.

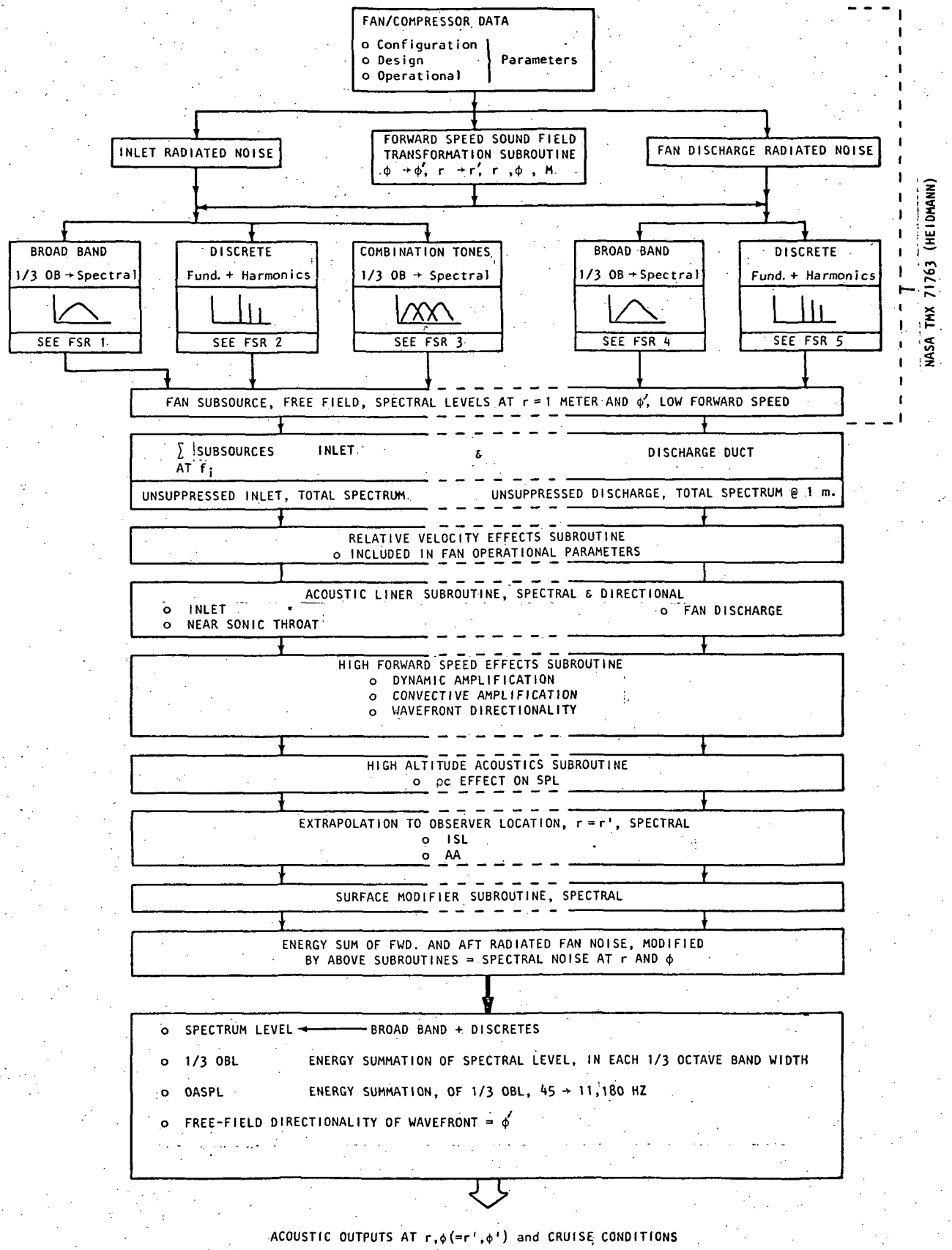

FIGURE 2-5. FAN/COMPRESSOR NOISE PREDICTION FLOW CHART

2.3.3.2 Turbine--The noise generated internally within the engine core and radiated from the engine nozzle in generally termed core noise. Core noise has several contributing noise components, some of which can be reasonably well identified. At low frequencies the noise sources are considered to be the combustion process and flow/surface interation noise, with combustion noise considered to be dominant. At high frequencies the dominant noise souce is the turbine. Much work, both experimental and analytical, has been performed recently to identify and quantify these noise components. In this study core noise is considered to be made up of the low frequency combustion noise, discussed in 2.3.3.3, and the high frequency turbine noise discussed in this section.

Turbine noise is generated by the core flow passing through the turbine; it radiates from the primary nozzle through the discharge efflux streams to the observers location. It has been shown to consist of discrete tones, usually associated with the blade passing frequencies of the last turbine stage, and broad-band noise centered at the same frequency, Reference 2-22 through 2-26. Typically, the tone frequencies are high, being above 5,000 Hz. Statically, measurements show that turbine noise is dominant in the aft quadrant, peaking at about 120° from the inlet.

The first comprehensive turbine noise study and proposed prediction method was that of Reference 2-22. This method was further developed in Reference 2-8 which presented a more complete (semi-empirical) prediction method including partial directivity and one-third octave band levels. Further methods, based on tests and analyses, were presented in Refrences 2-23 and 2-24.

A recent study of these turbine noise prediction methods was reported in Reference 2-25; there the method of Reference 2-8 was recommended as an interim turbine noise prediction method for use by the NASA/ANOPP office. Since then Reference 2-26 has been published and the proposed prediction methods there are developments of those presented in Reference 2-24 and are based on further extensive test and analyses. They also circumvent the criticisms of Reference 2-25 which were lack of sufficient directivity and spectra. Three methods are presented in Reference 2-26. First a "Preliminary Design" method which is shown to yield excellent correlation with CF6, TF34,

and NASA Engine "C" turbine noise. These engines have the kind of turbines which would be expected to be developed for use in advanced engine designs of the 1985 - 1990 time frame. It is referred to as the "Preliminary Design" method because it is a little simpler and requires less knowledge of turbine stage performance and configuration parameters and is more amenable for parametric studies.

However, the method could be expanded to the second or "comprehensive" detail design method, which requires individual turbine stage performance and configuration data. This kind of detail design information is not easily available and the increased accuracy at this time is probably not required. Such a method could be used closer to an actual airplane/engine selection. The third method is the "analytical method" which requires even more extensive turbine design details and, consequently, is even less applicable to the present study.

The method selected here for the prediction of static, unsurpressed, turbine noise is the "Preliminary Design" method of Reference 2-26. The only modification to that method is in the area of directivity. That method covers angles from 20° forward to 170° aft; the directivity was therefore linearly extended to cover the additional angles forward and aft so that the complete range was from directly forward, $\phi = 0^{\circ}$; to directly aft, $\phi = 180^{\circ}$. The method is not spectrally sensitive i.e., the same spectrum shape is held over the whole angle range. The prediction method and equations are summarized and defined in NASA CR-159105 "Cruise Noise Prediction Methods Manual." The Reference 2-26 methods also provide a methodology for the prediction of "hay stacking" effects. This is the interaction of the radiated discrete tones with the ad- jacent frequencies. This procedure could be included later, if desired, but is considered to be outside the scope of the current effort.

This turbine noise prediction procedure is for far-field (community) noise application. In the chosen method, the reference distance is on a 200 ft sideline at $\phi = 120^{\circ}$. Since it is a higher frequency noise radiating from an area which is larger than its wavelength the inverse square law would be expected to hold to distances very close to the nozzle. Thus it may be regarded as a point source radiator. Application to close-in distances is achieved by use of the inverse square law and atmospheric attenuation.

For prediction of turbine noise under cruise conditions, the turbine performance parameters corresponding to that flight condition must be employed, see Section 2.4.1. Since the noise is generated internally, airplane forward speed is not expected to otherwise directly influence the generated acoustic power. However, aircraft forward speed does effect the external propagation field, Section 2.4.2, and the coordinate transformation and convective effect are included in the cruise prediction method. The resulting acoustic free field would of course be modified by airplane configuration features as described in Section 2.4.3. Should turbine acoustic treatment be included in the nacelle design the noise reduction at cruise may be evaluated by use of the methods described in 2.3.3.7.

2.3.3.3 Combustion - Combustion noise, the other dominant component of core noise, is generated by the combustion process, propagates through the turbine and radiates from the primary nozzle, through the discharge efflux streams to the observer location. It has been shown to consist of low frequency broad band noise which has statically, little directionality.

Among the earlier detail reported combustion noise studies is that of Reference 2-27 dated 1972, which covered small gas turbine engines and auxiliary power units. Thus only recently has data of sufficient quality been obtained from which a definitive prediction scheme may be formulated. Also in 1972 core noise studies and analyses were presented for a T-64 turboshaft engine, Reference 2-28. Application to large turbofan engines was considered in References 2-29, 2-30, and 2-8.

Reference 2-31 presented a recent survey on low-frequency core noise prediction methods, and recommended an interim prediction method for use by the NASA ANOPP office. This method incorporates the sound power level equation of Motsinger, Reference 2-28, but with the directivity and spectrum shape given by Dunn and Peart, in Reference 2-8. This selection resulted from the general lack of substantiating data among the candidate prediction methods and for its simplicity and use of engine parameters that should be readily available to the acoustic analyst. Some uncertainty in the recommended directivity pattern was expressed in Reference 2-31 based mainly on the work of Strahle, Reference

2-32. A peak frequency of 400 Hz is recommended if this method predicts a frequency outside the range of 300 to 1000 Hz.

Consequent to the recommendations of Huff, et al, Reference 2-31, both Pratt and Whitney, Reference 2-33, and General Electric, Reference 2-34 and 2-26, have conducted extensive work in the area of core noise. Both companies have now developed and refined core noise prediction methods which should be a considerable improvement over the previous interim method. These methods have been developed from a substantial data base gathered from engine and burner-rig tests. The PWA correlations and prediction model relies mainly on versions of the JT8D engine core. GE present two prediction methods. The first is referred to as the "component" method and based on a correlation of their parametric test data. The second is the "engine" method derived from the engine data, Reference 2-34. The engine method is updated in Reference 2-26 with a new directivity for dual-flow engines. GE indicate that their "engine" prediction equation provides good agreement, not only with GE data, but with data of Garrett, PWA, Boeing, Rolls-Royce (RB211), and Allison (turboshaft). Furthermore, like the "interim" method, the GE equation is simple and uses mor readily available engine parameters. The GE "engine" method and the PWA method account for turbine transmission losses, while the GE "component" method does not. Both organizations have compared the others' and their own model to their measured data. However, the PWA methods does not appear to checkout with the GE data, and similarly, the GE model does not fair well with all the PWA data.

The GE "engine" method has been selected for the prediction of combustion noise at sea level static conditions since it appears to be based and validated over a wider range of engine cycles than the PWA method. This engine cycle range includes those likely to be developed for 1985/1990 application. The selected prediction method predicts the overall sound power level of the combustion noise. A spectrum shape and directivity are used to convert the sound power to one-third octave band sound pressure levels from 50 to 10,000 Hz and an overall sound pressure level at a specified point in the far-field for free-field, lossless conditions. The directivity of this method covers angles from 40° to 140° for dual flow engines and 10° to 160° for single flow engines. For application to this study the directivities have been linearly

expanded to cover the complete fore and aft quadrants. This is the only basic modification to that method.

This combustion noise prediction procedure is for far-field (community) noise application. However, even for close-in distances it may be treated as a point source radiator located at the primary exit plane.

The prediction method and equations are summarized and defined in NASA CR-159105 "Cruise Noise Prediction Methods." For prediction of combustion noise under cruise conditions, the combustion performance parameters corresponding to that flight condition must be employed; see Section 2.4.1. Since the noise is generated internally, airplane forward speed is not expected to otherwise directly influence the generated acoustic power. However, aircraft forward speed does effect the external propagation field, Section 2.4.2, and the coordinate transformation and convective effects are included in the prediction method. The resulting acoustic free field would of course be modified by airplane configuration features as described in Section 2.4.3. Should combustion acoustic treatment be included in the nacelle design, the noise reductions at cruise may be included by use of the methods described in Section 2.3.3.7.

2.3.3.4 Nacelle Case Radiation - Nacelle surfaces, may be in close proximity to potential laminar's flow control surfaces. Noise from the turbomachinery and combustion process can cause structureborne and airborne vibration excitation of the nacelle surface which in turn can radiate noise. Noise levels from this source have never been specifically identified and reported in the literature; no method is known for the estimation of such radiated noise levels. Case radiated noise levels are therefore expected to be low in comparison with the noise levels of other sources. At this time case noise is neglected.

2.3.3.5 Jet - The term jet noise refers to the noise generated within a nozzle efflux downstream of the nozzle exit plane. Jet noise can have three sub-components. The first is "jet mixing" noise, which is generated by the turbulent mixing of the jet with the ambient and neighboring fluids and is always present. The second and third are present when the nozzle operates at

supercritical pressure ratios (> 1.89) and when shock waves exist in the jet efflux, for example, in the case of a supersonic under-expanded flow. The jet shock noise components are broad band shock associated noise - which is generated by the convecting turbulent eddies interacting with the shock structure, and shock screech - which is a set of discrete tones created by a feedback loop between the nozzle and the shock structure. Should the exhaust flow be fully expanded through a convergent divergent nozzle operating at its design Mach number or pressure ratio then shock waves will not exist in the efflux and jet mixing noise only when be generated. The jet noise components must be predicted separately since they have different spectral characteristics and are generated at different locations in the jet. Further evidence exists that they respond differently to forward speed and have different convective amplification effects. For the propulsion systems expected to be of interest at takeoff and landing the nozzle exit pressure ratios are subcritical, e.g. 1.89, and the nozzle flows are locally subsonic. During cruise for the typical engine cycles expected the nozzle flow characteristics are those shown schematically in Figure 2-6. The primary nozzle efflux has the higher velocities and temperatures, but has a nozzle exit pressure ratio less than < 1.89 and hence has a shock free flow structure and is thus a source of jet mixing noise only. However, the fan duct exhaust flow has a nozzle exit pressure ratio greater than 1.89 and with the usual convergent nozzle the efflux is thus underexpanded and contains shock waves. At any location, the total jet noise in cruise could, therefore, be made up of four noise components e.g. primary mixing noise, fan-flow mixing noise, fan-flow shock-associated broad-band noise and possibly fan-flow screech, as shown schematically in Figure 2-7. Methods for the prediction of these jet noise sources are based upon noise characteristics and flow fields of static jets. During cruise the efflux flows (potential cores, mixing lengths) etc. could be different resulting in different noise source distributions and characteristics. These effects are not considered in the prediction procedures.

The following sections describe the methods for the independent prediction of the three jet noise sources.

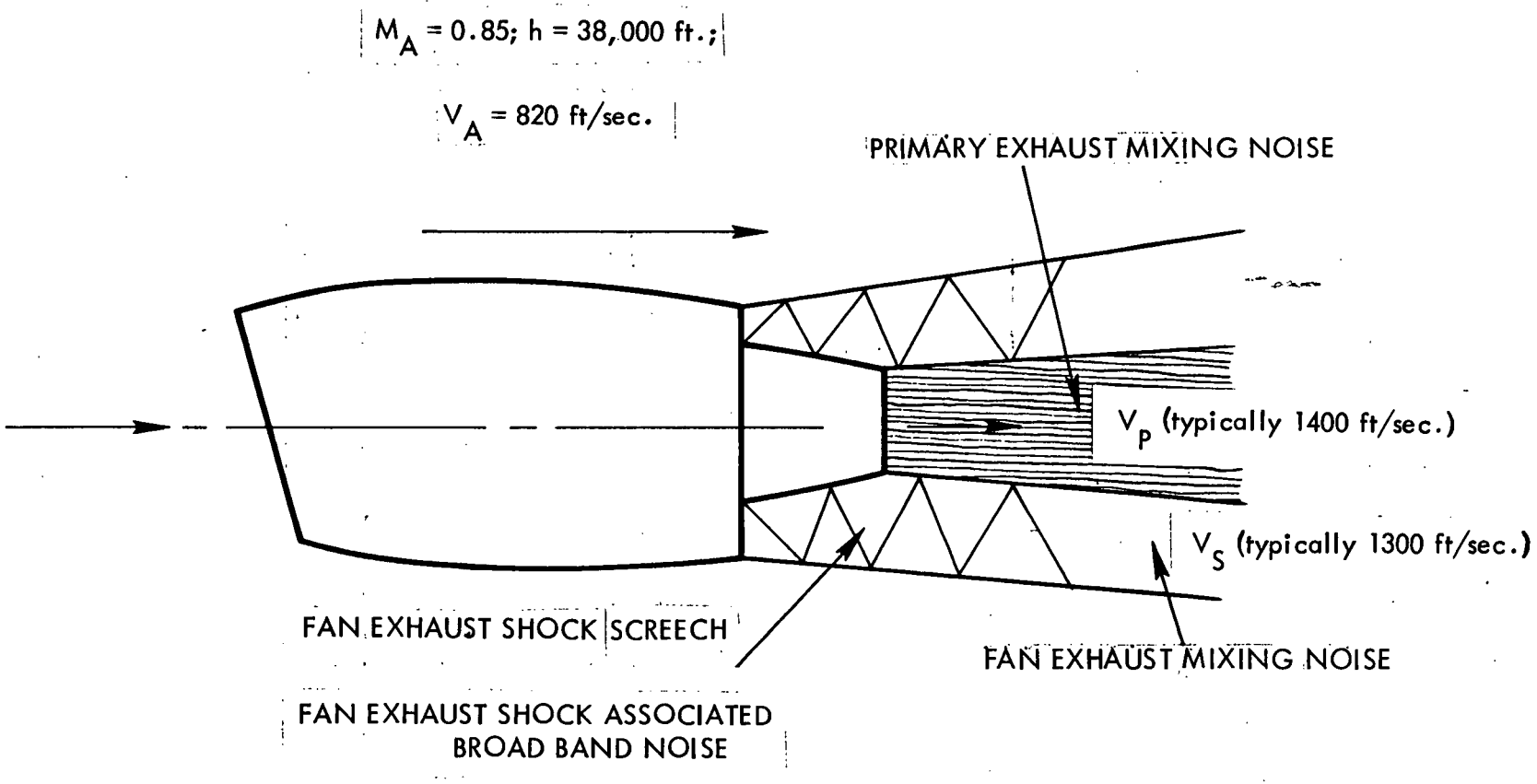

FIGURE 2-6. TYPICAL CRUISE JET FLOW PATTERNS AND NOISE SOURCES

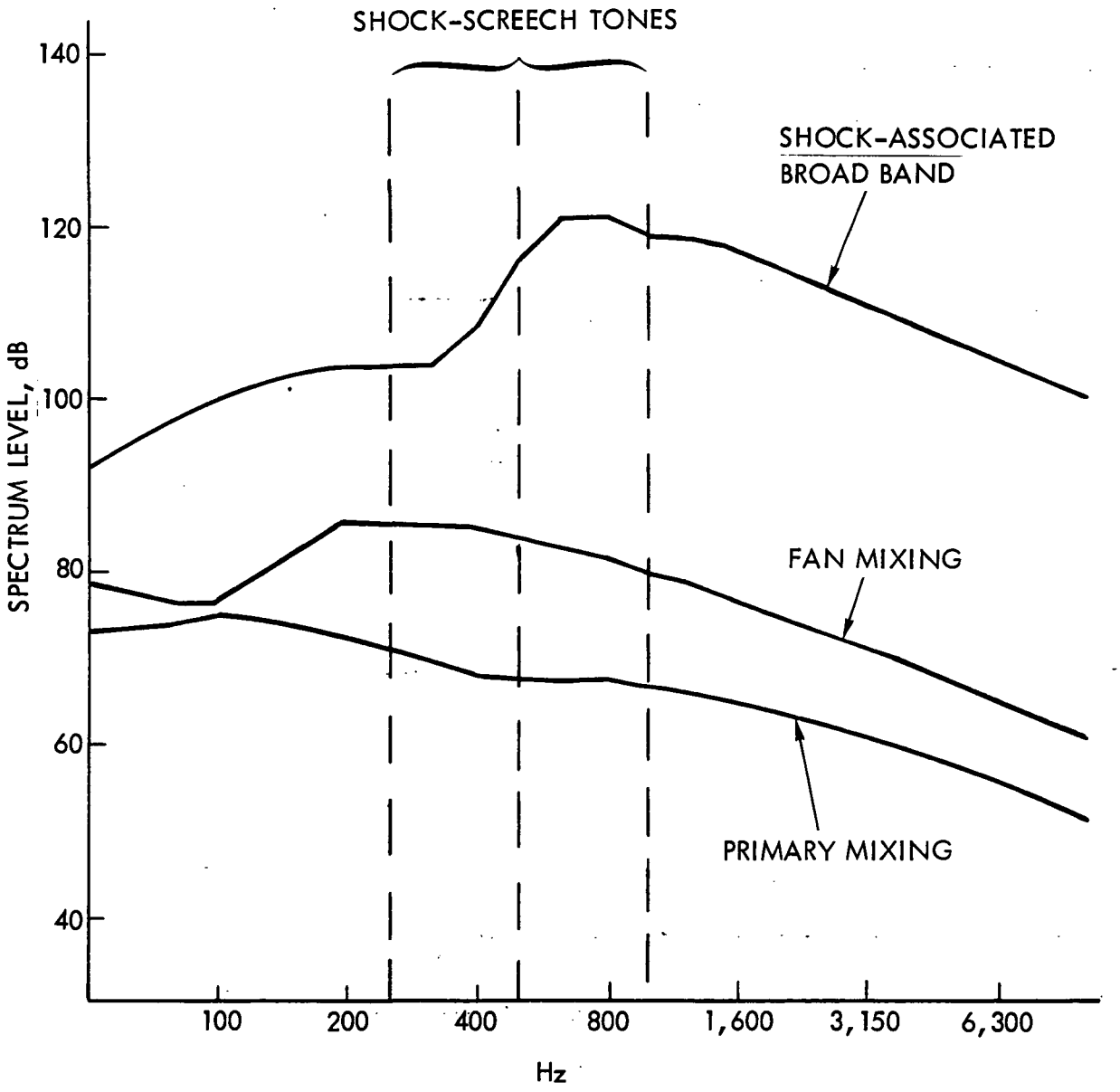

FIGURE 2-7. SCHEMATIC OF CRUISE JET NOISE COMPONENTS

Jet Mixing Noise

The mixing noise component is always present and is independent of the presence of shock waves. A review was made in References 2-6 and 2-7, of the various prediction schemes available. The most recent review of Reference 2-7 concluded that the most promising prediction of mixing noise from a single flow jet, in the near field, throughout the temperature and velocity range is that of Plumblee, et al., Reference 2-35. The prediction capability of this method was shown to be superior to that of the scaling methods of References 2-36, 2-37, and 2-38, all of which seem to inadequately consider the effect of temperature. The analytical methods of Chen, et al. 2-39, 2-40, 2-41 and Maestrello 2-42 were also investigated and compared with experimental data in Reference 2-7. The method of Chen, et at., is complex and shows the possibility of large errors; at least 10 dB under some conditions. Finally, Reference 2-7 indicates Maestrellos' analytical method, Reference 2-42, is not developed to the point where it is applicable to practical near-field preditions.

Thus, Plumblees method, described in References 2-6 and 2-35 is selected as the basic prediction scheme. In this scheme the prediction model is based upon extensive near field noise measurements of shock free jets. The jets were static, model scale, single flow jets. The near field measurements thus include the distributed nature of the noise sources within the jet and their directional effect at different frequencies. Further the method is valid over a wide range of jet temperatures and velocities. However, the mathematical model is limited to the above test conditions and prediction of an overall sound pressure level and acoustic pressure levels in three octave-bands (although noise levels over a much wider frequency were acquired and are presented). Thus, extensive development of the mathematical model was required to account for (1) an expansion of the frequency range from the three octave band to cover the frequency range of 50 to 10,000 Hz, (2) expansion of the directivity to include the forward quadrant, (3) co-axial nozzle flows, (4) different nozzle configurations, e.g., short, 3/4 or full length fan cowls and (5) airplane forward speed effects. These modifications are discussed in the following paragraphs.

To expand the frequency range of the static single flow jet the recommendation of Reference 2-7 was followed, which was that the four wide frequency non-dimensional spectra, derived in Reference 2-36 (which are based upon near field noise measurements of a full-scale, jet) be used. These spectra refer to four spatial zones in the aft quadrant. The appropriate shape is then fitted to the overall and three octave band points derived from Plumblees method. The spectum shape in the nozzle exit plane, X/D = 0, is also assumed to apply in the forward quadrant. This method can be used directly for the prediction of near field noise from static single flow jets such as a fully mixed flow.

To develop the above method for application to a dual flow jet the empirical procedure of Reference 2-8 is incorporated into the above prediction scheme as recommended by Reference 2-7. This method was developed mainly from model, cold-flow experiments and is strictly applicable to the far-field noise prediction of dual-flow jets. It is assumed to apply to near-field noise also. The approach is, first, to calculate independently, the sound pressure levels of the primary and secondary jets using the above single jet method. However, the primary jet noise is modified by a ΔdB correction to account for the relative velocity effect due to the presence of the secondary jet flow; in calculating the noise of the secondary jet, the mass flow-rated average values of the primary and secondary jets are used as the flow parameters. The sum of these two noise levels yields the total dual flow static jet noise level at any specified location. With this approach, the effect of aircraft forward motion is restricted to the secondary flow.

Plug nozzles are considered in the present prediction by adopting the far-field method developed by Stone 2-43. This method involves a correction to the overall level and a frequency shift as a function of nozzle geometry. It is assumed that these corrections developed from far-field data also apply to the near-field.

Forward speed has been shown in many model tests, References 2-44, 2-45 and others, to significantly effect the acoustic power output of a single flow jet at low forward speeds, e.g. up to a Mach number of about 0.2. The test results show that the static overall sound pressure levels are reduced by an

amount which is proportional to jet relative velocity raised to a power between 5 and 6. These reductions are, approximately, applicable to all frequencies at all angles. Figure 2-8 shows the relative velocity reduction, using a 5.5 component, for aircraft velocities up to the range applicable to cruise. It is seen that direct application of this low speed relationship predicts a very considerable cruise noise reduction. For example, with the jet velocity, V_J, held constant at 1300 ft./sec. the forward speed reduction amounts to some 24 dB.

In the computation of two flow jet noise the relative velocity effect is considered to occur twice e.g. between the primary and the secondary flow and between the secondary flow and the atmosphere. Appropriate relative velocities are used.

In the applicable transformations to acoustic characteristics at cruise, relative velocity is included as described; it affects both the level and the frequency. The noise is related to the jet structure which exists statically and does not allow for any flow changes which might occur due to cruise operation. Operating conditions and acoustic impedence used are those at cruise.

The forward speed propagation transformations include the co-ordinate transformation (using the different source frequency locations) and the dynamic effect, since jet mixing noise is a distributed source. The convective effect is already built into the basic jet noise model of Reference 2-40. Although the jet mixing noise sources move relative to a noise reception point on the aircraft, implying a Doppler frequency shift none is used here since, following Reference 2-7 there is lack of experimental data to support its existance.

The jet mixing noise prediction procedure and equations and the computational algorithm are summarized and presented in NASA CR-159105.

Shock-Associated Broad-Band Noise

The basic work on shock-associated broad-band was performed by Harper-Bourne and Fisher, Reference 2-46. They conducted noise surveys of static model jets containing shock flows in which the shock cell screech had been suppressed.

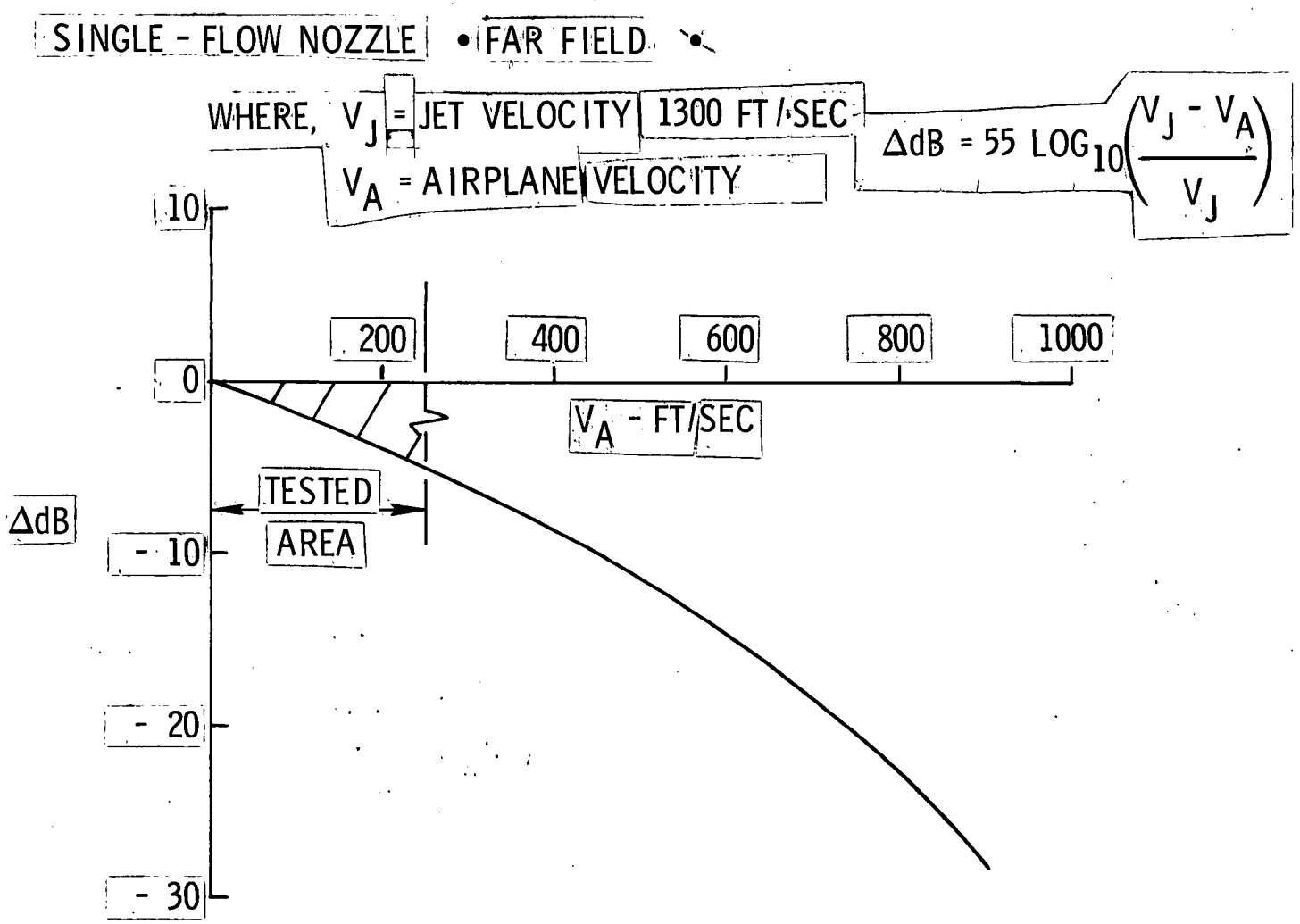

FIGURE 2-8. RELATIVE VELOCITY EFFECT ON JET MIXING NOISE

Using this data, together with a theoretical understanding of the problem a mathematical formulation of the phenomena was constructed. Later, a more extensive study was conducted on supersonic jet flows (again with the shock screech suppressed) and reported in Reference 2-47. This work has been recently summarized in Reference 2-48. Based on these measurements the original theory of Reference 2-46, with a few modifications, was verified. this methodology has recently been adopted by the Society of Automotive Engineers (SAE) as the recommended prediction procedure for far-field shock-associated broad-band noise. The method predicts the broad-band directional noise of a supersonically underexpanded flow discharge from a static conical nozzle. The shock flow field is assumed to be dominated by the first eight shock cells and the resulting noise is dominated by the turbulence-shock interaction. It does not include any contribution from shock-cell screech. The method assumes a point noise source located at the nozzle exit plane. For a static jet, levels of shock-associated broad-band noise increase rapidly with efflux flow Mach numbers above 1.0, and exceed those of jet mixing noise, which is also present and is unaffected by the presence of the shock waves. The spectrum peak frequency is related to the nozzle pressure ratio which controls the shock spacing. Increasing pressure ratio increases the shock spacing which decreases the spectrum peak frequency. The spectrum shape is broad-band in nature with steeper slopes than for jet mixing noise. The noise has virtually omni-directional characteristics.

The above method is the basic method selected for the prediction of static shock-associated broad-band noise at cruise. Developments made were: (1) the spectral frequency range was expanded to cover the 50 to 10,000 Hz range (which was accomplished by a linear extrapolation of the spectrum shape) and (2) the directivity was expanded to two complete quadrants (which was accomplished by a linear extrapolation of the available directivity). Application of the method to a single flow exhaust is straightforward. For a two flow nozzle configuration the sound pressure levels are related to the nozzle areas whose flow contains the shocks while the co-ordinate system is related to the outer diameter of the shock containing flow. The prediction method is basically applicable to the far-field with the noise source considered located at the nozzle exit plane. Some measured "close-in" far-field noise data was available and the method was used to predict this data. Reasonable agreement

was obtained; however, development of this method to more accurately predict "close-in" far-field noise is needed.

The effect of forward speed on shock-associated broad-band noise has been experimentally investigated on model jets contained in low speed co-flowing jets, References 2-49 and 2-50. There appears to be no relative velocity effect on was identified such as appears in jet mixing noise. However, a convective effect was identified, on overall sound pressure, and is $[1/(M_A \cos \phi)]^4$ factor applied to directionality.

In the applicable transformations to acoustic characteristics at cruise relative velocity does not effect the levels or spectral peak frequency. The noise is also related to the jet shock structure which exists statically and does not allow for any changes which might occur in the shock structure due to cruise operation. Operating conditions and acoustic impedance used are those at cruise, Section 2.4.1.

The forward speed propagation transformations include the co-ordinate transformation and the convective effect. The same convective effect identified at low forward speeds (corresponding approximately to $M_A = 0.2$) is assumed to hold for the much higher cruise Mach numbers. This noise source is currently predicted as a point source and so there is no dynamic effect. Since the source is fixed relative to a noise reception point on the aircraft these is no Doppler frequency shift, Section 2.4.2.

The shock-associated broad-band noise prediction equations and the computational algorithm are summarized and presented in NASA CR-159105.

Two examples of computed shock-associated broad-band noise at cruise are shown in Figure 2-9. Both spectra are at a wing location, the upper due to a wing mounted engine, the lower due to a rear fuselage mounted engine.

Shock Screech Noise

Shock screech is the second shock noise component which can be generated by jet flows containing shock waves, e.g. supersonic underexpanded jets. The

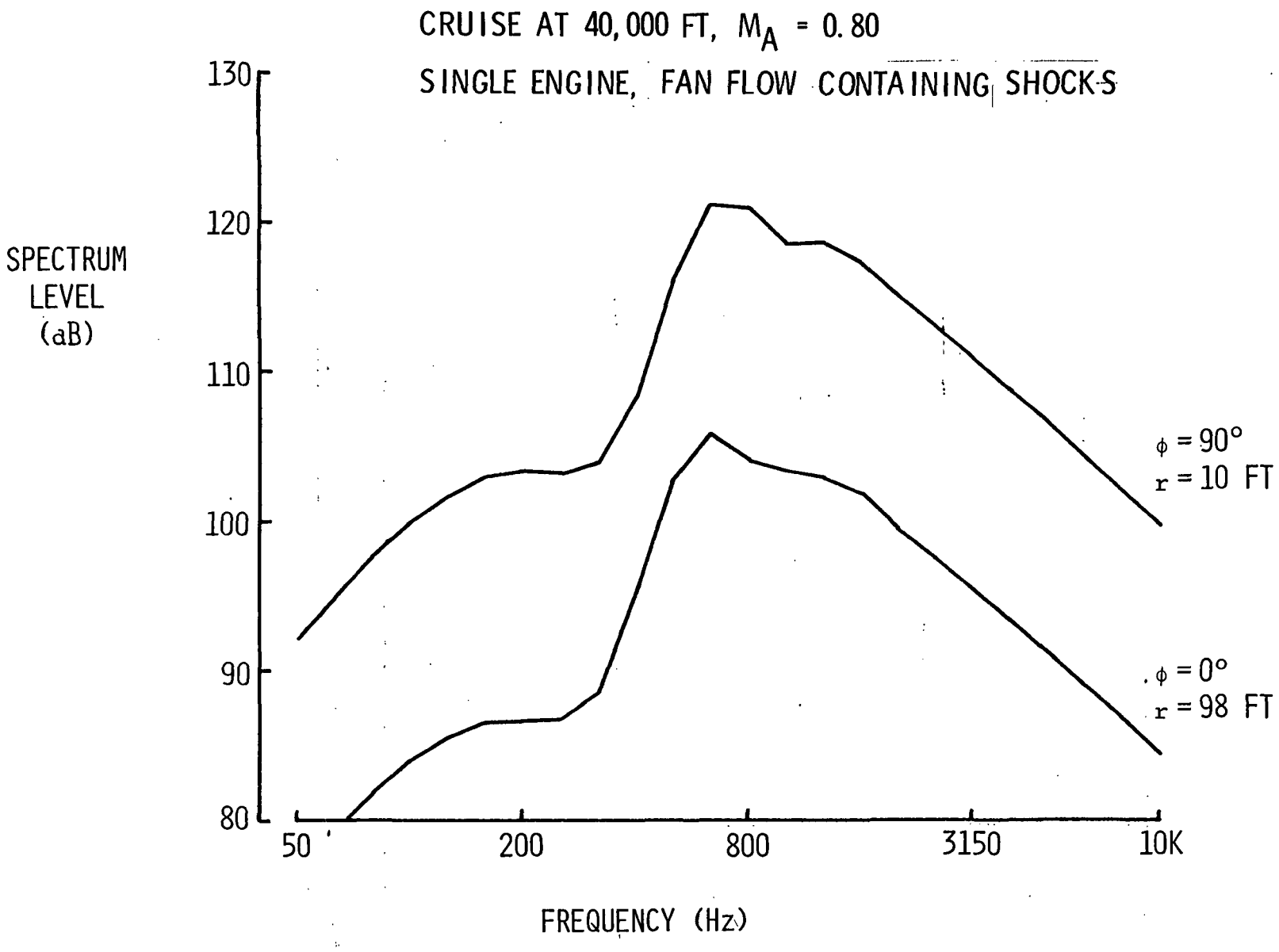

FIGURE 2-9. JET SHOCK-ASSOCIATED BROAD-BAND NOISE

screech has the form of intense discrete tones consisting of a fundamental and its harmonics. This noise is generated in addition to jet mixing noise and broad-band shock-associated noise. This noise was first described by Powell, References 2-51, 2-52, and 2-53; it appears to owe its origin to a feedback mechanism between the shocks and the nozzle lip, and it has been clearly identified on model nozzles. Under these conditions it may be suppressed by inserting small projections into the flow from the nozzle lip or by covering the nozzle lip with acoustically absorbtive material (which reduces the strength of the feedback mechanism). Then the radiated jet noise consists of mixing and shock associated broad-band noise, and the majority of acoustic studies on supersonic jet flows are made under these conditions. Some authorities state that the phenomena seldom occurs during flight on an aero engine configuration because the flows in the vicinity of the nozzle are too unsteady to permit the feedback to become established. Its existance during cruise is documented in References 2-54, 2-55, and 2-56 where the engines were of the low bypass ratio type. In Reference 2-55, structural damage during cruise is attributed to screech. Shock screech is believed to have been present during some of the X-21A flight testing, Reference 2-57, where the engine was a pure-jet. However, there are a great number of aircraft powered by various types of engines where its presence is not reported. Whether screech will occur on engines considered for the 1985-1990 time frame (probably high by pass ratio engines) is not known. Thus, it appears that should shock screech be present there is the possibility that it may be eliminated by some nozzle redesign. However, there are no available criteria available to define the onset of shock screech in terms of nozzle configuration and flight condition.

A review of methods and data available for the prediction of shock screech was reported recently in Reference 2-7. Based on References 2-51 through 2-56 and the extensive near-field noise measurement surveys conducted on static single flow nozzles operating in the "screech mode," References 2-58 and 2-59, a method was developed in Reference 2-7 for the prediction of shock screech. The screech frequencies, fundamental and second harmonic, were predicted using the equations of Reference 2-55, which include a forward speed effect. The absolute levels were obtained from the measured data of References 2-58 and 2-59. The screech noise levels may be neglected for nozzle exit pressure ratios less

than 2.0. Scaling was accomplished on an area basis. No criteria were presented to indicate whether screech is present or not therefore it is recommended that the predicted noise levels be regarded as "upper bound" levels. The noise source is considered to be a point source located 3.5 shock cell lengths downstream of the nozzle exit plane. The directivities for the fundamental and second harmonic were based on Powells lobed directivities, Reference 2-51 and 2-52, and centered on the source location.

The above described method was selected as the basic prediction method for shock screech. Developments included simplified equations to describe the directionality lobes. Application of the method to a single flow exhaust is straightforward. For a two flow nozzle configuration the sound pressure levels are related to the nozzle area whose flow contains the shocks while the co-ordinate system is related to the outer diameter of the shock containing flow.

Experimental studies of forward speed effects have recently been reported in Reference 2-49. The study was conducted on a 32 mm diameter circular nozzle. Low forward speed simulation was achieved by locating the nozzle in a larger co-flowing low speed jet. Statically, screech was identified to the fifth harmonic, with the second harmonic being the strongest. The measured harmonic noise level are up to 25 dB higher than the other jet noise sources - made up of jet mixing noise and shock associated broad-band noise. The effect of flight (90 m/s) shows that the screech tones are reduced in frequency and relative level. The use of the forward speed frequency equation gave the right trends, however, its use for the prediction of absolute frequency was not entirely satisfactory. Similar comment on the inflight frequency trends are reported in Reference 2-60.

In the applicable transformations to acoustic characteristics at cruise the effect of relative velocity is included in the frequency prediction but is not included in the level prediction. The noise is also related to the jet shock structure which exists statically and does not allow for any changes which might occur in the shock structure due to cruise operation. Operating conditions and acoustic impedance used are those at cruise, Section 2.4.1.

The forward speed propagation transformations include the co-ordinate transformation and the convective effect. The latter is assumed identical to that shown for shock-associated broad-band noise. Since this noise is considered as a point source there is no dynamic effect. Since the source is fixed relative to a noise reception point on the aircraft there is no Doppler frequency shift, Section 2.4.2.

The shock screech noise prediction equations for frequencies, levels, directionalities and the transformations are presented in NASA CR-159105.

2.3.3.6 Advanced Propellers - Advanced propellers refer to propeller designs which are currently under model development and are proposed for application high subsonic speed airplanes. Conventional propeller powered airplanes are limited to lower speeds. As currently configured these propellers would have approximately 8 to 15 blades and during cruise could be operating at supersonic tip Mach numbers. The blades could be swept and could have advanced blade sections. Application of this propulsion system to an LFC aircraft (for example in a pusher-type configuration) is a possibility, although not at present being studied. A very preliminary method for the prediction of cruise near field noise has been proposed by Hamilton Standard, Reference 2-61. However, this method only predicts overall sound pressure levels close to the propeller plane. A method needs to be developed which would include spectral (discrete and broad-band) and directional information. Acoustic tests of model advanced propellers in wind tunnels have recetly been accomplished and the data is being analyzed. One of the objectives of the analysis is to develop a more realistic and comprehensive model of the cruise near-field noise environment of an advanced propeller, although the directionality emphasis is on noise radiated in the plane of the propeller rather than directly forward. When this method becomes available it could, if necessary, be adapted into the present procedures as one of the possible noise sources.

In the meantime, if necessary, methods based on Reference 2-61 of estimating the cruise noise environment could be developed. However, they would require verification from the previously mentioned tests.

2.3.3.7 Duct Acoustic Treatment - Commercial airplanes must comply with the appropriate FAR 36 noise certification levels. Consequently, for new airplanes entering service in the 1990 time frame it can be anticipated that the engines will have some acoustic liner suppression of internally generated noise sources, e.g. fan, compressor, combustor and turbine. These acoustic liners could be optimized for either FAR 36 test conditions or cruise condition's. The assumption here is that the acoustic liners are designed for the former condition. It is thus necessary to evaluate the various liner acoustic performance under the cruise conditions. These attenuations are then combined with source hard wall noise generation characteristics to yield suppressed noise characteristics at cruise. An acoustic liner generalized attenuation prediction procedure is required which will include spectral and directivity effects.

In the literature a wealth of information exists on various aspects of acoustic liner design. For the selection and or development of an engineering procedure two of the most useful reference are References 2-8 and 2-62. The methods presented there are empirical and are based on extensive test data; they avoid the complication and expense of exact solution of wave propagation in a lined ducts. The attenuation predictions are experimentally correlated with the duct geometric and acoustic parameters and the duct Mach number. The liners are assumed acoustically optimized at the critical terminal design condition. Thus details of the liner design parameters are not specified in these evaluation methods.

The attenuation prediction method selected, with some development, is largely a simplified composite of these presented in References 2-8 and 2-62.

The method requires knowledge of the duct mean geometric, acoustic and aerodynamic properties, at the design and cruise conditions. The procedure can be used to estimate (1) the attenuation peak frequency at cruise, (2) peak attenuation at that frequency, (3) the attenuation spectrum shape and (4) the attenuation directivity.

The terminology used in this section is:

c_o speed of sound in duct at the design condition

c_c speed of sound in duct at the cruise condition

f_o liner peak frequency at the design condition

f_c liner peak attenuation frequency at cruise

H mean duct height between opposite liner faces

L effective length of treatment in the duct (with allowances made for fastening strips, etc.)

M_{d_o} mean duct flow Mach number at the design condition

M_{d_c} mean duct flow Mach number at cruise

S number of inlet splitter rings

ϕ angle from the inlet axis to the observer location

λ_o wavelength of sound in the duct at the liner peak frequency at the design condition

λ_c wavelength of sound in the duct at liner peak attenuation frequency at cruise ($= c_c/f_c$)

The above information (except f_c and λ_c) are required to compute the liner cruise attenuations.

25
24

Attenuation Peak Frequency

Based on Reference 2-62 the attenuation peak frequency at cruise is related to the peak frequency at the design condition by

$$\frac{f_c}{f_o} = 10^{\{0.306\ (M_c - M_o)\}} \qquad 3\text{-}1$$

The quantities f_o and M_o are required.

Attenuation Maximum Level

The important parameters are L/H, H/λ and M. The effect of L/H on maximum attenuation is shown in Figure 2-10 (for M = 0 and H/λ = 1.0). This curve is derived from References 2-8 and 2-62. The curve may be represented by

$$\Delta dB_{(H/\lambda = 1,\ M = 0)} = 10 \left(\frac{L}{H}\right)^{0.7} \qquad 3\text{-}2$$

The effect of H/λ is shown in Figure 2-11. The equation may be represented by

$$\frac{\Delta dB}{\Delta dB}_{(H/\lambda = 1,\ M = 0)} = \left(\frac{H}{\lambda}\right)^{-0.6} \qquad 3\text{-}3$$

The effect of duct Mach number is shown in Figure 2-12 which may be represented by

$$\frac{\Delta dB}{\Delta dB}_{(M = 0)} = 1 - \frac{M}{2}\left(2 - \frac{H}{\lambda}\right) \qquad 3\text{-}4$$

Since Equations 3-3 and 3-4 are multiplying factors on Equation 3-2, the general expression for the maximum attenuation is

$$\Delta dB_m = 10 \cdot \left(\frac{L}{H}\right)^{0.7} \cdot \left(\frac{H}{\lambda}\right)^{-0.6} \cdot \left\{1 - \frac{M_c}{2}\left(2 - \frac{H}{\lambda}\right)\right\} \qquad 3\text{-}5$$

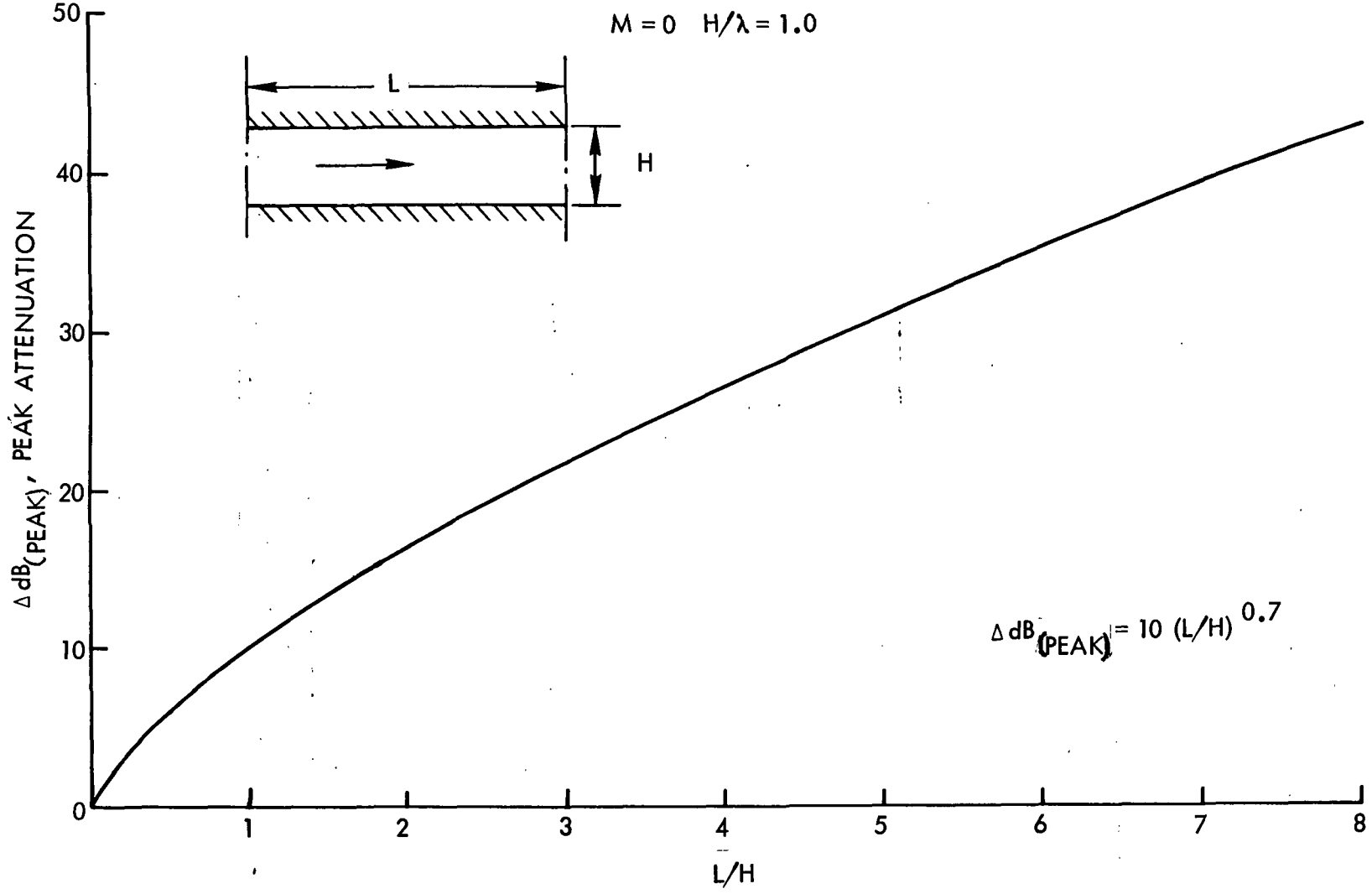

FIGURE 2-10. EFFECT OF TREATED DUCT LENGTH AND WIDTH ON PEAK ATTENUATION

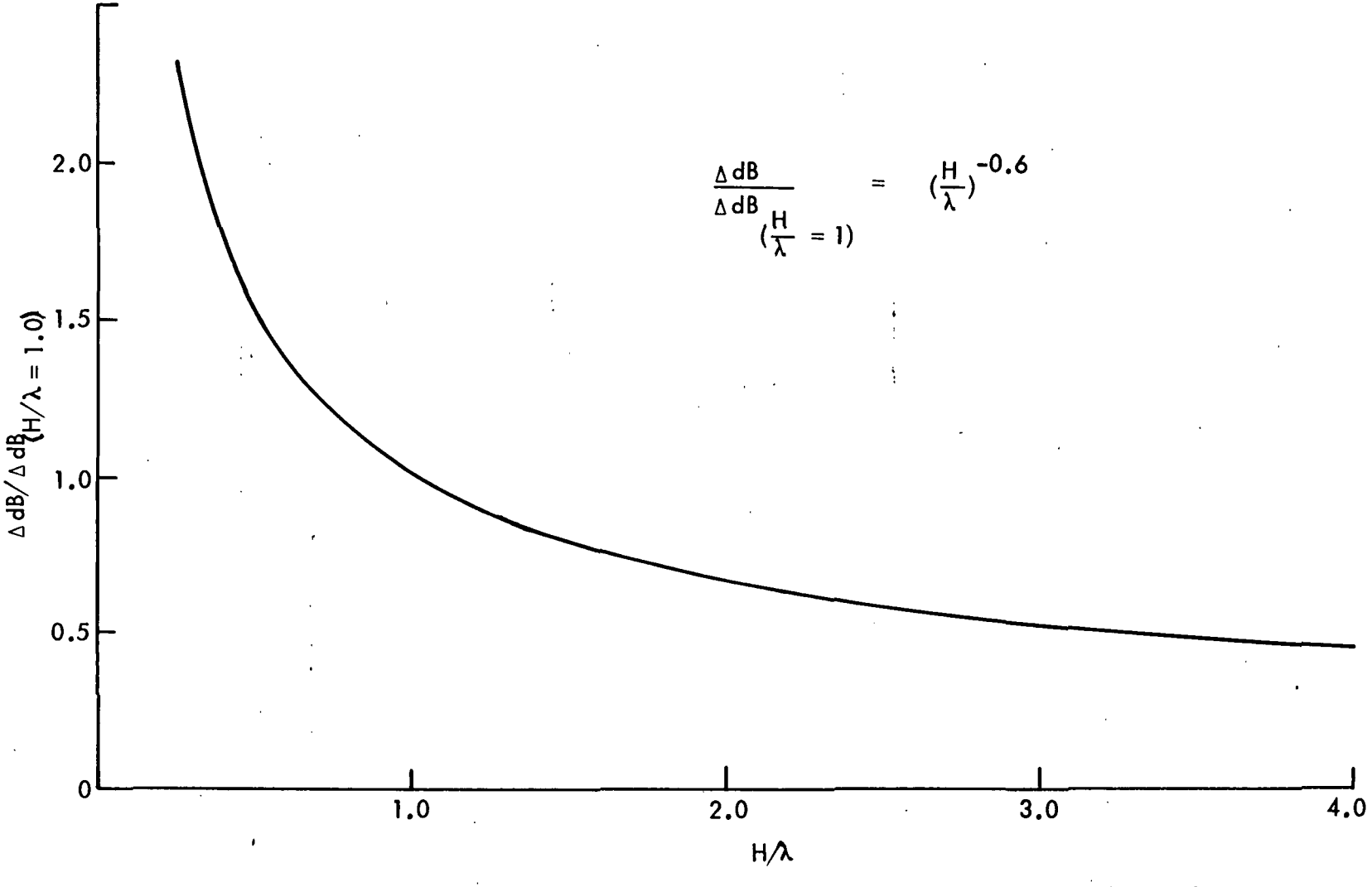

FIGURE 2-11. EFFECT OF WAVELENGTH AND DUCT WIDTH ON PEAK ATTENUATION

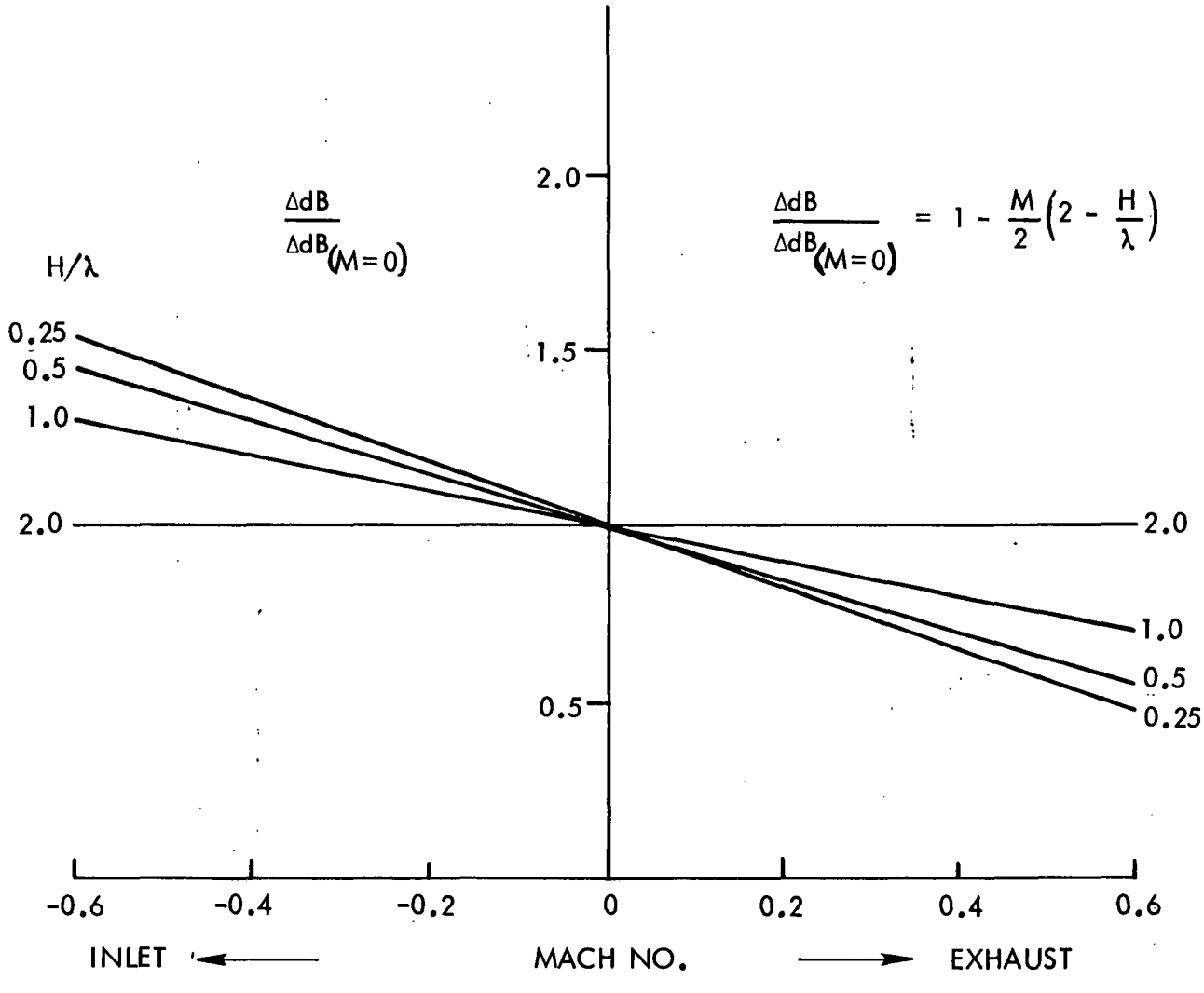

FIGURE 2-12. EFFECT OF MACH NUMBER ON PEAK ATTENUATION

At cruise the maximum attenuation becomes:

$$\Delta dB_{m,c} = 10 \cdot \left(\frac{L}{H}\right)^{0.7} \cdot \left(\frac{H}{\lambda_c}\right)^{-0.6} \left\{1 - \frac{M_c}{2}\left(2 - \frac{H}{\lambda_c}\right)\right\} \quad 3\text{-}6$$

where λ'_c corresponds to the cruise peak frequency defined in Equation (1).

At cruise the liners will be operating in a different duct acoustic characteristic impedance environment than at the design condition. The controlling criteria is the ratio of the acoustic impedance across the liner face sheet, which is the same at the design condition as at cruise. This change will not therefore directly affect the liner attenuation characteristics.

Attenuation Spectrum Shape

The spectrum shape (derived from mean, References 2-8 and 2-62) associated with the peak insertion is shown in Figure 2-13. Its shape may be represented using cruise notation, by

$$\Delta dB_f = \Delta dB_{m,c} \cdot \varepsilon \left\{\frac{\left|\log \frac{f}{f_c}\right|^{1.3}}{0.35}\right\} \quad 3\text{-}7$$

Attenuation Directivity

There is a marked directivity associated with the peak attenuation. This directivity for fan inlet and discharge noise has been derived from the NASA Quiet Engine static test results reported in Reference 2-63 and has been simplified to the trends shown in Figure 2-14. The directivities are expressed as

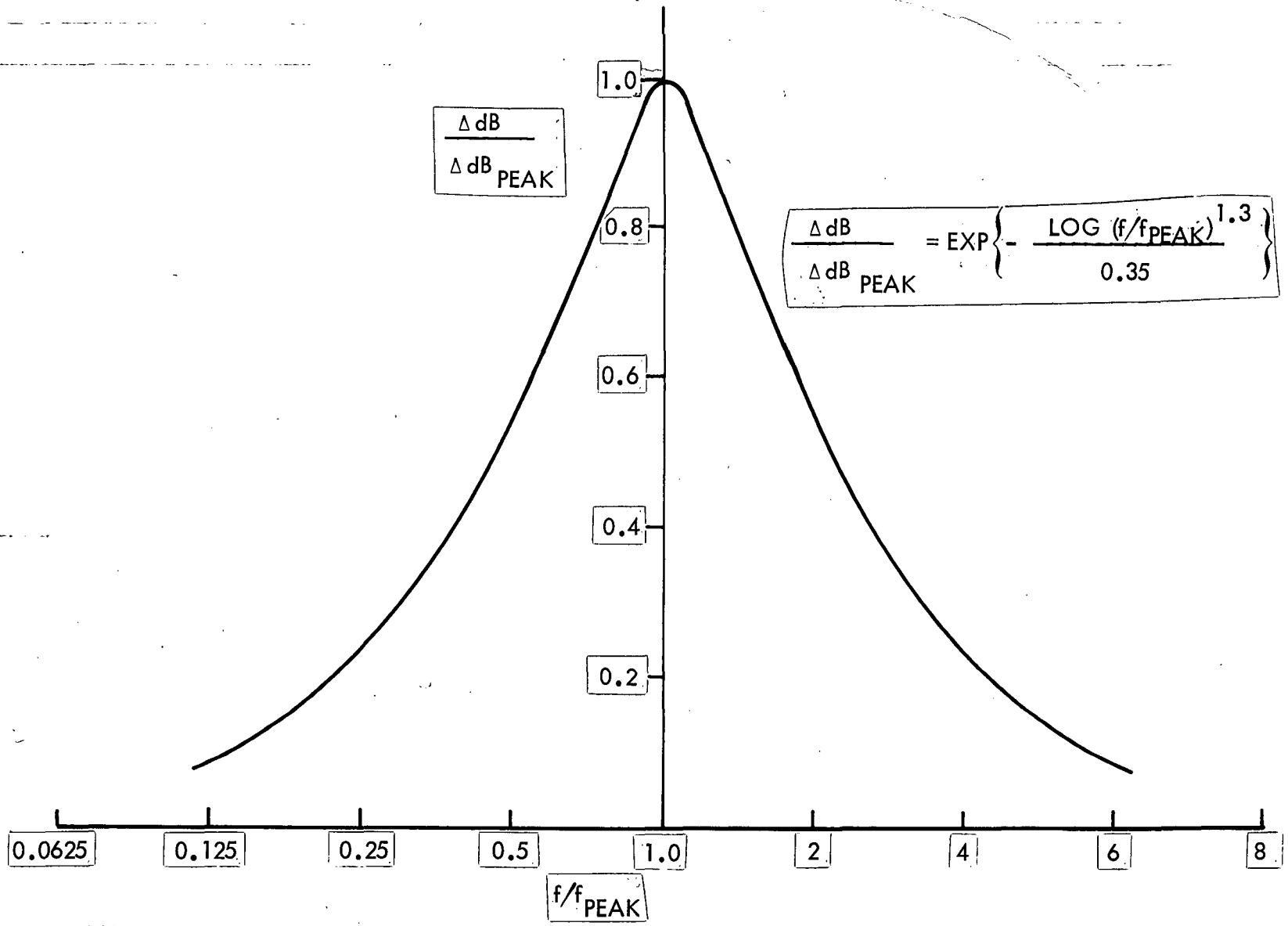

FIGURE 2-13. ATTENUATION SPECTRUM SHAPE

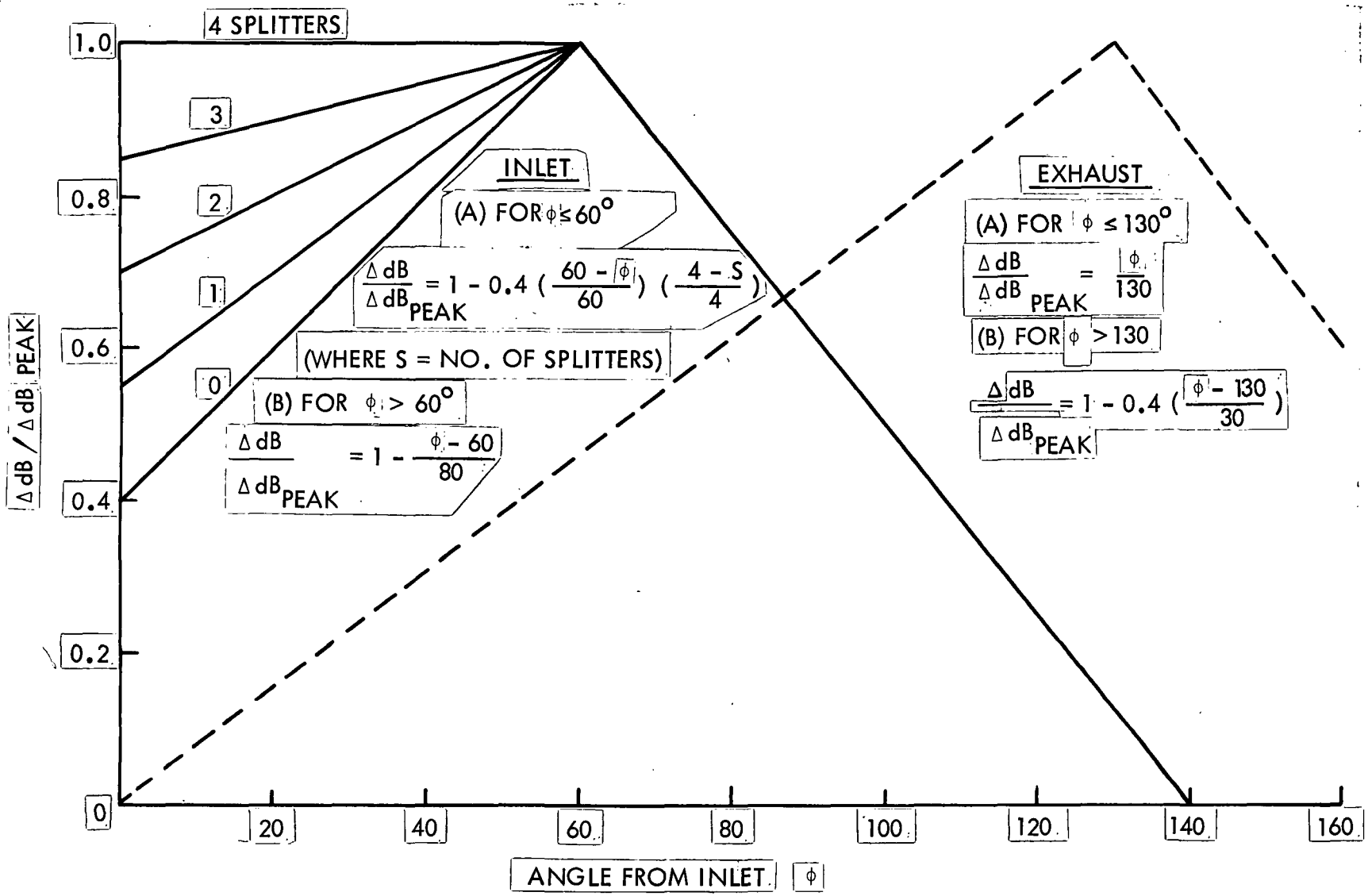

FIGURE 2-14. ATTENUATION DIRECTIVITY PATTERN

Inlet:

for

$$\phi \leq 60°, \quad \frac{\Delta dB(\phi)}{\Delta dB_m} = 1 - \left[\frac{60 - \phi}{60}\right] \left\{0.1\ (4-S)\right\}$$

$$\phi > 60°, \quad \frac{\Delta dB(\phi)}{\Delta dB_m} = \frac{140 - \phi}{80} \qquad 3\text{-}8$$

Exhaust duct:

for

$$\phi < 130°, \quad \frac{\Delta dB(\phi)}{\Delta dB_m} = \frac{\phi}{130}$$

$$\phi > 130°, \quad \frac{\Delta dB(\phi)}{\Delta dB_m} = \frac{205 - \phi}{75} \qquad 3\text{-}9$$

This method can be used for estimating the acoustic suppression characteristics of current technology liners designed for the attenuation of fan, compressor, combustion and turbine noise. Should advanced technology lines be used which have greater peak attenuations or wider bandwidths, these improved attenuations must be allowed for independently.

The computation algorithm for the duct acoustic treatment evaluation is given in NASA CR-159105.

2.3.3.8 High Mach Number Inlets - High Mach number inlets have been experimentally investigated as a possible means of reducing fan and compressor noise radiated from an inlet. The results of two such investigations, conducted statically on turbofan engines, are presented in References 2-64 and 2-65 and show high attenuations at higher throat Mach numbers. The noise reduction is also strongly dependent on the rotor tip speed and/or engine power setting. References 2-64 and 2-65 also show that the directional noise reduction is reasonably uniform and thus it may be considered as non-directional. This

attenuation may be considered as being independent of and additive to any attenuations arising from inlet acoustic treatment.

Figure 2-15 shows design curves derived from the above data for typical engine power settings. As an approximation, the $\Delta\Delta$PNL may be equated to a OASPL. This may be applied evenly across the spectrum to give a uniform spectral attenuation, at all angles. Thus the attenuation is independent of frequency and observer location.

2.3.4 Airframe Noise Sources

Airframe noise sources are associated with the interaction between airflows and turbulence convecting past rigid airframe surfaces, edges and other structural discontinuities. The turbulence can be that present in the incident airflow or that created by the relative motion between the airflow and airframe surfaces. Turbulence is a source of noise through two mechanisms. First, the fluctuating quantities (pressure and velocity) within the turbulence give rise to direct acoustic radiation, as in jet mixing noise. Second, the fluctuating quantities cause fluctuating forces (lift and drag) at the surface; these fluctuating forces then directly generate noise. The strength of these latter noise sources is related to the freestream dynamic head, the magnitude and scale of the turbulent pressure fluctuations and their interaction with the adjacent surface or edge. The resulting sound fields are "dipolish" in nature and exhibit an acoustic pressure dependent on velocity raised to the power between 5 and 6. These sources are treated quite independently of the propulsion system noise sources. Until recently, investigations of these airframe noise sources were aimed at ensuring that structures could withstand these near-field pressure loads and in determining their transmitted fuselage internal noise levels. A more recent interest has been from a far-field aspect in which the integrated effect of all the contributing airframe noise sources - at low aircraft speed and altitude - is to generate an aerodynamic noise floor for the airplane. These same noise sources contribute to the acoustic pressure environment over the airframe.

The possible airframe noise sources contributing to the acoustic pressure environment over a current high speed airframe during cruise can include sources described as:

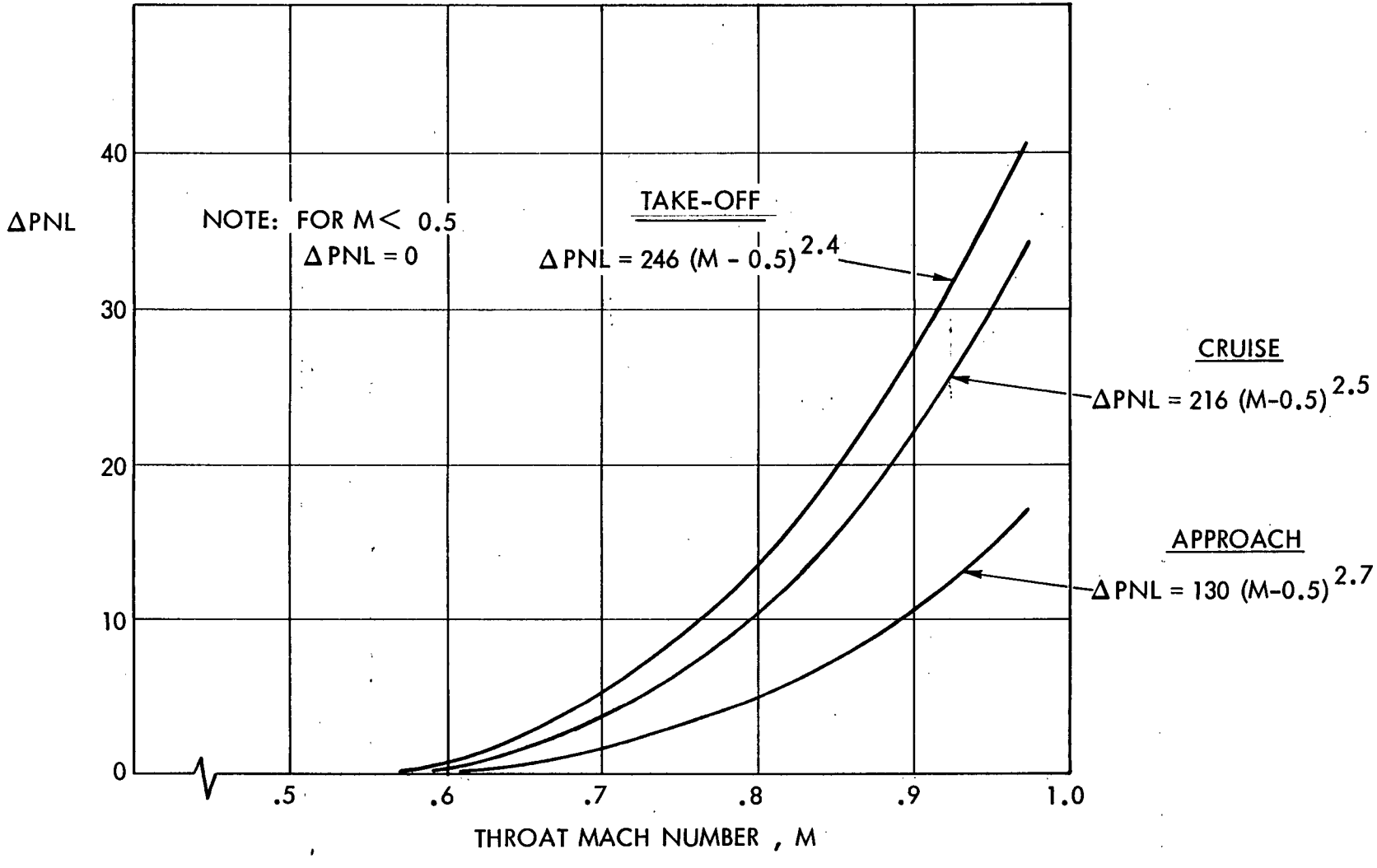

FIGURE 2-15. NOISE REDUCTION OF HIGH MACH NUMBER INLETS

- o disturbances convecting past whole surfaces
- o disturbances convecting past leading edges
- o laminar boundry layers
- o turbulent boundary layers
- o separated flows, buffeting
- o oscillating shock waves
- o projections, antenna
- o cavities
- o outflow valves
- o impinging and deflected flows
- o disturbances convecting past trailing edges
- o wakes
- o vortices
- o base pressure fluctuations

During cruise, aircraft are operated in a "clean" configurations e.g. landing gear, flaps and control surfaces are not deployed. Thus these projecting surfaces and associated cavities need not be considered separately as cruise noise sources. Prediction methods are required for the above noise sources which will be significant contributors to the acoustic pressure environment over the airframe in the cruise condition. First these sources will be described and ranked to determine their importance.

2.3.4.1 Source Ranking - The timeframe for the LFC airplane operation is in the 1990's. Such an airframe design would incorporate all applicable aerodynamic design technology and would be aerodynamically cleaner than present day airframes. Thus, there would be no areas of separated flow and no base pressure fluctuations; shocks on wings would not oscillate; projections and cavities will be designed out and outflow valves will be low-noise and located in a non-sensitive position. Impinging and deflected flows might occur for example from LFC suction unit exhaust systems. These exhaust flows would contain comparatively little energy, however, a direct (non-impinging) type exhaust would be preferable. The noise characteristics of a discrete vortex, such as may originate from a wing tip or other structural or aerodynamic discontinuity, is not really known except that the strength of these vortices will be minimized by design.

The noise radiated by a boundary layer must be related to the fluctuating quantities (pressure and velocity) within that boundary layers. These fluctuating quantities are much lower in a laminar boundary layer - if they exist at all - than in a turbulent boundary layer. For example, a technique for identifying transition of a laminar to a turbulent boundary layer is the use of a stethoscope to monitor the increase in wall fluctuating pressure level in the vicinity of the transition location. This leads to the concluson that surface fluctuating pressures and hence radiated acoustic pressures are much lower for laminar boundary layers than turbulent boundary layers. Thus the acoustic pressure radiated by an area of laminar boundary layers is believed to be low and may be neglected; no method will be developed for its prediction.

Noise producing disturbances convecting past whole surfaces and edges can include atmospheric turbulence and surface induced turbulence. Atmospheric precipitation or insect (if insects exist at cruise altitude) impingement are not considered. The scale of the convecting turbulence relative to the surface determines whether the acoustic source is a whole surface source (large scale and lower frequency) or a localized source (small scale and higher frequencies). Small scale atmospheric "inflow" turbulence can give rise to localized "leading edge incidence fluctuation" noise. Boundary layers convecting past trailing edges, and the resultant wake, contain small scale turbulence, which give rise to "trailing edge noise." Both of these disturbances, if of a sufficiently large scale can cause "whole body" noise.

At this stage the remaining airframe noise sources requiring evaluation are:

- o whole body
- o leading edge
- o turbulent boundary layer
- o trailing edge

The location of these sources can be on the fuselage, wings, horizontal or vertical control surfaces. The boundary layer sources are distributed over areas and the edge sources are distributed along lengths.

Some light on the relative magnitudes of these remaining noise sources is presented in the analysis and experiment reported by Sharland, Reference 2-66. There the total noise radiated by an airfoil placed in a jet flow is measured. The radiated noise level depends on whether the airfoil is located in the jet potential core (low inflow turbulence "quiet") or in the fully developed part of the jet (high inflow turbulence "noisy"). Sharland estimates the above listed noise component levels (he excludes the negligable laminar boundary layer) summates them and compares the total with the experimental measured total noise. He concludes that for the conditions of high inflow turbulence the dominant noise source is either whole body or leading edge. His equation for these noise components indicates a velocity dependency of V^4v^2 where V is the mean velocity and v is the root mean square value of the incident turbulent velocity fluctuations. In the absence of inflow turbulence, this equation would indicate that the whole body and leading edge noise components are absent. For the experimental case of the airfoil being located in the potential core (reduced inflow turbulence) the whole body, leading edge and trailing edge noise components were predicted to generate similar levels. His equation for trailing edge noise indicates a V^6 dependency and that the level is independent of inflow turbulence. The trend is that if there were no inflow turbulence the whole body and leading edge components are not present and trailing edge noise would dominate. The noise component always predicted to radiate the lowest noise level was the turbulent boundary layer; the equation for this noise component has a V^6 dependency. The tests covered velocities up to 800 ft/sec. Spectra or directionally of these noise sources are not discussed.

Further discussion of whole body and leading edge noise follow.

Whole Body Noise - When overall lift and drag fluctuations, act in phase over an entire airfoil then the whole airfoil can be considered as a point noise source. The noise source would be dipole in nature, with the lift dipole act-

ing at the center of pressure, and the drag dipole in the drag direction. The overall lift and drag fluctuations could be caused by (1) the airplane moving through atmospheric turbulence, (2) wakes shed from the airfoil trailing edge, and (3) wakes from upstream surfaces or propulsion systems impinging upon or connecting close to downstream surfaces. For whole body radiation to occur the wavelength , λ , of the excitation must be greater than the airfoil chord, c, e.g., $\lambda > c$, which means that the excitation consists of large scale fluid disturbances. For a wing typical chord of 20 ft., then $\lambda > 20$ ft. At cruise conditions the speed of sound is 968 ft/sec, thus the whole body radiated frequencies would be less than 50 Hz. For vertical and horizontal control surfaces these frequencies would be higher. Based on plausible assumptions, Sharland, Reference 2-66, estimated that the total acoustic power radiated from this source as:

$$W = \frac{\pi \rho}{40 c^3} \int_{SPAN} c V^6 \left[\frac{v}{V}\right]^2 dy$$

where

W = acoustic power
ρ = ambient atmospheric density
c = blade chord
V = free stream velocity
v = r.m.s. of turbulent velocity fluctuations
and c = ambient speed of sound

Similar equations are presented by Hayden, References 2-67 and 2-68. The directionality of this noise source is that associated with a free dipole e.g., $\sin^2\phi$, where ϕ is measured from a plane normal to the axis of the force in spherical co-ordinates. The turbulence intensity v is dependent upon the turbulence source.

The principal concern with atmospheric turbulence is airplane structural response in terms of large scale structural modes, e.g., whole wings, fuselage and empennage. For detail descriptions of free atmospheric turbulence pre-

diction see Reference 2-69 and 2-70. Structural frequencies of interest are generally, up to 10 Hz. This response is important at lower altitudes where large scale turbulence of sufficient intensity exists. The wavenumber spectrum of turbulence falls off rapidly (as $f^{-5/3}$) above about 10 Hz. Further, atmospheric turbulence decreases in overall intensity with altitude. Thus, it is considered that during high altitude cruise the residual atmospheric turbulence is of too large a scale and too low an intensity to produce any significant whole body noise. Thus, acoustically the inflow air may be considered undisturbed, quiescent, and non-noise producing.

During cruise the wing (with laminar flow control over the initial 75% of chord) and empennage Reynolds numbers are high enough that the wakes are turbulent. It is considered that they do not have enough large scale power to induce whole body noise, and that their effect is local in producing trailing edge noise.

From an aircraft design aspect it is unlikely that airframe surface components will be in the aerodynamic wakes of other parts of the aircraft. However, surfaces might be in propulsion system wake, an example being a wing/flap immersed in an advanced propeller slipstream. This last case would require separate investigation and evaluation. Apart from the last case, it is not considered that noise will be generated through the whole body mechanism.

From the above considerations a prediction method for "whole-body" noise will not be derived. If later it is considered that "whole body" could in fact be an important source, the approaches and ideas described in Reference 2-66, 2-67, and 2-68 would be considered as a starting point.

As the scale of the aerodynamic excitation is reduced, so the fluctuating forces over the main part of the airfoil cancel and do not radiate. This is for the case of < C, which is for higher frequency noise. However, there is non-cancellation at the airfoil edges (leading and trailing) at these higher frequencies. Thus, whole body noise deteriorates to leading and trailing edge noise which are discussed in the following sections.

Leading-Edge Noise - Leading edges become noise sources when the scale of the external fluctuating fluid disturbances incident upon them is small compared to the dimensions of the rigid airfoil, e.g., $\lambda < C$. Then, dipole like sources exist along the leading edge. These external disturbances can be either free atmospheric turbulence, turbulence from upstream aerodynamic or propulsion wakes or turbulence generated within an adjacent turbulent boundary layers.

During cruise, the intensity of small scale freestream turbulence is expected to be so low that it will generate extremely low levels of leading edge noise. By design leading edges will not be immersed in aerodynamic propulsive wakes. For the case of an (advanced) propeller powered puller airplane, the slipstream incident upon the leading edge could be a significant noise source. However this is probably not a practical LFC airplane design configuration.

At the wing and empennage roots, the airfoil leading edges are immersed in the turbulent boundary layers, developed over adjacent fuselage surfaces. This could lead to a localized production of leading edge noise, which might have to be eventually considered.

Thus, generally there will be very low levels of leading edge noise in conventional designs and a prediction method will not be developed for leading edge noise. Should a prediction method eventually be required the basis for formulating such a scheme could be the ideas presented in References 2-66, 2-67 and 2-68.

The two remaining airframe noise sources are:

- o turbulent boundary layer and
- o trailing edge

The above noise sources, for a clean advanced technology airframe, are considered to dominate the airframe acoustic pressure environment. Near-field noise prediction methods are developed for these two sources in the following sections.

2.3.4.2 Turbulent Boundary Layer - One of the most obvious of the airframe noise sources, but one of the most difficult to quantify, is the turbulent boundary layer which covers large external surface areas of the airplane fuselage, empennage and wings - except close to the leading edges and where laminar flow control exists. The surfaces do not include edges. A method for the estimation of noise radiated away from a high subsonic turbulent boundary layer which would include spectral directivity characteristics was therefore required. A review of the literature was made to identify such a procedure.

Literature Review - The acoustics of turbulent boundary layers has received much attention in the literature. Different aspects considered are: (1) theoretical mechanism of noise generation within the boundary layer, (2) fluctuating surface pressure levels felt by the surface over which the fluid flows, (3) surface structural response to the turbulent boundary layer excitation (which is the problem of fuselage acoustic transmission), and (4) theoretical analyses and measurements of the radiation of noise away from a turbulent boundary layer into free space. Generally the theoretical investigations of the subject appear to be probing and speculative in nature, References 2-71 through 2-77, the discussion revolving around the roles of surface dipole versus volume quadrupole type (and reflected volume quadrupole) mechanisms which translates into a question of whether the velocity dependancy exponent is 6 or 8. One of the first theoretical papers, Reference 2-71, shows after extensive theoretical analysis, that no noise is radiated away from a turbulent boundary layer of infinite extent. Tam, Reference 2-72, showed that this was an erroneous conclusion, created by a mishandling of an approximation, which stated that all space is incompressible! Many authors have concluded that the radiated level of turbulent boundary layer noise is "weak", without actually evaluating what it is. Other authors neglect it on grounds which might be theoretically correct, e.g., it is small compared to edge noise or wake noise, but again without any absolute prediction of level, References 2-73, 2-75, 2-77, 2-78 and 2-79. Often the interest is for low speed far field application whereas in this study the interest is for high speed and the close-in far field. Much of the knowledge of the acoustics of the turbulent boundary layer comes from the many measurements of the fluctuating pressure level at the surface. Generally, $\sqrt{\overline{p^2}} = 0.006q$ or the amplitude of the surface fluctuating pressure is proportional to V^4. Models of radiated noise are often built

around the surface pressure term. The most useful models are those of Lighthill, Reference 2-14, Sharland, Reference 2-66, and Tam, Reference 2-72. Tams complex procedure predicts many of the parameters, however, at the lower speeds it appears to overpredict the radiated noise (based on Wilson measurements discussed later) and at the higher speeds it does not allow for quadrupole radiation. Should the wall adjacent to the turbulent boundary layer be flexible, then the panel - responding to the turbulent boundary layer excitation - may, in certain frequencies, be a more efficient acoustic radiator than the turbulent boundary layer itself. What is missing is an absolute validated, simple, prediction scheme for this noise source which yields all the desired elements (acoustic power/unit area, directionality and spectrum) leading to the prediction of acoustic spectrum at any point over a wide range of velocities.

Although during many acoustic tests, the noise radiated by a turbulent boundary layer is frequently a contributing noise component, it is rarely a dominant noise source and thus can rarely be positively identified. In the literature only two experiments are reported where direct radiated turbulent boundary layer is claimed to be the dominant source. The first was from a rotating disc, Reference 2-80, and the second was from a rotating cylinder, Reference 2-81. The data acquired during the X-21A related measurement programs, Reference 2-57, and then interpreted as boundary layer noise could possibly be noise from some other source. These experiments and results are described in the following.

The first experiment to isolate and measure the noise radiated from a turbulent boundary layer is that reported by Hubbard, Reference 2-80. The test configuration was a rotating disc, with rotational speeds up to 350 ft/sec. At a location within two boundary layer thicknesses of the disc, the mean square sound pressure increased as $(\text{velocity})^4$ whereas further away it increased as $(\text{velocity})^8$. Single point OASPL is the only reported data. In this experiment the disc edge travels at high speeds so that the radiated noise could be contaminated with some form of edge noise. Further the boundary layer is not uniform across the noise generating surface.

The second attempt to measure turbulent boundary layer alone noise is that by Wilson, Reference 2-81, and dealt with the noise of a rotating cylinder at circumferential speeds up to 350 ft/sec. In this test, close to the cylinder, the mean square sound pressure followed a $(\text{velocity})^4$ law and the total acoustic power radiated to the far field followed a $(\text{velocity})^6$ relationship. Some spectra are also presented in this report. This test configuration has less edge effect than that of Hubbard and it also has a constant surface velocity, which is the noise generating velocity.

A third attempt to measure aircraft radiated turbulent boundary layer noise in the far-field is reported and discussed in References 2-82 and 2-83. Flyover noise data was acquired from gliding T-33 and F-100 airplanes at speeds up to M = 0.8. Selected final results are presented in Reference 2-84. At the higher speeds (M = 0.48) for the T-33, the total airplane (glide) acoustic power, based on the flyover noise measurements, is deduced to vary with M to the power 8. At M = 0.8, a single F-100 point lies on the same line. However, the reported directivity is more directional than reported recently in numerous unpowered flyover noise tests. Experimental test details have not been studied, except through the Reference (which is an abstract) where there are no comments on engine power setting or flap setting at the high speed glide. These tests were reported in 1956. Non-powered flyover noise, for a clean configuration, at lower speeds, is currently considered to be dominated by wing and empennage trailing edge noise rather than radiated surface turbulent boundary layer noise. However, at that time, 1956, the above measured noise was attributed to radiation from the turbulent boundary layer. From the reported description, especially the increase in the noise radiated forward the dominant noise source could have been convectively amplified core noise at low engine power settings.

Fourthly, measurements of the noise field in close proximity to an airframe during high speed cruise was reported in References 2-84, 2-85, 2-86, and 2-87. This extensive and complex measurement program was in support of the X-21A program. The results were reported over the period of 1960 to 1967. Not all results are available. Airplane configurations were the F94-C, NB-66 and the X-21A. The data acquisition system developed was of a flush mounted

microphone installed in a laminar flow housing located external to and close to various surfaces. The intent was to prevent the microphone signal from being masked by pressure fluctuations of its own turbulent boundary layer. The objectives were to measure the close-in cruise noise environment, to source separate the measured data and to develop cruise noise prediction procedures. One of the main results of these series of tests was that, generally, at the lower flight Mach numbers and the higher engine power settings the OASPL's, at a point, decreased with increasing airplane Mach number, although there is much scatter in this data. This was interpreted as showing that propulsion noise (which was assumed to be basically jet noise) generally decreased with forward Mach number. Another principal result was that at the higher Mach numbers ($M > 0.6$) and lower engine power settings the OASPL's, at a point, generally increased with increasing Mach numbers. Again there was much scatter and the claim that the increase was proportional to Mach number to the power 8 appears to be an over simplification. However, this was interpreted as showing that, in this case, the noise was dominated by radiated turbulent boundary layer noise. This conclusion was also based on the fact that a turbulent boundary layer noise prediction method (based on previously described T-33 and F-100 far-field flyover noise tests) yielded levels which compared quite favorably with the measured levels at the higher Mach number. However, the final figure of Reference 2-100 shows measured inflight noise levels from an X-21A flight with the laminar flow control mechanism operating over the wings. Four of the microphones are adjacent to large wing areas where laminar boundary layers existed. On comparison with measured data under similar flight conditions in the presence of a turbulent boundary layer the OASPL's - within measurement tolerance - are essentially the same. This would appear to indicate that the measured noise close to the surface is not dominated by the turbulent boundary layer radiated noise, but by noise from another source. Noise sources not considered in that analysis include: (1) wing trailing edge noise, (2) engine core noise, and (3) jet shock associated broad band noise. The last two, especially when convectively amplified could be the dominant noise source at these locations at speed and not the turbulent boundary layer. In fact, the analyses of this present report would suggest exactly that. It is apparent, and very desirable, that more work be performed to more confidently define the exact noise source contributions at the X-21A measurement locations. This would be an extremely useful exercise - assuming that the basic measured data is of good quality.

In Reference 2-85, prediction procedures were proposed for the noise radiation from fuselage wakes and turbulent boundary layers. The prediction method used an equivalent jet for both sources (acoustic power $\sim V^8$). Estimates of T-33 and F-100 aircraft glide acoustic power were made and the indicated agreement, Reference 2-85, Figure 2-19 is extremely good. However, no breakdown is indicated as to the relative magnitudes of the two noise sources. Neither is any spectral data provided. The equation derived these for the OASPL from a surface area element of turbulent boundary layer, expressed in the notation and format of this report, is

$$OASPL(r,\phi) = 10 \log A + 80 \log M - 20 \log r + 10 \log f(\phi) + 139$$

There is a correction for altitude (Δ dB = 20 log $\frac{\rho_c c_c^2}{\rho_o c_o^2}$) and a forward speed co-ordinate correction, r,ϕ to r',ϕ'. The directivity is the previously mentioned measured flyover directivity, Reference 2-82. No spectral data are presented. Use of this equation for the noise radiated from a turbulent boundary layer predicts high noise levels. Further, it predicts noise levels some 18 dB greater than that the prediction method developed later in this section.

Development of Turbulent Boundary Layer Cruise Noise Prediction Procedure - Based on the survey of the literature, it would seem that a comprehensive validated prediction scheme for the direct acoustic radiation from a turbulent boundary layer, which takes into account all sources does not exist. A method was, therefore, partially, developed and is described as follows. Based on the concepts of Powell, Lighthill, and Tam, the noise radiated away from an infinite turbulent boundary layer is considered to be generated by three sources within the boundary layer, as shown in Figure 2-16, and described as follows: (1) a surface distribution of dipoles - caused by the fluctuating pressures within the flow causing fluctuating forces on the rigid surface and hence radiating noise. The strength of these dipoles can be related to the measured characteristics of the surface fluctuating pressure levels - called pseudo-sound. Noise from a surface area element is $\propto [A_i V_i^6 f(\phi_i)]/r_i^2$, (2A) a volume distribution of quadrupoles (generated by the fluctuating pressures within the turbulent boundary layers, in a manner similar to jet mixing noise)

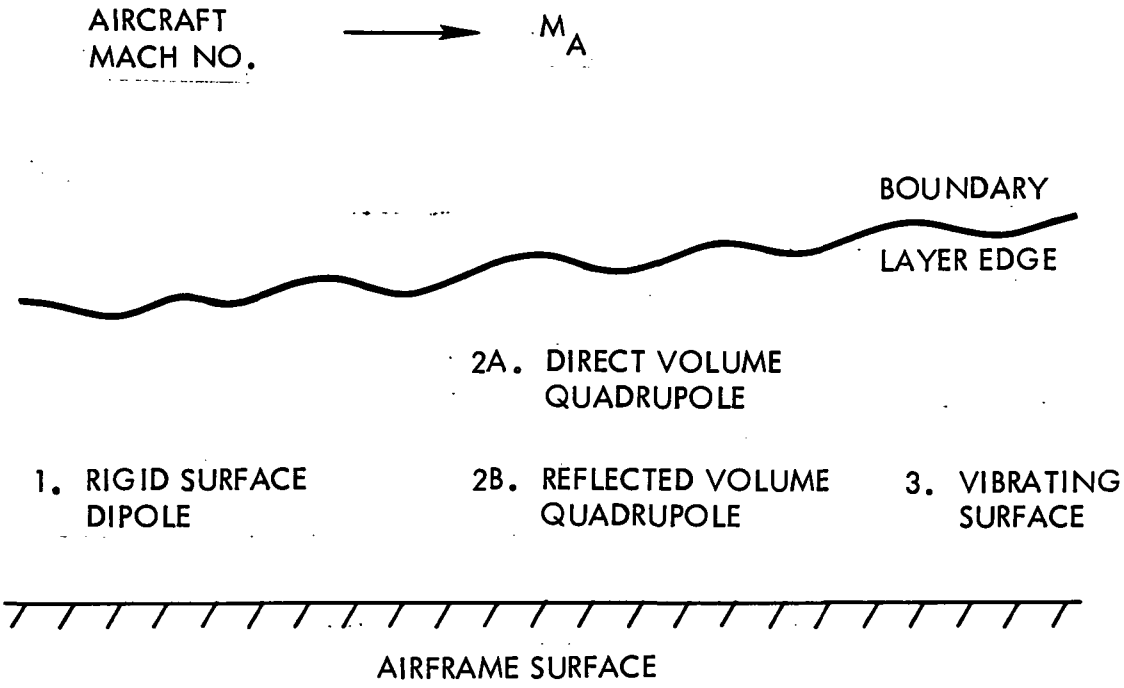

FIGURE 2-16. MECHANISMS OF TURBULENT BOUNDARY LAYER NOISE GENERATION

and (2B) reflected volume quadrupole noise. Noise from a volume element of turbulence is $\alpha[(A_i \delta_{ii}) V_i^8 f(\phi_i)]/r_i^2$, and (3) the noise radiated by the flexible surface as it responds to the turbulent boundary layer excitation. The last noise component radiates internally and externally. For conventional subsonic airplanes it can be shown that this does not represent a high acoustic power. Internal noise levels are constrained within the cabin and are modified by soundproofing. During cruise, internal overall noise levels exist close to the wall of 90 to 100 dB. This same panel motion radiates noise externally. It is less than the internal noise by 10 log $(\rho c)_{cabin}/(\rho c)_{ambient}$ (which is about 7 dB) and further it is not constrained but freely radiated. The external noise due to panel induced vibration might therefore be expected to be about 85 to 95 dB, OASPL at about 1 ft. from the fuselage.

All these noise sources are distributed over large areas and the noise is to be estimated within very close proximity to these large areas. The method therefore considers the noise radiated by an area element of the turbulent boundary layer, to a selected observer location. The total noise is obtained by computing the noise from a series of such area elements (with its own element source strength, element to observer distance and directionality) and logarithmically combining these individual spectra to yield the total spectral noise.

The noise sources originally considered in the method were the first two components e.g., the surface dipoles and the volume quadrupoles. In terms of ranking it is possible that at the lower subsonic speeds the surface dipole terms (αV^6) dominate while at the higher subsonic speeds the volume quadrupole terms (αV^8) might dominate. Where the cross over is not known, and remains a subject for further study. In the method developed here, only the surface dipole model was developed. The model was then "calibrated" against limited available test and analytical data previously described. The prediction scheme yields absolute values of OASPL, spectrum and directivity radiated from a large surface. Extension to include the volume quadrupole component is required.

(a) Overall Sound Pressure Level and Directivity - The acoustic power radiated by the surface dipole distribution in a turbulent boundary layer is assumed to have the form:

$$W = k_1 A V^6 \qquad 3\text{-}10$$

where

W is the acoustic power, watts,
A is the wetted area, ft.^{2}
V is the surface velocity, ft./sec.,
k_1 is a constant

This equation may be expressed as

$$PWL = 10 \log A + 60 \log V + K_2 \qquad 3\text{-}11$$

where PWL is the acoustic power with reference to 10^{-13} watts.

Now the radiating surface is considered the equivalent of a dipole. For a dipole the relationship between acoustic power and acoustic pressure can be shown to be:

$$PWL = OASPL_M(r) + 20 \log (r) + 5.7 \qquad 3\text{-}12$$

where $OASPL_M(r)$ is the maximum sound pressure level at radius r (ft).

Further, dipole acoustic radiation directivity is given by

$$OASPL\ (r,\phi) = OASPL_M(r) + 20 \log (\cos\phi) \qquad 3\text{-}13$$

where ϕ is measured away from the dipole axis.

Combining equations 3-11, 3-12, and 3-13 yields the acoustic sound pressure level directionality as follows

$$OASPL(r,\phi) = 10 \log A + 60 \log V - 20 \log r + 20 \log (\cos\phi) + K_3 \qquad 3\text{-}14$$

The constant of equation (5) is now determined from the experimental work of Wilson and Hubbard, and the theoretical work of Lighthill, Sharland and Tam.

(i) Value of Constant, Based on Wilson, Reference 2-81.- There it was shown, that up to a cylinder surface velocity of 350 ft/sec, that the radiated acoustic power was proportional to surface velocity to the power of 6 which suggests that the dominant radiators are of dipole type. From that data, the constant in Equation 3-11, K_2 can be shown to be -66.4 and the constant in Equation 3-14, K_3 becomes -72.1. Thus,

$$OASPL(r,\phi) = 10 \log A + 60 \log V - 20 \log r + 20 \log (\cos\phi) - 72.1 \qquad 3\text{-}15$$

(ii) Value of Constant Based on Hubbard, Reference 2-80 - Hubbards experimental results were evaluated in a similar manner to Wilson's. The single point measured acoustic pressure was assumed to be that at maximum directivity. Although the reported measured acoustic pressure increases with velocity to the power 8 it was forced to fit a V_6 type relationship. The resulting SPL relationship was

$$OASPL(r,\phi) = 10 \log A + 60 \log V - 20 \log r + 20 \log (\cos\phi) - 57.6 \qquad 3\text{-}16$$

This equation gives an OASPL which is 14.5 dB higher than that given by Equation 3-15.

(iii) Value of Constant Based on Lighthill, Reference 2-14.- Lighthill, in Equation 13 of the reference presents an equation for the mean square sound pressure produced by a unit area of turbulent boundary layer, which may be rewritten as

$$p^2(r,\phi) = 6.5 \times 10^{-10} (p^2/c^2) [(A V^6 \cos^2\phi)/r^2] \qquad 3\text{-}17$$

where

p is the acoustic pressure, lb/ft.
p is the ambient air density, slugs/ft^3
a is the ambient speed of sound
A is the area of the radiator, ft^2
V is the flow velocity, ft/sec.
ϕ is the angle to the observer location from the normal
r is the polar distance to the observer location

This equation may be re-expressed as

$$OASPL(r,\phi) = 10 \log A + 60 \log V - 20 \log r + 20 \log (\cos\phi) - 77.7 \qquad 3\text{-}18$$

This equation give an OASPL which is 5.6 dB lower than that of Equation 3-15.

(iv) Value of Constant, Based on Sharland, Reference 2-66 - Development of some of Sharland's equations and data showed that the constant in the equation should be -73.9, which is 1.8 dB lower than Equation 3-15 at -73.9.

(v) Value of Constant Based on Tam, Reference 2-72.- Application of Tam's equations showed that the constant in the equation should be 16.5 dB higher than Equation 3-15 at -55.6.

(vi) Selected Value of Constant - It is seen that there is some variation in the constant. Wilsons, Lighthill and Sharland are -72.1, -77.7 and -73.9, respectively. Hubbard and Tam's are -57.6 and -55.6, respectively. Because it is based on test measurements from what is considered the best test configuration, it is proposed to use the constant based on Wilson's results, e.g.,

$$OASPL(r,\phi) = 10 \log A + 60 \log V - 20 \log r + 20 \log (\cos\phi) \quad -72.1 \quad 3\text{-}19$$

The above derivation assumes that the noise radiated away from a turbulent boundary layer has the characteristics of a dipole, and that it can be related to the fluctuating pressure level induced on the surface by the turbulence within the boundary layer. This is the approach considered by Lighthill, Sharland, Tam and Maestrello. Powell considers that the quadrupole noise arising from the turbulence alone within the boundary layer could be an important contributor to the noise radiated away from the boundary layer, especially at high speeds. This would mean that in addition to the surface dipole noise of Equation (10) a volume quadrupole noise would exist. Formulation of this component requires knowledge of the turbulent structure within the boundary layer. Development of the scheme to predict absolute noise levels and directivities would then require comparison with the acoustic power output of a volume element of turbulence. This could be estimated by comparison with noise radiation and turbulence characteristics of a subsonic circular jet. The effect is recommended as a program follow-on item.

(b) Peak Frequency - Throughout the literature there is even less reference to the spectral peak frequency or spectrum shape of radiated turbulent boundary layer noise, the discussion is generally limited to an overall type sound pressure level. The only specific information on the peak frequency of radiated turbulent boundary layer noise are the computed data of Tam, Reference 2-72, and the measured data of Wilson, Reference 2-81. Both indicated the broad band nature of the spectrum. The peak frequency of the radiated acoustic pressure spectrum is taken from the work of Tam.

FIGURE NUMBER

ILLUSTRATION TITLE

Tams computations indicate that the peak frequency has some small sensitivity to directionality and flow Mach number, generally, however, the peak frequency, of the spectrum is given for flow Mach numbers to 0.8, (Reference 2-72, Figure 3, 6, and 7) by:

$$S_n = \omega\delta^*/V = 0.055 \qquad 3\text{-}20$$

where

S_n = Strouhal number
ω = circular frequency
δ^* = boundary layer displacement thickness, ft.
V = flow velocity, ft/sec.

This equation can be re-expressed as

$$f_p = 0.00875 \; V/\delta^* \qquad 3\text{-}21$$

where f_p = peak frequency in Hz.

This equation estimates the peak frequency as measured by Wilson, quite reasonably. Therefore, the above equation of Tam is used directly. The peak frequency is for a spectral distribution. The radiated peak frequencies are inversely proportional to boundary layer thickness. Hence, the higher frequency noise is radiated by the thinner boundary layers.

(c) Spectral Shapes - The only specific data available in the literature concerning the spectrum of radiated turbulent boundary layer noise are again the measured data of Wilson, and the computed data of Tam. Both spectra have broad band characteristics and have similar peak frequencies. However, the shapes are different. To aid in the selection, of one of these shapes, these spectra were compared to another known aerodynamic noise spectrum shape. This was jet-mixing noise. Wilson's shape was chosen because it fell off at a higher rate at the higher frequencies than Tams and was closer to the

FIGURE NUMBER

jet-mixing spectrum shape. The selected non-dimensional shape, (in one-third octave band levels) with the slope definitions is shown in Figure 2-17.

ILLUSTRATION TITLE

(d) Total Noise from an Area - Computation of the OASPL radiated by a large area of turbulent boundary layer to a specified point in space is achieved by considering the boundary layer as a series of area elements, A_i. If the point in space is defined by r_i, ϕ_i from the center of each element then the total OASPL is obtained by summation of each individual element OASPL radiated to that point, e.g.,

$$OASPL_{TOT} = \sum_i OASPL_i(r_i, \phi_i) \qquad 3\text{-}22$$

Similarly the spectrum at a point is obtained by computing the spectra from each element and logarithmically adding the element spectra.

(e) Transformations to Cruise Conditions - The basic prediction is for conditions of sea level and low speed. Transformation to cruise conditions must include: cruise operating conditions, acoustic impedance, co-ordinate transformation, convective effect and the dynamic effect.

Example of Turbulent Boundary Layer Noise Computation - Figure 2-18 shows the computed free-field OASPL radiated by a large length of fuselage, as a function of distance normal to the fuselage, at the cruise conditions shown. The fuselage length was approximated by five large flat element areas.

2.3.4.3 Trailing Edge - During cruise, wing and empennage control surfaces are not deployed, thus the wing, horizontal and vertical surfaces may be considered as streamlined or "clean" airfoils which are immersed in a non-turbulent high-speed flow.

Model airfoils immersed in clean (non-turbulent) air flows have been shown, theoretically and experimentally, to be a source of noise. As previously described, the dominant noise component is considered to be the trailing-edge

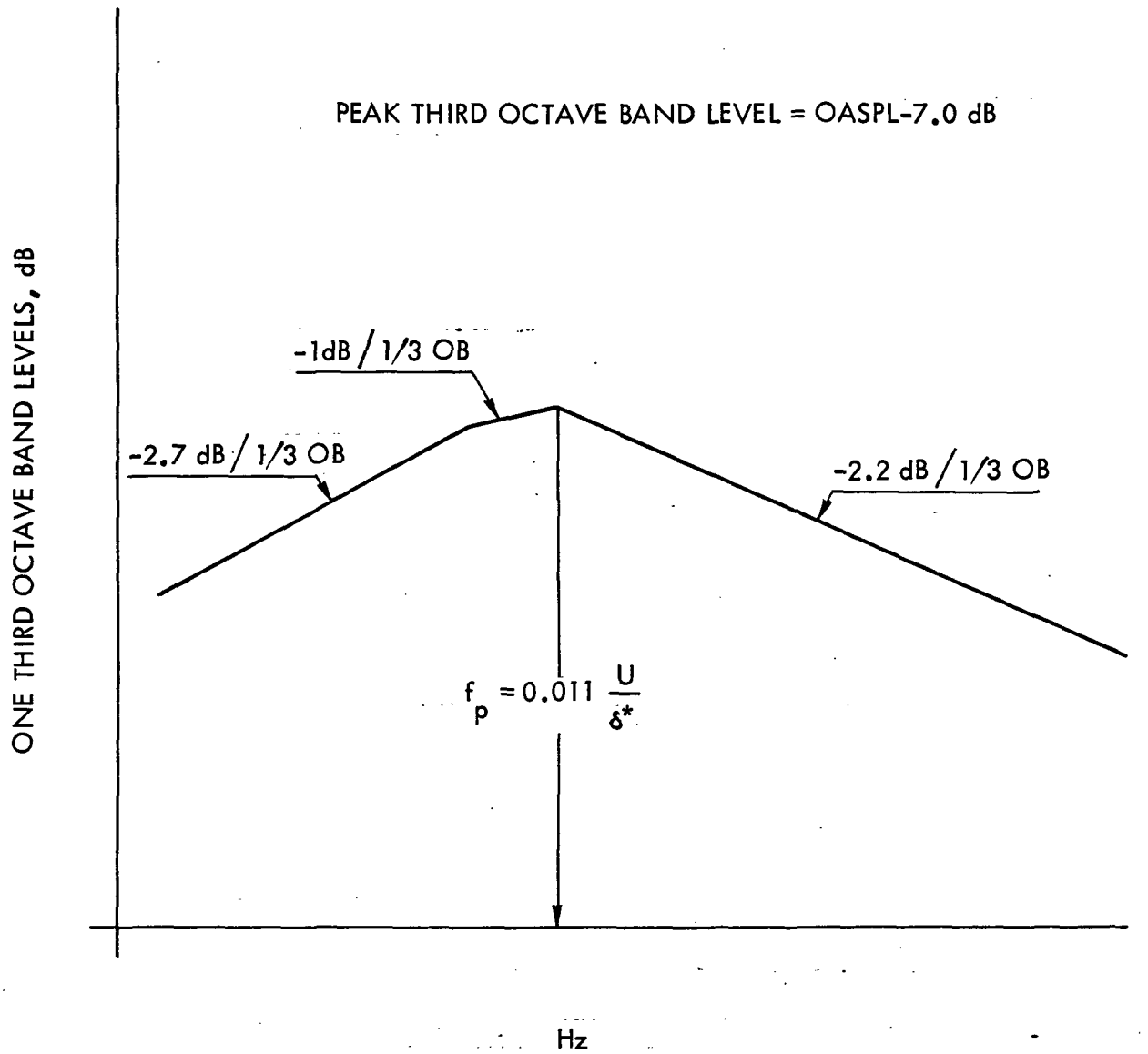

FIGURE 2-17. RADIATED TURBULENT BOUNDARY LAYER NOISE SPECTRUM

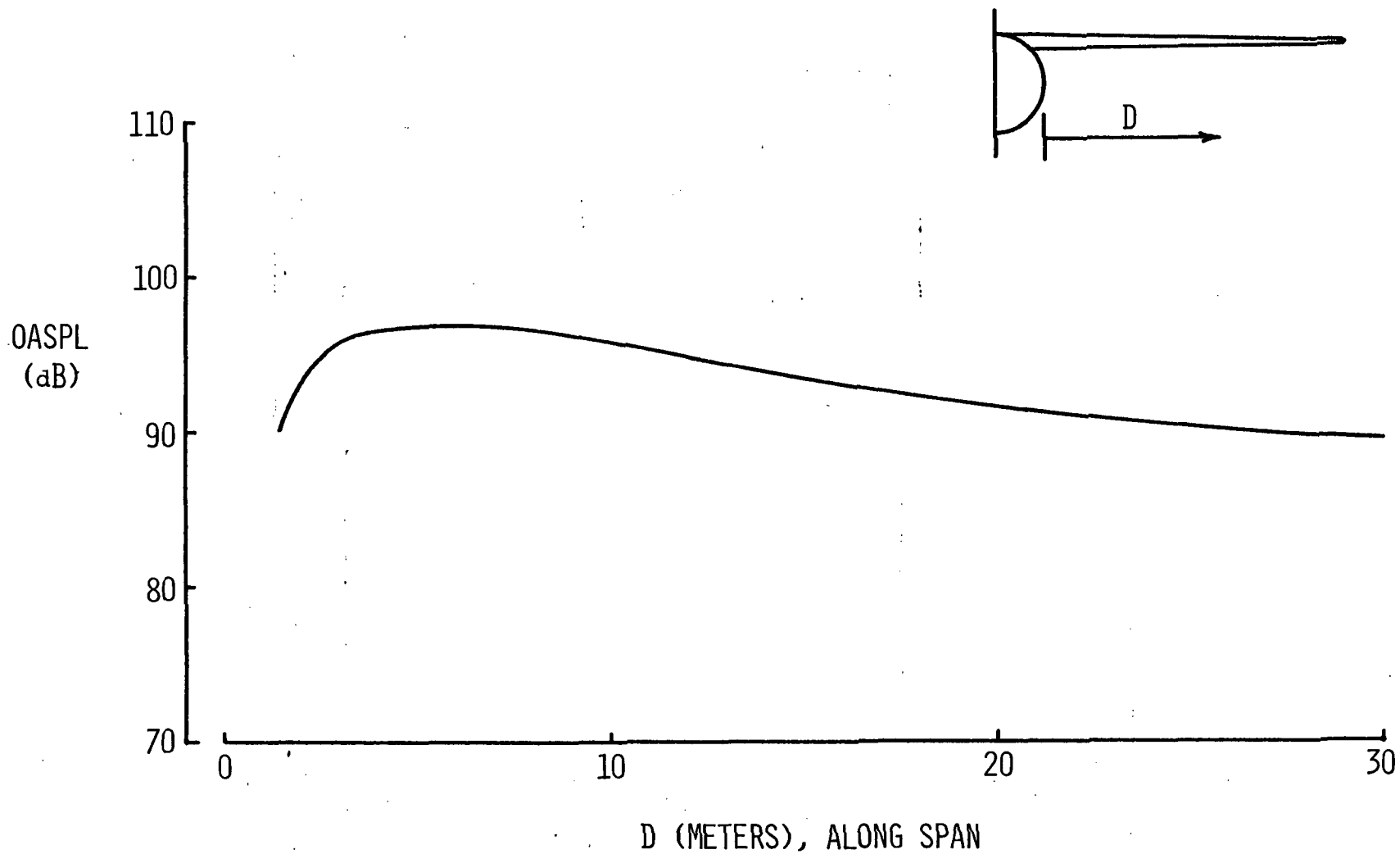

FIGURE 2-18. FUSELAGE RADIATED TURBULENT BOUNDARY LAYER, CRUISE

noise. In the generation of trailing-edge noise the participating elements are the boundary layers - whether laminar or turbulent - from both surface sides, the trailing edge and the resulting wake. The noise generation mechanism is considered to be the boundary layers which in convecting past the surface trailing edge adjust themselves to the sudden change in impedance environment, releasing pressure waves which give rise to acoustic radiation. The acoustic radiation is described analytically in Reference 2-88. Trailing edge noise, at lower aircraft speeds, with turbulent boundary layers, has been shown to be dipolish in nature, and to have a velocity exponent dependancy of between 5 and 6.

Recently much attention has been focussed on the far-field noise radiated by large airframes (comprising fuselage and lifting surfaces) which is in addition to that radiated by the propulsion system. The state of the art of airframe noise was recently reviewed in References 2-78 and 2-89 and 2-90. For a clean airframe, (flaps up, gear up and wheel well doors closed) it has been generally concluded that the dominant noise source again is the trailing edge, with contributions from wing, vertical and horizontal surfaces. Turbulent boundary layer noise radiated from the whole airplane to the far-field was considered to be comparitively low and neglected. Three methods have been proposed to predict far-field, clean, airframe noise. Reference 2-89 describes the "total aircraft" method and the "drag element" methods which are part of NASA's Aircraft Noise Prediction Program (ANOPP). References 2-78 and 2-90 discuss these methods and their ability to predict measured (clean) airframe noise. In these references, the author, M. R. Fink, develops an alternate prediction method which, he shows, yields improved predictions of clean airframe far-field overall noise levels and their spectrum shapes than do the previous methods. For the jet aircraft considered, turbulent boundary layers existed at the trailing edges. Separate contributions from the different surfaces (trailing edges) are considered. It is this method which is developed here for the prediction of trailing-edge overall sound pressure levels, spectrum levels and directionality in the near field. The method is applicable to surfaces which have turbulent boundary layers at their trailing edges. Laminar flow control surfaces, which would have partial laminar flow control (extending to typically 60 to 80% of chord) will have turbulent boundary layers at their trailing edges but with a modi- fied boundary layer

thickness replacing the natural turbulent boundary layer thickness. However, should a laminar boundary layer exist at the trailing edge, a different phenomena - wing singing would occur. A prediction methodology would need to be developed for this situation. For the turbulent boundary layer situation, first the basic equations of References 2-78 and 2-90 are reviewed, then they are developed for application to the prediction of the near-acoustic-field.

Review of Clean Airframe Equations (Far-Field) - The noise prediction equations used here are taken from References 2-98 and 2-90. They have been derived from aircraft (airframe) flyover noise measurements (with propulsion noise extracted) at altitudes of 300 to 500 feet and at aircraft speeds up to 350 knots (most at about 200 knots). The data have been normalized to reference conditions. The equations are thus far field equations. Further, the airframes are low-noise airframes. The 1990 LFC airframe is assumed to be in this category.

(a) Overall Sound Pressure Level and Directivity - Taken from Reference 2-78, Equation 4 and Reference 2-90, Equation 10. Based on communication with the author, the constant is 101.3. The equation for overall sound pressure level and its directivity

$$OASPL = 50 \log(V/100 \text{ kt}) + 10 \log(\delta b/h^2) + 10(\cos\gamma \sin\xi \cos\phi/2)^2 + 101.3 \text{ dB} \qquad 3\text{-}23$$

This OASPL includes effect of ground reflection. To obtain free-field predictions a value of 3 dB should be subtracted from this equation. The notation is summarized below and in Figure 2-19.

δ = wing (horizontal or vertical tail) turbulent boundary layer thickness at the trailing edge

b = wing (horizontal or vertical), tail span

h = altitude, measured from trailing edge, and $h = r \sin\xi$

V = flight velocity, true air speed

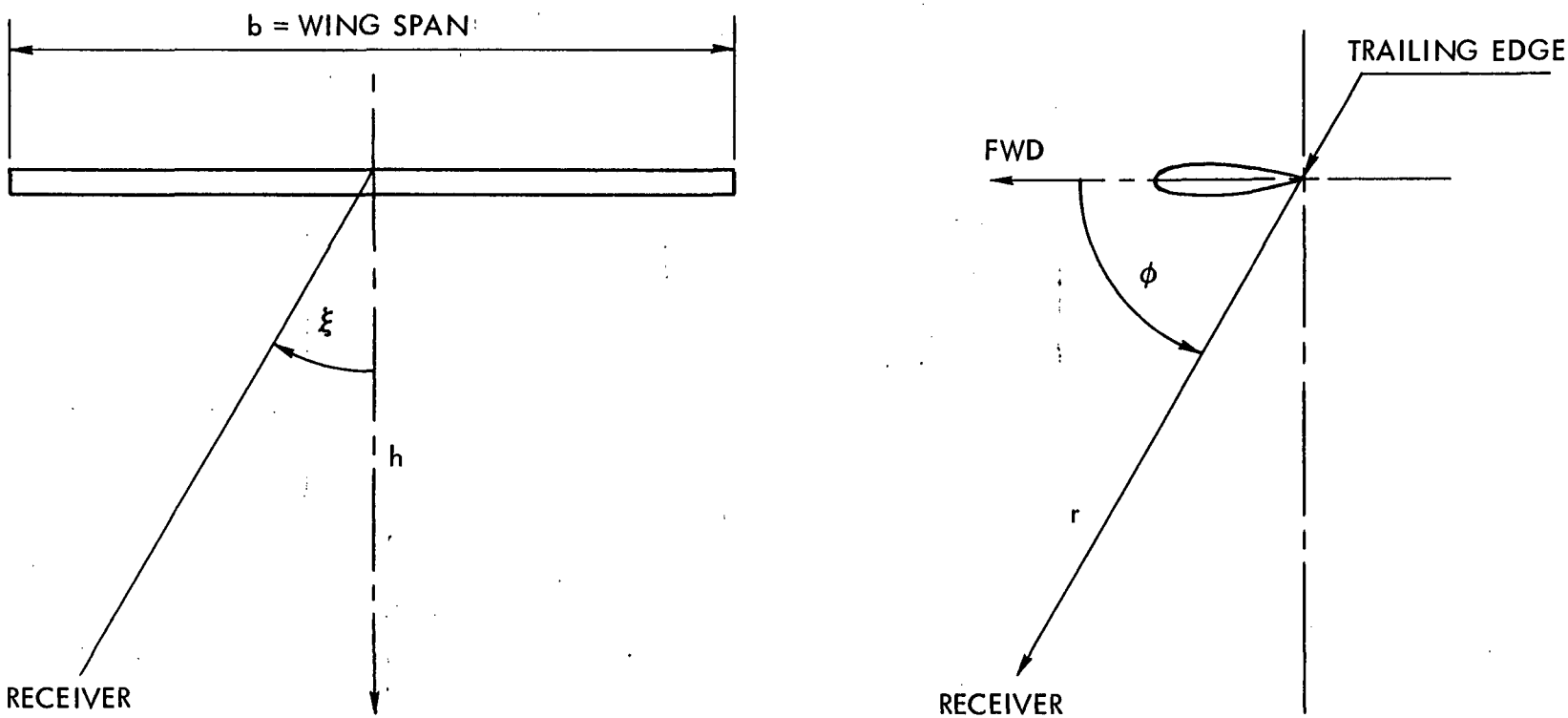

FIGURE 2-19. AIRFRAME NOISE TERMINOLOGY

ϕ = angle measured forward from trailing edge, directly forward = 0°, directly aft = 180°

ξ = sideline angle from trailing edge

and

$$\delta = 0.37\ (S/b)\ (V\ S/b\ 1/\nu)^{-0.2} = 0.37\ C\ (VC/\nu)^{-0.2} \qquad 3\text{-}24$$

C = mean aerodynamic chord = S/b

S = gross area of wing, horizontal or vertical tail

ν = kinematic viscosity

In the equation, the $\cos^2 \phi/2$ directionality term represents directionality in the flyover plane. Trailing edge noise is modeled after a dipole whose axis is normal to the trailing edge. A free dipole has a $\sin^2 \phi$ directionality where ϕ is measured normal to the dipole axis. However, when the dipole is located at the wing trailing edge (which can be represented by a semi-infinite plane or baffle) the directionality is considered to be modified by the $\cos^2 \phi/2$ and the dipole becomes a "half baffled dipole". This modeling is common to References 2-66, 2-67, and 2-68. Its importance lies in the change in angle of maximum noise radiation from $\phi = 90^\circ$ (along the axis of the dipole) to $\phi = 0$, which is forward along the baffle (or wing). Thus, trailing edge noise will be most directly felt by the generating surface rather than adjacent surfaces.

(b) Peak Frequency - The acoustic spectrum for trailing edge noise, with a turbulent boundary layer, has a broad band shape. The peak frequency is given by Equation 7 of Reference 2-78 and is

$$f = 0.1\ V/\delta \text{ Hz} \qquad 3\text{-}25$$

(c) Spectrum Shape - The normalized one-third octave band spectrum shape is taken from Reference 2-78, Equation (5) and Reference 2-90, Equation (7), and includes the 0.613 factor. The third-octave band sound pressure level, relative to the Equation 3-23 overall sound pressure level, at center frequency f relative to the peak frequency f_p is obtained from

$$SPL_{1/3}(f) - OASPL = 10 \log 0.613 \left\{ (f/f_p)^4 \left| (f/f_p)^{3/2} + 0.5 \right|^{-4} \right\} \qquad 3\text{-}26$$

This 1/3 octave band spectrum is, broad band and non-directional, i.e., independent of angle and is related to the OASPL only. The high frequency atomospheric attenuation terms of References 2-78 and 2-90 based on sea level condition of temperature and humidity are omitted because of the small distance considered.

Conversion to spectral levels, SL, from one-third octave band levels are obtained by

$$SL_i = 1/3\ OBL_i - 10 \log (\Delta f)_i$$

(d) Noise Source Location - The source location of the trailing-edge noise probably includes the trailing edge and some of the mixing region downstream of the trailing edge and thus is more properly a volume source, see for example Reference 2-91. The noise source location, too, is probably frequency dependent. Because of lack of definitive trailing edge noise source location data, the source location will be treated as being at the appropriate trailing edge. In the plane of the wing it is thus a line source along the trailing edge extending over the span of the wing.

Development of trailing-Edge Cruise Noise Prediction Procedures - The above equations are developed for application to small source to observer distances and for cruise conditions.

(a) Overall Sound Pressure Level and Directivity - First, equation (1) is converted to free field conditions by subtracting 3 dB from the constant and secondly, h is replaced by $r/\sin\phi$. Then

$$OASPL = 50 \log(V/100 \text{ kt}) + 10 \log(\delta b/r^2) + 10 \log(\cos\xi \cos\phi/2)^2 + 98.3 \qquad 3\text{-}27$$

Equation (5) considers the trailing-edge noise behaving as a point source and is thus applicable for predictions in the true far-field where the inverse square law holds. At smaller distances trailing-edge noise may be regarded as a finite line source, extending along the span of the wing - or other surface - and, to a good approximation, being of constant strength. It may also be regarded as being a distribution of uncorrelated sources. Reference 2-11 shows that the limit on the use of the inverse square law in this situation is limited to source to observer distances, r, greater than the span divided by π, $(r > b/\pi)$. For closer in distances $(r < b/\pi)$ the situation exists, as shown in Figure 2-20; the effect of the finite length of the line source must be considered. This region may be called the "close-in" far field. In this region, because of the finite size of the radiator, the noise drops off at 3 dB/doubling of distance. Thus, it is necessary to convert Equation (5) into the more general form which allows for propagation in the far field and the close-in far field. This is achieved, following the formulation of Reference 2-11, by replacing the $1/r^2$ in Equation (1) by $\alpha_2 - \alpha_1/rb$ Thus, the OASPL directivity equation at small distances from the trailing edge becomes.

$$OASPL = 50 \log(V/100 \text{ kt}) + 10 \log(\delta(\alpha_2 - \alpha_1)/r) + 10 \log(\cos\xi \cos\phi/2)^2 + 98.3 \text{ dB} \qquad 3\text{-}28$$

where α_2 and α_1 are the angles subtended to the observer by the ends of the line source, see Figure 2-21, and b is the "local" noise

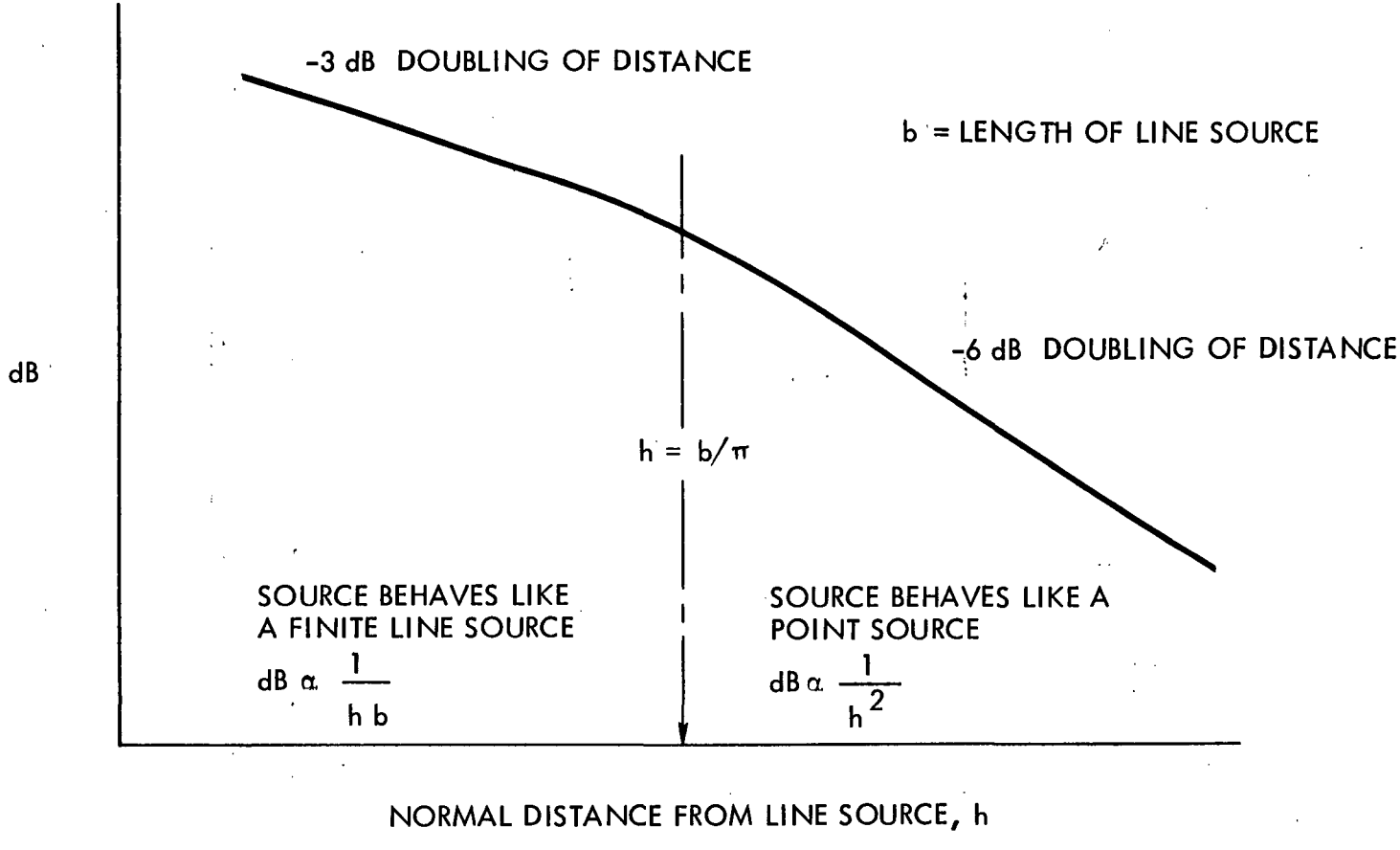

FIGURE 2-20. ACOUSTIC PROPAGATION FROM TRAILING EDGE

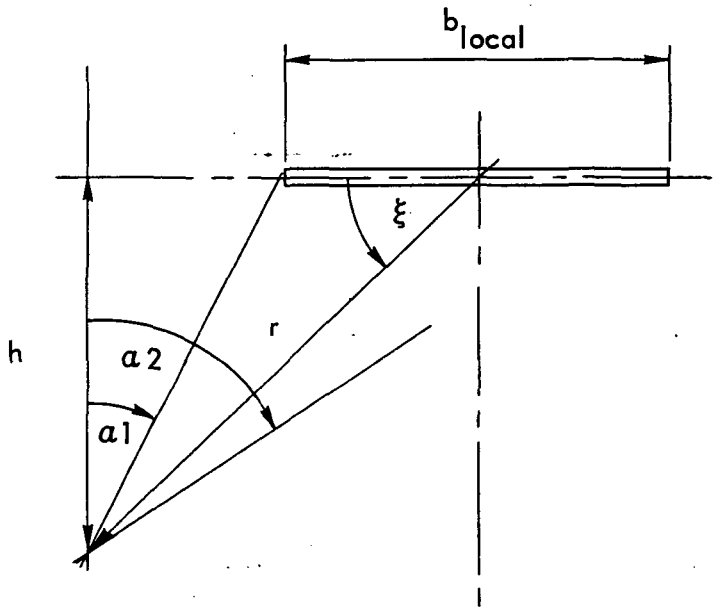

FIGURE 2-21. TRAILING EDGE NOISE TERMINOLOGY

generating span. Thus, for a wing and a horizontal a semi-span should be used while for the vertical the full span should be used.

During cruise, the LFC system would probably be operating on the wing and empennage surfaes. For example, the wing could have LFC on the upper and lower surfaces to about 75% chord. The empennage could have LFC, typically to 65% on both surfaces. At the end of the LFC surface, the laminar boundary layer will transition into a turbulent boundary layer. Trailing-edge noise is predicted on turbulent boundary layer characteristics at the trailing edge. The resulting noise will have broad band characteristics. For a conventional airfoil the use of flat plate boundary layer thickness as opposed to airfoil boundary layer thickness is discussed in Reference 2-78. There, Fink concludes that for low-speed conditions the effect of lift coefficient on boundary layer thickness can be neglected. Whether this is true for high-speed cruise applicationis not known at this time. For application to surfaces with LFC, the boundary layer thickness at the trailing edge, in the presence of LFC operation, should be used.

If the boundary layer at the trailing edge should be laminar (i.e., low Reynolds numbers, much less than 1×10^6, more typical of model data and for small high performance sail planes), then strong discrete frequencies will occur in the spectrum, Reference 2-92. This phenomenon, often known at "wing singing", is not expected to occur on LFC airplanes considered in this study. Should it occur, an additional prediction method would need to be developed.

(b) Peak Frequency - The peak frequency is predicted using Equation 3-25 with the appropriate boundary layer thickness, δ, at the trailing edge.

(c) Spectrum Shape - The spectrum shape is predicted using Equation 3-26.

(d) Noise Source Location - The noise source is assumed to be uniformly distributed along the span of the appropriate trailing edge. However, the noise radiation characteristics of each trailing edge (wing or empennage) are predicted using the parameters appropriate to each edge.

(e) Wing Sweep Angle - The equations do not indicate any sensitivity to sweep angle. Many airplane surfaces have some trailing edge sweep. This effect is considered small and is neglected.

(f) Control Surface Deflection - Small deflections of wing control surfaces may occur during cruise for trim and gust alleviation purposes. The trailing edge noise is sensitive to flap deflection as shown in Reference 2-93. There for the VC-10 airplane flap deflections of 20°, 35° and 45° are reported to generate OASPL increments (relative to the clean configuration) of +4.5, +7.5 and +9.5 dB. The VC-10 has very large area flaps and large flap deflec- tions compared to those considered for trim control. However, if necessary this reference (and others) could form a basis to determine the sensitivity of a noise increment due to a flap (of given area) deflection.

(g) Transformations - The applicable transonic transformations are: forward speed transformation (r, ϕ to r', ϕ'), acoustic impedance, convective effect and dynamic effect. The roles of convective effect and dynamic effect on this noise source are questionable. The original data were acquired under the conditions of airplane (= noise source) forward speed, and if convective amplification is applicable to this noise source (which is questioned in Reference 2-78) the original data need to be normalized for this effect.

The trailing edge OASPL is related to velocity exponent to the power 5. Should, at the higher aircraft speeds the wake noise component of the trailing edge noise become more dominant then trailing edge noise could become proportional to a higher velocity exponent.

Application of method estimation of trailing edge noise at this time should be probably limited to $\xi = 0$. This would yield a fairly uniform distribution of noise level and spectra along the wing leading edge.

Example of Trailing-Edge Noise Computation - Computed trailing-edge OASPLM's for a large airplane (TOGW = 566,961 lb.) are shown in Figure 2-22 as a function of distance from the trailing edge for $\phi = 0^{\circ}$. The only transonic transformation included in this example is the c effect. The lower two lines refer to the approach case (original equations); the single upper line refers to the cruise prediction. Cruise noise levels are some 15 dB higher than on approach. This is basically because of the OASPL $\propto V^5$ relationship. The influence of the trailing edge being a point source versus a line source (at distances $r < b/\pi$) can be seen. These levels would be the same for the upper surface and the lower surface.

Comparative third octave band spectra are shown in Figure 2-23. During cruise the influence of the higher speed is apparent not only in the levels but in the upward shift in frequency. The directivity of the radiated noise is that of a half-baffled dipole type based on the trailing edge radiating preferentially forward along the generating surface.

A further example is shown in Figure 2-24. This shows how the free field OASPL varies on a percentage of wing chord for the above airplane during cruise, with all transformations applied. A spectrum at a central span location is shown in Section 2.6.

2.3.5 Laminar Flow Control Noise Sources

A laminar flow control system which is currently considered representative for application to the 1990 type airplane is shown in Figure 2-25. The system, which would operate during cruise only, basically consists of a suction unit (a power generator and a suction pump) and the duct system. The actual configuration e.g., numbers, size and location of the suction units and the extent and distribution of the ducting system would depend on the airplane design. The basic elements of a flow control system design are as follows:

a. Power generators (which could consist of an inlet, compressor, combustion chambers, turbine, drive shaft and external exhaust) to drive the suction pumps. For a large long range airplane, for example the sys-

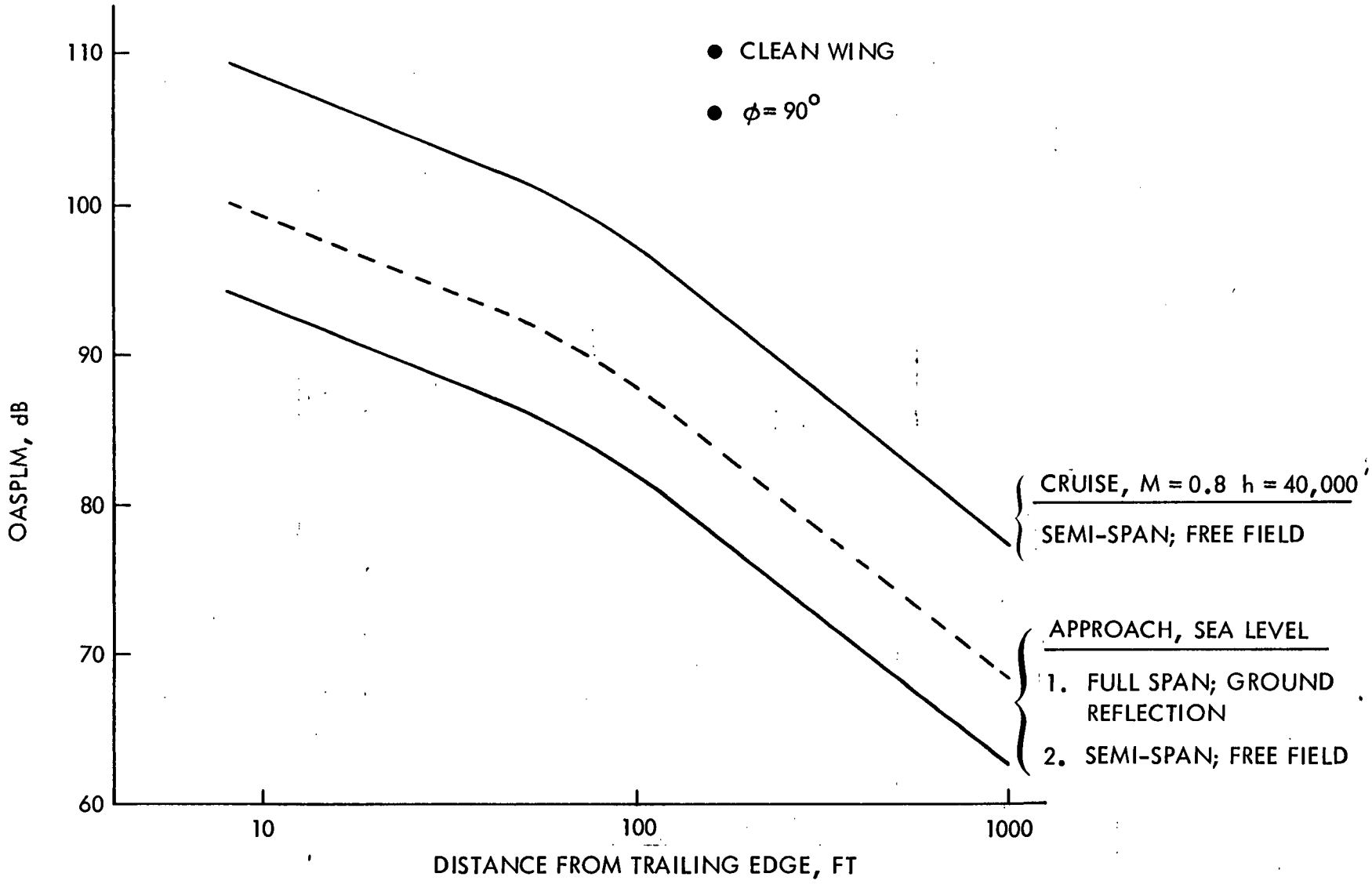

FIGURE 2-22. WING TRAILING EDGE NOISE, OASPLM

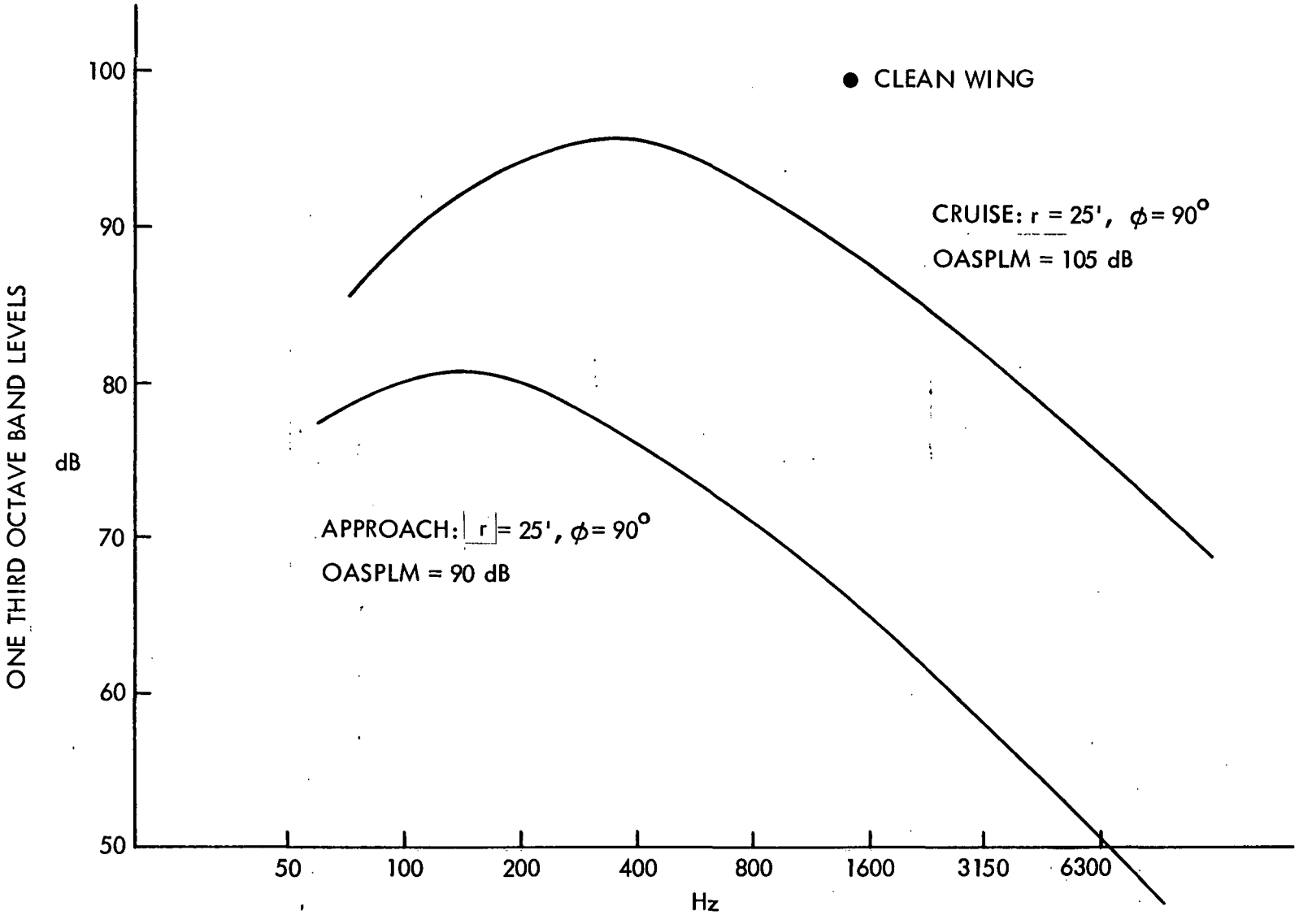

FIGURE 2-23. WING TRAILING EDGE NOISE SPECTRUM

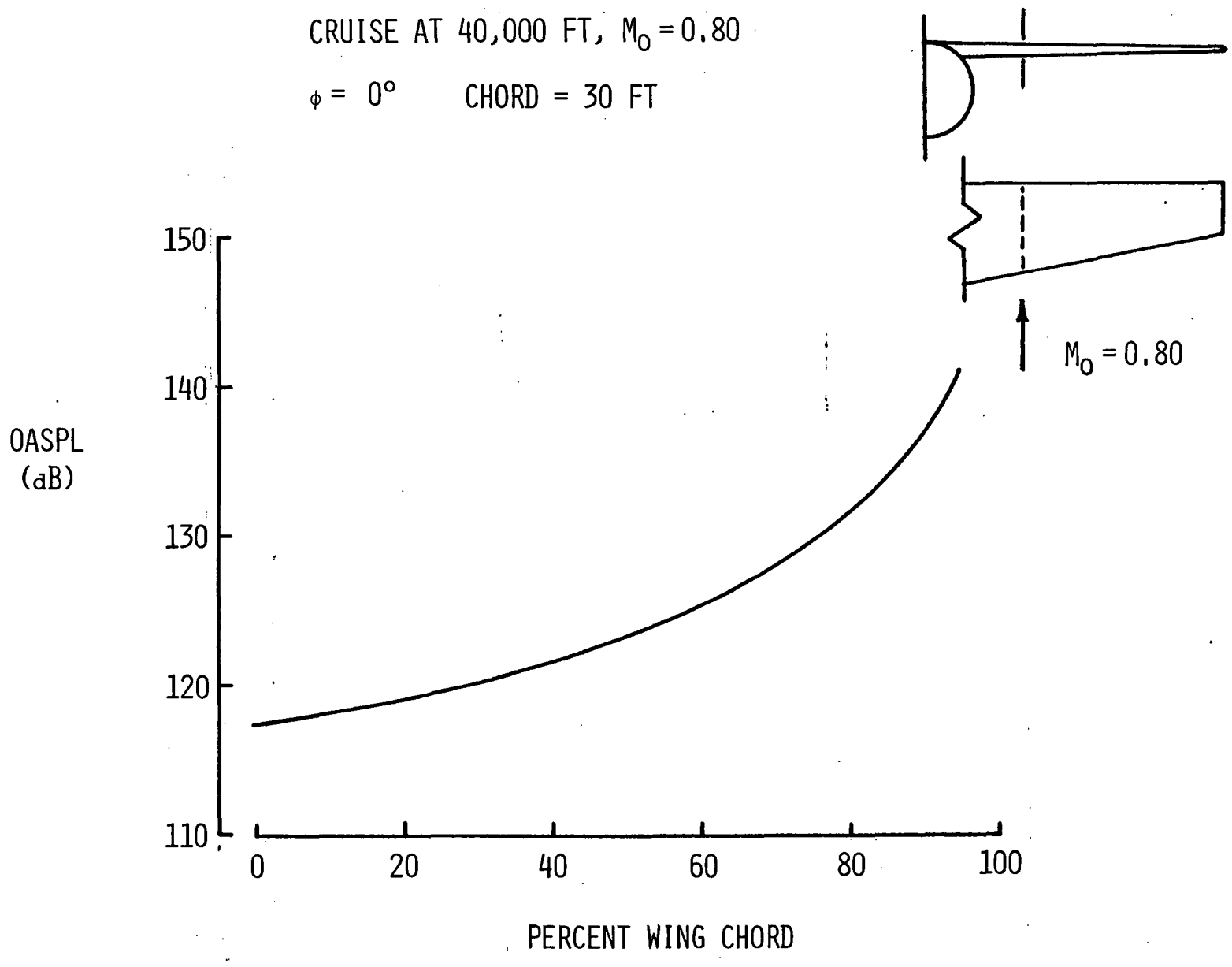

FIGURE 2-24. WING TRAILING EDGE NOISE, OASPL

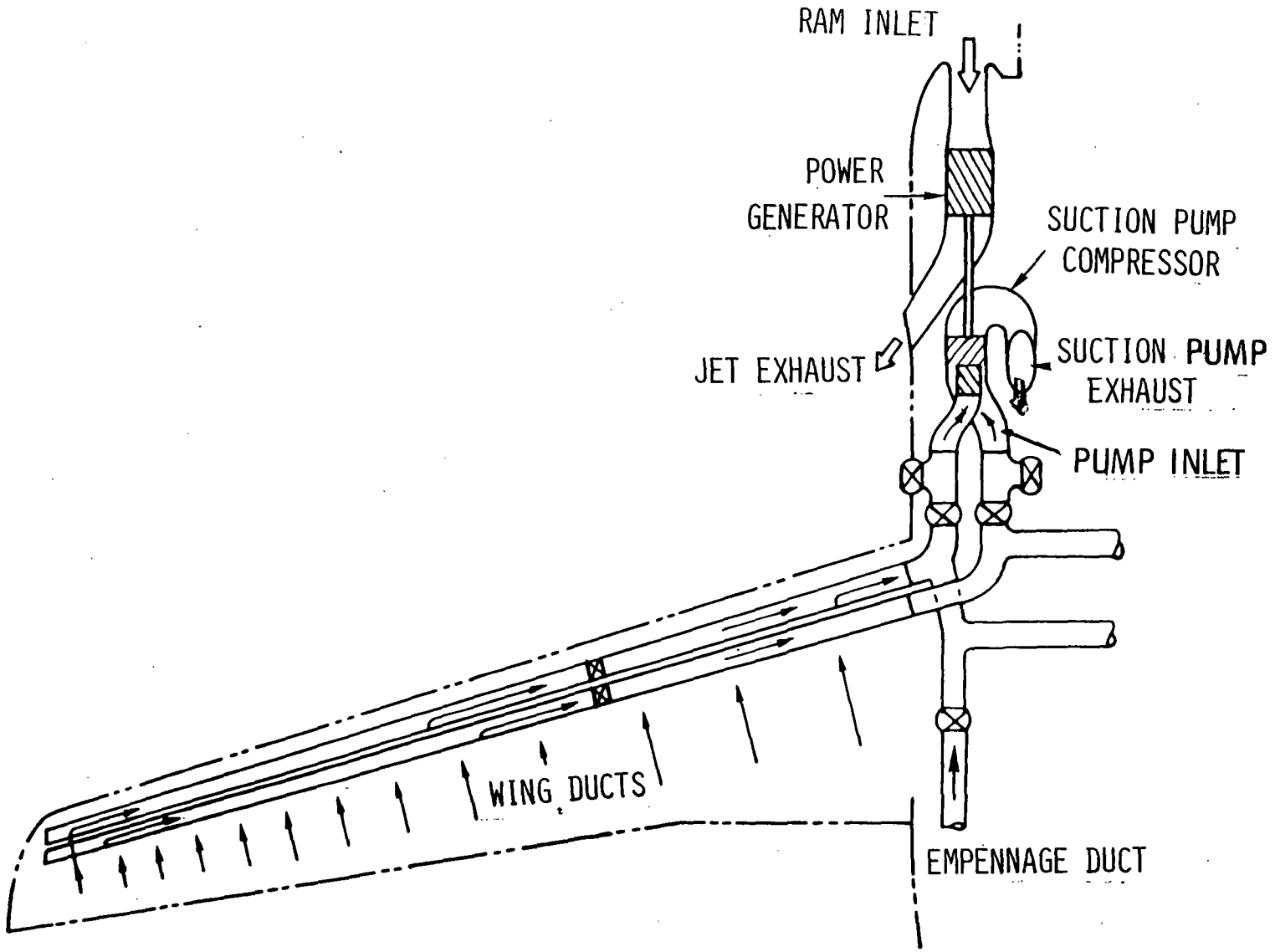

FIGURE 2-25. TYPICAL FLOW CONTROL SYSTEM AND NOISE SOURCES

tem might require two of these generators each being between 1,000 and 2,000 horsepower each.

b. Suction pumps (which could consist of a drive shaft, a compressor with the inlet facing into the duct and an external exhaust).

c. Suction duct system (with associated air flows, bends, junctions, valves, spoilers, etc.). Typical duct flow Mach numbers during LFC operation may be between 0.1 and 0.3.

d. Surface suction (which could be either discrete suction through slots or a distributed suction) and a plenum chamber system. For a slot design, the slots could be typically 0.010" wide spreading in the spanwise direction at about 10" spacing. Typical flow velocities in the slot are estimated to be between 50 and 150 ft/sec. Slot design Reynolds numbers (based on slot width) would be, typically, between 35 and 100. LFC surfaces would be primarily on the wings and empennage, but could be on the fuselage as well.

The above system components can be sources of (1) external noise, which is noise radiated through the atmosphere to the airframe surface, (2) internal noise which is noise propagated through or generated in the ducting and incident upon the flow control inner surface and producing a disturbance in the boundary layer, and (3) suction slot wake instabilities, which can produce a disturbance in the boundary layer.

2.3.5.1 External Noise Sources - Sources contributing to the external noise environment are compressors, combustors, and turbines radiating from the appropriate inlet and discharge ducts and the jet effluxes themselves. Cruise noise prediction methods for these sources would be those described in the Propulsion Noise Source section, 2.3.3, together with all the applicable transformations (to allow for forward speed and altitude). Should acoustic liner treatment be installed then its suppression capability on the appropriate noise source would be estimated from the Duct Acoustic Treatment section. The actual cycles of the suction unit system components are not yet specified and since the noise prediction methods are semi-empirical they are

somewhat configuration dependent. Thus, the direct application of the propulsion prediction methods to these similar sources would require some care.

The rotating machinery would probably operate at high speeds and consequently give rise to high frequency tones and whines, e.g., 5,000 Hz. Since the inlet and discharge ducts would be small, all the noise sources could be regarded as point sources radiating from those locations. Both the power generator jet exhaust and the suction jet exhaust would be operating at nozzle exit pressure ratios only high enough to discharge the exhaust, thus the only jet noise component present will be jet mixing noise. Although the suction unit may be physically smaller, less powerful and create less acoustic power than the propulsion system, it could be located close to an LFC surface thus requiring a full acoustical evaluation.

2.3.5.2 Internal Noise Sources - The way that internal noise can effect the boundary layer is by it being the origin of a fluctuating velocity disturbance introduced into the boundary layer at the suction slot.

These noise sources are constrained within the duct geometry and thus are not dependent upon aircraft forward speed nor are they subject to any of the forward speed transformations. The high altitude (ρc) effects are present however. Noise sources contributing to the internal duct sound pressure levels are :

a. The suction pump compressor, the acoustic power of the compressor can be predicted using the fan/compressor noise prediction procedure of 2.3.3.1, with the turbulent inflow factor. The compressor acoustic power is then shared by the ducts and propagates upstream through a complex hardwall duct geometry. Although much work has been accomplished recently in the field of noise propagation in ducts in the presence of flow (for application to turbofan noise control), for example see Reference 2-94, application of these sophisticated methods to a much more complex duct geometry would be extremely difficult. Also, prediction of the noise levels arriving at the plenum chamber, using techniques such as those discussed in standard text books, e.g., References 2-95, 2-96 and 2-97, would have a wide prediction toler-

ance. Control of these noise sources can be readily out by conventional acoustic liner techniques.

b. The noise generated by the cold low density turbulent airflow in the duct and its interaction with bends, junctions, valves and flow control devices, etc. Typical duct flow Mach numbers, M, are expected to be within the range of 0.1 to 0.3. The strength of these noise sources is related to M^6 or M^8. The low duct flows are, therefore, believed to be inherently low-noise for example, no noisy choked flow exists in the duct system. Reference 2-98, for example, reports noise levels in a duct system with flow Mach numbers up to 0.6, of up to 125 dB. Prediction of these effects is complex and difficult to generalize.

c. Noise level amplifications due to standing waves and resonances. These effects are very configuration oriented and again difficult to generalize.

In order to quantify the severity of the above three disturbance sources, a review was made of the X-21A internal noise level investigations. Faced with similar assessment of the impact of internal noise, Northrop embarked upon an elaborate test program encompassing wind tunnels, laboratory tests and a full scale X-21A flight test program. The results are summarized as follows:

a. Wind tunnel tests, References 2-99, 2-100, and 2-101. Tests were conducted on a laminar flow suction wing (10 foot chord, 7 foot span and 33° sweep) in the presence of a suction controlled laminar boundary layer. Noise, in addition to the ambient duct noise, was introduced into the duct system. These tests showed that premature transition could be induced depending upon the sound pressure level, the frequency and the suction rate. At low chord Reynolds number, internal noise induced premature transition was eliminated by increasing the suction flow, at high Reynolds number increasing suction brought about transition due to an aerodynamic disturbance in the suction system, discussed in 2.3.5.3. The mid chord region of the specimen was most sensitive to internal sound. The critical frequencies were those of

the Tollmien-Schlicting theory of amplified oscillation. Because of these results, laboratory duct tests and flight tests were conducted.

b. Laboratory Duct Noise Test. The goal of this test was to determine the perturbation velocity from the suction slot resulting from an acoustic pressure in the main spanwise duct as a function of duct flow Mach numbers and slot flow Mach number. The test specimen was part of the X-21A lower wing surface. The test and the results are described in detail in Reference 2-102. Suction, flow rates and altitude effects were simulated, however, there was no external flow (or boundary layer). A sound generator was located downstream of the panel, slot perturbation velocities were measured with a hot wire anemometer. An expression for the transfer function relating the slot perturbation velocity and the duct sound pressure level was obtained. Application of this method to the X-21A flight tests indicated that the laminar boundary layer would not be affected by the introduced sound.

It was during this test that the discovery was made that, at the higher slot Reynolds number, the suction slot wake flow oscillated as it exited from the slot and that under these conditions this disturbance could dominate over the disturbance arising from duct normal sound pressure levels, see 2.3.5.3.

c. X-21A Flight Tests. Flight Tests were conducted, on the X-21A, to determine the effect of internal noise on laminar flow control. These tests covered, for the X-21A configuration, all aspects of the problem, namely generation of noise by compressors and duct flow components, noise propagation through complex duct designs, and the final effect on the laminar boundary layer. The results are summarized in Reference 2-87. The first part of the tests was to measure ambient duct sound pressure levels existing in representative spanwise ducts at suction system settings used to obtain laminar flow at an altitude of 40,000 ft. Overall sound pressure levels measured were in the range of 103 to 121 dB. In the second part of the tests, sound generators were installed on the airplane and additional sound (discrete

tones and broadband noise between 500 and 10,000 Hz) was introduced into selected ducts during M = 0.75 cruise at 40,000 ft. with laminar flow control surfaces in operation. The introduced sound was generally 6-15 dB above the ambient duct overall sound pressure level in the duct and 10-20 dB above the corres- ponding duct noise spectrum level. No evidence of any deterioration of the wing laminar flow was reported during these introduced sound tests.

Although it is not possible to state that internal sound is a negligible factor in the design of a laminar flow wing, a conclusion of Reference 2-87, based on internal noise tests in wind tunnel, laboratory work and X-21A LFC flight test is that the lack of any evidence of deterioration in the laminar flow with sound 10 to 15 decibles higher, on a spectral basis, than the normal (X-21A) sound pressure levels provides reasonable assurance that internal sound is not a factor of primary concern in the maintenance of laminar flow. Although this conclusion is directly applicable to the X-21A configuration, it could be representative of LFC suction systems in general, particularly those with low duct flow Mach numbers. Further, suction compressors for the 1990's will probably be quieter than those used in the X-21A Program. However during any future LFC program, with a different configuration, it is recommended that duct internal noise measurements be taken in order that the situation be re-assessed.

For the above reasons, and because of the difficulty of formulating a generalized prediction procedure for such a complex geometry, no methods for the direct prediction of internal noise levels in the duct are presented, although some suggestions are made as to a starting point here it is deemed necessary.

2.3.5.3 Internal Aerodynamic Disturbance Sources - The stability of a boundary layer, in the presence of disturbances emanating from suction slots, has recently been analyzed in Reference 2-103 for low suction velocities.

In addition to internally generated noise producing a disturbance at the suction surface, an aerodynamic disturbance generated by the slot flow wake in

the plenum chamber can propagate back through to the suction surface. The disturbance intensity from this aerodynamic source can, under certain flow conditions, be more intense than that created by the internally generated noise and thus be the dominant disturbance. This situation is believed to have existed in the wind tunnel LFC tests of References 2-99, 2-100 and 2-101. The presence of such a disturbance was confirmed in the laboratory test work reported in Reference 2-102, and is discussed in detail in Reference 2-104. The conclusion is that with the suction system configuration of the X-21A and at slot Reynolds numbers ($R = Vw/\nu$, where V is the slot mean flow velocity and w is the slot width) above 120 to 140 the wake of the slot flow oscillates and creates a disturbance that can propagate through the slot to the wing surface and disturb a laminar flow. The presence of this phenomena is probably also a function of the slot and plenum chamber design.

Since this phenomena is more related to unsteady aerodynamics than internal noise, no prediction of this phenomena is included in this study. However, it could provide an upper limit on design slot Reynolds numbers. Its importance in other configurations might require further investigation.

2.3.6 Other Disturbance Sources

2.3.6.1 Structural Vibration - Tests and analyses were conducted to determine whether vibratory suction duct wall motion induced by structural response to aero-acoustic loading, by mechanical excitation or by transmission of vibration could result in a pumping action which would induce high suction slot velocity at the wing surface, Reference 2-87. This would originate from a fluctuating duct volume arising from duct wall oscillatory motion. Conservative analyses showed that the induced slot velocity is negligable for the duct vibration amplitudes measured. Further, in the experiments (conducted over a wide range of flight conditions with the wing possessing both a laminar and turbulent flow) there was no discernible evidence that any deterioration of the maintenance of laminar flow could be related to such a pumping action.

Flight tests were also conducted on the X-21A to determine the effect of LFC panel vibration on LFC operation, Reference 2-87. The panel was forcibly excited in the frequency range 400 to 1,800 Hz at vibration levels higher than

normally existed. The test procedure was to establish laminar flow over the test area of the wing and then slowly vary the frequency of vibration between the frequency limits. Tests were conducted up to M = 0.8 at 40,000'. The effects of the forced panel vibration on the laminar boundary layer were monitored by two flush mounted microphones located immediately aft of the vibrated panel. The difference in the microphone spectra between laminar and fully developed turbulent flow for normal vibration was established. During the forced vibration test there was essentially no difference in the microphone response with induced vibration except at the frequencies of the induced vibration. These tests showed that for the X-21A airplane and structural configuration: 1) that the normal vibration environment did not affect the maintenance of laminar flow and 2) that vibration within the frequency range 400 to 1,800 Hz at magnitudes far in excess of the normal vibration environment did not affect the maintenance of laminar flow. These results can probably be attributed to the fact that the structural vibration response spatial characteristics are "in-phase" over panel areas large (such as an overall panel response) compared to suction slot sizes. More local vibrations could be more harmful.

Based on these results it is considered that comparative levels of structural excitation on any LFC design would have similar non harmful effects. Especially if the future LC aircraft were to be constructed from composite materials which have inherently higher structural damping. These effects were not considered further in this study. For further information see Reference 2-49.

2.4 CRUISE TRANSFORMATIONS

The basic noise prediction methods predict noise at their best data base. For propulsive type noise sources these conditions are static sea level. For airframe type noise sources they are at low forward speed and at low altitude. It is necessary to transform these predictions to the conditions of cruise altitude (30,000 to 50,000 ft.) and cruise Mach number (0.7 to 0.95) and to allow for airplane configuration and flow field effects. The transformations may be considered as being in three categories, as shown in Figure 2-2, and are discussed as follows. Since not all of the transformations may be applicable to any given noise source the appropriate transformations for each noise source are defined.

2.4.1 Cruise Effects on Acoustic Strength

The first set of transformations describe the acoustic conversion from the best data base to cruise altitude, at the cruise operating conditions. This includes the effect of speed on acoustic power (relative velocity effects); the effects of forward speed on propagation and airframe presence effects are covered in the next sections. These transformations yield the equivalent of a "static" acoustic free-field of a single noise source at cruise altitude.

2.4.1.1 Cruise Operating Conditions - Using the basic prediction methods the noise fields are predicted using the values of the noise sensitive parameters which exist at required cruise conditions. Thus the propulsive type noise characteristics require knowledge of the appropriate cruise mass flows, temperatures, pressure ratios, etc.

2.4.1.2 Relative Velocity - The strength of some noise sources are related to the relative velocity between the exhaust flows and the ambient medium. Of the propulsive sources jet mixing noise is directly effected. For a single model jet flow, experimental evidence, References 2-44, 2-45, and others, show that the overall sound pressure level radiated in the direction 90° to the inlet varies as $V_R = (V_J - V_A)$ raised to the power between 5 and 6. Thus the inflight effects may be approximated by:

FIGURE NUMBER

ILLUSTRATION TITLE

$$\Delta dB(V_R) = 55 \log \left\{ \frac{V_J - V_A}{V_J} \right\}$$

This relationship is presented in Figure 2-8 for a single flow jet nozzle efflux velocity, V_J, of 1300 feet/second. The range of experimental confirmation covers low aircraft forward speeds, V_A, up to about 250 feet/second. Applying this equation to an airplane cruise velocity of some 800 feet/second a reduction due to forward speed of 23 dB is predicted. In the jet mixing noise prediction procedure, for a single jet, this correction factor is applied to noise levels at all frequencies and in all directions. (A further refinement here would be to relate the spectral peak frequency and the directivity of jet mixing noise to V_R, based on low speed model test work). In the prediction of the jet mixing noise of a two flow jet, the effect of relative velocity is allowed for between each of co-flowing fluids, e.g. between primary and secondary and between secondary and the atmosphere.

Propulsion noise sources originating from within the engine are dependent upon aircraft velocity in that the engine cycle is designed to operate at the cruise altitude and Mach number. Thus the aircraft cruise velocity influences the value of the engine noise sensitive parameters (such as mass flows, pressures and temperatures) used in the computation of fan, compressor, combustion and turbine cruise noise levels. These noises then radiate from the inlet or discharge ducts (except for sonic throat and acoustic treatment attenuation effects), independent of aircraft velocity or any relative velocity. This conclusion, at least for low speeds is supported by the experimental work reported in Reference 2-50 and 2-105. Similar comments apply to the laminar flow control external noise sources.

The airframe noise sources (the turbulent boundary layer and the trailing edge) are a direct result of the freestream airflow. In these cases the free stream velocity is the acoustic generating velocity.

2.4.1.3 Change in Jet Efflux Structure at Cruise - At cruise conditions the jet efflux flow structure will probably be different to that at sea level static. The changes could include: 1) different jet mixing characteristics,

2) different shock cell spacing characteristics and 3) the presence of boundary layers shed from the nacelle. The three jet noise components (mixing noise, shock associated broad band noise and shock screech), could well have their source location and acoustic radiation characteristics influenced by these flow field changes. These effects are not allowed for in these predictions. However, they do need to be quantified to assess their importance.

2.4.1.4 Acoustic Characteristic Impedance - At cruise altitude the acoustic propagation environment is significantly different from sea level. The air is cold, rarefied and very dry. A comparison of acoustical parameters at sea level and a typical cruise altitude are shown in Figure 2-26. The main acoustic differences are the lower speed of sound, the reduced acoustic characteristic impedance and the change in atmospheric attenuation. These last two effects are discussed in the following sections.

In this study, the acoustic characteristic impedance, Z, has two important roles. First, acoustic impedance, defined as $Z = p/u$, relates acoustic pressure and particle velocity. For a plane wave $Z = \rho c$. It is thus dependent upon altitude and its value reduces from 40.7 c.g.s. rayls on a standard day at sea level to a value of 9.6 c.g.s. rayls at an altitude of 38,000 feet. Figure 2-27 illustrates the variation with altitude. Secondly, the acoustic power of a stationary noise source, W, and its acoustic pressure ratiation field are also related by acoustic impedance. Now acoustic power $W = \iint_A I dA$ where I is the acoustic intensity of the sound wave through an elemental area dA. Since $I = p^2/\rho c$, then for non-directional spherical radiator at a given radius, r, $dA = A(r)$ and

$$W = \frac{p^2(r)}{\rho c} \cdot A(r) \qquad 3\text{-}30$$

Thus at sea level

$$W_o = \frac{p_o^2(r)\ A(r)}{\rho_o c_o} \qquad 3\text{-}31$$

		SEA LEVEL	38,000 FT
Temperature	^{o}F	59.0	-69.7
Speed of Sound	ft/sec	1,116	968
Air Density	$Slugs/ft^3$	0.002378	0.000646
Density Ratio		1.000	0.272
Air Pressure	lb/ft^2	2116	432.6
Pressure Ratio		1.000	0.204
Kinematic Viscosity	ft^2/sec	0.0001572	0.0004594
Acoustic Characteristic Impedance (ρc)	c.g.s. rayls	40.7	9.6
Characteristic Impedance Ratio		1.000	0.236

FIGURE 2-26 COMPARISON OF SEA LEVEL AND ALTITUDE ACOUSTIC PARAMETERS

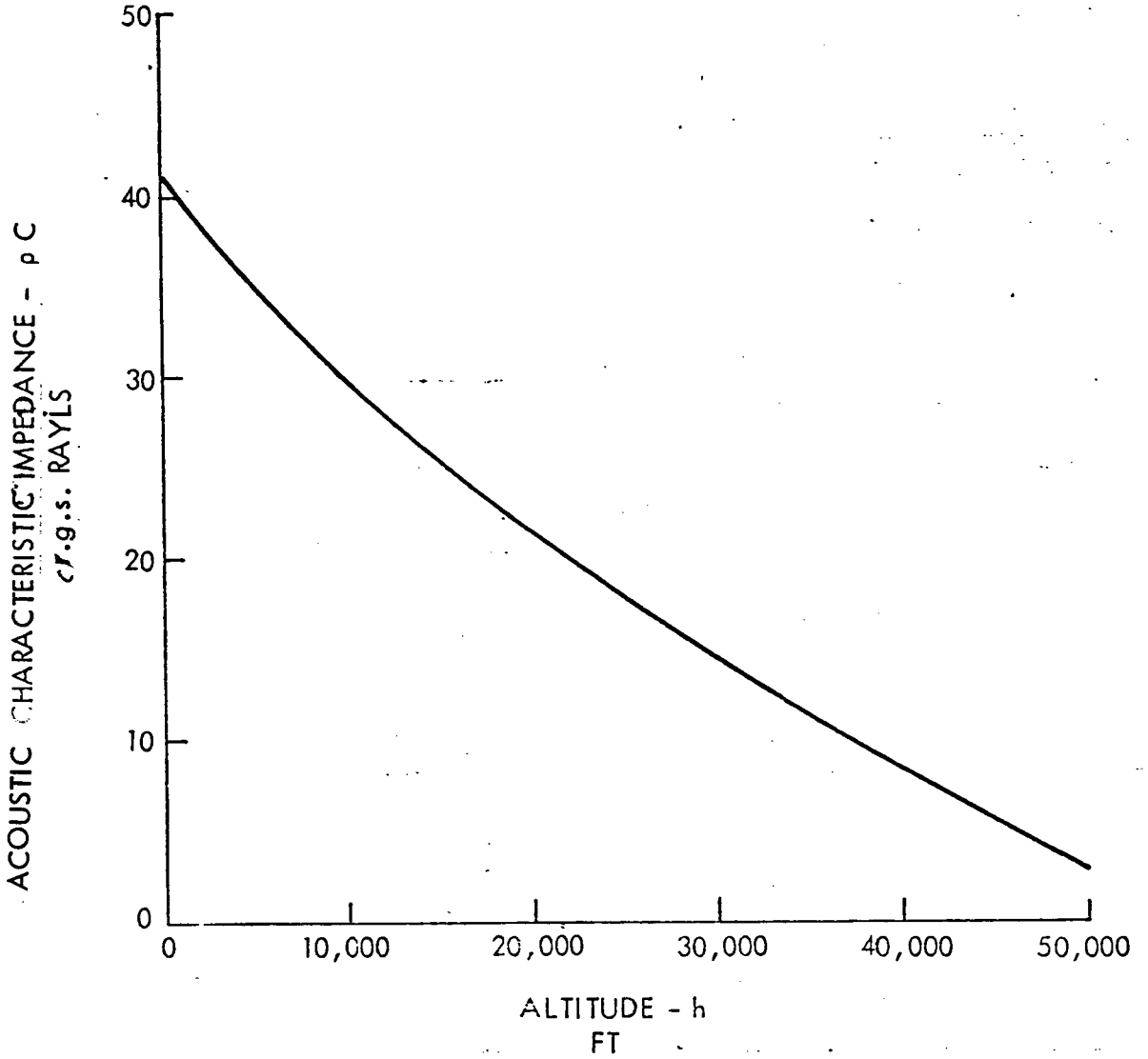

FIGURE 2-27. ACOUSTIC CHARACTERISTIC IMPEDANCE AND ALTITUDE

This equation may be re-expressed as:

$$PWL_o = SPL_o(r) - 10 \log (\rho_o c_o) + 10 \log A(r) + K \quad 3\text{-}32$$

At altitude h, the power level for the same source is

$$PWL_h = SPL_h(r) - 10 \log \rho_h c_h + 10 \log A(r) + K \quad 3\text{-}33$$

From which

$$SPL_h(r) = SPL_o(r) + (PWL_h + PWL_o) + 10 \log \left[\frac{\rho_h c_h}{\rho_o c_o}\right] \quad 3\text{-}34$$

The sound pressure level at altitude is thus derived from three terms. The first, $SPL_o(r)$, is the noise level which would be made at sea level by the source with the source operating at sea level conditions. Thus, the acoustic prediction would be made using the noise sensitive parameters, e.g., mass flows, densities, temperatures, pressure ratios, velocities, revolutions/ sec, etc. The second ($PWL_h - PWL_o$) represents the change in acoustic power between sea level and cruise altitude conditions (due to the change in noise sensitive parameters) but still at sea level (which assumes operating at sea level impedance). In this study the first and second terms are effectively combined since the noise level at sea level using cruise source operating conditions is calculated directly. (The effect of other factors such as relative velocity on acoustic radiation are considered separately.) The third term, 10 log is the correction for the change in characteristic impedance between sea level and altitude. This factor is shown in Figure 2-28. It is applicable to all the noise sources. At 38,000 ft. this correction factor is -6.3 dB applied to the sound pressure. It can be seen that for a noise source which has constant acoustic power output, increasing altitude reduces the radiated acoustic

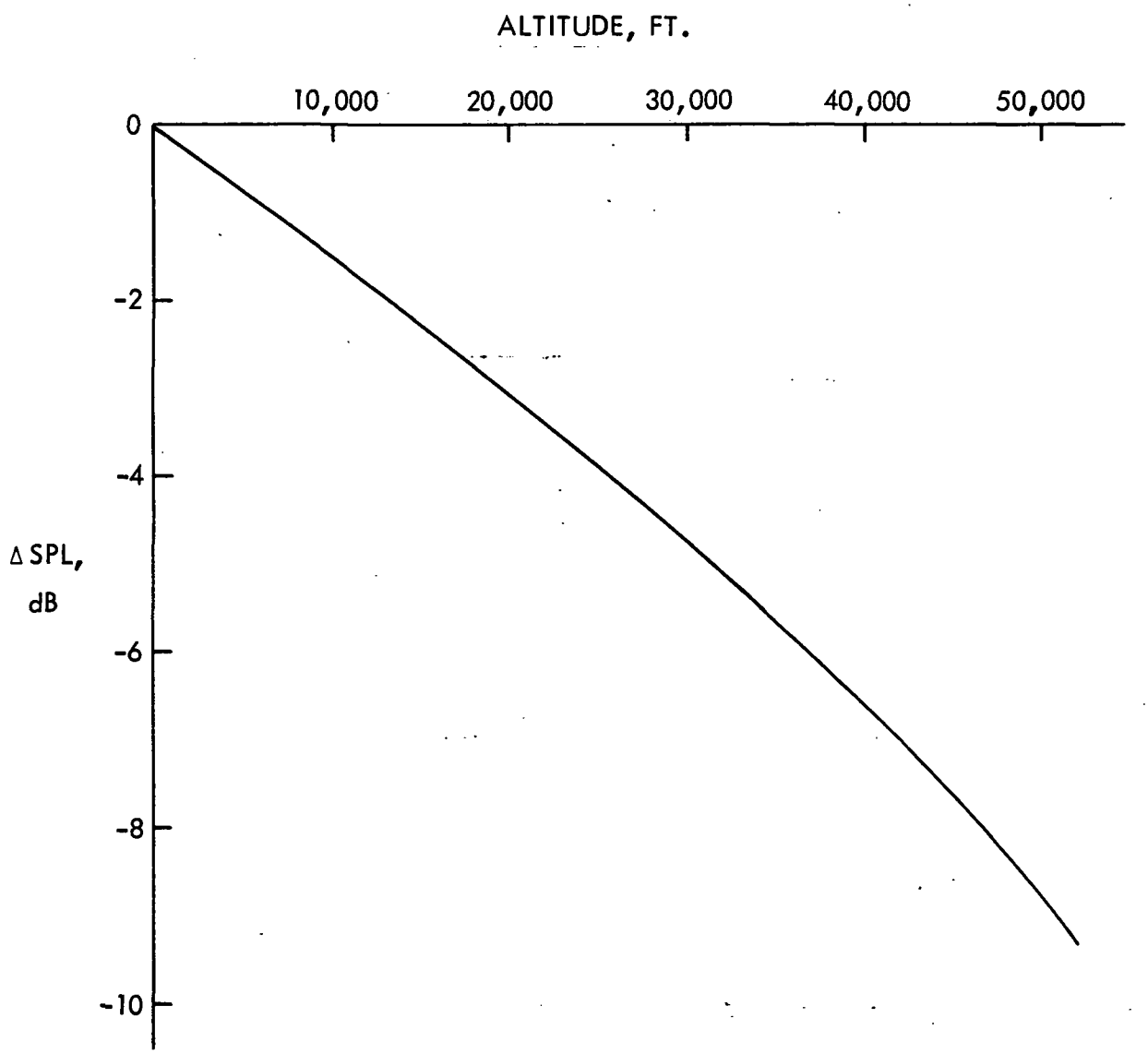

FIGURE 2-28. ALTITUDE CHARACTERISTIC IMPEDANCE CORRECTION ON SOUND PRESSURE LEVEL

pressure. However, from the above equations, it can be shown that the corresponding particle velocity increases, as shown in Figure 2-29.

2.4.1.5 Atmospheric Absorption - The atmospheric absorption of sound in quiescent air can be well predicted, as a function of frequency, over a wide range of temperature (0° to 100°F) and relative humidity (10% to 100%) conditions at near sea level altitudes, References 2-106 and 2-107. The attenuations are most significant over large distances and at higher frequencies. For cruise noise predictions some large propagation distances could be involved. The pressure, temperature and relative humidity at 40,000 ft. ($18.75(10)^3$ N/M^2 and 216.7°K (with zero relative humidity), are far outside the range of the curves of Reference 2-122 or the data of Reference 2-123). There appears to be no method available to predict the absorptive characteristics of the atmosphere at high altitudes.

Both of the above references relate atmospheric absorption coefficients, , (dB/1000 ft or dB/M) as a function of frequency to temperature, pressure, and relative humidty. One of the more obvious trends in this relationship is that at sea level pressure, with the other factors constant, as temperature decreases the absorption coefficients reach a peak and then reduce to smaller values at the lower temperatures, as shown in Figure 2-30. The equations of Reference 2-107 (which have not been verified for temperatures below 0°F (255°K)), have been used to generate a "reference" set of absorption coefficients, α_{cruise}, for the conditions at 40,000 ft. on a standard day, and are shown in Figure 2-31. Also shown are the corresponding 1/3 O.B. level reductions at a distance of 50 ft. as a result of atmospheric absorption alone. Note, however, that at Mach 0.8 an observer distance of 50 feet will translate into a varying propagation path length of from 250 ft. to 28 ft. for observer positions directly in front of to behind a moving source, respectively. The projected dB reduction at 250 ft. is therefore included in Figure 2-31. In this case the absorption becomes significant only at the high frequencies.

Even though these attenuations have been extrapolated well outside the applicable ranges of their controlling parameters it is felt that the results indicate that this correction to the predicted cruise noise levels may be omitted. In any event, this approach will be somewhat conservative.

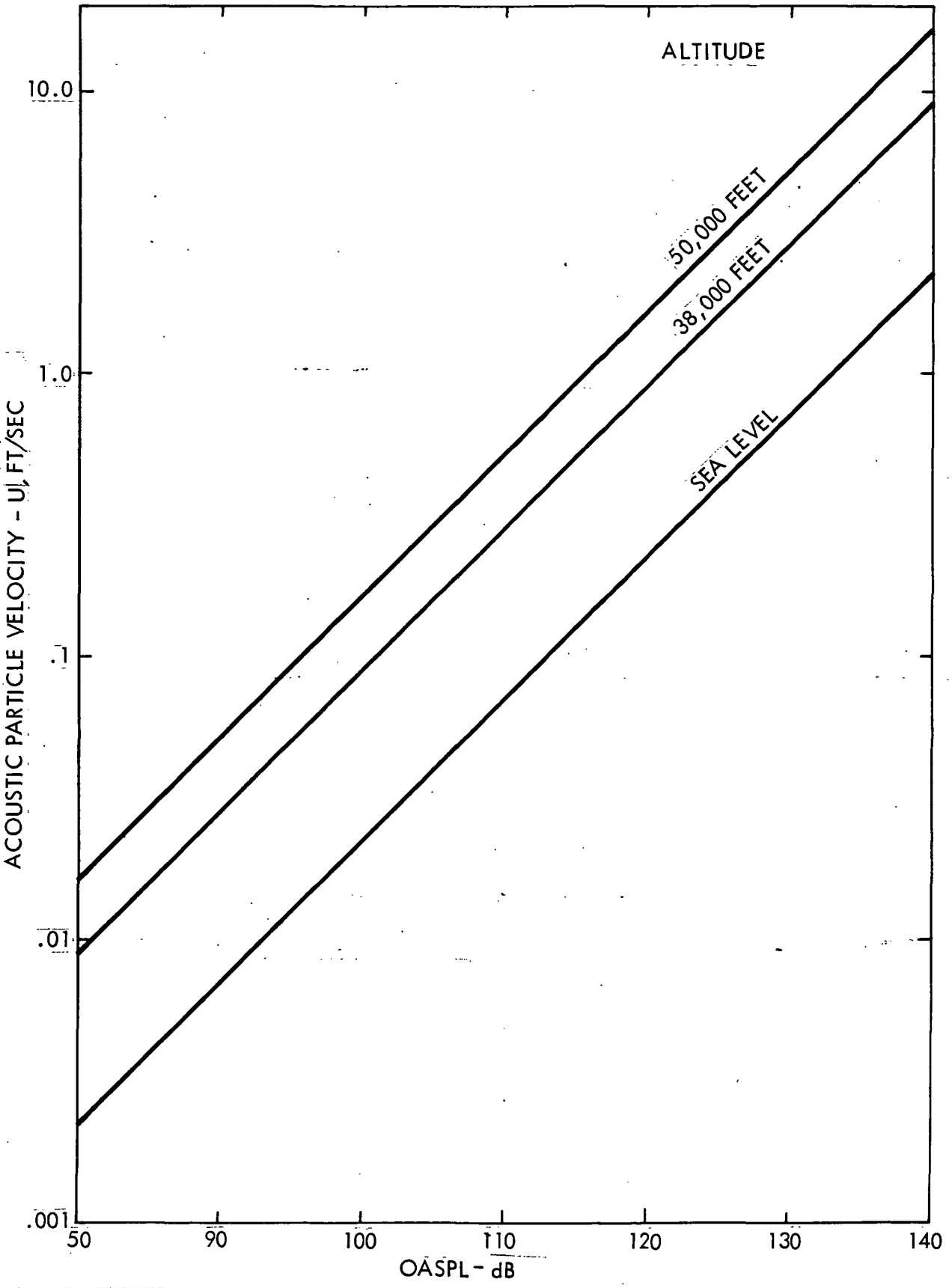

FIGURE 2-29. ACOUSTIC PARTICLE VELOCITY AS A FUNCTION OF OASPL AND ALTITUDE

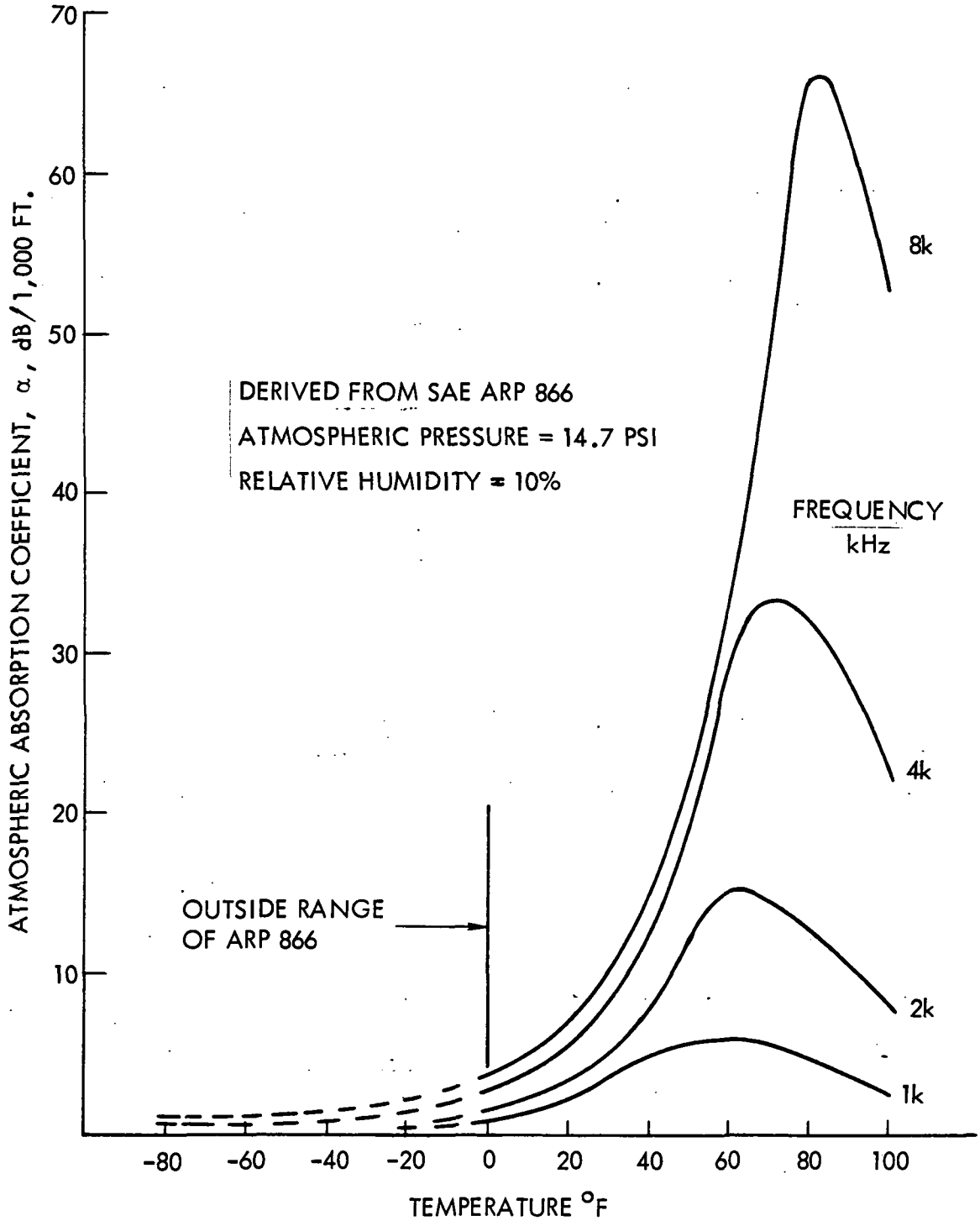

FIGURE 2-30. ATMOSPHERIC ABSORPTION COEFFICIENT, AT SEA LEVEL

1/3 O. B. CENTER FREQUENCY (Hz)	α_{cruise}, dB/1000 ft.	ΔdB 50 ft.	ΔdB 250 ft. *
50	0.01	0.0	0.0
63	0.01		
80	0.01		
100	0.01		
125	0.01		
160	0.01		
200	0.02		
250	0.02		
315	0.03		
400	0.04		
500	0.06		
630	0.10		
800	0.15		
1000	0.23		0.1
1250	0.36		0.1
1600	0.59		0.2
2000	0.91		0.2
2500	1.42	0.1	0.4
3150	2.25	0.1	0.6
4000	3.63	0.2	0.9
5000	5.66	0.3	1.4
6300	8.98	0.4	2.2
8000	14.48	0.7	3.6
10000	22.63	1.1	5.7

* This column is for an observer (moving with the source) located 50 ft. directly in front of the source moving at Mach 0.8. ($\bar{r}$ = 50 ft., r' = 250 ft.)

FIGURE 2-31 ESTIMATED ACOUSTIC ABSORPTION COEFFICIENTS AT 40,000'

2.4.2 Forward Speed Effects on Acoustic Propagation

This set of transformations describes four changes in the noise field due to the motion of the noise source and the receiver (moving along with the noise source) through a stationary medium.

2.4.2.1 Cruise Co-ordinate Transformation - Noise prediction procedures are generally applicable to the case of the noise radiated by stationary source and observed by a stationary observer, e.g., a test stand type situation. For application of static type data to the cruise condition, allowance must be made for the effect of the moving source and moving receiver. This movement changes the perceived location of the receiver in the sound field and necessitates a cruise co-ordinate transformation which is developed as follows.

During cruise, through a stationary, homogeneous medium, the airplane noise sources travel along with the airplane at the airplane Mach number, M_A. A receiver location, situated on the airframe also travels in the same direction and at the same speed, as illustrated in Figure 2-32 (where the noise source example is the forward fan noise). The sound field radiated by the moving source has a propagation velocity, relative to the stationary medium of the speed of sound, corresponding to M = 1.

Relative to the moving noise source, the airframe co-ordinates are r, ϕ,; the co-ordinate system moves with the aircraft, these co-ordinates are thus physical co-ordinates of the airframe receiver point.

The receiver perceived location in the moving sound field is different to the physical, real, location of the receiver. The reason for this can be seen in Figure 2-32. Because of the source/receiver velocity, a receiver located at r, ϕ actually hears the noise radiated to another location r', ϕ', where r' and ϕ' are the static distance and directivity in the sound field. r' and ϕ' define the real travel distance and directivity of the acoustic ray. The relationship between r, ϕ and r', ϕ' must be established in order to convert from the receiver apparent location to the receiver actual perceived location. The new location is the location to be used for applying static (test stand) acoustic prediction methods.

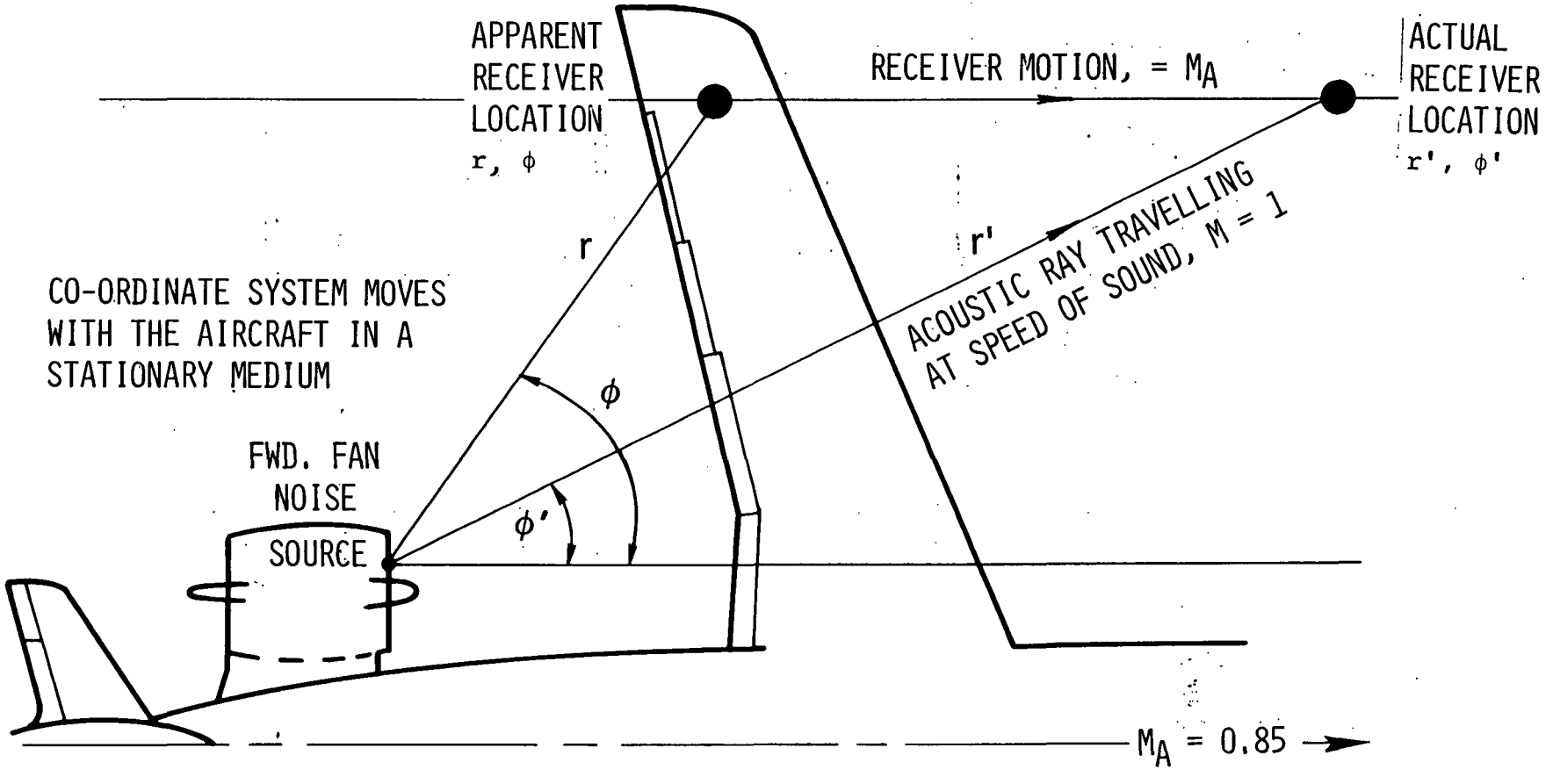

FIGURE 2-32. CRUISE CO-ORDINATE TRANSFORMATION

FIGURE NUMBER

ILLUSTRATION TITLE

In the time that the noise source, and the receiver travel a distance Δx ($= x' - x$) the sound wave travels a distance r'. Thus

$$\frac{\Delta x}{M_A \cdot c} = \frac{r'}{c}$$

Further from geometric relationships, $\cot\phi = \frac{x}{y}$, $\cot\phi' = \frac{x'}{y}$, and $r'^2 = x'^2 + y'^2$. From which it can be shown that:

$$\cot\phi' = \frac{1}{1 - M_A^2}\left[\cot\phi + M_A\sqrt{1 - M_A^2\cot\phi}\right] \qquad 3\text{-}35$$

and

$$r' = r\,\frac{\sin\phi}{\sin\phi'} \qquad 3\text{-}36$$

Figure 2-33 shows the relationship between ϕ and ϕ' for a range of Mach numbers. Effectively, the static noise directivity is swept back by the aircraft motion, so that ϕ is equal to ϕ' at 0° and 180°, but elsewhere is less than ϕ'.

Figure 2-34 shows, at M = 0.82, the relationship between r and r' for various ϕ'. Ahead of the noise source r'> r while aft of the noise source r' < r. The effect of distance transformation on sound pressure level, for a non-direc- tional source, is shown in Figure 2-35, where it can be seen that there is a reduction in noise level ahead of the noise source and an increase behind the source.

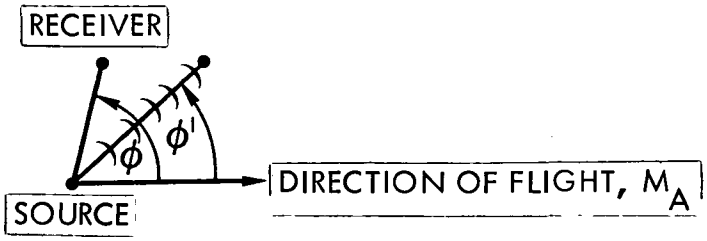

ϕ RECEIVER LOCATION AT EMISSION

ϕ' RECEIVER LOCATION AT RECEPTION

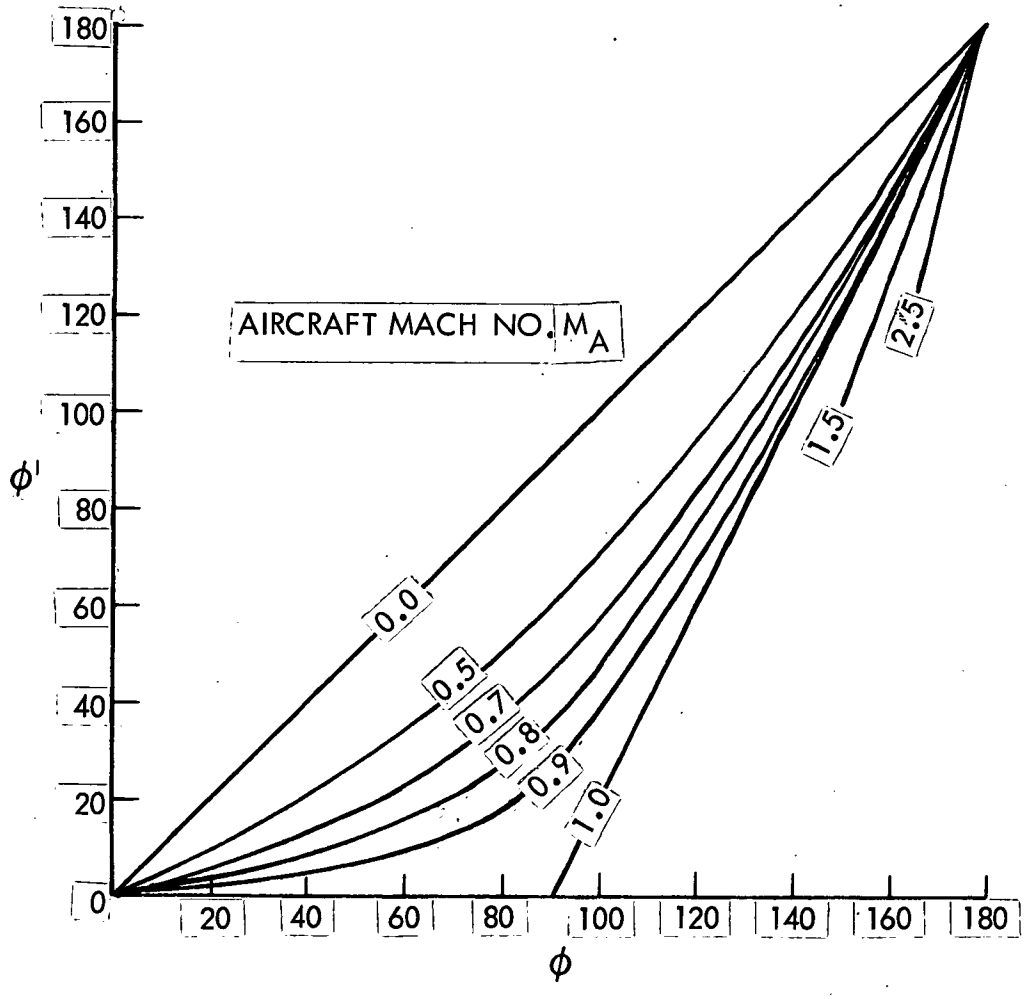

FIGURE 2-33. CRUISE ANGULAR TRANSFORMATION

108

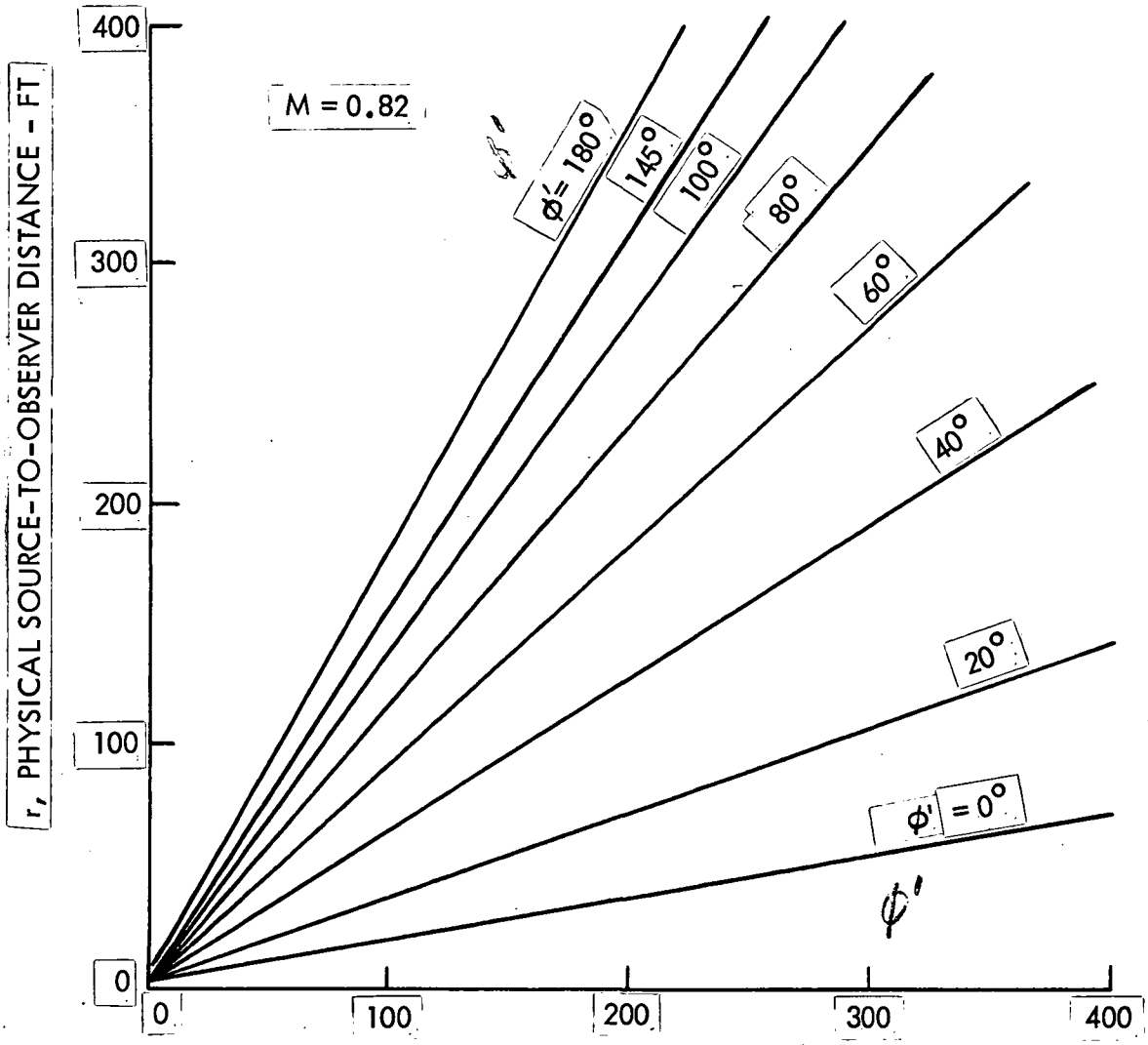

CRUISE

FIGURE 2-34. CRUISE DISTANCE TRANSFORMATION

FIGURE NUMBER

ILLUSTRATION TITLE

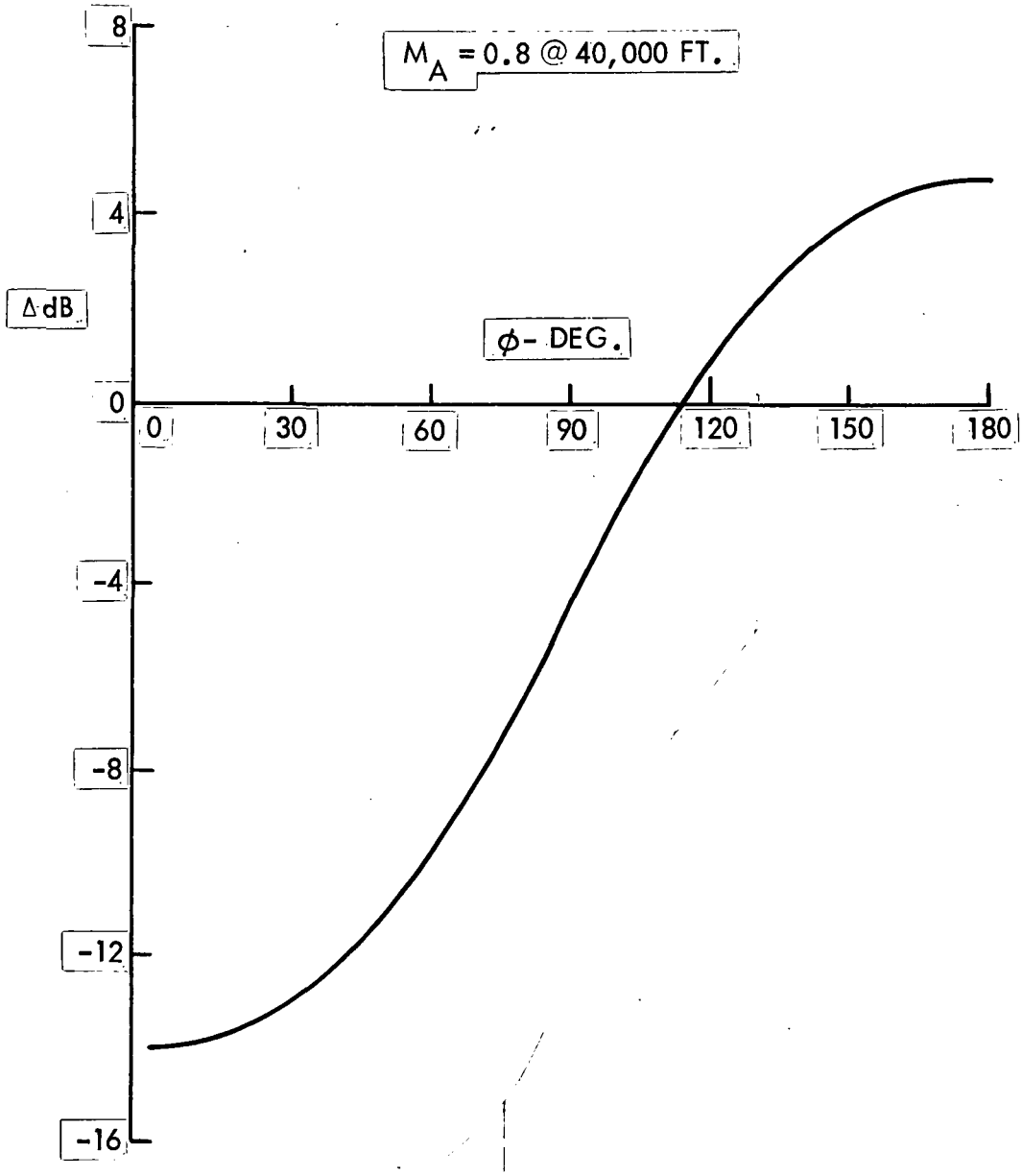

FIGURE 2-35. EFFECT OF CRUISE DISTANCE TRANSFORMATION ON A NON-DIRECTIONAL SOURCE NOISE LEVEL

110

FIGURE NUMBER

ILLUSTRATION TITLE

A further effect of source and receiver motion is to change the observed wavelength (and hence wavenumber) of the acoustic signal relative to the receiver.

Thus, to calculate the noise at the cruise co-ordinates r, - which are the physical co-ordinates - one of the first steps is to determine the transformation to the equivalent static co-ordinates r', ϕ', where the static noise is then calculated. This transformation is required for all external noise sources. In all the noise prediction progresses this is achieved by specifying r, ϕ and M.

2.4.2.2 Doppler Frequency Shift - A stationary observer listening to a stationary noise source, when both are in a stationary medium, hears the source radiated true frequency. When relative motion exists one to another, changes in observed frequency and wavelength occur. The general equation for the frequency shift has been defined in Reference 2-108, Equation (14). For cruise noise prediction the medium is assumed to be stationary and both observer and source are in parallel motion. That equation then simplifies to

$$f_o = f_s \frac{c_o + |V_m| \cos\phi_{ms}}{c_o + |V_s| \cos\phi_{ms}} \qquad 3\text{-}37$$

where

f_o = observer detected frequency

f_s = source true frequency

c_o = speed of sound

V_m = moving observer velocity

V_s = moving source velocity

ϕ_{ms} = angle between source and observer

Two cases are of interest. First, when the observer and the noise source are travelling together at the same speed and in the same direction, the above equation indicates no change in frequency. This applies to noise sources which are fixed relative to the airframe, e.g. fan, turbine, core, jet broad band shock associated, and trailing edge noise. The second case is when the noise sources travel at a speed different to the observer. Examples of this are jet mixing noise, where the sources move aft relative to the nozzle, and turbulent boundary layer noise, where the sources move aft relative to the fuselage surface. The observed frequency shift is then given by the above Equation. This effect has not been included in the prediction of these two noise sources. A special case is of jet shock screech where the feedback loop time is influenced by airplane forward speed. This effect is included in the computation of cruise screech frequencies.

2.4.2.3 Convective Effect - It has been theoretically shown that subsonic motion of a noise source changes its static directionality as heard both by a stationary observer and by an observer moving with the noise source, References 2-14, 2-50, and 2-109. The change in acoustic intensity is proportional to $(1 - M_c \cos\phi')^N$, where M_c is the source convection velocity and ϕ' is measured from the direction of motion. Some authors, Reference 2-14, indicate that the exponent, N, is dependent upon the type of noise source, e.g., N is equal to 2, 4, or 6 for a single monopole, dipole, or quadrupole, respectively. Others, Reference 2-50, indicate that the exponent N is equal to 4 independent of noise source. For N = 4, the change of sound pressure level is

$$\Delta dB_{CE} = 40 \log \left(\frac{1}{1 - M_c \cos\phi'} \right) \qquad 3\text{-}38$$

This relationship is shown in Figure 2-36, for two convection Mach numbers. Thus, in motion the acoustic pressure field carried along with the noise source has a preferential radiation forward and a reduced radiation aft. This phenomena is often referred to as convective amplification, here it is re-

CONVECTIVE EFFECT - THE EFFECT OF SOURCE MOTION ON ACOUSTIC DIRECTIVITY

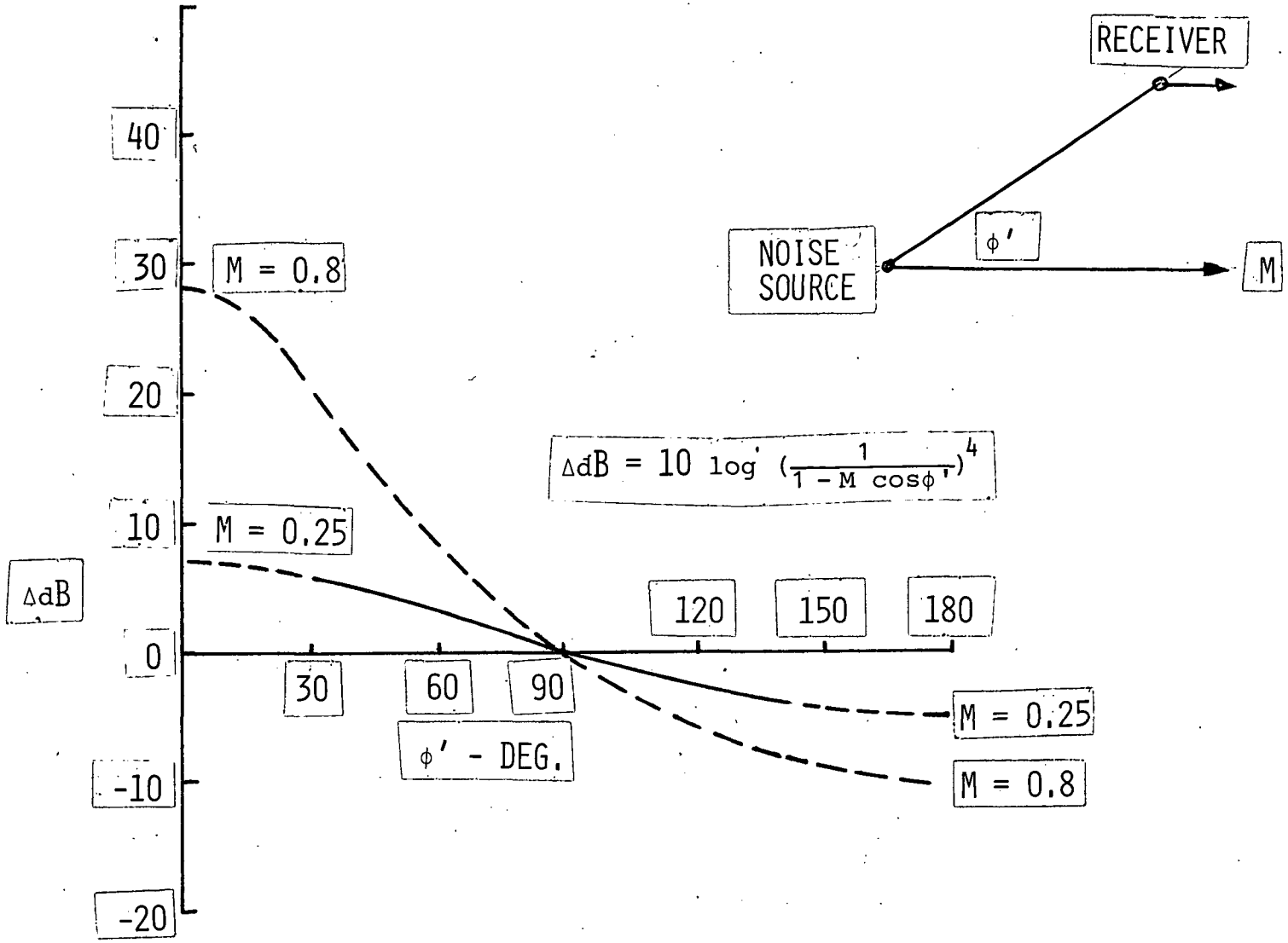

FIGURE 2-36. CONVECTIVE EFFECT

FIGURE NUMBER

ferred to as the convective effect. This effect is in addition to any change in observed frequency - known as the Doppler Effect.

ILLUSTRATION TITLE

Recently the convective effect has been identified experimentally, for low forward speeds (M = 0.1 → 0.25). References 2-110, 2-111, and 2-112 report an analysis of the effect of forward motion on various engine noise components for large airplanes. In correlating static and flyover noise, on a source separated basis, the convective effect, including the strong forward arc lift, was shown to hold for fan, core, and turbine noise. For all the above noise sources the exponent N was equal to 4. In Reference 2-49, again at low speeds, model tests with simulated forward speed in an acoustic wind tunnel showed, for shock associated broad band noise and for upstream generated noise, that the convective effect, with N = 4, was clearly evident. Reference 2-50 also showed the same effect for model tests with simulated forward speed with N = 4 for shock associated broadband noise. Thus, at low Mach numbers the convective effect, for a wide range of noise sources appears to be reasonably well validated.

In jet mixing noise, even for a static engine, the noise sources are convected downstream. Jet mixing noise prediction theory uses the convective effect concept, as applied to a distribution of moving quadrupoles. The theory accurately predicts the directionality of mixing noise, with the directionality peaking in the aft quadrant, in the direction of motion of the noise sources. The theory covers a wide range of subsonic convection velocities.

An analysis of static to flyover noise, at lower airplane speeds, reported in Reference 2-113, incudes the convective effect on an individual noise source basis. High and low by-pass ratio engines are examined. The reported correlations are good. The convective effect applied to engine core noise helps explain why forward quadrant noise stays high at forward speed.

For application to the prediction of cruise noise the convective effect as described in the above Equation is used directly for all of the noise sources, with M_c equal to the airplane Mach number, M_A, except (i) jet mixing noise (where the convective effect is already built into the prediction model) and (ii) turbulent boundary layer noise (where $M_c = 0.18\ M_A$).

From Figure 2-36, it can be seen that in the forward quadrant at M = 0.8 some high incremental noise levels (to +28 dB) are predicted; at 90° it drops to zero and in the aft quadrant noise level reductions (to -10 dB) are predicted. The test work has verified the convective effect for angles from 30° to 150° at Mach numbers up to 0.25, as shown by the full line. In view of the large impact at the higher Mach numbers, experimental validation at these speeds is urgently required.

2.4.2.4 Dynamic Effect - This is a factor introduced by Lighthill, in his derivation of the noise radiated by distributions of convected turbulence (jet mixing noise and turbulent boundary layer noise) when that region of turbulence moves through the atmosphere, Reference 2-14. This factor is sometimes referred to as dynamic amplification. For jet mixing noise, Lighthill states that the directional distribution of intensity is modified by the factor $\frac{1}{1-M_A \cos\phi'}$ (using the notation of this report) or that the sound pressure level is changed by:

$$\Delta dB_{DE} = 10 \log \left(\frac{1}{1 - M_A \cos\phi'} \right) \qquad 3\text{-}39$$

This relationship is shown in Figure 2-37 for the case of M_A = 0.25 and for M_A = 0.8. It shows an increase in observed sound pressure level in the forward quadrant, no change at 90° and a reduction in the aft quadrant. The effect is small for the case of aircraft at low speeds, M = 0.25, (typical of takeoff and landing) being between ±1 dB. However, at higher cruise Mach numbers, M = 0.8, the effect is much larger, showing a maximum increase of 7 dB in the forward quadrant.

For radiated turbulent boundary layer noise, the equation becomes

$$\Delta dB_{DE} = 10 \log \left(\frac{1}{1 + M_A \cos\phi'} \right) \qquad 3\text{-}40$$

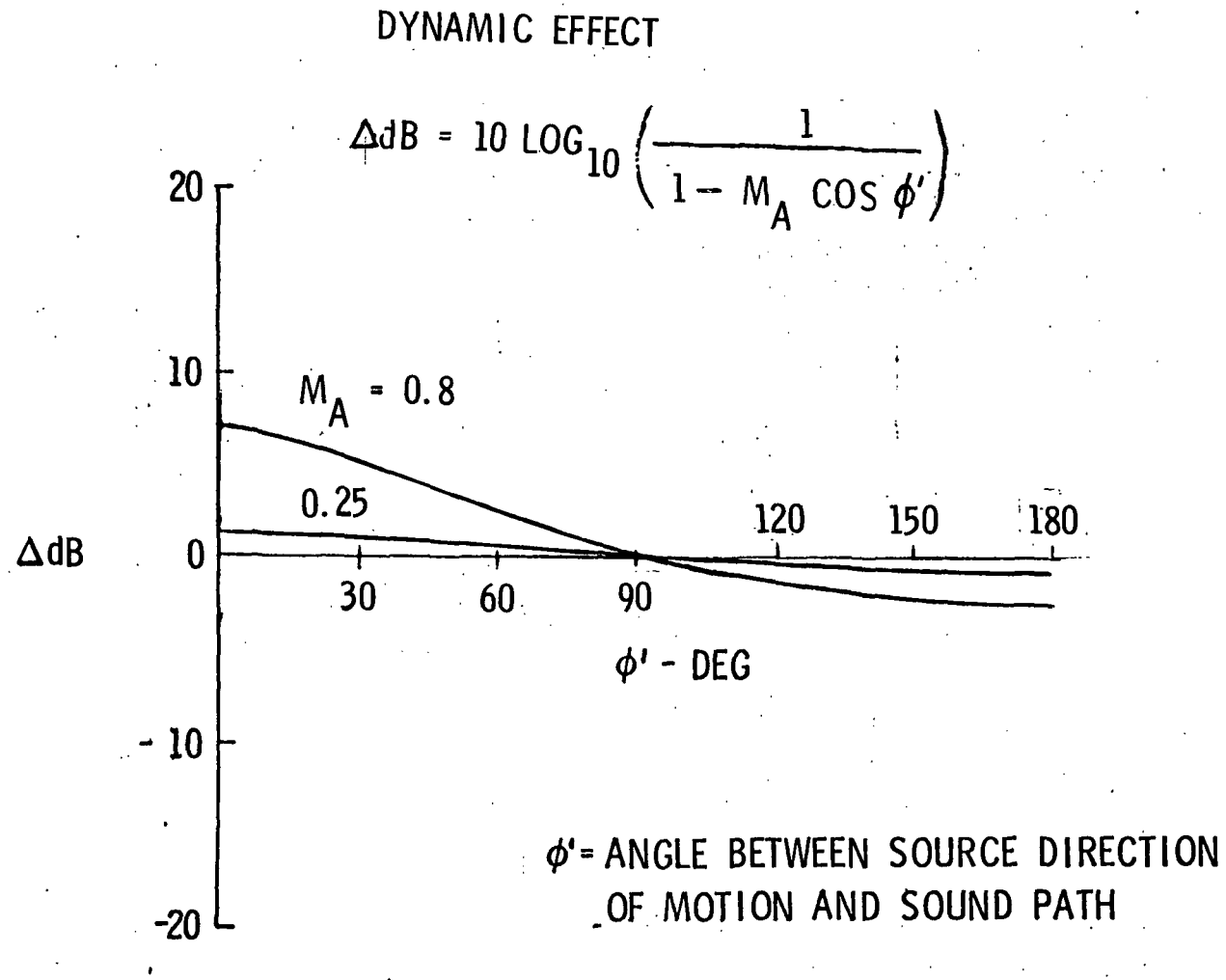

FIGURE 2-37. DYNAMIC EFFECT ON JET MIXING NOISE

since the turbulent boundary layer noise producing eddies are moving in the same direction as the fuselage wall, relative to the ambient air. The effect is shown in Figure 2-38, it is opposite to that for jet noise.

The dynamic effect phenomena is applicable only to distributions of sources (jet mixing noise and radiated turbulent boundary layer noise) and not to point source noise (fan, core, turbine, jet broadband shock associated, jet screech and trailing edge noise). It is included in the predictions for the former group of sources.

There do not appear to be any reports or data where this effect has been identified, either at low speed, where the effect is small or at high speed. Effort is required to understand and confirm the validity of this factor throughout the speed range. Application to high aircraft Mach numbers where the effect is for more significant, is therefore questionable. Whether the effect is equally applicable to point sources as well as distributed sources also requires clarification. The effort to better define the applicability of this effect to observer locations - either stationary or moving with the source - needs further study both theoretically and experimentally.

2.4.3 Aircraft Configuration Effects

The noise prediction methods, with their transformations to cruise conditions, provide a free-field sound field moving along with each single source, and uninfluenced by the presence of the airframe. However, the sound field which is required is that at locations on, or in the vicinity of, the airframe surface. The presence of the airframe can modify the free field noise levels through the number and location of sources, by incorporation of noise control devices and by physical shielding. Further the aerodynamic flow field around the airframe creates boundary layers, wakes and vortices, and shock waves which can influence the acoustic propagation. On arrival at the airframe surface the sound field is subject to reflection and diffraction effects. These airframe modifications (installation effects) to the sound field are discussed in this section and, where possible, methods proposed for their evaluation.

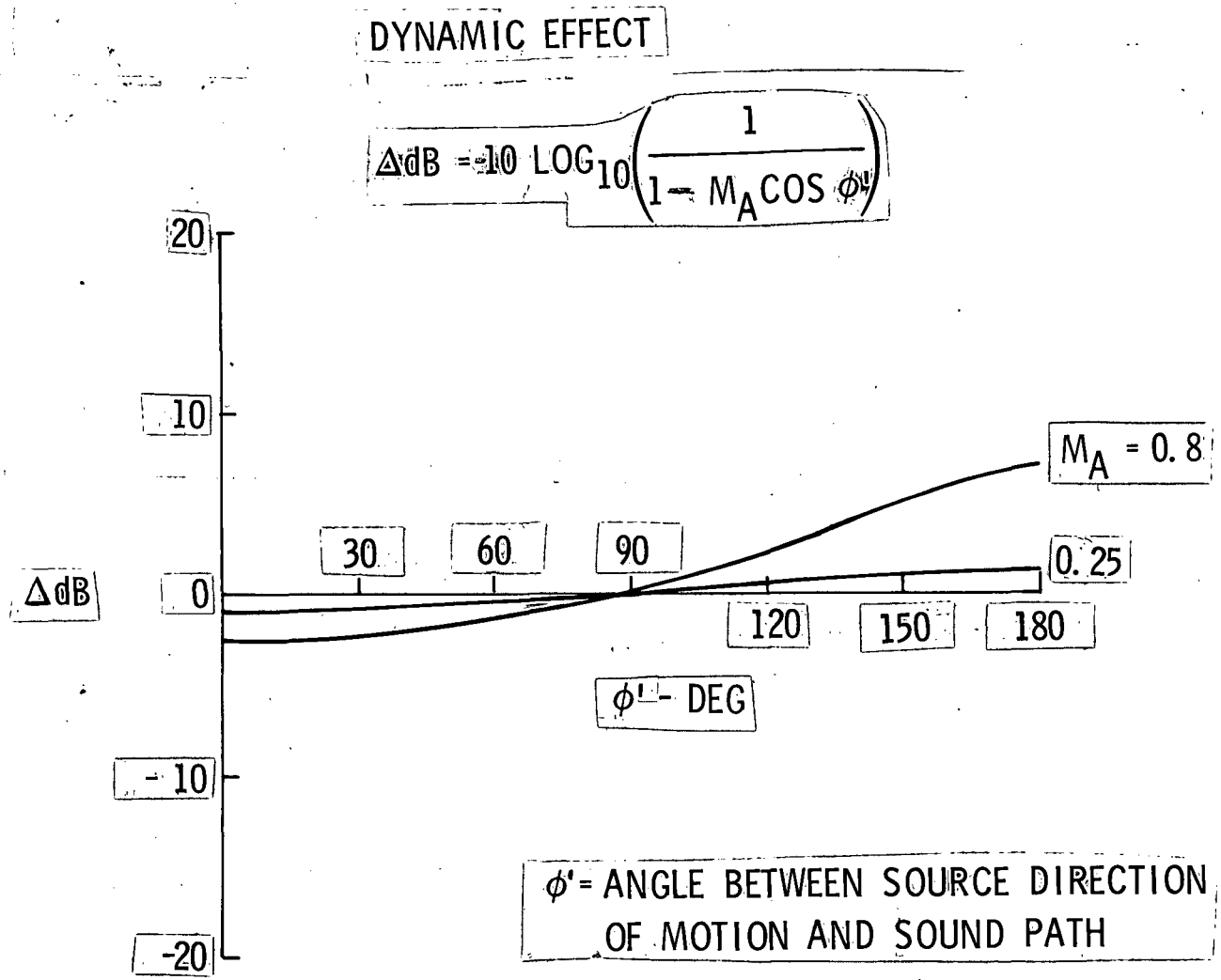

FIGURE 2-38. DYNAMIC EFFECT ON TURBULENT BOUNDARY LAYER NOISE

2.4.3.1 Number and Location of Noise Sources - The prediction procedures estimate the noise from a single noise source. On an airframe, multiple sources usually exist (e.g., propulsion units, suction units and trailing edges).

Acoustically is would be simple if the identical noise sources could be grouped together, then the single source sound level field would be modified by:

3-41

$$\Delta dB = 10 \log N \qquad 3\text{-}41$$

where N is the number of noise sources. However, this simplification can only be justified where the individual source to observer distances, r_i are much greater than the individual source separation distance, d_i, e.g., $r_i > d_i$; the cluster of noise sources thus appear as a single source. Further, there should be no structural shielding between sources. An example of where this approximation would be permissible is for propulsion units located adjacent to each other (such as mounted on the same side of the empennage) and the noise is to be predicted on the wing. However, where the predictions require the estimation of noise close to the source, this approximation is not valid and the noise contribution for each unit must be evaluated separately.

2.4.3.2 Noise Suppression Devices - Modifications to the predicted free field noise can occur through the incorporation of noise suppression devices applied to the various noise sources. For example the application of acoustic liner treatment to propulsive and flow control inlets and discharge ducts can be used to attenuate fan, compressor, core and turbine noise. Such acoustic treatment might be introduced for noise control either during terminal operations or for cruise operation. A method for estimating noise source attenuations due to acoustical linings in terms of spectral directivities is presented in Section 2.3.3.7. The same section includes procedures for the estimation of spectral directivity attenuations arising from inlet operation at high throat Mach number.

Jet noise control may be obtained through nozzle design. The jet noise prediction procedures of Section 2.3.3.5 cover the acoustics of single flow (mixed flow) and two flow nozzle designs.

Should any other type of acoustic suppression device be applied to any of the propulsive, airframe or flow control noise sources,then the effect on radiated noise levels can be determined if the spectrally directive attenuations of that device can be estimated during cruise operation.

2.4.3.3 Airframe Flow Field Modifiers - The aerodynamic flow around the airframe creates super-velocity fields around the lifting surfaces, boundary layers, and edge wakes as schematically shown, for an engine under the wing installation, in Figure 2-39. All these features detract form the assumption that the sound field propagates through a homogeneous atmosphere. The resultant magnitude of the scattered, refracted and reflected sound field is extremely difficult to assess.

During cruise the turbulent wakes, especially those shed from the wing trailing edges provide shear layers through which, often, the acoustic rays of interest must propagate. An acoustic analysis of the impact of the wake transmission is beyond the scope of this effort. However, Rawlins, Reference 2-114, shows analytically that a wake has a shielding effect which becomes more prominent with increasing Mach number, up to M = 0.9. Some analyses to account for this problem is reported in Reference 2-115, which uses Rudds concept of sound scattering by turbulence, Reference 2-116; this study was performed for low airplane needs. This problem, especially at the high cruise speeds of interest requires further evaluation. No allowance for the influence of wakes on acoustic propagation is included in these predictions.

At high cruise speeds, the lifting surfaces are surrounded by a flow field whose local velocities can be much higher than that of the speed of the airplane. On the upper surface especially regions of supersonic flow exist, which are terminated by a shock wave. Since an acoustic wave travels at the local speed of sound the presence of this region could be an effective barrier to upstream noise propagation. This effect has not been specifically investigated in this study. Estimates of the noise attenuation could possibly be made using an "equivalent barrier" approach.

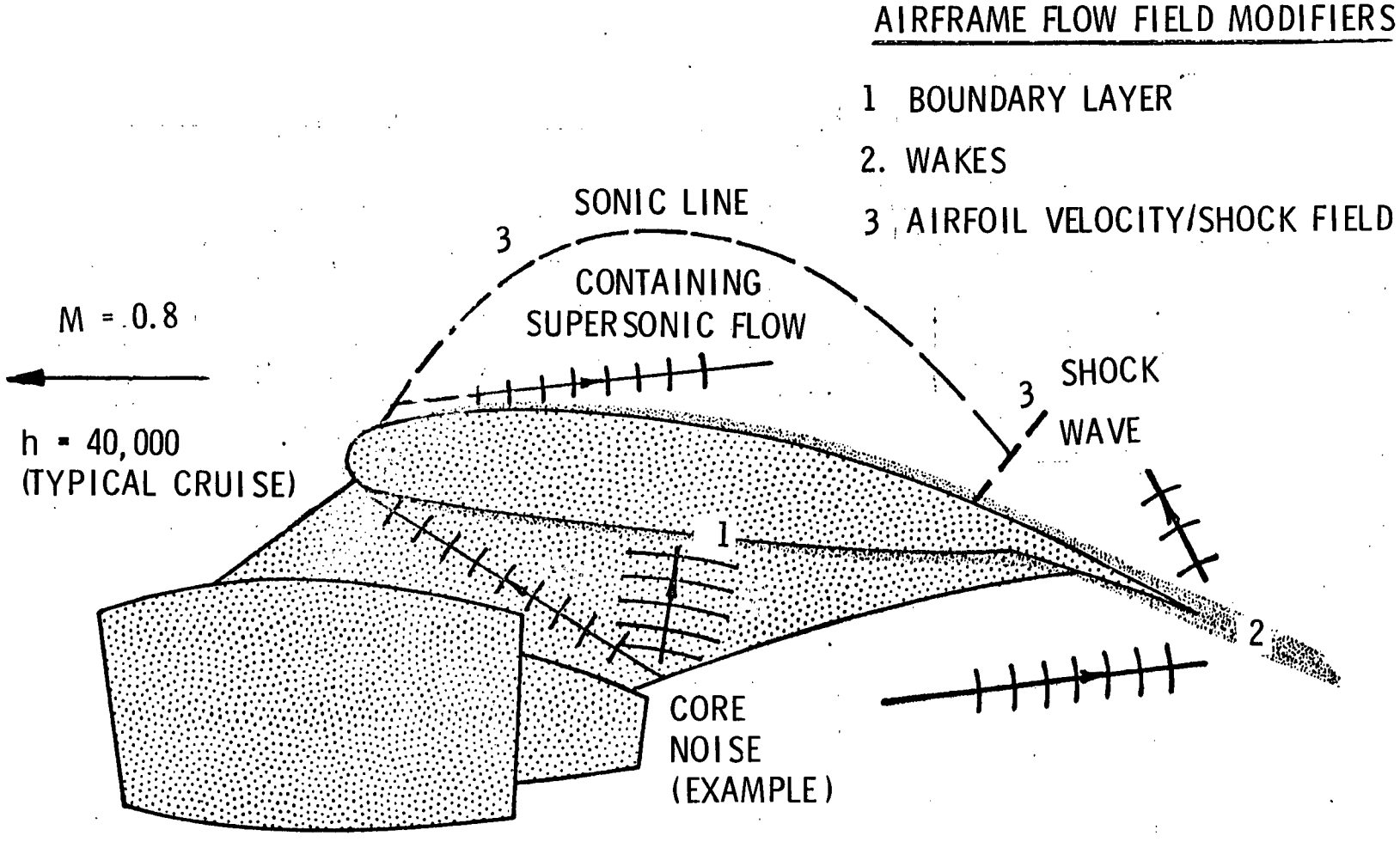

FIGURE 2-39. AIRFRAME FLOW FIELD PROPAGATION MODIFIERS

FIGURE NUMBER

ILLUSTRATION TITLE

For the sound field to finally reach the airframe surface it must travel through the adjacent boundary layer - which in this case must be laminar. Interaction with the boundary layer velocity gradient causes refraction (change of direction) of the incident wave front. This effect is included, for plane waves, in Section 3.

2.4.3.4 Airframe Shielding - The presence of an airframe surface in an acoustic free-field has two effects. First, a structural surface placed between a noise source and the receiver point can provide shielding, e.g. a reduction in observed noise. Second when the noise field is incident upon a surface an acoustic pressure increase can occur at the surface. These effects are shown schematically in Figure 2-40.

The beneficial effects of shielding have been investigated, analytically and experimentally largely in connection with static, far field point sources and stationary receivers. However, during cruise a moving noise source could be shielded by a moving surface. The noise source can be a point or a distributed noise source and the shielding effect of the surface will often be required in the near field. The simpler approach to estimating shielding effects (static, point source far field) predicted in References 2-117 to 2-120 and the most recent and extensive investigation of low speed wing shielding of Reference 2-121 were considered for use in this study.

References 2-117 and 2-118 present an analytical equation derived by R. O. Fehr for estimating the excess attenuation due to a rigid barrier. The experimental data as shown in these references show good agreement with Fehr's equation. The measured data do, however, show a practical limit of about 20 dB which Fehr's optical-diffraction theory does not predict. However, this equation is only applicable to a point source and a receiver located on the ground separated by a semi-infinite barrier in a still and homogeneous atmosphere.

Reference 2-121 presents a rather detailed and involved procedure for the estimation of wing shielding effects on turbomachinery noise at low speeds. This method was developed from experiment (using models and at low speeds)

M = 0.8

h = 40,000

(TYPICAL CRUISE)

AIRFRAME SURFACE MODIFIERS

1. BARRIER SHIELDING
2. EDGE DIFFRACTION
3. SURFACE REFLECTION

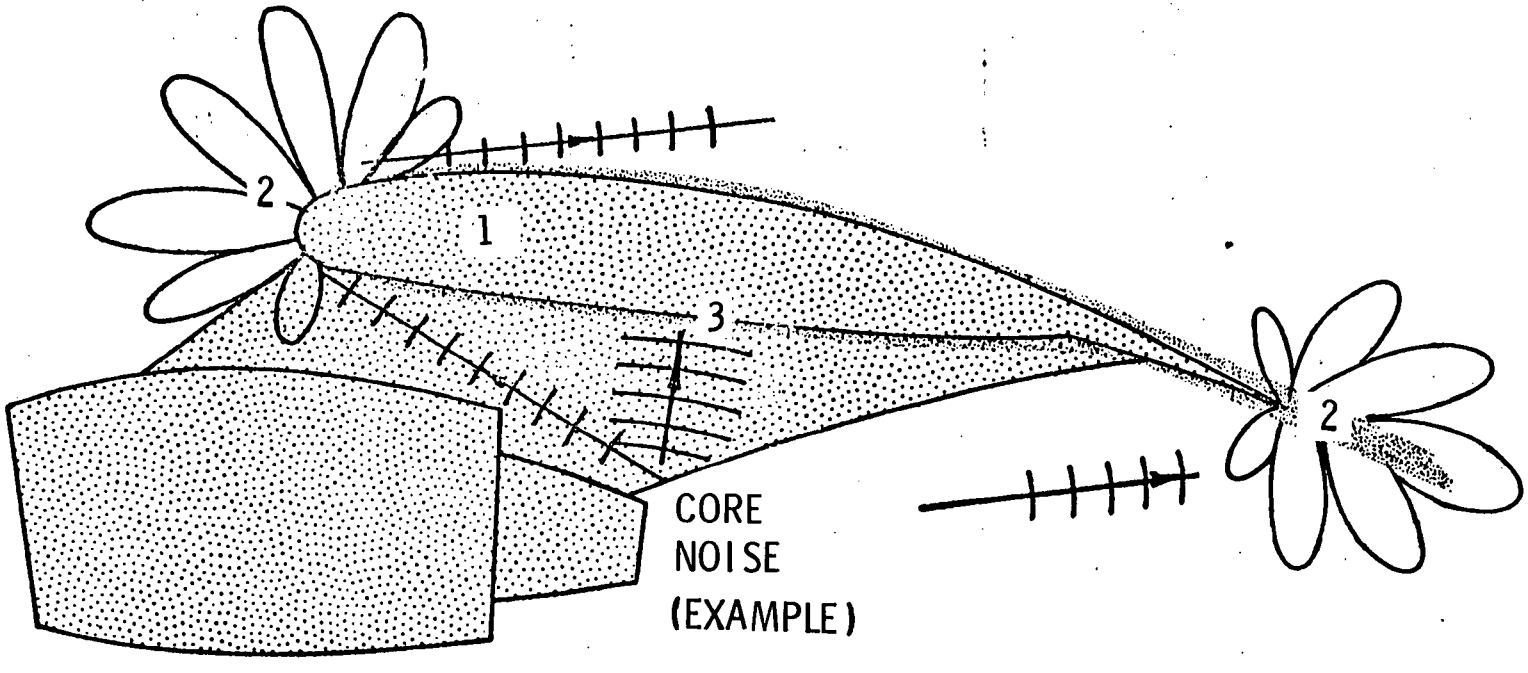

FIGURE 2-40. AIRFRAME SURFACE PROPAGATION MODIFIERS

using a theoretical model based on refraction and diffraction theory. Exhaust turbomachinery noise is said to appear as a distributed source which may be represented by two point sources. The effect of forward speed is treated by coordinate transformations for wave propagation in flow. Their empirically-adjusted theoretical model predicts a significant increase in shielding effectiveness with forward speed, but their wind-tunnel results show little if any effect. Sound scattering by the wing wake is said to account for this observation. Finally, it is recommended that low speed flight effects on shielding effectiveness be assumed negligible. Furthermore, it is not clear how this method might be applied to wing shielding of aft-fuselage mounted engines. Reference 2-121 also presents a method for estimating fuselage shielding. However, it is rather tentative in nature.

For application to shielding of point noise sources, considering the relative complexity of the method of Reference 2-121 - still a far-field predictor - and the uncertainty of forward speed effects, the simplified method has been selected for use in the present study. This method is considered to yield a reasonable estimate of wing or fuselage shielding effects although it is clear that considerable improvement is required in this area.

This shielding estimation procedure has not been verified for application to the near-field. However, if the basic prediction equation is applied to the near-field, the results indicate an increase in shielding effectiveness of about 5 dB regardless of frequency. Therefore, until a better method is developed, the equation will be applied to the near-field or, where the shielding surface cannot be represented by a simple barrier, the noise reductions of Figure 2-41 may be used. The noise sources which may be considered as point sources are the fan (forward and aft), core, turbine and jet shock screech. The locations of these noise sources has been identified elsewhere. Jet shock associated broadband noise is a distributed noise source. For shielding evaluation purposes it is proposed to treat this source as a point source whose location is at the first shock cell - a distance of 1.1L, downstream of the jet exit on the jet centerline.

For application to distributed noise sources, the single point shielding method can be extended on a source distribution basis. Here the noise source/

1/3 O.B. CENTER FREQUENCY (Hz)	SHIELDING dB
50	5.7
63	6.7
80	7.8
100	8.7
125	9.7
160	10.8
200	11.7
250	12.7
315	13.7
400	14.8
500	15.7
630	16.7
800	17.8
1000	18.7
1250	19.7
1600	20.0
2000	20.0
2500	20.0
3150	20.0
40000	20.0
5000	20.0
6300	20.0
8000	20.0
10000	20.0

FIGURE 2-41 ESTIMATED ONE-THIRD OCTAVE BAND NEAR-FIELD NOISE SHIELDING REDUCTIONS

FIGURE NUMBER

barrier/noise-receiver-location-geometry would vary for each element of the

ILLUSTRATION TITLE

distributed noise source - each of which would be regarded as a point source. The total noise level at the receiver would then be the sum of the individual shielded contributions. Should shielding affects need to be evaluated for radiated turbulent boundary-layer noise this method should be used. Then each elemental area, A_i, of the scrubbed surface would be treated as a point source. However, for jet mixing noise Reference 2-121 presents a completely empirical equation for far-field wing-shielding of jet noise. This prediction equation is said to include the effects of forward speed since shielded jet noise appears to scale on velocity in the same relationship as unshielded jet noise. This equation also accounts for the distributed source nature of jet noise. Therefore, this method is used to estimate wing-shielding effects for pylon-mounted engine configurations. The equation is modified by a constant, to approximate near-field values, to be consistent with near-field estimates for shielded point turbomachinery noise sources.

In the near-field a more precise knowledge of the acoustic pressure distribution may be required on the edge and in the vicinity of a shielding surface - such as the wing leading edge. Diffraction patterns exist around edges of shielding surfaces as shown schematically in Figure 2-40. An analysis of these patterns is beyond the scope of this study.

2.4.3.5 Airframe Reflection - Acoustic waves incident upon rigid surfaces are reflected. At the surface the acoustic sound pressure level can be increased over the free-field value. For example, a flat surface exposed to a normally incident plane wave will experience an increase of acoustic pressure of 6 dB over far-field pressure (surface pressure doubling), whereas for grazing incidence there is no increase in pressure. The increase in pressure is a function of the incidence angle. Thus wings, fuselage and empennage will have different local acoustic pressure surface amplification factors dependent upon their orientation relative to the noise source. The sound pressure level increase at the surface may be approximated by

$$\Delta dB = 20 \log_{10} (1 + \sin\theta)$$

3-42

FIG

1266

PAGE NUMBER

where θ' is the angle between the incident ray and the local tangent to the surface. For the cruise case the incidence to be used must be that associated with the transformed $\hat{\phi} = \phi'$.

However, in the interaction between noise and the boundary layer the acoustic pressure distribution is required not only at the surface but throughout the boundary layer. The acoustic criteria analysis section only requires as input the free field acoustic pressure, and the methodology there computes the necessary acoustic pressure changes throughout the boundary layer and at the surface.

FIGURE NUMBER

2.5 CRUISE-NOISE-PREDICTION-METHODS-MANUAL

ILLUSTRATION TITLE

The prediction methods manual, "Near-Field Noise Prediction for Aircraft in Cruising Flight" NASA CR159105, is a completely separate but companion document to this study volume. That volume is the result of the study reported here. Whereas this volume contains the background material for methods and transformation development, the Noise Prediction Methods Manual summarizes and explicitly defines all the prediction methods and equations. There the methods have been organized as computational algorithms. Each noise source has its own computational algorithm, from which computer programs may be developed. Computer programs are not a specific output of this study.

However, computer programs have been developed from the computational algorithm. The acoustical output of each program is the free field noise spectrum level at a specified point. To obtain the total noise at a point requires the use of all the separate noise prediction modules. To obtain a noise contour would require multiple use of the modules. Examples of these acoustical outputs are used as illustrations both in CR159105.

FIGURE NUMBER

2.6 AIRPLANE EXAMPLE

ILLUSTRATION TITLE

An example of the application of the cruise noise prediction methods is shown in Figure 2-42. The airplane configuration is high wing with engines mounted under the wing. The engines are advanced high bypass ratio turbofan engines (of the 1985-1990 time frame technology); the inboard engines are spaced 20 feet from the fuselage side wall. The airplane cruises at a Mach number of 0.8 at an altitude of 40,000 feet. The noise is computed at a point midway between the fuselage and the inboard engine at a wing midchord location. All the appropriate noise source cruise transformations have been applied. The noise levels are spectrum levels and are free field. In this example, the dominant noise sources are seen to be propulsion noise sources - jet shock associated broadband noise, fan and turbine noise. In this example no acoustic treatment has been applied to the fan inlet or discharge duct or to the turbine. Incorporation of an acoustically treated nacelle would considerably reduce the fan and turbine noise levels shown and leave the jet shock associated broadband noise as the dominant noise source throughout the frequency range. For the airframe noise sources, at this location, trailing edge noise is predicted to be higher than the noise radiated from the turbulent boundary layer.

At other locations, and for different engine/airframe configurations, different conclusions as to the relative importance of contributing noise sources could be drawn because of noise source directionalities and transformation effects.

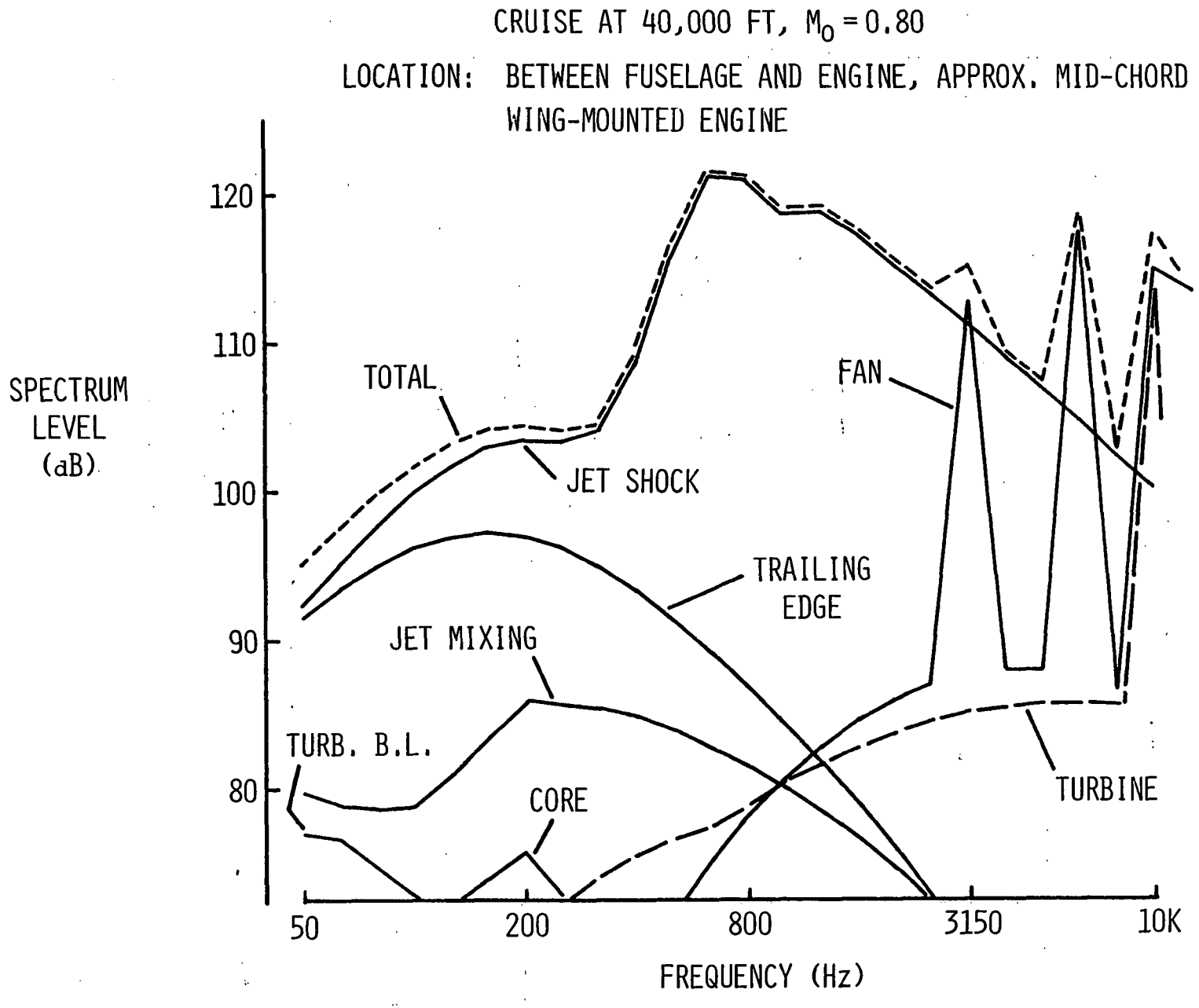

FIGURE 2-42. COMPOSITE NOISE SPECTRUM EXAMPLE

2.7 CONCLUDING REMARKS

The basic noise prediction techniques selected for use in this report represent significant advances in acoustic prediction technology over those available in the X-21A time period, 10 to 15 years ago. In fact some new noise sources have become apparent.

In the propulsion area, fan, compressor, core and turbine noise prediction techniques have recently been developed for far-field application to current high by-pass ratio turbofans. These turbomachinery noise components are considered similar to those appropriate for 1985 - 1990 engine time frame technology. It is shown here that these methods are also applicable to prediction of near-field noise. Each source requires its own co-ordinate system. The impact of low forward speed on these sources is still being explored. For jet noise the past near-field emphasis has been on mixing noise at low speeds. During cruise however, shock waves could exist in the jet efflux flow. But much work has recently been performed on the far-field noise of jet shock associated broad-band noise at low speeds and this data was used to predict jet shock associated broad-band noise. This data needs to be extended for better near-field representation.

In the airframe noise area it was concluded that for an advanced technology airframe that the dominant noise sources would be the turbulent boundary layer and the trailing edge. Methods were developed for the prediction of near-field noise fields of these distributed noise sources. It was concluded that by accounting for noise source elemental distribution and directivity and using inverse square law on these elements that predictions of the close in far-field total noise - which deviates from the inverse square law - could be made.

Laminar flow control system noise sources were separated into 1) external noise sources - which can be predicted using the propulsion noise source prediction techniques and 2) internal noise sources which are readily controllable.

Transformations for these noise sources to convert from the best noise data base, which were static or low speed at sea level, to the transonic condition of high subsonic speeds at altitude were developed. These covered 1) cruise effects on acoustic strength, 2) forward speed effects on acoustic propagation and, 3) aircraft configuration effects.

The final result, for each noise source, is the ability to predict acoustic spectrum levels, at the cruise operating conditions, from 45 to 11,000 Hz at any location. However, many recommendations for improving the validity and accuracy of these cruise noise prediction methods are made in Section 4.0.

The propulsion noise prediction methods of this report could also be used to predict 1) noise levels incident on fuselage at cruise for use in determining fuselage internal noise levels and soundproofing requirements and 2) noise levels incident on the airframe at static takeoff power for determining vibration and sonic fatigue acoustic loadings.

3.1 INTRODUCTION

From the point of view of design and operation of laminar flow control (LFC) wing surfaces subjected to noise fields, it is desirable to be able to predict whether a sound pressure level (SPL) at an arbitrary point on the surface is likely to cause premature transition to a turbulent state of an otherwise laminar flow. It has been established from experiments that sound can cause premature transition if the sound pressure level exceeds a critical value. This critical SPL is a function of the geometry of the surface and various parameters of the sound and mean flow fields.

In this section of the report the state of the art in the determination of the critical SPL relevant to the LFC/Acoustic criteria is discussed. Although the sensitivity of shear layers to sound under some conditions has been known for more than a century, it was not until the early nineteen sixties, the design period of the X-21A LFC wing, that quantitative tests were undertaken to establish LFC/Acoustic criteria for engineering applications (References 3-2, 3-3, 3-4). A summary of the findings of these and other tests and the factors and concept that led to the establishment of the X-21A LFC/Acoustic criteria are discussed in Section 3.2. In Section 3.3, limitations of the X-21A LFC/Acoustic criteria are discussed, and in Section 3.4 a semi-analytic method is proposed to overcome the limitations and some numerically computed critical SPL spectra are presented. An example case of the application of the improved criteria is also shown.

The X-21A LFC/Acoustic criteria are empirical criteria based on the concept that "Noise is expected to cause transition through much the same process as freestream turbulence". Certain observations on the response of boundary layer disturbances to sound and certain characteristic features of sound induced transition suggest the need for a more fundamental and rational approach in which the coupling between a sound wave and a boundary layer disturbance can be quantitatively evaluated. Such an analysis has been developed at Lockheed-Georgia, and is described in Section 3.5. It is based

on the hypothesis that boundary layer disturbances are governed by the linearized fluctuating vorticity transport equation (Orr-Sommerfeld equation) and that if sound is to excite such disturbances, it must be able to produce fluctuating vorticity or a fluctuating flux of vorticity. An analysis of the acoustics of shear layers shows that sound can induce both fluctuating vorticity and fluctuating vorticity flux and that such effects are limited to the boundary layer region only. The derived governing equation obtained by linearizing the vorticity transport equation is in the form of an inhomogeneous Orr-Sommerfeld equation with source terms proportional to the sound field. Integral solutions are obtained for the general case. Numerical solutions are then computed for the special case of low frequency sound impinging in the boundary layer of a rigid semi-infinite plate. The results compare favorably with a corresponding set of measurements.

In Sections 3.6 and 3.7, comments are respectively made regarding excitation by more than one discrete component of the sound field and on sound induced disturbances in the presence of cross-flow.

FIGURE NUMBER

3.2 OBSERVATIONS ON SOUND INDUCED TRANSITION AND THE X-21A LFC/ACOUSTIC CRITERIA

ILLUSTRATION TITLE

3.2.1 On Transition Mechanisms

Based on the experimental observations of Schubauer and Skramstad (Reference 3-5), transition is preceeded by selective amplification of boundary layer disturbances. Such disturbances (in the boundary layer of a flat plate) were predicted, long before they were observed experimentally, by Tollmien (Reference 3-6) as solutions of the Orr-Sommerfeld equation, and are known as Tollmien-Schlichting (T.S.) waves. The Orr-Sommerfeld equation, which is the linearized form of the convected vorticity transport equation, has been the most widely studied equation in recent years and is indeed the basis for all stability and transition prediction schemes. The nature of the solutions of the Orr-Sommerfeld equation and the stability limits are governed by the mean flow profiles which are in turn governed by the geometry of the surface and the mean pressure gradients (Reference 3-1). Boundary layer disturbances associated with two-dimensional flows over flat or convex surfaces are categorized as Tollmien-Schlichting waves, and are influenced by the viscous forces (Reynolds number). In flows over concave surfaces (or mean flows whose streamlines are concave, for example near suction slots), boundary layer disturbances are categorized as Taylor-Gortler vortices, and are influenced by the centrifugal force arising from the curved streamlines. Another class of instability commonly known as inflectional instability, occurs when the mean velocity profile contains an inflection point; such profiles are found in many practical flows, for example in regions where the pressure increases in the direction of the flow, and in particular the spanwise flow on swept wings.

Although the Orr-Sommerfeld equation describes adequately the propagation and amplification or decay of boundary layer disturbances, it is not adequate to describe the transition mechanisms which appear to correspond to some kind of breaking up of the coherent boundary layer waves accompanied by spectral broadening. No complete theory is available for describing the transition mechanisms. For this reason a combination of theory and empiricism has been the basis for the best transition prediction.

Based on linear stability analysis, a total amplification corresponding to e^9 appears to correlate and predict reasonably well the effects of body shape, pressure distribution and suction effects on transition (Reference 7). On the other hand, measurements on transition induced by freestream turbulence show that the turbulent intensity exerts a decisive influence on the location of transition. The transition Reynolds number $[R_T]_T$ reduces with increase of freestream turbulence intensity. If the beginning of transition can be associated with the attainment of some threshold value for the disturbance velocity ratio after amplification, as shown by the measurements of Klebanoff and Tidstrom (Reference 3-8), then it follows that the initial amplitude (level) and spectrum of freestream disturbance play a key role as shown by the measurements of Wells (Reference 3-9) and Spangler and Wells (Reference 3-10.)

For reasons similar to turbulence induced transition, acoustically induced transition can at best be a similar combination of theory and empiricism.

3.2.2 Observations of the Effects of Sound on Boundary Layers

Apart from establishing that transition is preceeded by selective amplification of boundary layer disturbances, Schubauer and Skramstad (Reference 3-5) showed that sound of a given frequency could excite T.S. waves of the same frequency even though the wave-lengths (of the sound and the T.S. waves) were vastly different. Phase measurements showed that the T.S. wave propagates with a phase speed of less than half of the freestream mean velocity (a result in agreement with stability calculations). Sensitivity to sound of attached or free shear layers, including jets and wakes, has been known for a long time. For sound induced transition prediction, although it appears a sufficient condition that sound excites boundary layer disturbances which can then be related to transition induced by freestream turbulence, it is desirable to understand physically the mechanisms involved and express them mathematically with view to evaluating the coupling. This is discussed further in Section 3.5.

Schubauer and Skramstad did not specifically investigate quantitatively the influence of SPL on transition, but noted "transition could be moved one or two feet ahead of its natural position by the right combination of sound intensity and frequency. In general, random noise from the loudspeaker produced similar results, but the effect on the oscillations (boundary layer response) was not so marked". A significant result is the observation that, in regions prior to transition, the amplitude of the sound excited boundary layer disturbance is linearly related to the SPL (Reference 3-11 thru 3-14).

Klebanoff and Tidstrom (Reference 3-8) made a very comprehensive experimental investigation of natural and externally excited transition mechanisms, but did not use sound as their boundary layer disturbance. They used instead, a vibrating ribbon and studied effects of level of excitation. One important set of results shows that the location of transition could be moved upstream by increasing the level of excitation, and more importantly for their particular setup (flat plate without suction), transition occurred whenever the ratio (u'/U) amplified to a value of about 7.5% irrespective of the level of excitation. These results are reproduced in Figure 3-1 of this report for two reasons. First, it shows the importance of level of excitation and the threshold value at transition of (u'/U_∞) (where u' is the boundary layer fluctuating velocity component in the flow direction and U is the freestream mean velocity). Second, when we discussed a similar set of measurements (in the next paragraph), but with sound as the exciting field, we shall be able to distinguish the difference between a localized (vibrating ribbon) and an extended source of excitation.

Shapiro (Reference 3-14) investigated the boundary layer fluctuation on a flat plate excited by a sound wave propagating in the direction of the mean flow. One interesting feature of his results was that boundary layer fluctuations of the same frequency as the sound were detected and their growth rates measured along the plate. This set of results is reproduced in Figure 3-2 for comparison with Figure 3-1 showing results of Klebanoff and Tidstrom using a vibrating ribbon. Although both sets of curves show that the externally

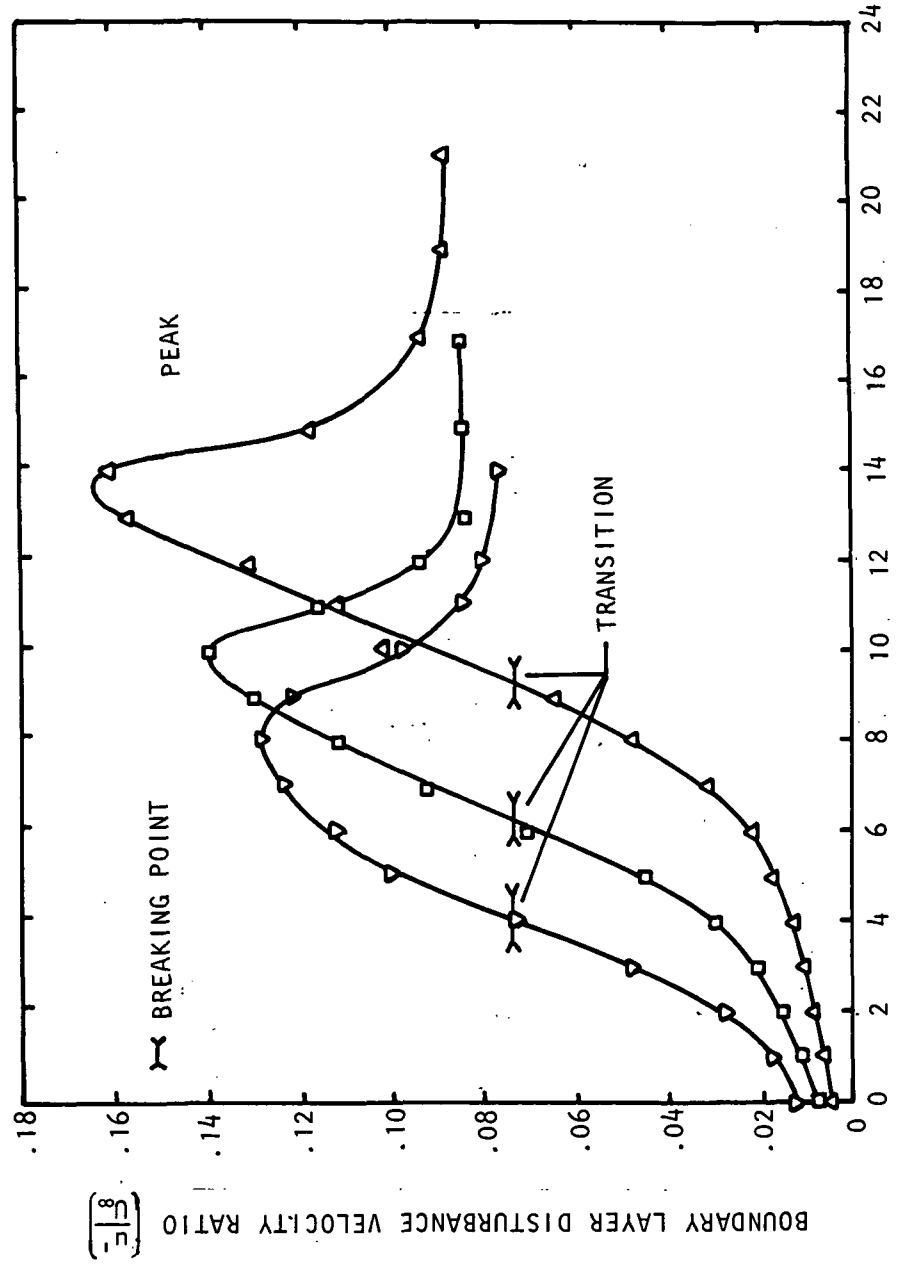

Figure 3-1. Growth in wave intensity in boundary layer of a flat plate for different input levels of vibrating ribbon. $y = 0.046$ inch; frequency, 145 cps. From Klebanoff and Tidstrom, reference 3-8.

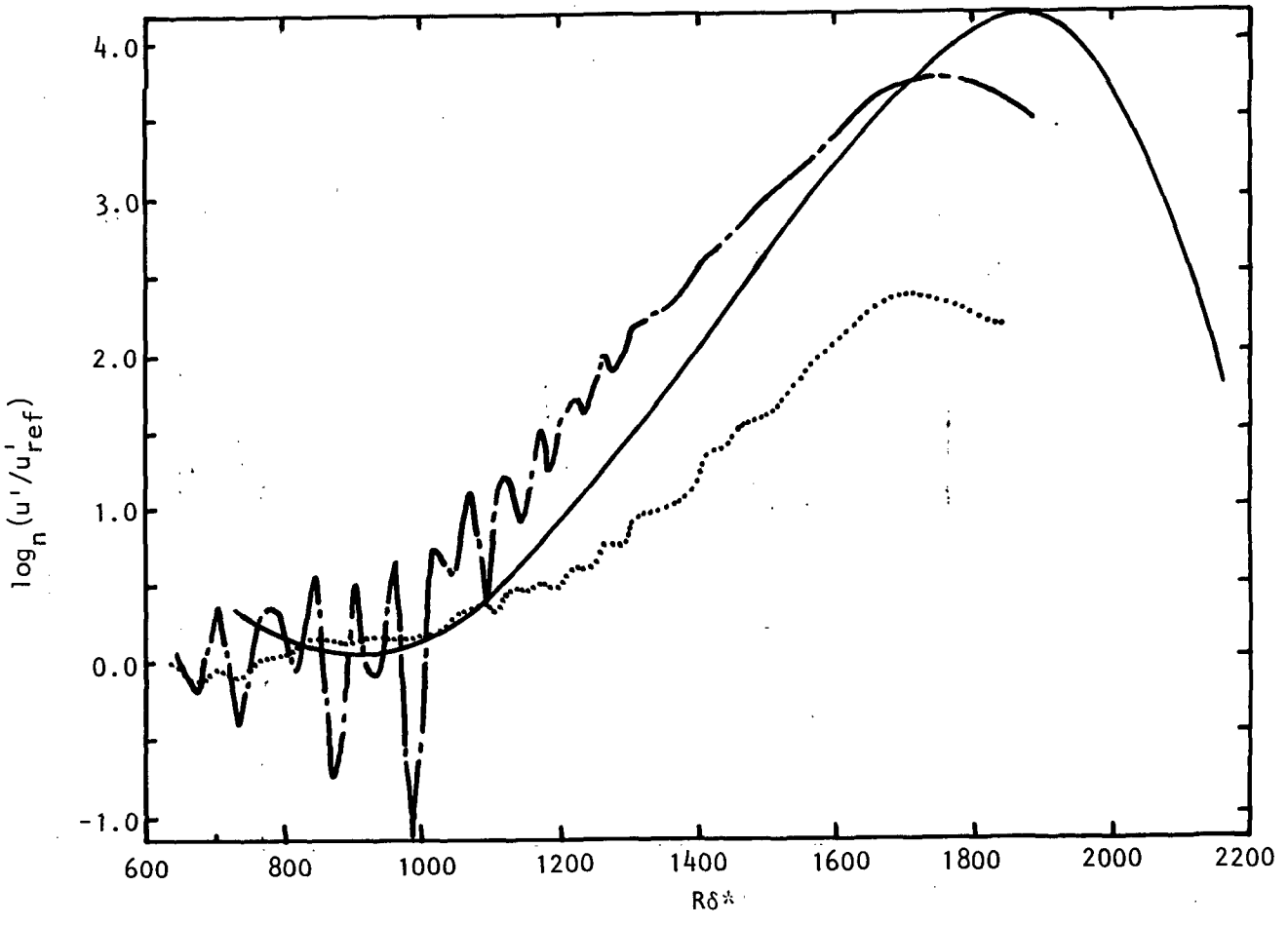

Figure 3-2. Natural and sound (plane wave along flow) excited Tollmien-Schlichting growth data U_∞ = 29 m/sec, f = 500 Hz from measurements on a flat plate by Paul Shapiro, reference 3-14.

excited boundary layer disturbances amplify as they propagate, at least in the range considered, the amplitude of the sound induced disturbance appears to be modulated spatially, especially in the regions where the amplitude is relatively lower. Such spatial modulation has also been observed by Schilz (Reference 3-15) and Mechel and Schilz (Reference 3-16) and no doubt is also related to the chordwise striations observed by Pfenninger using Napthalene sublimation test. This will be discussed further in later sections. This marks the first difference between boundary layer disturbance excited by a vibrating ribbon which constitutes a localized source and by a sound field which constitutes an extended source.

In a series of tests connected with development of LFC/Acoustic criteria for the X-21A design, a straight and a swept airfoil were subjected to sound fields of varying amplitudes and spectra (References 3-2 thru 3-4). On flat plates and sucked airfoils, it was shown that sound can induce transition if the sound pressure level exceeds a critical SPL. This feature (the SPL having to exceed a critical SPL) is similar to transition by freestream turbulence. This belief is reinforced by the further evidence that the critical SPL can be increased by increasing the suction velocity, similar to stabilizing flows with high freestream turbulence intensity.

3.2.3 The X-21A LFC/Acoustic Criteria

Based on the hypothesis that "Noise is expected to cause transition through much the same process as freestream turbulence", the X-21A LFC/Acoustic criteria (Reference 3-3) were derived using empirical data relating transition Reynolds number and disturbance velocity ratio as shown in Figure 3-3. The disturbance velocity, used in computing the velocity ratio corresponding to transition for each of the test points, primarily represents total tunnel turbulence which normally contains energy over a wide range of frequencies, except for AMES data (both for flat plate and sucked airfoil) in which case the fluctuating particle velocity was calculated from the noise level measured at one point in the tunnel using plane wave acoustics for an ambient medium.

A regression line drawn through the sucked airfoil data appear to link up most of the data points and this line was used as the transition criterion for the

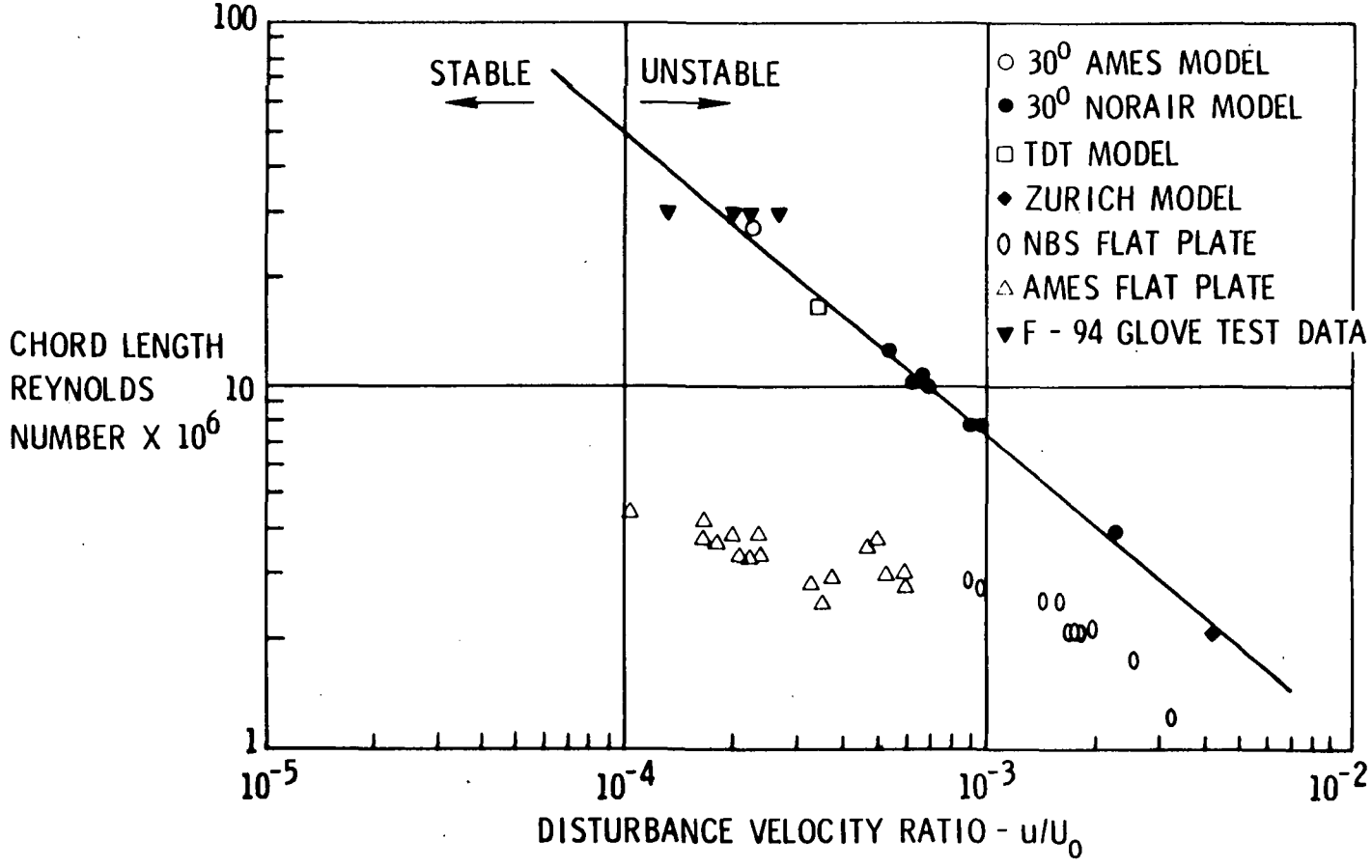

Figure 3-3. The X-21A LFC/acoustic criteria (reference 3-3)
disturbance velocity ratio u'/U_∞
chord length Reynolds number x 10^6

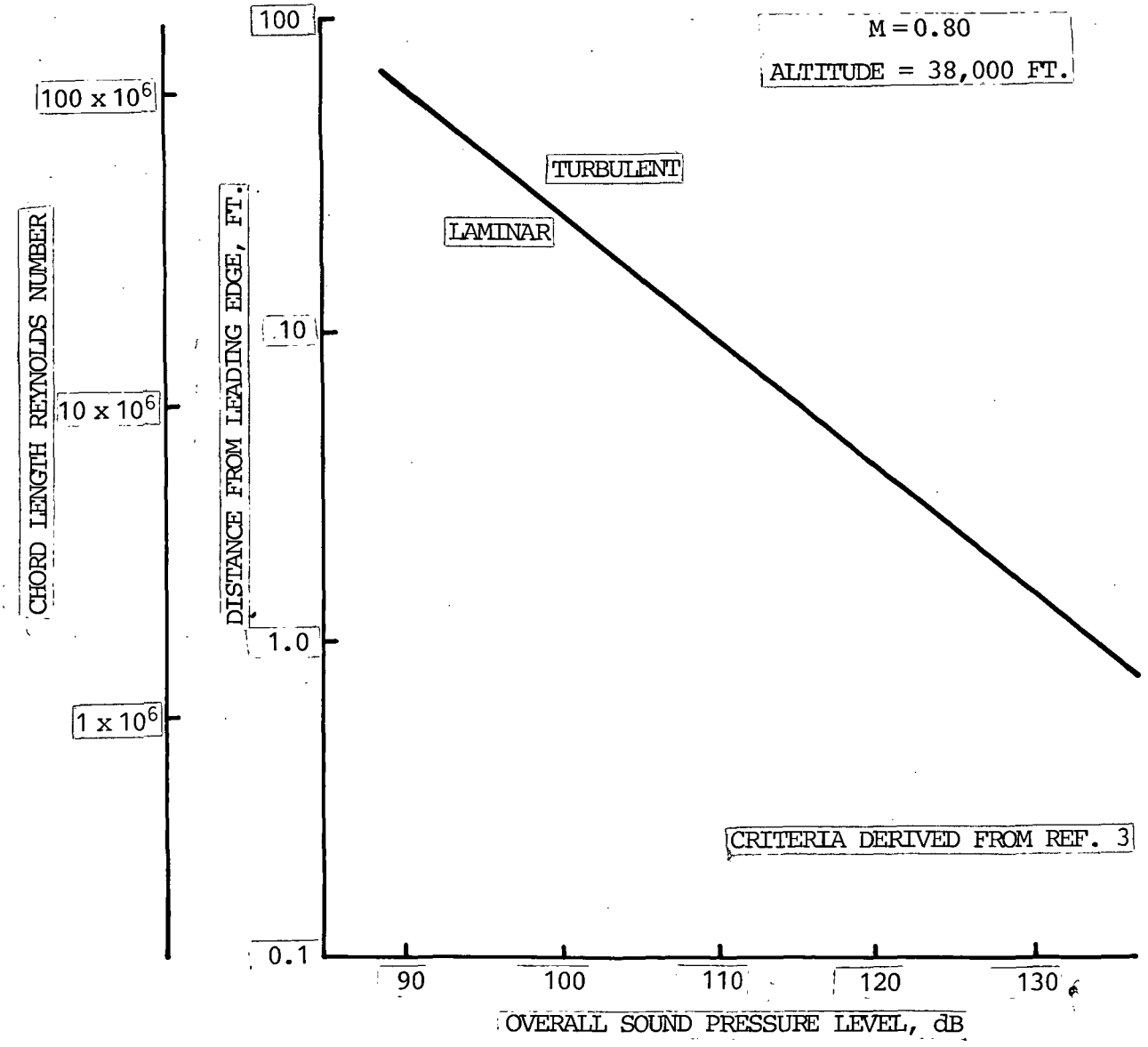

Figure 3-4. Initial Lockheed/X-21A acoustically induced transition criteria, derived from reference 3-3 for cruise speed of Mach 0.8 and altitude of 38,000 feet. Distance from leading edge in feet.

X-21A design. On the assumption that "noise is expected to cause transition through much the same process as freestream turbulence", the critical disturbance velocity ratio can be converted into critical SPL using the following plane wave relationship: If

ILLUSTRATION TITLE

$$SPL = 20 \log (P/P_{ref}) \qquad (3\text{-}1)$$

where $P_{ref} = 2 \times 10^{-4}$ dynes cm^{-2}

Then $P = 10^{(SPL/20 - 3.7)}$

and using $u' = P/\bar{\rho}c$

$$\frac{u'}{U_\infty} = \frac{P}{\rho c^2 M_\infty} = \frac{10^{(SPL/20 - 3.7)}}{\gamma P_\infty M_\infty} \qquad (3\text{-}2)$$

With $M_\infty = 0.8$ and the mean pressure P_∞ at an altitude of 38,000 feet, a curve equivalent to Figure 3-3 was produced, relating the transition Reynolds number to critical SPL, and is shown in Figure 3-4 and represents the early Lockheed/X-21 LFC/Acoustic criteria (Reference 3-17.)

Curves like those depicted in Figures 3-3 and 3-4 are extremely useful design tools because of their simplicity, except for some limitations and reservations about the basic hypothesis. Assuming the hypothesis is correct, the curves allow determination of whether a specified SPL at an arbitrary point along the chord of a wing is likely to exceed the critical SPL (above which premature transition takes place) and by how much, permitting corrective steps to be taken if necessary.

Corrective measures involve one of two alternatives. First, the amplitude of the incident sound field could be reduced to values such that the SPL or associated particle velocity ratio is less than the critical SPL or $(u'/U)_{crit}$ respectively corresponding to the particular suction level on the airfoil. The second measure is to alter the suction level either as a whole or in local areas, and is discussed next.

3.2.4 Effects of Suction on Criteria

Both stability analysis (Reference 3-1) and Northrop Norair test results (Reference 3-3) show that for any specific model, a major controllable parameter influencing the critical value of (u'/U_∞) and the corresponding critical SPL is the suction velocity as shown in Figure 3-5. The stabilizing effect of increased suction is due to two reasons: (1) a reduction in the boundary layer thickness, and (2) a modified velocity profile that is more stable. Although it appears natural to use suction as a controllable parameter for corrective measures just in case the incident SPL exceeds the critical SPL, unfortunately there are other constraints that limit to what extent such a measure can be used. For example, if the suction is increased to the point where the boundary thickness is smaller than the surface irregularities, then a new source of velocity fluctuation due to surface roughness can trigger transition.

Sometimes it is possible to increase the critical value for (u'/U_∞) and the corresponding critical SPL by modifying the suction distribution rather than increasing suction uniformly. The sensitivity of critical SPL to suction quantity $C_q/C_{q_{opt}}$ (normalized by suction quantity for minimum drag) taken from Reference 3-3 is shown in Figure 3-6 both for uniform and modified suction distributions. C_q is defined as $(\bar{\rho}\bar{V})_{wall}/(\bar{\rho}U)_\infty$. It is evident that modified chordwise suction distribution is more desirable than a uniform increase. At the time of the X-21A test program, finding a suitable suction distribution had to be done by trial and error and as such was more of an art.

Quite recently Nayfeh and Elhady (Reference 3-18) and Lekoudis* of Lockheed-Georgia have shown from numerical solutions of the stability equation that distributed suction (suction through slots) can be made to yield amplification rates of the same order as with uniform suction.

Thus, from Figure 3-6, it appears that if the incident SPL exceeds the critical SPL by as much as 10dB, transition can be avoided if the suction quantity could be increased by about 20% using a modified distribution; if the suction had to be increased uniformly, it appears that transition could not have been avoided due to the asymptotic nature of the curve. An increase of 60%

*Private communication.

in the suction quantity only shifts the critical SPL by 8dB. The sensitivity of critical SPL or (u'/U_∞) on suction rates, frequency, pressure gradient and geometry can also be evaluated from solutions of the stability equation and will be discussed further in Section 3.3, following a discussion of the limitations of the X-21A and early Lockheed-X21A LFC criteria.

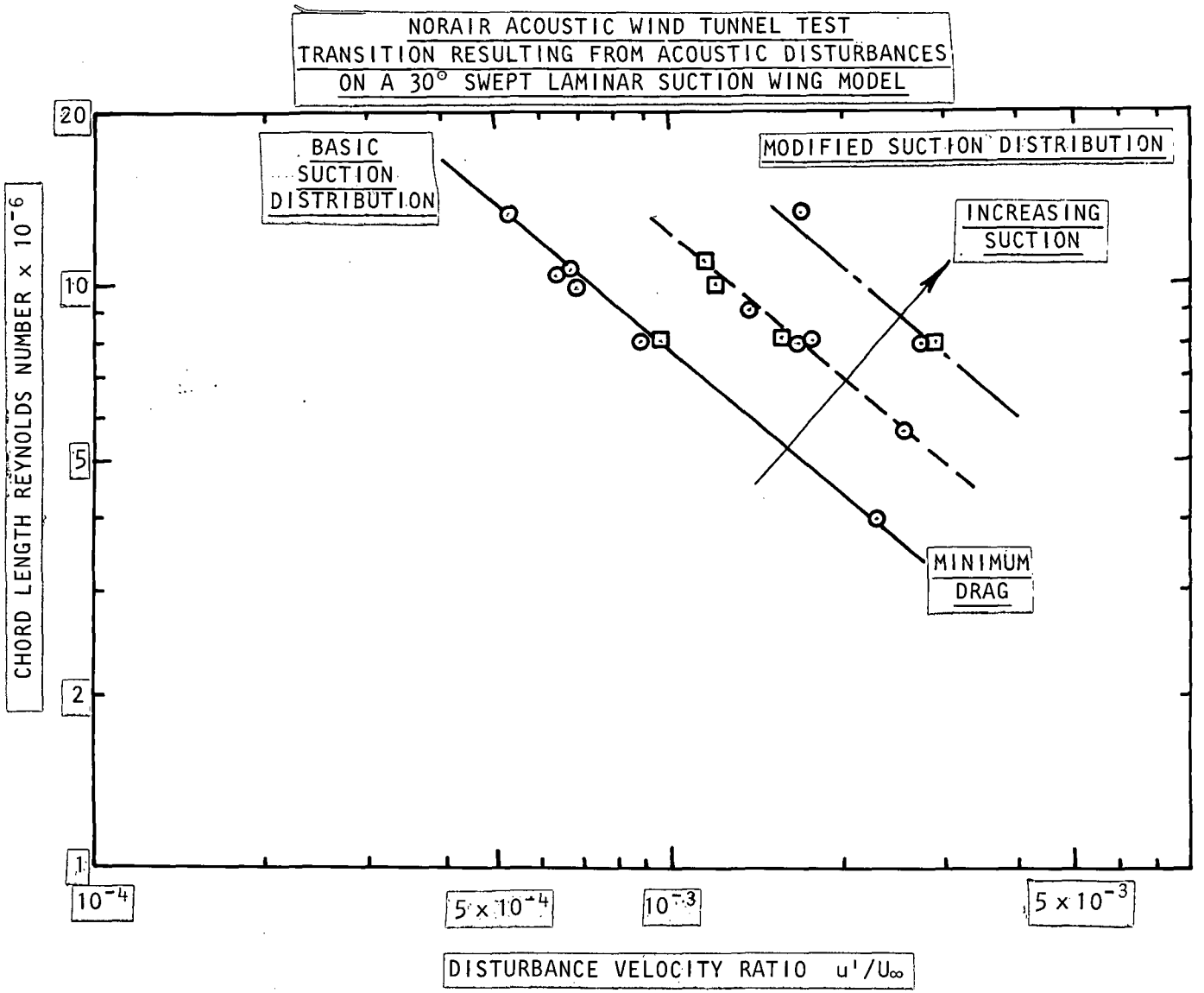

Figure 3-5. Influence of suction on Reynolds number at transition from reference 3-3.

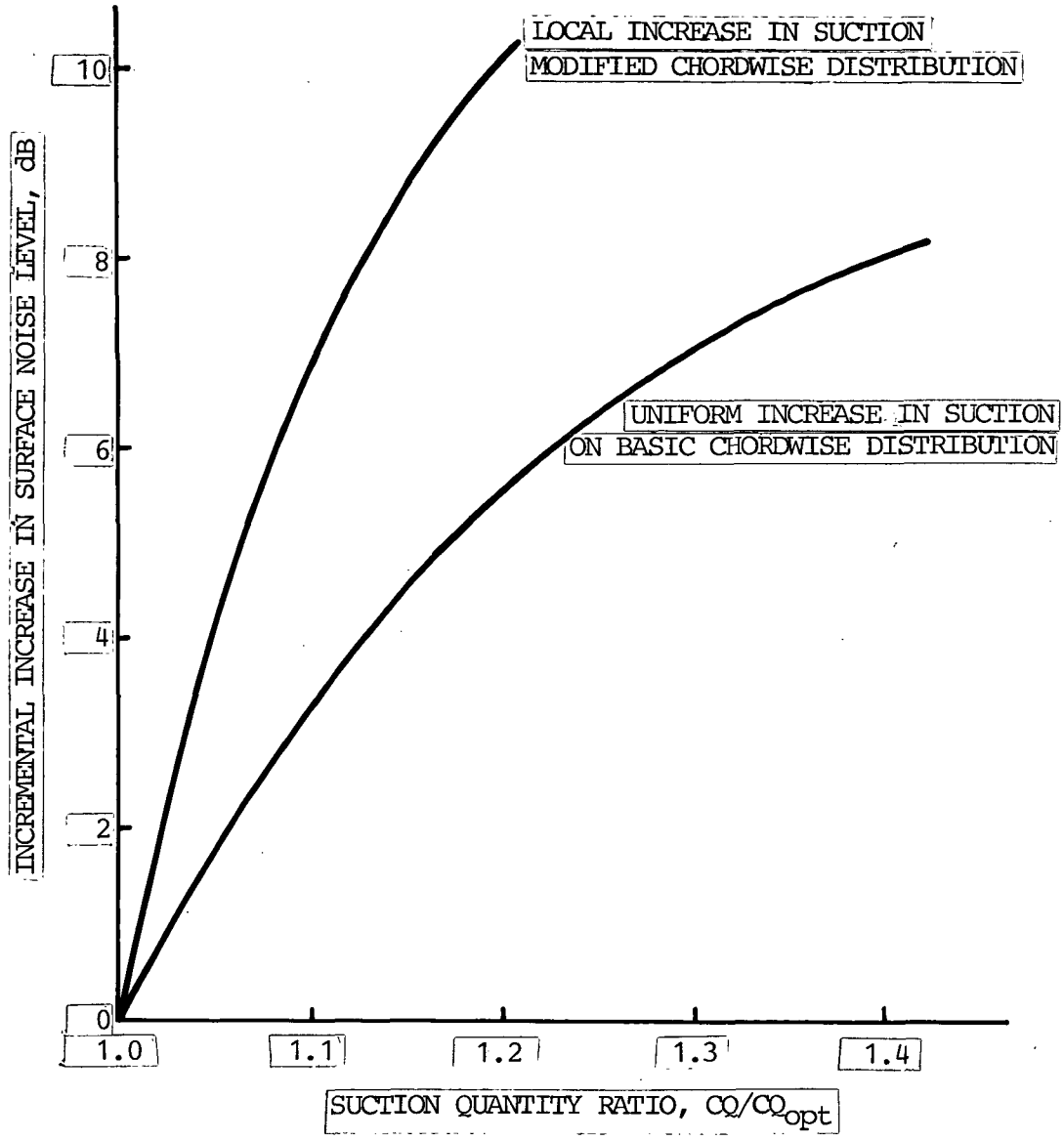

Figure 3-6. Sensitivity of critical SPL with increased suction, from references 3-3 and 3-17

3.3 LIMITATIONS OF X-21A LFC/ACOUSTIC CRITERIA

3.3.1 Frequency Sensitivity of Sound Induced Transition

Linear stability analysis predicts that the amplification of boundary layer disturbances is frequency dependent and in Section 3.2.1 (on transition mechanism), it was asserted that the initial amplitude (level) and spectrum of freestream disturbance must play a key role on the location of transition (an experimentally established fact). Using similar arguments it can be expected that the spectrum of the incident sound field is as important as the amplitude. The measurements of Wells (Reference 3-9) and Spangler and Wells (Reference 3-10) have shown how very sensitive the transition Reynolds number is to the spectrum of the turbulence and to the sound field, respectively. The results of Spangler and Wells are reproduced in Figure 3-7. These sets of curves of R_T versus (u'/U_∞) (for unsucked flat plate) are plotted in the same traditional manner as those used on the X-21A criteria for sucked airfoils. The disturbance velocity ratio (u'/U_∞) corresponds to the spectrally integrated value. For this reason, the curve corresponding to the X-21A criteria cannot be expected to show frequency sensitivity and affects the degree of confidence on the predicted critical SPL. In fact, the Northrop team went at length to assess the frequency sensitivity. Their results reproduced from Ref. 3-4 are shown in Figure 3-8a in the form SPL_{crit} in dB vs frequency for discrete and octave band sound impinging externally on a 30° swept sucked wing at a chord Reynolds number of 12.5×10^6. The main observation from this figure is that with both discrete and octave band sound, critical SPL is sensitive to frequency. Discrete frequency is more effective in inducing transition in that it requires a lower SPL compared to the broadband sound.

The depth of the trough in the plot of SPL_{crit} vs frequency of Figure 3-8a, is a measure of the lack of confidence in the use of the X-21A or the related early Lockheed/X-21A LFC criteria. For that particular airfoil and the prevailing suction and Reynolds number, the depth of the trough is 15dB. It will be shown later in the section on proposed extension of the X-21A criteria, that the depth of the trough is a function of suction, Reynolds number and directionality of the sound field.

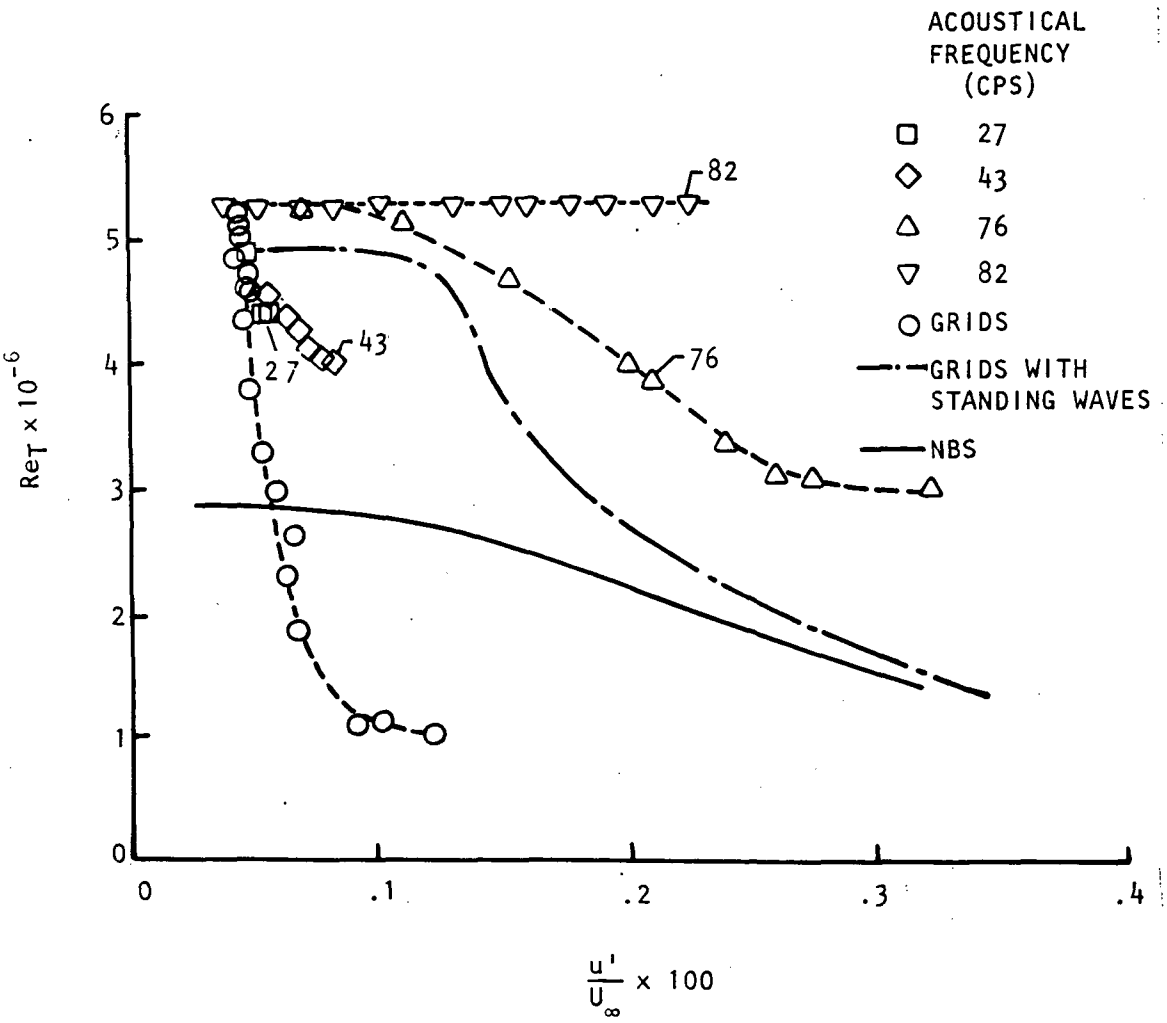

Figure 3-7 Effects of freestream disturbances containing narrow band acoustic components on boundary layer transition from Spangler and Wells, reference 3-10.

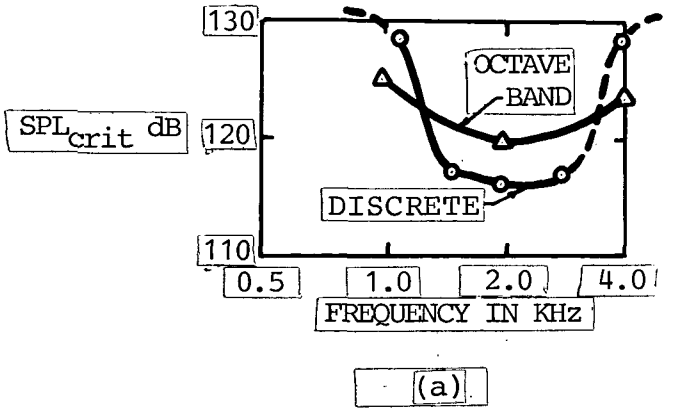

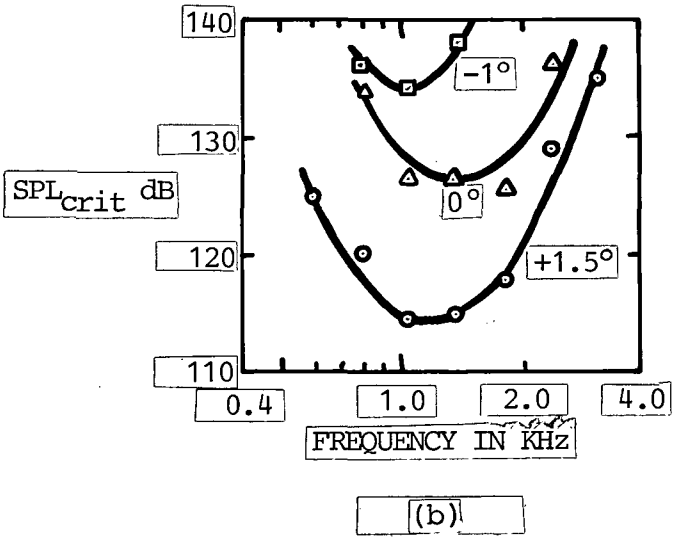

Figure 3-8. Sensitivity of critical SPL spectrum with
(a) acoutic spectrum
(b) angle of attack

FIGURE NUMBER 19

Other Frequency Effects - Mechel, Mertens and Schliz (Reference 3-19) observed that the flat plate boundary layer response to sound can be divided into three frequency ranges.

ILLUSTRATION TITLE

a. At sound frequencies below a critical value, there appears to be no interaction.

b. At intermediate sound frequencies there is an increase in the boundary layer disturbance which can lead to premature transition.

c. At high sound frequencies the interaction is such as to reduce the level of natural disturbance, leading to delayed transition.

In both intermediate and high frequency ranges, it was observed that sound modified the propagation exponent of the boundary layer disturbance.

Although the low and intermediate frequency effects can be qualitatively explained by stability analysis alone, the high frequency observations require a coupled acoustic and boundary layer field approach which will be discussed in Section 3.5.

3.3.2 Sensitivity to Internal Noise and Angle of Attack

Another observation with the X-21A test program was that internal noise through the suction slots could also induce transition and that the critical SPL was frequency selective as with external sound fields. Further, the critical SPL spectrum was a function of the angle of attack as shown in Figure 3-8b.

3.3.3 Effects of Acoustic Standing Waves

To investigate the effects of acoustic standing waves in an LFC suction system, Aiutolo* used a discrete tone to set up a spanwise standing wave in a chamber beneath a suction slot. Using napthalene sublimation tests, it was observed

Oral presentation during workshop on Laminar Flow Control held at NASA/Langley, April 1976.

that the external flow field was turbulent in regions along the span where the standing wave pressures were maxima; and in regions where the standing wave pressures were minima, the flow field was still laminar. This standing wave induced transition mechanism is similar to a setup by Mechel, Mertens and Schliz (Reference 3-19) who used a loudspeaker behind a porous plate enclosed in an airtight chamber. It was suggested by the authors of Reference 3-19 that the sound radiation through their porous plate (or slot for the Northrop test) could be regarded as periodic suction and blowing. The strong influence of a small amount of suction on a marginally unstable flow is well known and has been briefly mentioned earlier. If a flow is marginally stable, then in the blowing phase of the standing wave pattern, it can be expected to go turbulent. This was confirmed from the measurements of Reference 3-19 in a low frequency experiment in which the period of the sound signal was large compared to the time of turbulent spot generation. Even if the blowing phase did not cause transition directly, as will be the case when there is also present a mean steady suction, the resulting fluctuating suction at the slot gives rise to a source of fluctuating vorticity which may amplify as it convects downstream. This will be discussed further in Section 3.5.

3.3.4 Effects of Directionality of the Sound

The only investigation of the effects of directionality of an incident plane sound wave on the boundary layer response over a flat plate was carried out in the same series of tests undertaken for the X-21A program, and was limited to two angles, along (longitudinal) and at right angle (transverse) to the mean flow. The relevent results were shown in Figures 20 and 21 of Reference 3-2. The main conclusions that can be drawn from those results are as follows. Both longitudinal and transverse sound waves excite T-S waves. The critical SPL (for acoustically induced transition) are frequency dependent in both cases. In the case of transverse sound waves, the initial SPL is slightly higher than for the corresponding longitudinal case; depending on frequency and Reynolds number, the difference varies between 2 and 10dB.

3.3.5 Summary of Limitations of the X-21A LFC/Acoustic Criteria

The disturbance velocity ratios (u'/U_∞) in the X-21A LFC/Acoustic criteria represent spectrally integrated values and cannot be expected to show sensitivity to the frequency and directionality of the sound wave. Thus the degree of confidence on the critical SPL predicted using the X-21A criteria is of the order of the maximum variation of the measured critical SPL with frequency and/or directionality. These are of the order of 10 to 25dB for frequency, depending on spectrum of the sound field (less for broadband and more for discrete tones), and 2 to 10dB for directionality, and possibly more if the sound was travelling upstream (no data available for this case).

To improve the degree of confidence in the use of the X-21 criteria, the latter must be modfied to include at least the frequency and directional effects. To achieve this in a completely empirical manner, the limited frequency tests have to be repeated over the whole range of Reynolds number and several angles of incidences, including upstream acoustic waves. An alternative approach is a semi-empirical method which is discussed next.

3.4 IMPROVED LOCKHEED/X21A LFC ACOUSTIC CRITERIA

Presented in this section are semi-empirical criteria that have been evolved from the use of an approximate solution derived from a fundamental approach (developed at Lockheed-Georgia and discussed in Section 3.5) that relies on an empirical constant. This empirical constant defines the level to which the acoustically induced boundary layer disturbance must amplify before transition sets in. For example, for a flat plate in the absence of pressure gradients, Klebanoff and Tidstrom (Reference 3-8) found (u'/U_∞) at transition to be equal to 7.5%. This value can be quite different for a sucked airfoil and is therefore left as an empirical constant.

The fundamental approach to acoustically induced transition is derived from a linearization of the vorticity transport equation and is based on the concept that when sound intercepts a boundary layer, an acoustically induced fluctuating vorticity field is set up. Although the relative phase of such a vorticity field is the same as that of the sound field, its convection, propagation, amplication (or decay) and ultimate diffusion are governed by the linearized convected diffusion equation, which in another form is the Orr-Sommerfeld equation. Thus the equation governing sound induced boundary layer disturbances is expected to be in the form of an inhomogeneous Orr-Sommerfeld equation and for the two dimensional case may be written in the form (see Section 3.5 for more details).

$$L\psi = Q(\omega, u_a, v_a, U, U', U'') \qquad (3\text{-}3)$$

where ψ is the stream function associated with the boundary layer disturbance; L, the Orr-Sommerfeld operator is given by

$$L = \nu \nabla^4 - \frac{\bar{D}}{Dt} \nabla^2 - \frac{d^2U}{dy^2} \frac{d}{dx} \qquad (3\text{-}4)$$

and Q is the rate of change of the acoustically induced fluctuating vorticity, including convective transport. U, U' and U" are the mean flow profile and its first and second transverse derivatives. u_a and v_a are the streamwise and transverse particle velocities associated with the sound field, and may be expressed in terms of the incident sound pressure level, angle of incidence and

spectrum. In this concept, it is not the particle velocity of the sound field that is equated to that of the TS wave which is then allowed to amplify, but rather that terms proportional to the fluctuating vorticity associated with the sound wave (in the boundary layer) constitute the source term for exciting the TS wave.

When evaluating the source term, the scattering of the incident acoustic field by the flat plate (reflection from the surface and diffraction from the leading edge) and the convection and refraction of the combined field must theoretically be taken into account. These effects can be evaluated by solving the convected acoustic wave equation. Once the amplitude and spatial distribution of the acoustically induced fluctuating vorticity source term of Equation 3-3 are known, a formal solution for the acoustically induced boundary layer disturbance velocity ratio (u_b/U_∞) may be derived from the stream function solution and may be written in the form (see Equation 3-26)

$$\frac{u_b}{U_\infty}(x,\eta,\omega) = \bar{g}_o \frac{\partial\phi}{\partial\eta} \frac{P_i}{\bar{\rho}c^2} 2R_\delta \frac{D(\theta i, M_\infty)}{M_\infty} A\{x, x_o, \alpha(\omega, U, U'', R_\delta)\} \quad (3\text{-}5)$$

where $\phi(\eta)$ is the eigen-vector associated with the most amplifying solution of the homogeneous Orr-Sommerfeld equation,

P_i is the incident sound pressure amplitude,

D is a function of the directionality of the incident sound field, the freestream Mach number M_∞, reflection from surface and refraction in the boundary layer,

A is a factor expressing the chordwise variation of the boundary layer disturbance,

α is the amplification rate and is a function of frequency and suction rate and distribution

The evaluation of $A\{x, x_o, \alpha(\omega), U, U', U'', R\delta)\}$ in its exact form involves a volume and a surface integral (as shown in Section 3.5), and requires specification along the chord of the sound field distribution as well as the complex eigenvalue variation. The latter is obtained numerically by solving the homogeneous stability equation for the specific sucked airfoil.

For boundary layer excitation from a localized region (x_o) along the chord, $A(x,x_o,\alpha)$ would represent the propagation and amplification along the chord as determined by the homogeneous Orr-Sommerfeld equation. The volume and surface integral effectively account for the distributed source of excitation as is expected of a sound field in contrast to a vibrating ribbon. Such volume and surface integrals have been evaluated for the case of a sound wave impinging on the boundary layer of a flat plate. In addition to the initial decay, followed by an amplification and a subsequent decay, regions characteristic of boundary layer disturbances, $A(x,x_o,\alpha)$ also contain a spatial modulation in amplitude and phase. The peaks of the modulated amplitude follow a curve somewhat lower than that corresponding to excitation from a localized region, and are discussed in Section 3.5.

3.4.1 Proposed Approximation

For the sucked airfoil case, in view of the fact that our aim is to improve the X-21A criteria by adding sensitivity to frequency and directionality, it is proposed that a simplified form for $A(x,x_o,\alpha)$ be used but still retaining its sensitivity to frequency and suction distribution. The simplest form would be that corresponding to a localized excitation. This involves "only" the determination of the complex propagation constants as a function of distance along the chord (eigenvalues of the homogeneous Orr-Sommerfield equation) without having to evaluate the volume and surface integrals. Obviously some information is lost in this approximation, for example, contributions to the boundary layer disturbance from the interaction of sound at the surfaces of the slots, and details of the receptivity. However, some of these can be absorbed in the single empirical constant suggested initially for defining the level at which transition sets in. For this simplified situation, A becomes $A\{x,x_o,\alpha(\omega,V)\} = \exp \int \alpha(\omega,V)dx$, where V represents the local suction velocity.

3.4.2 Critical Sound Pressure Level Determination

Within the approximation discussed above, Equation 3-5 relates the response at an arbitrary point x due to an incident sound field at an arbitrary angle θ_i. The fluctuating boundary layer disturbance velocity ratio is linearly related

to the amplitude of the incident sound field. Let a threshold value for (u_b/U_∞) at transition be defined by $(u_b/U_\infty)_{crit}$ and let the corresponding acoustic pressure amplitude be defined as P_{crit}. The critical sound pressure level can now be obtained from Equation 3-5 as follows

$$SPL_{crit} = 20 \log_{10} \left(\frac{P_{crit}}{P_{ref}}\right) = 20 \log_{10} \left(\frac{u_b}{U_\infty}\right)_{crit} - 20 \log_{10} \left(\bar{g}_o \frac{\partial \phi}{\partial \eta}\right)$$

$$- 20 \log_{10} \left(\frac{P_{ref}}{\bar{\rho}_o c_o^2}\right) - 20 \log_{10} \left(\frac{\bar{\rho}_o c_o^2}{\bar{\rho} c^2}\right) + 20 \log_{10} (M_\infty)$$

$$- 20 \log_{10} (2R_\delta) - 20 \log_{10} \{D(\theta_i, M_\infty)\}$$

$$- 20 \log_{10} \{A(x, x_o, \alpha(\omega)\} \qquad (3\text{-}6)$$

The critical sound pressure level SPL_{crit} is obtained by multiplying Equation 3-6 by 20. In the above equation P_{ref} is the standard reference pressure for sound pressure level normalization and is 20 x 10^{-6} N/m^2. $\bar{\rho}$ and c are mean density and mean adiabatic speed of sound; $\bar{\rho}_o$ and c_o are reference values. In the above expression for a fixed distance from the surface the first three terms are constants; the fourth term, which can be reduced to $\log_{10} (\gamma_o \bar{P}_o / \bar{\gamma} \bar{P})$, accounts for altitude effects. The fifth term is only a function of the freestream (or cruise) Mach number. The seventh term is not only a function of the directionality of the incident sound wave, but also of the freestream Mach number. The last term, which has already been discussed in reducing it to its approximate form, is a function of the frequency, suction distribution, distance along the chord, and Reynolds number.

Thus for a constant altitude and cruise speed, the critical SPL may be written in the form

$$SPL_{crit} = \text{constant} - 20 \log_{10} D(\theta_i, M_\infty) - 20 \log_{10} \{A(x, \alpha(\omega, U, U', U'')\} \qquad (3\text{-}7)$$

In the above form, the critical SPL becomes sensitive to sound directionality, frequency and suction distribution; the constant is empirical and may have to be determined from measurements. Function $D(\theta_i, M_\infty)$ expressing the directionality of the sound field is approximately given by

$$D(\theta_i, M_\infty) = \log_e\{1+M_\infty \cos\theta_i\}/M_\infty \qquad (3.8)$$

and is obtained by integrating the acoustically induced vorticity source across the boundary layer as shown in Section 3.5, eq. (3-19).

Equation 3.7 has been evaluated for the following specific case:

Airfoil characteristics: Lockheed swept wing LFC AF10-3

Leading edge swept angle = 25°
Trailing edge swept angle = 16.7°
Chord length = 22.81 ft

Suction distribution:
From 0 to 8% of chord: tapered suction rate from 0.044% to 0.008%
From 8 to 73% of chord: constant suction rate of 0.008%

The suction rate is defined as $(\bar{\rho}\bar{V})_{wall}/(\bar{\rho}\bar{U})_\infty$

Cruise speed = 0.822 Mach
Altitude = 38,000 feet

For the above specific case, the 2D Orr-Sommerfeld eigenvalue problem has been solved for different frequencies corresponding to pure tones. The velocity profiles used were the ones in the direction of the normal chord. The amplification rates for different frequencies are determined as a function of distance along chord and are shown in Figure 3-9A. In Figure 3-9B a cross plot shows the amplification spectrum for different chord locations.

From these two sets of curves, it can be immediately deduced that for the specific case considered, the region and frequency range of concern are respectively between 14% to 26% of the chord and 2 to 6 kHz. For stations

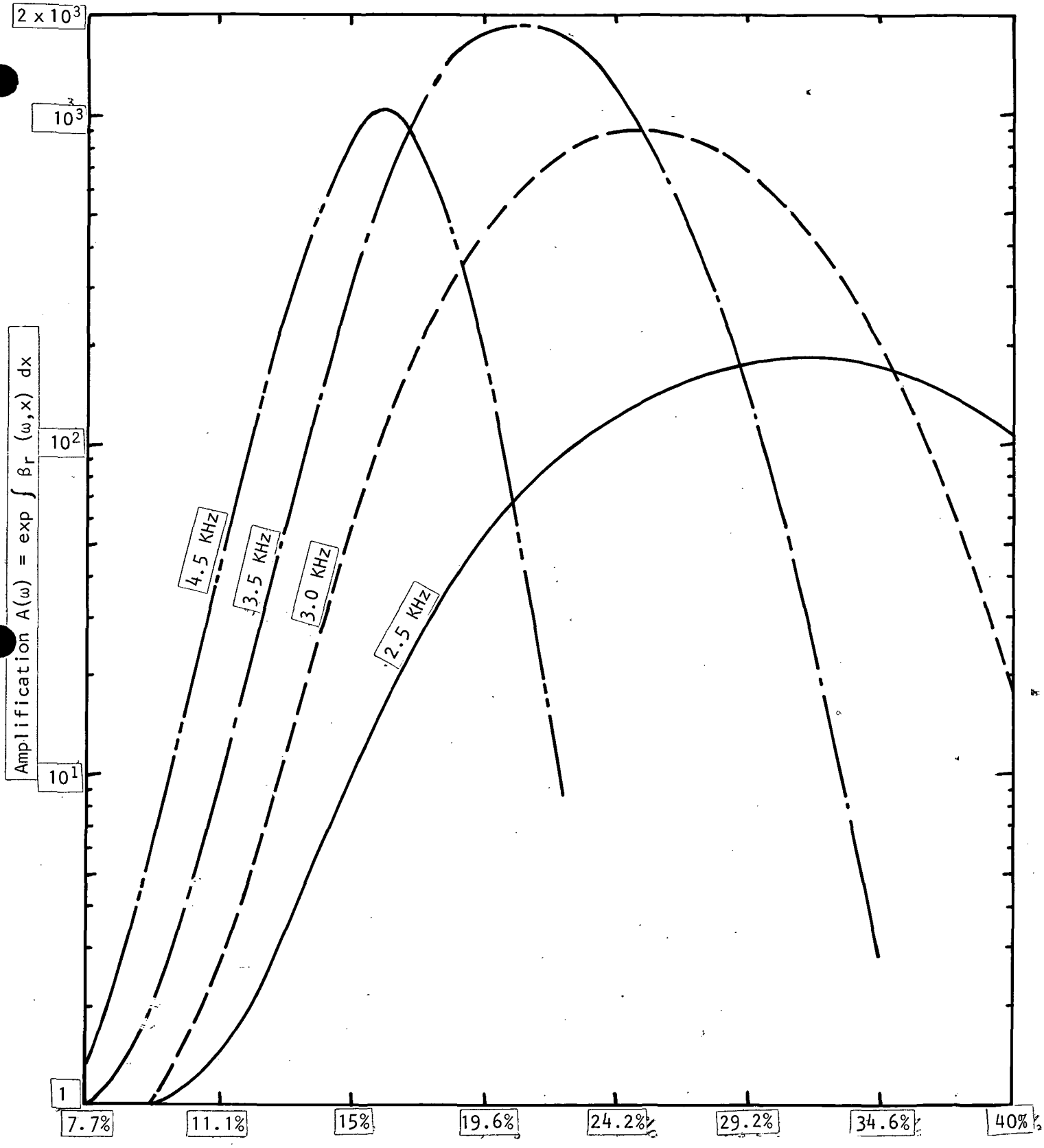

Figure 3-9a. Variation of amplication A(ω) for T·S waves along Lockheed LFC airfoil chord for suction rate = 0.044% from 0 to 8% of chord and 0.008% from 8 to 73% of chord

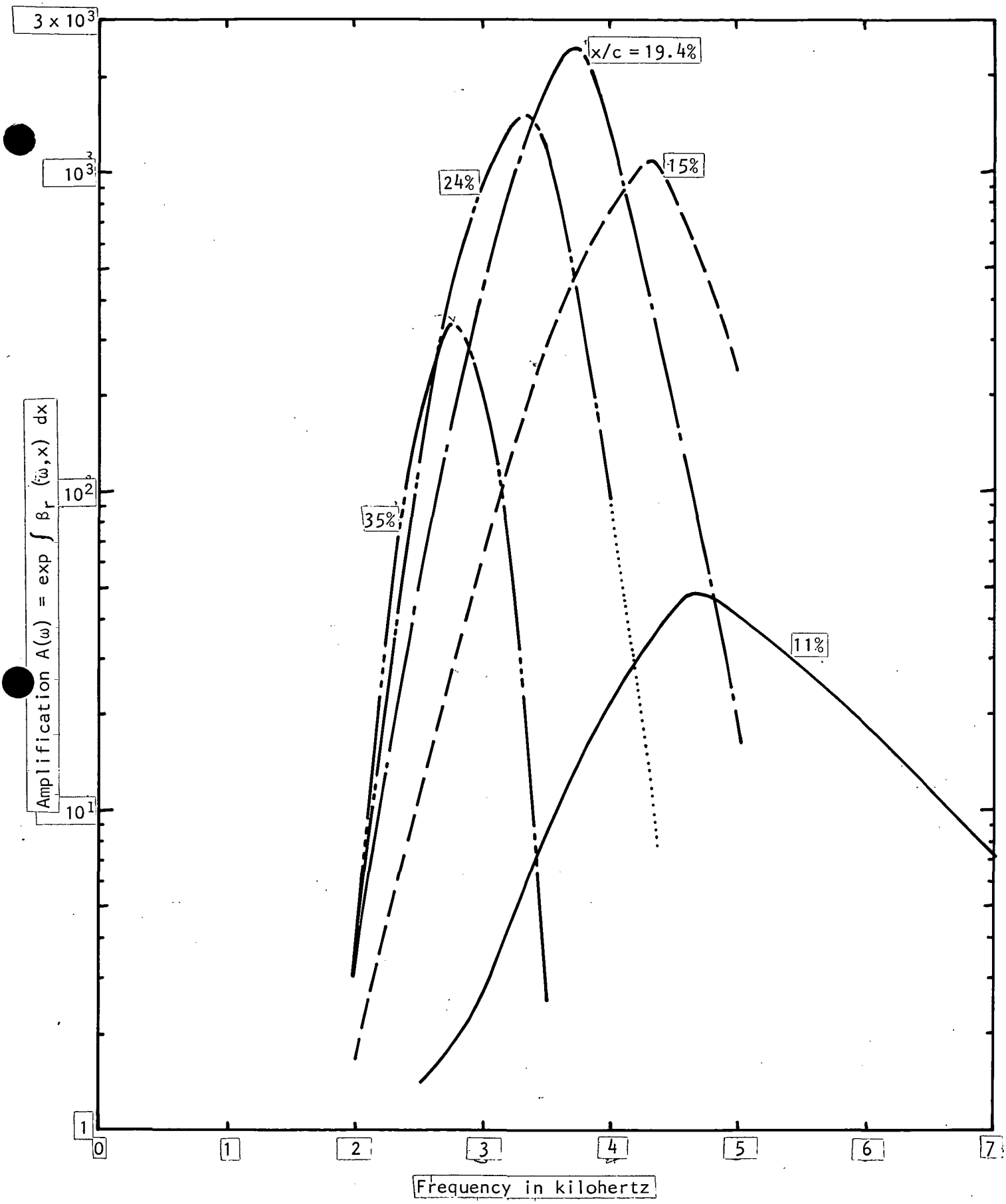

Figure 3-9b. Tollmien-Schlichting amplification spectrum $A(\omega)$ on Lockheed LFC airfoil computed for suction rate = 0.044% from 0 to 8% of chord and 0.008% from 8 to 73% of chord

1600

160

along the chord further away from the leading edge, it is the lower part of the frequency range that is of concern, whereas for stations closer to the leading edge, it is the high frequency range that is important.

3.4.3 Critical SPL Spectra

For each of five chord stations, the amplification spectra are substituted in Equation 3-7 and the relative critical SPL spectra were evaluated for sound incident on the airfoil in the same direction as the mean flow ($\theta_i = 0°$). The constant has been taken to be zero. The results are plotted in Figure 3-10. These curves exhibit the frequency sensitivity of the critical SPL at each of five chord locations. Each of these curves is similar to measurements reported in Reference 3-2, 3-3, 3-4 of which two sets are reproduced in Figure 3-8. For comparison, the curve corresponding to the pure tone is relevant.

In Figure 3-11, the critical SPL spectrum is plotted for a fixed chord location, namely 18%, for different angles of incidence. An interesting feature of this set of curves is that as the angle of incidence increases, the critical SPL in the whole frequency range first increases, then decreases and is not symmetrical about 90°. The critical SPL spectrum for 180° is as much as 10dB below that for 0° angle of incidence. Although there is not sufficient data to compare variation of the critical SPL with angle of incidence, the slight increase in critical SPL from 0° to 60°, of the order of 5dB, is in the right range when compared to the Northrop test using longitudinal and transverse sound.

3.4.4 Effect of Suction

The depth of the initial SPL spectrum is a function of the suction rate and distribution. The amplification spectrum and the corresponding critical SPL spectrum are plotted in Figures 3-12a and 3-12b, for the same Lockheed airfoil under the same condition except for the suction distribution which is as follows:

From 0 to 8% of chord, tapered suction rate from 0.044% to 0.0135%.
From 8% to 73% of chord, constant suction of 0.0135%.

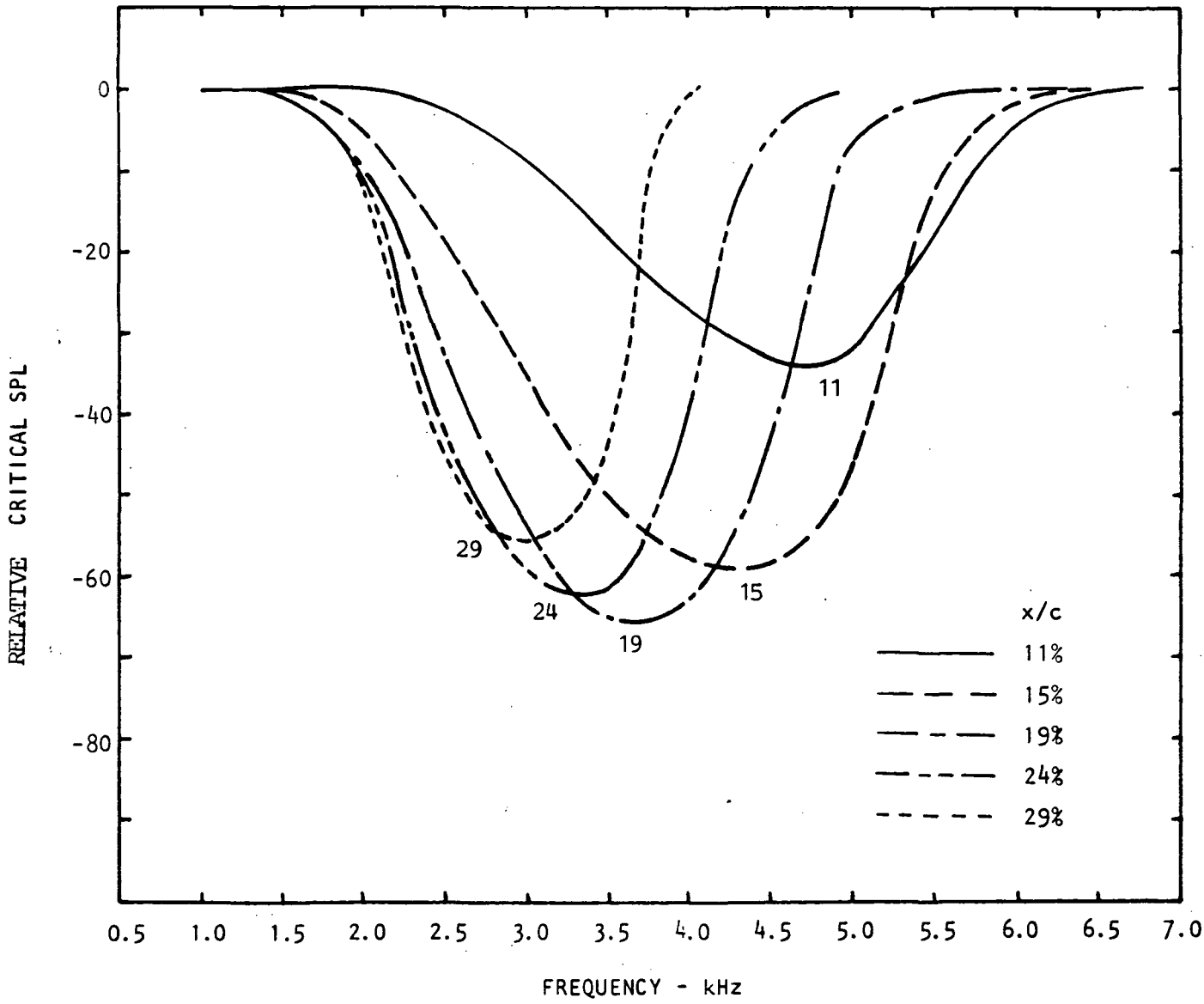

Figure 3-10. Variation of critical SPL with frequency for different (x/c) locations on airfoil and for plane sound wave incident 0° (x/c) = 19%.

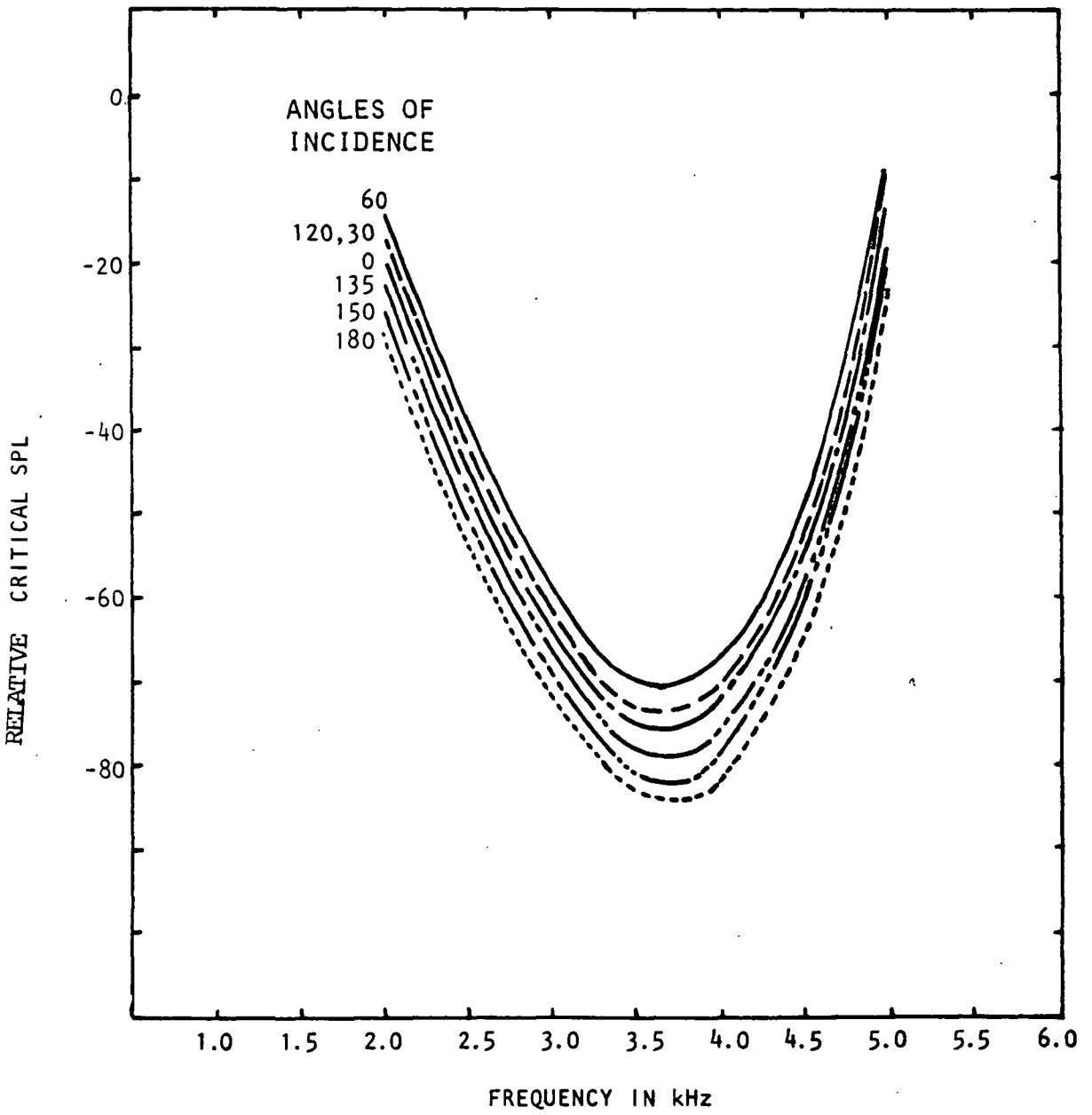

Figure 3-11. Variation of critical SPL with frequency for different angles of incidence at (x/c) = 18%.

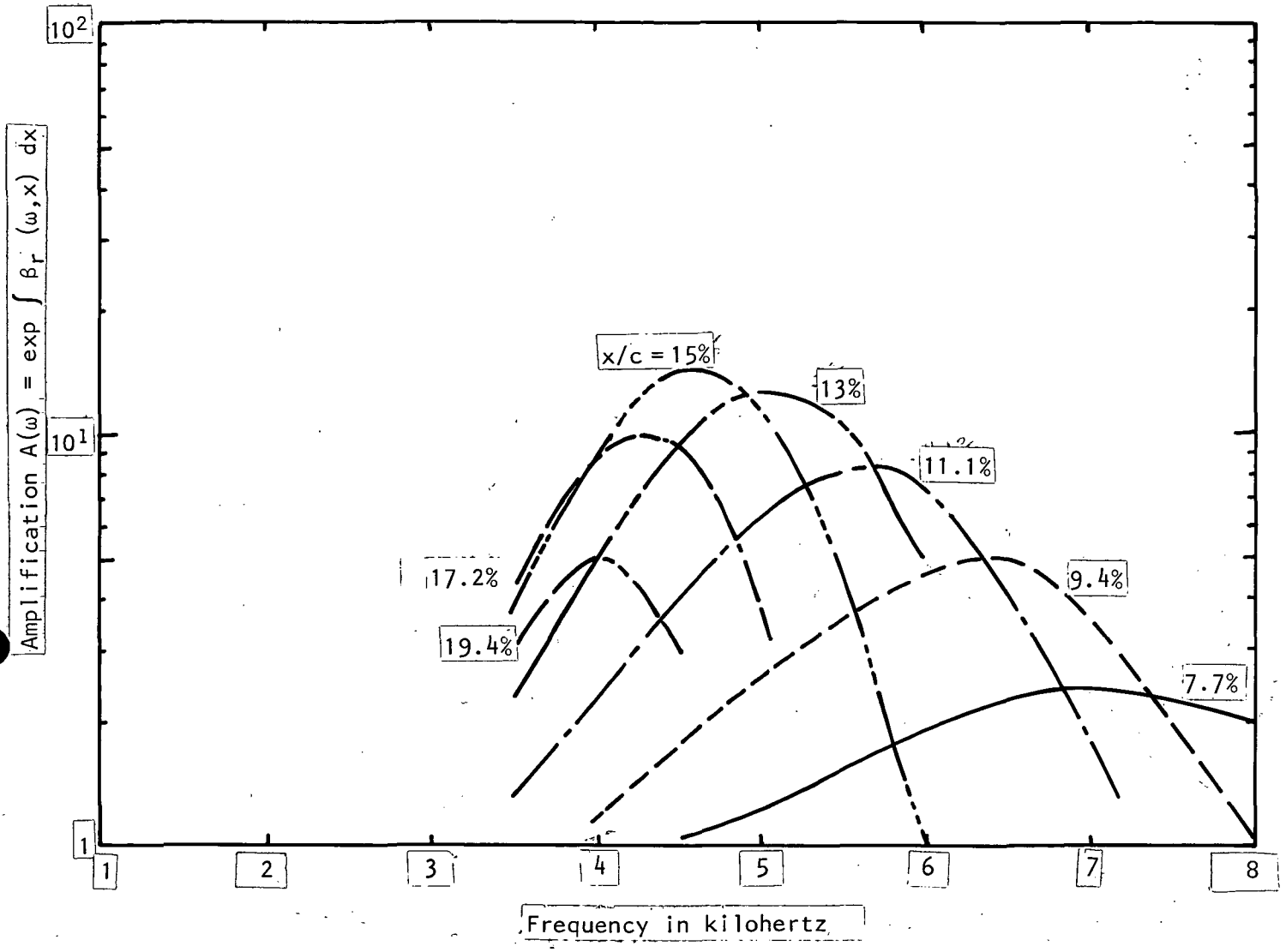

Figure 3-12a. Tollmien-Schlichting amplification spectrum $A(\omega)$ on Lockheed LFC airfoil computed for suction rate = 0.044% from 0 to 8% of chord and 0.0135% from 8 to 73% of chord

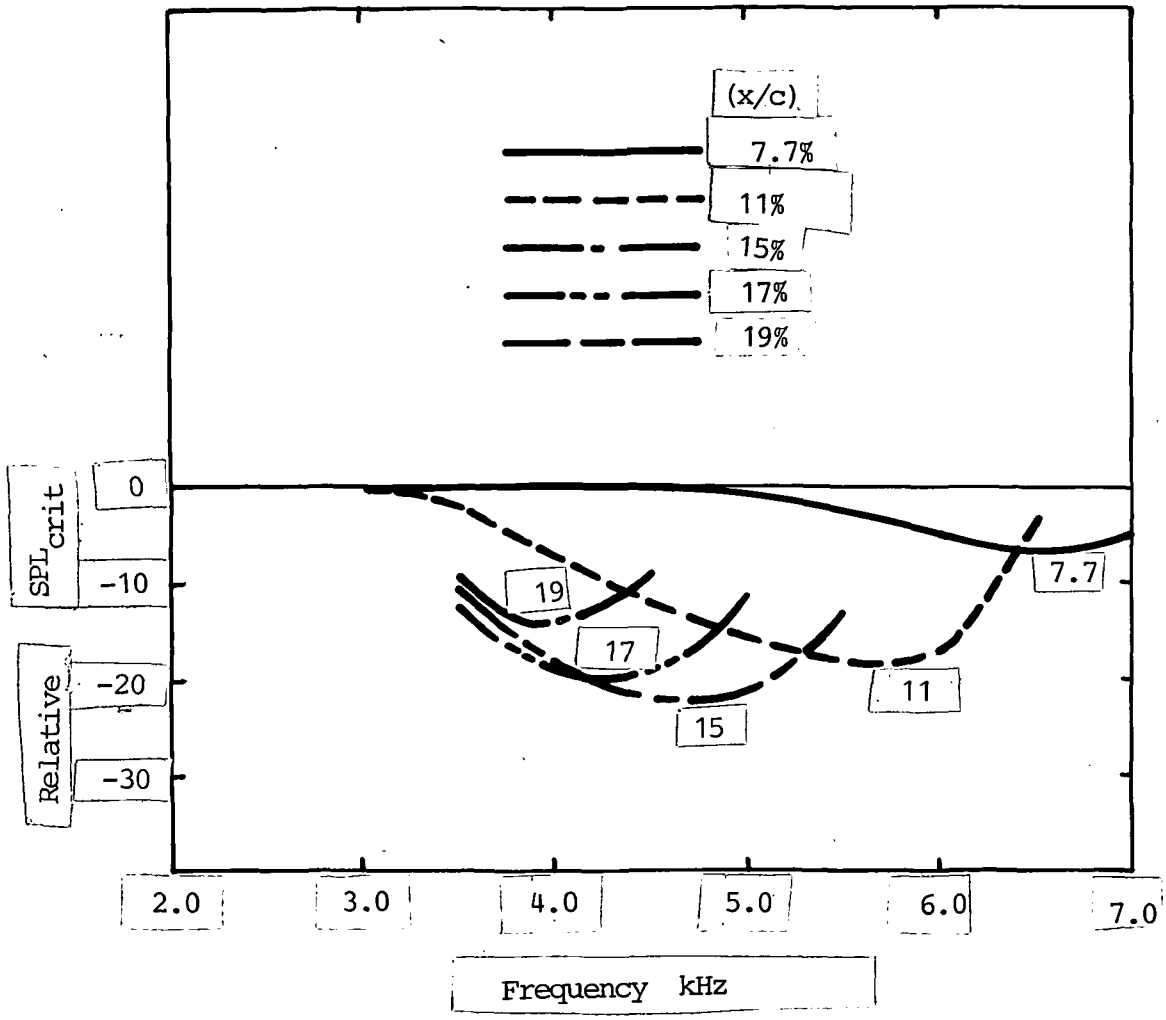

Figure 3-12(b). Critical SPL spectrum for different (x/c) locations on airfoil, for plane sound wave incident at 0° and for suction rate and distribution as defined on page 161.

Comparing Figures 3-10 and 3-12b, it can be seen that an increase in the suction rate not only reduces the depth of the critical SPL spectrum but also shifts the critical frequency and the critical region along the chord.

3.4.5 An Application Example

As an example, the impact on transition on the upper surface of a wing due to noise from a tail mounted engine is considered. The purpose of this exercise is to determine whether the critical SPL pertinent to this wing has been exceeded; and if so, by how much; and to determine (a) the regions of the wing where transition is most likely, and (b) the components of the engine noise which are responsible for exceeding the critical SPL. These results may then be used to take remedial actions.

If the wing, its shape and its aerodynamic characteristics are similar to those defined in Section 3.4.2 and 3.4.3, namely the Lockheed LFC AF 10-3, then the critical SPL spectra already computed, Figures 3-10 and 3-11 are relevant. These spectra, however, are relative because the constant of Equation 3-7 was arbitrarily set to zero. For determining transition location, the relative critical SPL spectrum must be adjusted to yield an absolute critical SPL spectrum by adding a constant dB level, which in effect defines a $(u_b/U_\infty)_{crit}$. Such a constant has to be determined empirically from a set of measurements, for example like that in Figure 3-8a. If the aerodynamic parameters corresponding to this set of measurements were the same as the case being considered here, then the relevent constant is 130 dB. Alternatively, the computed relative critical SPL spectra can be used as a supplement to the original spectrally integrated Lockheed/X21 criteria. For the relevent length Reynolds number, the spectrally integrated critical SPL is deduced using Figure 3-4. This level is used as the upper limit in the ordinate of Figures 3-10 and 3-11. For the example case, we shall assume this level to be 130 dB.

The next step is to overlay on the critical SPL spectrum, Figure 3-10, the jet engine noise SPL spectrum at 18% chord predicted from Section 2 of this report (since for this wing, location near the 18% chord is most critical). The intersections of the engine noise spectrum with the sets of critical SPL

spectra allow determination of the engine noise sources and the amount the levels are exceeded, as shown in Figure 3-13. In this example case, it can be deduced that the shock associated noise and the fundamental of the fan inlet noise are the only two sources that exceed the critical SPL.

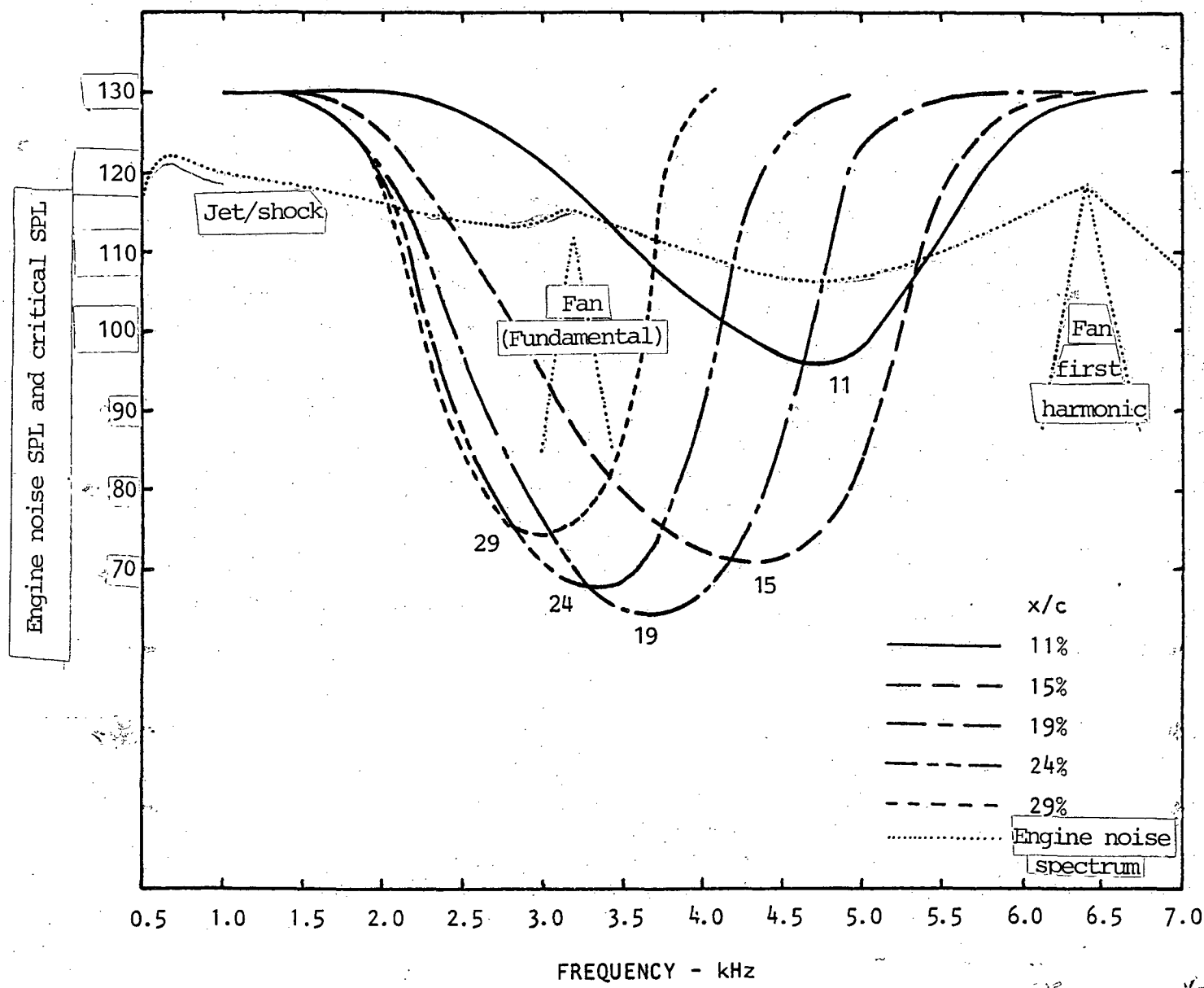

Figure 3-13(a) Identification of sources and regions along wing chord where engine noise spectrum exceeds critical SPL, for suction distribution defined on page 158 (reduced suction).

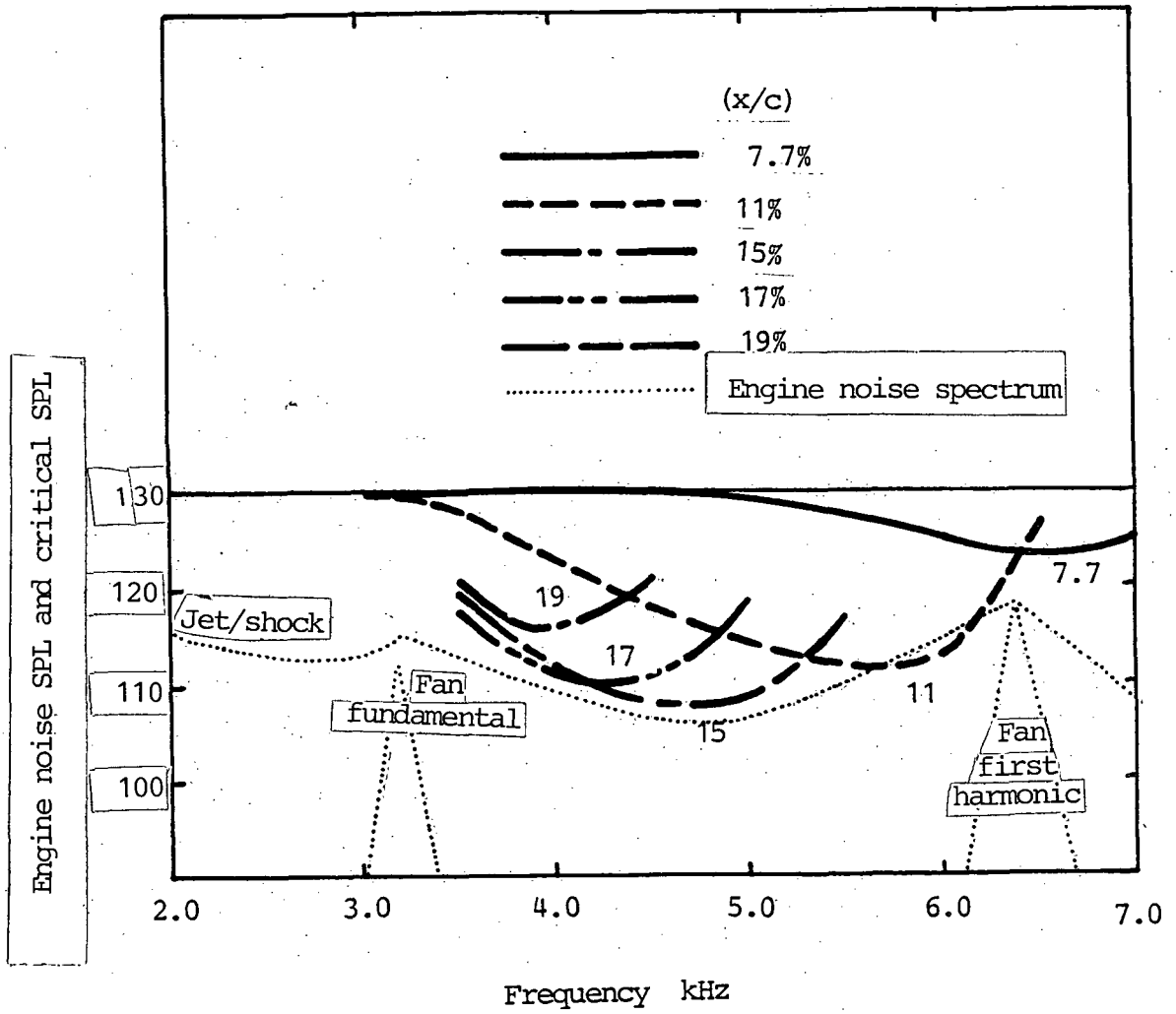

Figure 3-13(b) Identification of sources and regions along wing chord where engine noise spectrum exceeds critical SPL, for suction distribution defined on page 161 - (increased suction).

? ?

161

1/89

In this section, a physical mechanism is hypothesized based on the measurable observed differences between acoustic and boundary layer disturbance fields. These are then translated into a mathematical formulation of the process to allow quantitative evaluation. The formulation is applicable for sound interaction with the general class of boundary layer disturbances (T.S., inflectional or Taylor-Gortler). Numerical results are then presented on the acoustic excitation of Tollmien--Schlichting waves on a flat plate in the absence of pressure gradients.

3.5.1 Sound and Boundary Layer Disturbances

Before discussing possible coupling mechanisms, it is instructive to note the basic similarities and differences between an acoustic and a boundary layer disturbance. Among the similar properties, the first is that both types have space-time fluctuating velocity components. Depending on the source of excitation, both types of disturbances can have periodic or random phase variations. However, space-time phase measurements of coherent disturbances of both kinds show that boundary layer disturbances "propagate" with phase speed proportional to but less than the freestream mean velocity, and acoustic disturbances propagate with phase speed proportional to the vector sum of the abiabatic speed of sound and the mean freestream velocity. Thus, in the limiting case of the freestream mean velocity reducing to zero, the acoustic disturbance propagates with the adiabatic speed of sound and the boundary layer disturbance stops "propagating"; in fact, the latter reduces to a diffusion process. From this point of view, boundary layer disturbances are some form of convected (diffusion) disturbances, like turbulence, whereas sound is a truly propagating disturbance. These are further evidenced by the fact that measurements on boundary layer disturbances correlate with solutions of the Orr-Sommerfeld equation which is a linearized form of the convected vorticity transport equation (of the diffusion type) and represents a balance of fluctuating vorticity dissipated by viscosity and the substantial time derivative. Acoustic disturbances on the other hand are governed by the convected wave-equation which represents a balance between compressional and inertia forces; the particle velocity and density fluctuations being related

to the pressure fluctuation through the speed of sound vanish in the limit of incompressibility. Particle velocities associated with boundary layer disturbances are still finite in the limit of incompressibility. For this reason, boundary layer disturbances and turbulence are often looked upon as incompressible disturbances, especially for subsonic flows.

3.5.2 Hypothesis and Governing Equation

In view of the fact that the boundary layer disturbances are governed by a vorticity conservation equation, then for sound to be able to excite boundary layer disturbances, it must somehow be able to induce a fluctuating vorticity field or a fluctuating vorticity flux. In a medium at rest or uniformly convecting, the field associated with a sound wave constitutes an irrotational field, and therefore, the fluctuating vorticity derived from the particle velocities of the sound field is identically zero. However, for sound propagating in non-uniform mean flows, the fluctuating vorticity derived from the acoustic particle velocities has a non-zero component (see Appendix A). This sound induced fluctuating vorticity field has the same phase distribution as the sound field. The rate of change of such an acoustically induced vorticity field can be a potential source for boundary layer disturbance excitation. This and other sources in terms of the acoustically induced fluctuating vorticity field can be formally derived by perturbing and linearizing the vorticity transport equation and is shown in Appendix B. The boundary layer disturbance is shown to be governed by an inhomogeneous Orr-Sommerfeld equation, with source terms linearly proportional to the sound field and for the case of a two-dimensional flow is given by

$$\nabla^4\psi - \frac{1}{\nu}\frac{\bar{D}}{Dt}\nabla^2\psi - \frac{1}{\nu}\frac{\partial\psi}{\partial x}\frac{d^2U}{dy^2} = Q_a(\Omega_a, \underset{\sim}{w}_a, \bar{\Omega}, x, y, t) \qquad (3\text{-}9)$$

where

$$\bar{Q}_a(\Omega_a, \underset{\sim}{w}_a, \bar{\Omega}, x, y, t) = \frac{2}{\nu}\left[\frac{\partial}{\partial t}\,\Omega_a + \text{div}\,(\underset{\sim}{w}_a\bar{\Omega}) - \nu\,\nabla^2\,\Omega_a\right] \qquad (3\text{-}10)$$

$\bar{\Omega}$ = mean vorticity = $-\frac{1}{2}\frac{d^2U}{dy^2}$

$\underset{\sim}{w}_a$ = the acoustic particle velocity vector whose x and y components are u_a and v_a, respectively

Ω_a = fluctuating vorticity attached to the sound field and is given by (Appendix A, eq. A-11)

$$= \frac{1}{2\bar{\rho}c}\left[\left\{\frac{2K^2}{(1-MK)^2} - 1\right\}\frac{dM}{dy}P(x,y,\omega) + \frac{1}{k^2(1-MK)^2}\frac{d^2M}{dy^2}\frac{dP}{dy}\right] \qquad (3\text{-}11)$$

$K = k_x/k = \omega/c$

$P(x,y,\omega)$ = sound pressure field

The source terms, Equation 3-10, exciting boundary layer disturbances, represent a volume distribution of acoustically induced fluctuating vorticity of multipole orders, and may be evaluated if the sound field distribution is known. The first term represents a time rate of change of fluctuating vorticity, similar to acoustic radiation by a source corresponding to time rate of change of mass. The second term is the divergence of the vorticity flux induced by the particle velocity associated with the sound, similar to acoustic radiation from a dipole or the divergence of a force (or mass flux). The third term in the form of a double divergence is not a vorticity production term, but rather a vorticity absorption term by viscosity with an acoustic analogue coresponding to a quadrupole.

The second term when expanded and expressed in terms of the acoustic pressure, yields the source terms discussed in Reference 3-20. However, the first and third terms of the present analysis were missing. This is due to the fact that the acoustic field in Reference 3-20 was associated from the outset to the irrotational component of the general vector decomposition and as a result the curl of such velocity components and, therefore, the associated fluctuating vorticity vanished.

Before writing down formally a general solution of Equation (3-9), it must be pointed out that Q_a ($\Omega_a, w_a, \bar{\Omega}, x, y, t$), the acoustically induced fluctuating vorticity source, is assumed known and indeed may be evaluated if the sound field distribution in the boundary layer is known explicity. Such a sound field may either be measured directly or evaluated in terms of the incident

sound field. For a sound wave impinging on an airfoil or a finite length flat plate at an arbitrary angle of incidence, the sound field distribution in the boundary layer (needed for evaluation of Q_a) consists of the incident sound wave, an acoustic field representing reflection from the surface, and two scattered fields representing diffraction from the leading and trailing edges of the airfoil or flat plate. As sketched schematically in Figure 3-14, all four component fields are subject to convective and shear refraction. The evaluation of leading and trailing edge near-field diffraction in the presence of a non-uniform mean flow is outside the scope of the present contract. The influence of convective and shear refraction on the combined incident and reflected sound waves has been investigated numerically by solving the convected wave-equation in the boundary of an infinite flat plate and matching the numerical solution to analytic solutions outside the boundary layer. The analysis and results are presented in Appendix E, where the sound field in the boundary layer and the acoustically induced vorticity flux corresponding to the second term of Equation 3-10 have been evaluated for different frequencies and angles of incidences. It is also shown that for frequencies $k\delta \leq 1$, the sound pressure distribution across and in the boundary layer is uniform, implying negligible effects of refraction, so that the terms containing the transverse acoustic velocity and transverse pressure gradients on the right hand side of Equation 3-9 (source terms) may be neglected. The above deduction is, of course, limited to a sound field over a rigid surface.

Although the acoustic analysis can be easily extended to non-rigid surfaces, the evaluation of the coupling will become slightly more complicated and will have to be evaluated numerically. However, if the analysis is restricted to rigid surfaces, part of the coupling may be approximated by analytic expressions allowing useful trends to be deduced without excessive numerical computation. Although the approach used in the next section is applicable to general situations, some of the integrals will be evaluated for sound waves of

SOUND FIELD EVALUATION INSIDE BOUNDARY LAYER

- INCIDENT SOUND
- REFLECTED SOUND
- DIFFRACTED SOUND

} MODIFIED BY CONVECTION & REFRACTION

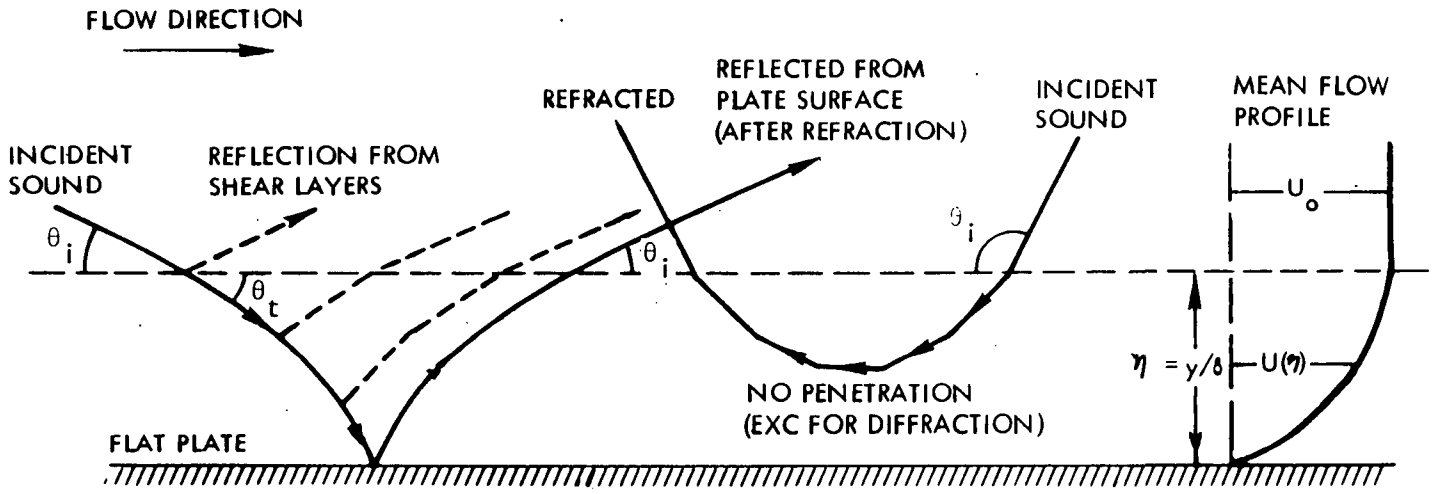

Figure 3-14. Convection and refraction of incident and reflected plane sound wave in the boundary layer of a rigid flat plate.

frequencies $k\delta \ll 1$ and propagating at arbitrary angles of incidence θ_i over rigid surfaces.

3.5.3 General Solution

In view of the fact that Equation 3-9 governs the boundary layer disturbance in a mean non-uniform flow that is considered locally parallel, the general solution can be expressed in terms of Fourier transform integrals. If Equation 3-9 is non-dimensionalized (by setting $\eta = y/\delta(x)$) with respect to the boundary layer thickness $\delta(x)$, then a general solution may be written in the form,

$$\psi(x,\eta,t) = \iiint \delta^4(x_s)\, \bar{Q}_a(x_s,\eta_s,\omega_s)\, g(x,x_s,\eta,\eta_s,\omega_s)\, dx_s\, d\eta_s\, d\omega_s \qquad (3\text{-}12)$$

where subscript s refers to source (region and frequency) and $g(x,x_s,\eta,\eta_s,\omega_s)$ is the Green's function representing the hydrodynamic response at a point (x,η) due to a point source excitation located at (x_s,η_s), similar to that from a vibrating ribbon. Equation 3-12 is equivalent to treating each elementary volume of the source region as a point source. Two of the integrals correspond to summation of each elementary source and are to be carried in the source regions. The third integral is over the source frequencies. When evaluating the integrals, it must be remembered that both the amplitude and phase of the sound field and therefore of the source terms can be functions of space and frequency. Complicated spatial modulations can be expected if the sound field consists of more than one discrete frequency. In fact, numerical results (discussed below) indicate spatial modulation even in the case of a single discrete frequency sound. This is due to the fact that the phase of the sound varies much slower than that of the Tollmien-Schlichting (T.S.) waves; so that a T.S. wave generated in an earlier part of the source region interferes with those generated further downstream. If more than one discrete frequency is present, then more interferences can be expected. Equation 3-12 should in principle account for all these effects.

In what follows, the evaluation of Equation 3-12 is restricted to discrete frequency sound. For the case of acoustically induced vorticity Ω_a, or vor-

ticity flux field, $\operatorname{div}(\underset{\sim}{w}_a \bar{\Omega})$, the source region extends transversely from the plate surface to the edge of the boundary layer, and streamwise from the leading edge to the point of evaluation which most often lies inside the source region. If Equation 3-10 is substituted in Equation 3-12, $\psi(x,\eta,\omega_s)$, the temporal Fourier transform of the harmonic response of the boundary layer disturbance, may be written as the sum of two volume integrals which may be evaluated separately. Thus,

$$\psi(x,\eta,\omega_s) = \psi_1(x,\eta,\omega_s) + \psi_2(x,\eta,\omega_s) \qquad (3\text{-}13)$$

where

$$\psi_1(x,\eta,\omega_s) = 2\iint \delta^4(x_s)\{j\frac{\omega_s}{\nu} - \nabla_s^2\}\,\Omega_a(x_s,\eta_s,\omega_s)\,g(x,x_s,\eta,\eta_s,\omega_s)\,dx_s\,d\eta_s \qquad (3\text{-}14)$$

and

$$\psi_2(x,\eta,\omega_s) = \frac{2}{\nu}\iint \delta^4(x_s)\,\operatorname{div}(\underset{\sim}{w}_a \bar{\Omega})\,g(x,x_s,\eta,\eta_s,\omega_s)\,dx_s\,d\eta_s \qquad (3\text{-}15)$$

The above integrals, although still valid for all frequencies, arbitrary surface conditions and arbitrary angles of incidences, will now be evaluated for the limiting case of low frequency sound, $k\delta \ll 1$, impinging at arbitrary angles of incidences on a rigid flat plate. As mentioned previously this low frequency limitation allows evaluation of the above integrals in the form of semi-analytic solutions allowing useful trends to be deduced. Extension to high frequencies and surfaces with suction slots will require the double integration to be carried out numerically, thus making extensive computation necessary for deducing trends for each of the many parameters involved.

For the limiting case of low frequency, $k\delta<1$, and a rigid flat surface, the volume integral for ψ_1 of Equation 3-14 has been evaluated in Appendix C and is given below. In Appendix D the integral for ψ_2 of Equation 3-14 has been expressed as the sum of a volume and a surface integral and has been evaluated in the form shown below.

$$\psi_1(x,\eta,\omega_s) = \delta(x)\,\phi(\eta)\,\frac{P_w}{\rho c}\,R_\delta\,\bar{g}_o\,e^{j\pi/2}\,k\delta\,D_1(\theta_i,M_\infty)\,A_1(x,x_o,\omega_s) \qquad (3\text{-}16)$$

and

$$\psi_2(x,\eta,\omega_s) = \delta(x)\ \phi(\eta)\ \frac{P_w}{\bar{\rho}\bar{c}}\ R_\delta\ \bar{g}_o\ D_2(\theta_i,M_\infty)\ A_2(x,x_o,\omega_s) \qquad (3\text{-}17)$$

where $R_\delta = U_\infty \delta(x)/\nu$

$\delta(x)$ = local boundary layer displacement thickness.

P_w = the constant sound pressure level in the boundary layer of the rigid flat surface in the low frequency limit of $k\delta < 1$ and is twice the SPL of the incident sound.

$\phi(\eta)$ = eigen-function of the most amplifying boundary layer disturbance and is obtained by solving the homogeneous Orr-Sommerfeld equation.

g_o = a constant corresponding to the receptivity, that is, the effectiveness of boundary layer disturbance excitation by a point localized source of fluctuating vorticity.

D_1 & D_2 are functions of the freestream Mach number and the directionality of the sound field, and have the following forms

$$D_1(\theta_i,M_\infty) = \left\{\frac{2\cos\theta_i}{1 + M\cos\theta_i} - 1\right\} \qquad (3\text{-}18)$$

$$D_2(\theta_i,M_\infty) = \frac{\log_n(1 + M_\infty\cos\theta_i)}{M_\infty} \qquad (3\text{-}19)$$

$A_1(x,x_o,\omega_s)$ and $A_2(x, x_o, \omega_s)$ are complex functions expressing the relative variations of the amplitude and phase of the component disturbance along the mean flow direction. They may be written in the form

$$A_1(x,x_o,\omega_s) = \int_{x_o}^{x}\left[\left\{\frac{\delta(x_s)}{(x)}\right\}^3 f(k_x,\beta(x_s),x_s)\right] dx_s \qquad (3\text{-}20)$$

$$A_2(x,x_o,\omega_s) = A_{21}(x,x_o,\omega_s) + A_{22}(x,x_o,\omega_s) \tag{3-21}$$

$$A_{21}(x,x_o,\omega_s) = \int_{x_o}^{x}\left[\left\{\frac{\delta(x_s)}{\delta(x)}\right\}\left\{4\,\frac{d\delta(x_s)}{d\,x_s} + j\beta\delta(x_s)\right\} f(k_x,\beta(x_s),x_s)\right]dx_s \tag{3-22}$$

$$A_{22}(x,x_o,\omega_s) = \delta(x)\; f(k_x\beta(x),x) - \frac{\delta(x_o)^3}{\delta(x)^2} f(k_x\beta(x_o),x_o) \tag{3-23}$$

and

$$f(k_x,\beta(x_s) = \exp -j\{k_x x_s + \int_{x_s}^{x} \beta(x_s)\; dx_s\} \tag{3-24}$$

In the above Equation (3-21), A_{21} arises from a volume integral and A_{22} from a surface integral. A comparison of Equations 3-16 and 3-17 shows that the relative magnitude of ψ_1 with respect to ψ_2 is of the order of (k/β) which, for a Tollmien-Schlichting disturbance over a flat plate, is of the order of 0.3 M. It then follows that for subsonic flows, the contribution to the boundary layer disturbance is dominated by the second term, namely $\psi_2(x, \eta,\omega_s)$.

In the next section, some numerical solutions are presented showing the amplitude and phase variations of the two components of $\psi_2(x,x_1, \omega_s)$ and a comparison is made with the measurements of Shapiro (Reference 3-14).

3.5.4 Numerical Evaluation of the Acoustically Excited Boundary Layer Disturbance

As shown in the last section, the main contribution to the excitation of boundary layer disturbance (TS waves), for subsonic flows, comes from the source term of Equation 3-10, corresponding to the divergence of the acoustically induced fluctuating vorticity flux, and may be written in the form, (see Equation 3-17),

$$\psi(x,\eta,\omega_s) = \delta(x)\;\phi(\eta)\frac{P_w}{\bar{\rho}c} R_\delta\, \bar{g}_o\, D_2(\theta_i,M_\infty)\{A_{21}(x,x_o,\omega_s) + A_{22}(x,x_o,\omega_s). \tag{3-25}$$

The streamwise fluctuating particle velocity $u_b(x,\eta,\omega_s)$ associated with this boundary layer disturbance is given by

$$u_b(x,\eta,\omega_s) = \frac{\partial\phi}{\partial\eta}\frac{P_w}{\rho c} R_\delta \bar{g}_o D_2(\theta_i,M_\infty) \{A_{21}(x,x_o,\omega_s) + A_{22}(x,x_o,\omega_s)\} . \qquad (3\text{-}26)$$

From the above expression, it may be deduced that an acoustically excited TS disturbance is linearly proportional to P_w, which on a flat plate is twice the SPL of the incident wave. The apparent linear dependence on R_δ, the Reynolds number is misleading, for A_{21} and A_{22} not only depend on x, x_o and ω_s but also on R_δ, M_∞ and directionality through the factor k_x and $\beta(x_s)$.

The evaluation of $A_{21}(x,x_o,\omega_s)$ and $A_{22}(x,x_o,\omega_s)$, expressing the relative streamwise variation of the amplitude and phase of u_b, requires as input not only the variation along x, the streamwise coordinate, of the amplitude and phase of the sound field, but also of $\beta(x)$, the complex eigenvalue of the homogeneous Orr-Sommerfeld equation for the relevant mean flow field. The variation of $\beta(x)$ with x can be related to the variation of β with R_δ, the displacement thickness Reynolds number, using the relationship $\delta = 1.72\sqrt{\nu x/U_\infty}$. The variation of complex β with R_δ has been computed for different frequencies using a computer program developed by Saric (Reference 3-21) and is shown in Figure 3-15 for the case of the stability frequency parameter $F = (\omega\nu/U_\infty^2) = 56 \times 10^{-6}$. This frequency parameter has been chosen to simulate the measurements of Shapiro (Reference 3-14) for his case of sound frequency = 500 Hz and freestream flow of 29 m/sec. The variation of the complex β with R_δ is introduced into the integral expression for A_{21} and A_{22} after suitable transformation from x to R_δ, and the integrals have been evaluated numerically and the results are shown and discussed below.

Figures 3-16 and 3-17 show numerical solutions of the amplitudes of the two components of u_b (volume integral and surface integrals respectively, see Equation 3-26) in the form $\log_n A_{21}(x,\eta,\omega_s)/A_{21}(x_o,\eta,\omega_s)$ and $\log_n A_{22}(x,\eta,\omega_s)/A_{22}(x_o,\eta,\omega_s)$ as a function of Reynolds number R_δ which is proportional to square root of x. Because of the normalized form of the ordinate, these curves also correspond to $\log_n u_b(x,\eta,\omega_s)/u_b(x_o,\eta,\omega_s)$ as a function of R_δ. The dashed curve in each figure corresponds to the amplification of a Tollmien-Schlichting wave if it was excited by a point source at the reference location and corresponds to the axial variation of the amplitude of the Green's function referred to in the section on general solution. Several aspects of these numerical solutions deserve comments.

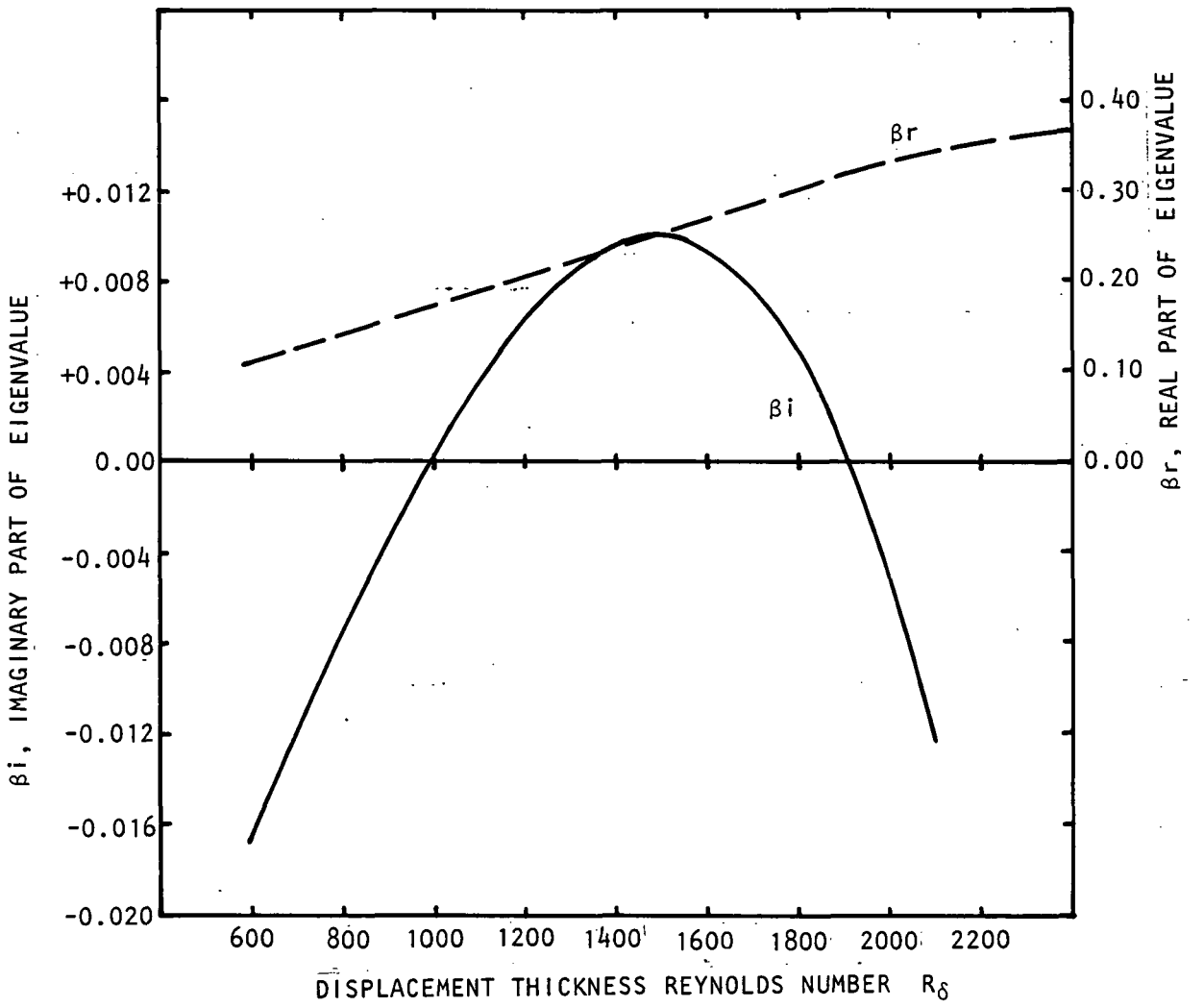

Figure 3-15. Variation of complex eigenvalue ($\beta_r + j\beta_i$) with Reynolds number from solution of homogeneous Orr-Sommerfeld equation for frequency parameter $F = \nu\delta/U_\infty^2 = 56 \times 10^{-6}$.

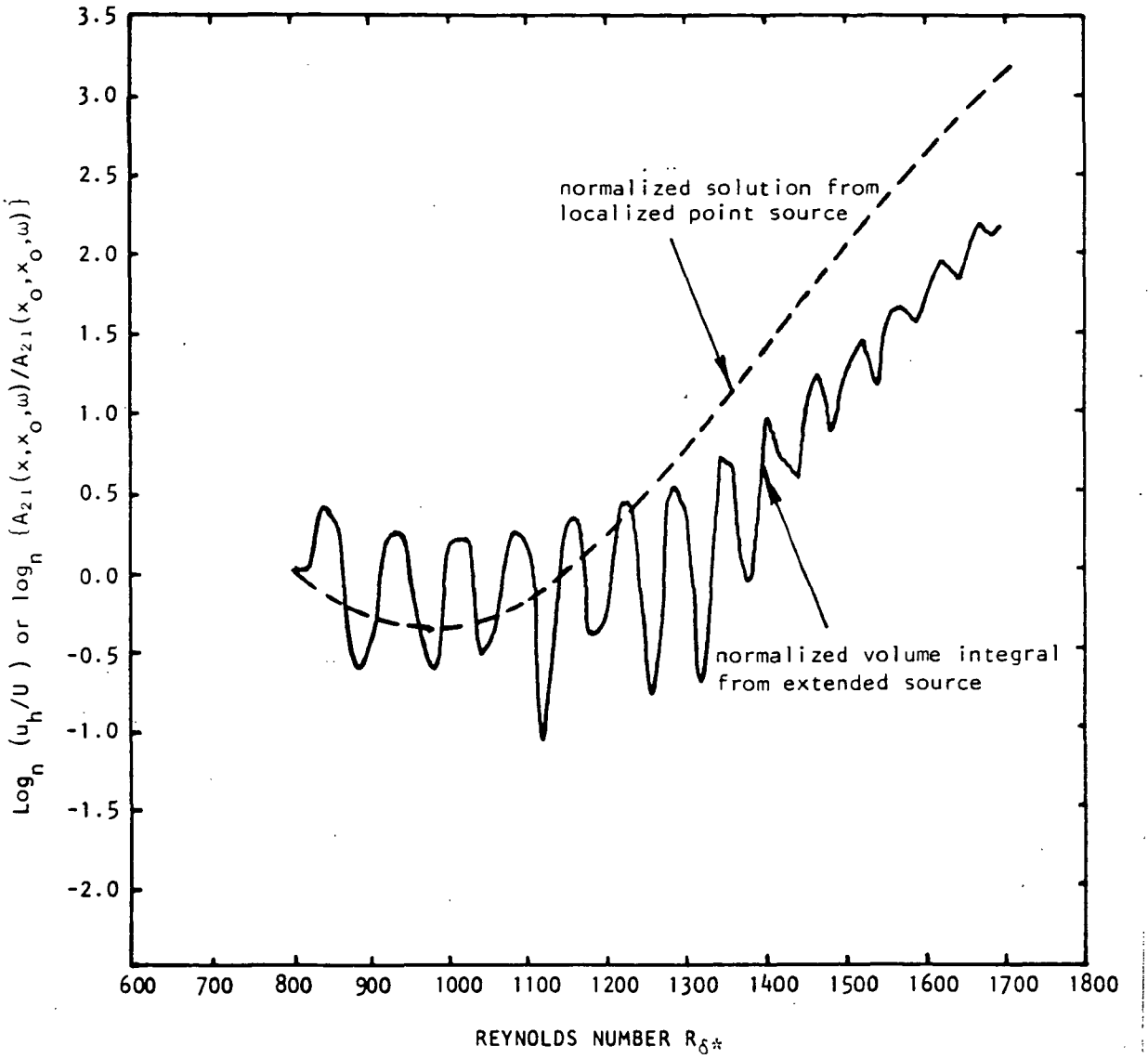

Figure 3-16. Volume integral component A_{21} to numerical solution of sound induced TS wave.

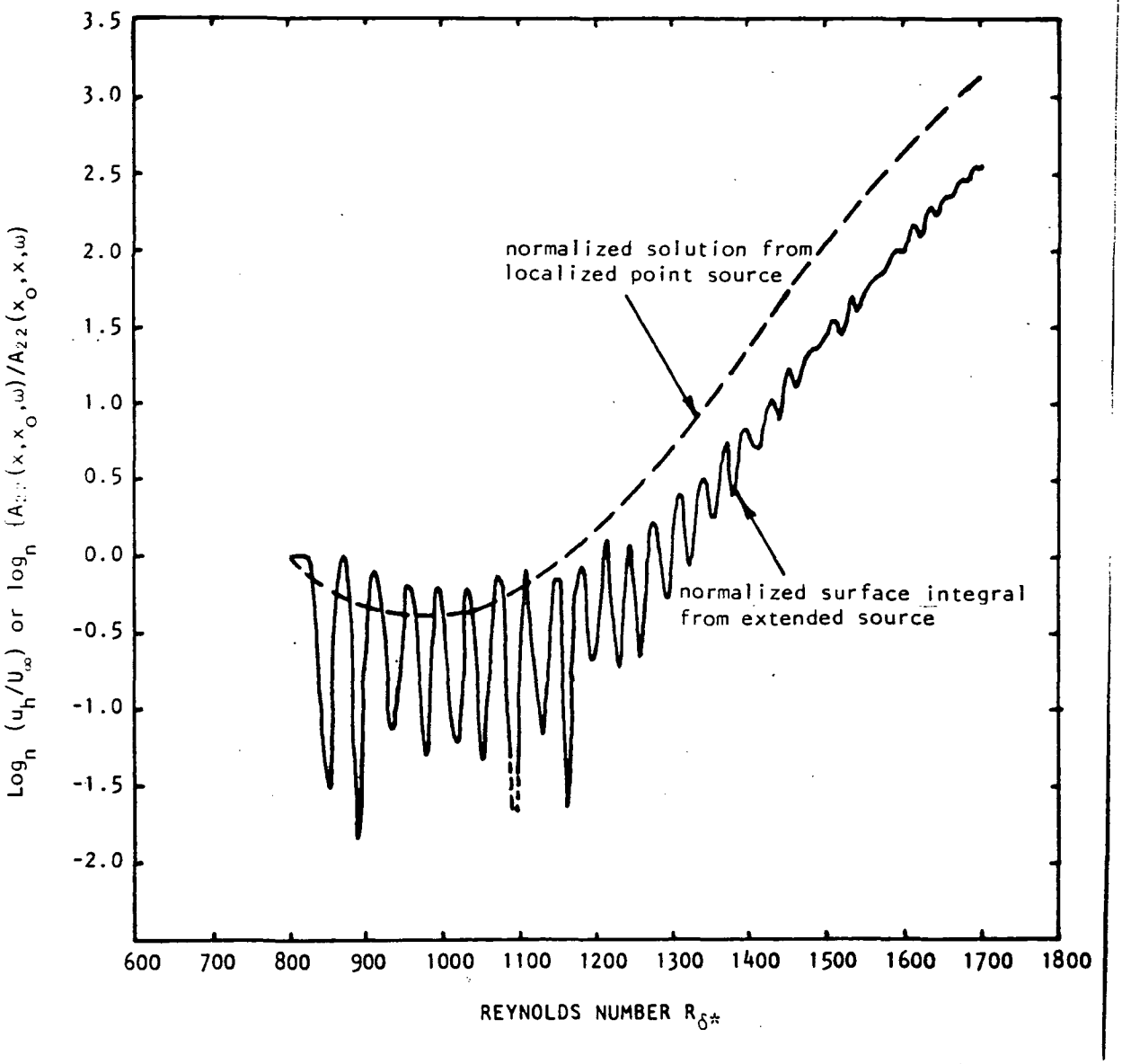

Figure 3-17. Surface integral component A_{22} to numerical solution of sound induced TS wave.

The first observation is that the amplitudes of both A_{21} and A_{22} are spatially modulated unlike the corresponding localized point source solution which monotonically decays initially and amplifies subsequently. However, the peaks of the spatial modulation do follow a trend somewhat similar to the localized point source solution.

A second observation is that in the initial region along the R_δ coordinate, which includes the damped region, the peaks of the extended source solution lie above the localized point source solution. Further downstream, the reverse is true, the extended source solution lies below the localized point source solution.

There are about twice as many maxima and minima in the amplitude of the surface integral than that in volume integral. The ratio of the maximum to the minimum amplitude in each curve reduces as one proceeds downstream. One may be tempted to call this a standing wave ratio, but whether the disturbance is standing or propagating is determined, not from the spatial modulation of the amplitude, but rather from the phase distribution which is investigated next.

Figure 3-18 shows $\chi_1(x)$ and $\chi_2(x)$, the phase variations with (x/x_{ref}) or $(R_\delta/R_{\delta_{ref}})^2$ of the volume and surface integrals A_{21} and A_{22}, respectively. The phase variation of the sound wave is also included to contrast the vast difference in wavelength of the "exciter" disturbance (the sound wave) and the "excited" disturbance (the boundary layer disturbance).

From the linear variation of χ_1, it can be deduced that the volume integral A_{21}, corresponds to a propagating disturbance, in spite of the fact that the amplitude is spatially modulated. The wavenumber and the corresponding phase speed can be determined from the slope of the phase vs distance plot. For the case of 500 Hz, and freestream flow U_∞ = 29 m/sec, the slope of χ_1, is equivalent to a disturbance of phase speed = 26.5 m/sec (= 0.91 U_∞ or a Mach number of 0.08). Such a disturbance, although convecting with a speed slower than the freestream, cannot be associated with a TS wave which propagates with a phase speed closer to 0.3 U_∞.

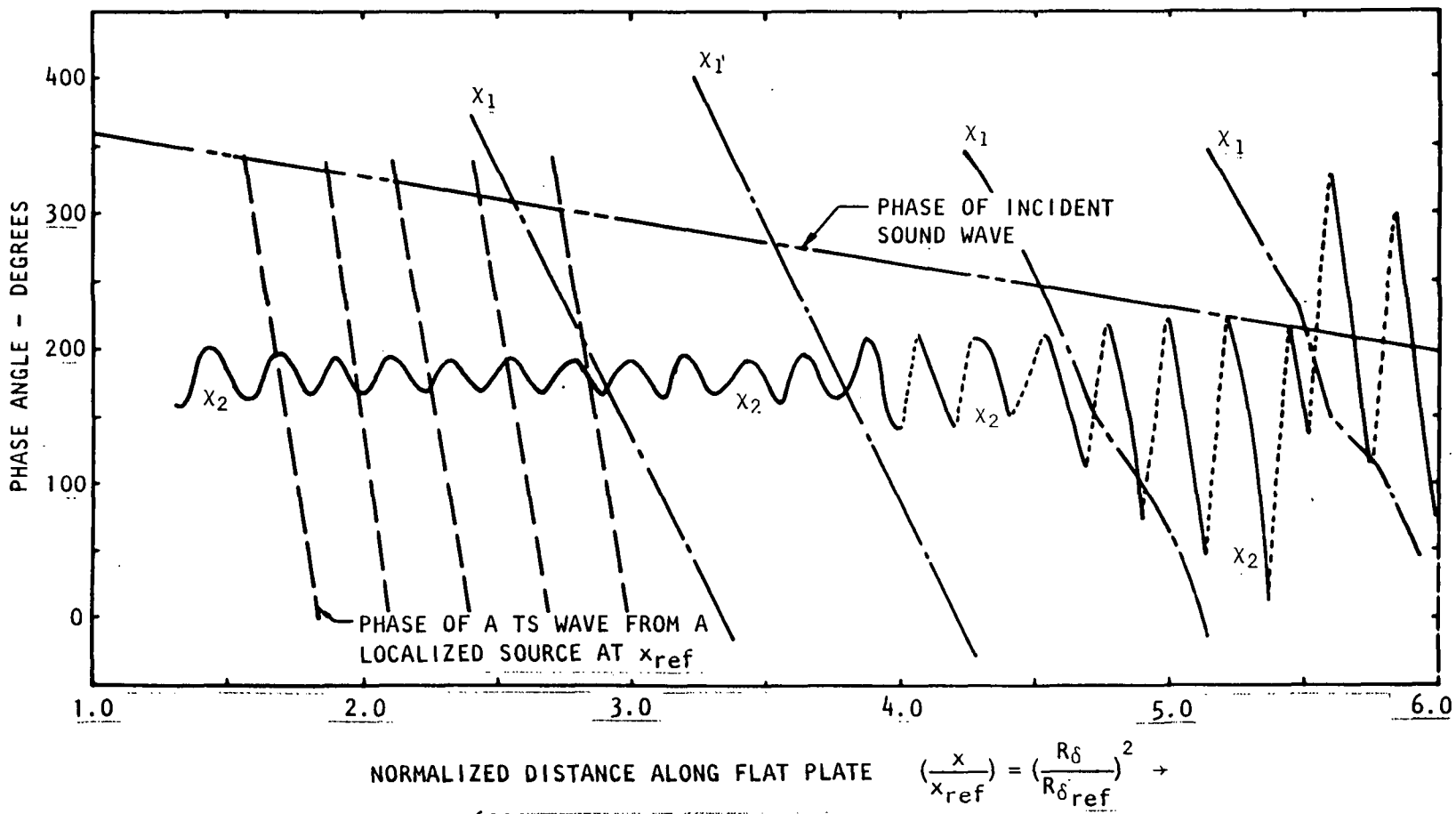

Figure 3-18 Calculated Phase Variations Along a Flat Plate for An Incident Sound Wave and for the Components of the Boundary Layer Disturbance Excited by the Sound.
$X_1(x)$ = Phase of Component Arising from Volume Integral.
$X_2(x)$ = Phase of Component Arising from Surface Integral.
Phase of a TS Wave from a Localized Source at x_{ref} (from Homogeneous OS equation)

Unlike χ_1, the variation of χ_2, the phase of A_{22}, (due to surface integral) does not become linear until some point downstream of the reference location; and when it does become linear, the associated phase speed is 6.3 m/sec or 0.22 U_∞ compared to 0.30 U_∞ for a TS wave. In the initial region, phase χ_2 fluctuates about a reference phase with an "amplitude" growing from 30° until the region downstream where it starts propagating. In this initial region, the surface integral component is not only amplitude modulated in space, but is also phase modulated. Such a phase modulation lies somewhere between that of a standing wave and that of a propagating wave. In this context, in the initial region, the disturbance corresponding to the surface integral can be looked upon as a crawling wave until further downstream it starts to "run" or propagate.

3.5.5 Comparison of Numerical Results with Measurements and Relevent Observations

The numerical results described in Figures 3-16 and 3-17 may now be compared separately or together with the corresponding measurements of Shapiro (Reference 3-14) reproduced here in Figure 3-2. The spatial modulation of the amplitude is similar to that described in the numerical solution, especially the diminishing ratio of the maximum to the minimum. Shapiro's measured phase given in Figure 3-19 shows evidence of the presence of phase modulation and the slow or crawling wave. Further downstream, the measured phase gradient suggests a phase speed of 0.88 U_∞ which compares with the value of 0.91 U_∞ from the numerical solution, arising from the volume integral component. The dashed curves of Figures 3-16 or 3-17 correspond to a localized point source and may be compared with the measurements of Klebanoff and Tidstrom, reproduced here in Figure 3-1.

Thomas and Lekoudis (Reference 3-22) in an attempt to explain the spatial modulation observed by Shapiro suggested that the observation could be a simple interference between a sound wave and a TS wave, and accordingly evaluated such a model allowing the TS wave to amplify and keeping the sound wave amplitude constant. Their results look similar both to the measurements of Shapiro and to the numerical results presented here for the surface integral, $A_{22}(x, \eta, \omega_s)$. The agreement is not surprising, for if one considers the

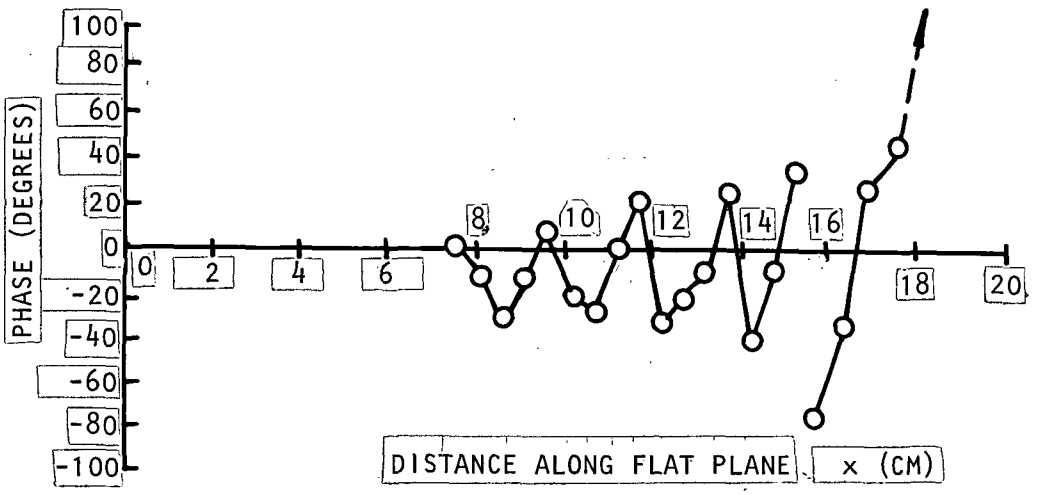

Figure 3.19 Measured phase of boundary layer disturbance excited by a plane incident sound. $U_\infty = 29$ m/s, f = 500 Hz, from Shapiro reference 3-14.

simplified form of $A_{22}(x,\eta,\omega_s)$ by ignoring the streamwise gradient of the boundary layer thickness, (that is $\partial\delta(x)/\partial x << \beta(x)\,\delta(x)$, then $A_{22}(x,\eta,\omega_s)$ does represent an interference pattern of the kind considered by Thomas and Lekoudis.

The above mentioned sound excited spatial modulation of the amplitude of the boundary layer disturbance was also observed and reported by Mechel and Schilz (Reference 3-16) and is probably related to the chordwise striations observed by Pfenninger (Reference 3-4) on a swept wing, (Naphthalene sublimitation experiment) using discrete frequency noise. Pfenninger added that such vortices were not observed in the absence of noise. In view of the fact that the contribution of A_{22} to the total disturbance corresponds to a "crawling or nearly standing" wave, it may well be associated with the striations or vortices.

Spatial amplitude modulations have also been measured in sound excited mixing layers of jets (References 3-13 and 3-23 thru 3-26). The mechanism of acoustically induced vorticity can be applied to such flows as well, provided the Green's function is suitably constructed from the relevant eigenvalue.

3.5.6 The Effect of Sound on Phase Speed and Rate of Amplification of Boundary Layer Disturbance

As mentioned in the preamble to the hypothesis of the present analysis, the propagation and amplification or decay of a TS wave is governed by the Orr-Sommerfeld equation. For a specified arbitrary frequency, the rate of amplification or decay according to stability analysis is a function of the mean flow field only (freestream velocity, kinematic viscosity and velocity profile). The measurements of Mechel, Mertens and Schliz (Reference 3-19) showed that the propagation exponent of the boundary layer disturbance excited by sound can be considerably different to that excited by a vibrating ribbon or by natural turbulence. Above a critical frequency, sound causes a reduction in the amplification rate, and thus has a stabilizing effect. Further, the measured phase speed of acoustically excited boundary layer disturbances was found to be greater than that of TS waves, varying between 0.45 to 0.625 of the

freestream, depending on frequency. Stability calculations (homogeneous Orr-Sommerfeld equation) indicate that a TS wave for $F = 56 \times 10^{-6}$ ($= \omega\tilde{\nu}/U_\infty^2$) should propagate with a phase speed close to $0.3\ U_\infty$.

The numerical solutions of the sound induced inhomogeneous Orr-Sommerfeld equation discussed above shows that the rate of amplification in the amplifying region is indeed lower than that corresponding to a TS wave excited by a localized point source. The sound induced source has been treated as an extended source and not a localized point source. The reduction in the amplification rate is due to interferences not only between a sound wave and the resulting vorticity wave (shown in the surface integral), but also among vorticity disturbances excited by different portions of the sound wave.

The sound induced disturbance at low Reynolds numbers that has a defined characteristic phase speed is that associated with the volume integral. In the range $600 \leq R_\delta \leq 750$, the corresponding phase speed is $0.61\ U_\infty$ and increases steadily to $0.91\ U_\infty$. Further downstream the component associated with the surface integral starts propagating with a phase speed close to $0.22\ U_\infty$. In view of the fact that both integrals have the same weighting, then in the Reynolds number range where both contributions are propagating, the average phase speed will be of the order of $0.56\ U_\infty$, which is in agreement with the measured increased phase speed due to acoustic excitation.

3.6 COMMENTS ON BOUNDARY LAYER EXCITATION BY TWO OR MORE DISCRETE SOUND FIELDS

The prediction of the spatial modulation of the boundary layer disturbance excited by a pure tone, the increase in phase speed, and the decrease in the amplification rate seems to be borne out by measurements. Since all these effects appear to be caused by interferences due to the "extended source of acoustically induced fluctuating vorticity," then more interactions of a similar nature can be expected if more than one pure tone is used. Such effects should show up when evaluating the last of the three integrals in Equation 3-12 with respect to $d\omega_s$. Such a study can and should be pursued, but is outside the scope of this investigation, and is therefore recommended for future studies.

3.7 COMMENTS OF SOUND INDUCED DISTURBANCES IN PRESENCE OF CROSS-FLOW

On a swept wing, in addition to the flow along the chord, there is a mean cross-flow along the span direction whose velocity profile is inflectional.

Brown (Reference 3-27) and Pfenninger (Reference 3-28) computed the stability characteristics of such an inflectional cross-flow profile and found the critical Reynolds number to be much lower than that of a Blasius profile. If the cross-flow was the only component of the flow field, the boundary layer disturbance would propagate along the cross-flow direction, and sound induced excitation of such disturbances could be treated in exactly the same way as that just described for the TS wave in the Blasius boundary layer along a flat plate. The difference would be that the variation of the propagation exponent with distance in the Green's function would have been different.

The flow field on a swept wing is three-dimensional, so that the boundary layer disturbance does not propagate along the chord or the span but at some angle to the freestream. This angle varies with frequency and location on the wing due to the changing magnitude and profile of the cross-flow. In such a 3D mean flow field, the disturbance is also three-dimensional. The analyis of spatial stability of three dimensional disturbances is recent and not fully developed yet (References 3-29 thru 3-32). Consequently, the evaluation of sound induced cross-flow instability must await such development.

The factors and concept that led to the X-21A LFC/Acoustic criteria have been discussed. Its main limitation is its inadequacy to take into account the spectrum and directionality of the sound field. A semi-empirical method based on numerical solutions of the homogeneous Orr-Sommerfeld equation has been applied to provide sensitivity to frequency, suction distribution and suction rates. A directionality factor, based on analytic solution of a more fundamental formulation of the problem, is proposed. A critical SPL spectrum for different angles of incidence are computed numerically and shown graphically. An example case of the application of these critical SPL spectra is also shown, using a tail-mounted jet engine noise spectrum.

The more fundamental problem of how does a sound wave excite boundary layer disturbances and the physical mechanisms involved in the process are discussed in Section 3.5 of this report. The hypothesis is that, boundary layer disturbances being governed by the linearized unsteady vorticity transport equation, for sound to excite such disturbances it must generate fluctuating vorticity or fluctuating flux of vorticity. These are discussed in detail and an inhomogeneous Orr-Sommerfeld equation is derived with source terms proportional to the amplitude and phase of the sound field. Numerical solutions of this inhomogeneous governing equation are computed in the form of volume and surface integrals. The results show spatial modulation of the amplitude and phase of the boundary layer disturbances and are in agreement with the measurements of Shapiro. Other measurements where striations on an airfoil have been observed in the presence of a sound field are relatable to these spatial modulations. Measured effects of a sound field on the amplification and phase speed of boundary layer disturbances can also be explained by the analysis. The numerical solutions have been restricted to low frequency sound impinging on the boundary layer over a rigid flat plate. Non rigid surfaces and the effects of slots can be, but have not been analyzed. Diffraction by the leading edge has also been excluded from the analysis.

This study has identified specific technology gaps and problem areas relative to both cruise noise prediction and LFC noise criteria.

4.1 NOISE PREDICTION METHODS

The cruise noise prediction methods are based largely on acoustic data acquired at sea level under static or low forward speed conditions. To confirm the validity and to increase the accuracy of the methods which have been developed for the prediction of noise, under transonic conditions, requires that analytical and test programs be conducted covering the following subjects, as summarized in Figure 4-1 and detailed as follows.

1. Methods Validation

To validate the cruise noise prediction procedures, an experimental flight test program is required where high quality cruise noise data would be acquired at a (wing) surface in the presence of a laminar boundary layer. This will prevent masking of the acoustic signal by the adjacent turbulent boundary layer and thus provide the uncontaminated incident total noise originating from the propulsion and airframe noise sources. Such a test program could be conducted on an airplane where the microphones could be located in the natural laminar flow of the wing leading edge or on a laminar flow control glove. The methods of this report would be used to predict the measured total noise levels. Any differences would be used as feedback data to allow modification of the prediction procedures for improved accuracy of both component and total noise.

Measured cruise noise data from the X-21A and any which is available from high by-pass ratio turbofan powered airplanes (measured in the presence of a turbulent boundary layer) also needs to be evaluated to provide an assessment of the prediction method accuracy.

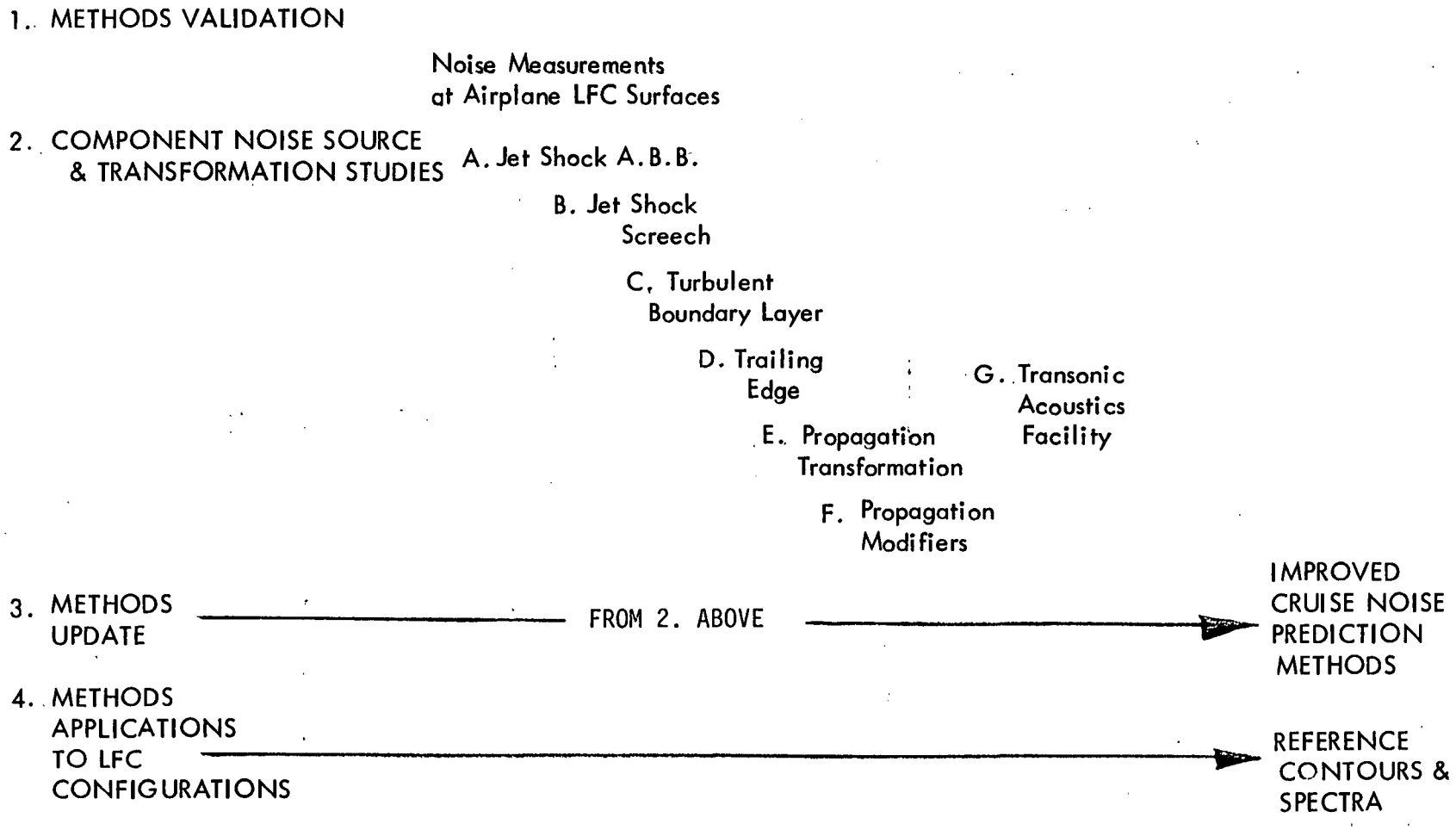

FIGURE 4-1. AREAS FOR IMPROVED CRUISE NOISE PREDICTION TECHNOLOGY

2. Component Noise and Transfomation Studies

A. Jet Shock Associated Broad Band Noise

(i) Update. More experimental information has recently become available on the acoustic spectral directivity characteristics of shock associated broad band noise at simulated low forward speeds, Reference 2-46. This noise source prediction computational algorithm needs to be updated to include this new data.

(ii) Experimental and Analysis Program. A test program is required to measure the shock associated broad band noise characteristics of a two flow jet representative of 1995's propulsion system cycle and nozzle configurations. Nozzle pressures and temperatures need to be simulated. Data would be acquired in the complete foward and aft quadrant and at near field distances, as a funcion of simulated aircraft forward speed Mach numbers, to as high a Mach number as possible. Facilities for an experimental investigation of this kind, at lower speeds, exist at the Lockheed-Georgia Company and at other companies.

Based on theoretical and experimental data the measured noise would be adjusted to correct for 1) higher aircraft forward speeds, corresponding to cruise conditions and 2) change in jet flow structure at cruise conditions. Other applicable transformations would be reviewed.

B. Jet Shock Screech

An experimental model program is required to investigate the possible occurrence of shock screech in two flow jets, representative of 1995's propulsion system cycle and nozzle configurations, at cruise conditions. This is required since no criteria are available to indicate the onset of screech.

Such a test could be conducted in conjunction with the jet broad band shock associated noise test discussed in the last section.

Results would be subject to the same limitations as discussed there. Avoidance criteria may be established.

C. Turbulent Boundary Layer Noise

A theoretical and experimental study of the noise radiated by a turbulent boundary layer is required. In the current empirical prediction procedure, the parts (OASPL, spectrum and directionality) have been derived from different sources in the literature, and are limited to surface velocities of about 350 ft/second. The prediction procedure needs to be expanded to include other turbulent boundary layer noise sources e.g. volume quadrupole which, because of the higher noise producing velocity exponent associated with quadrupoles, could be the dominant component at higher subsonic speeds. This extension could be developed analytically by first comparing the flow characteristics of a turbulent boundary layer and a subsonic jet. Then since the noise characteristics of a subsonic jet are well defined, the boundary layer would be equated to an equivalent distribution of jets whose acoustic strength would be modified depending upon the flow comparison.

A test program is essential to validate these methods. All flow facilities have radiated turbulent boundary layer noise as a contributing noise source. What is needed is an experiment where radiated boundary layer noise can be positively identified. Such a condition would be obtained using a rotating cylinder installed in an anechoic environment. Much attention would be required to suppress any cylinder drive or other extraneous noise. Further, surface velocities up to 900 feet per second would be required. Sound pressure levels and spectra would be measured as a function of rotational speed throughout the speed range and the resulting data would be used to modify the prediction procedures.

D. Trailing Edge Noise

The acoustics of edges in turbulent flows is a new field. The near field trailing edge prediction model is developed from

measured airframe far-field acoustic data at low aircraft speeds. This near field prediction model requires verification. Further, it requires extension to higher speeds representative of cruise, since other edge/flow mechanisms might be contributing at higher speeds. An experimental investigation of high speed trailing edge noise might be difficult to devise since positive identification of this noise source could be difficult. However, some experimental verification is required.

E. Propagation Transformations

The acoustic propagation from moving noise sources is different to that of stationary noise sources. Two effects are the so-called convective amplification and dynamic amplification modifications. There are numerous references to these effects in the literature and some experimental confirmation at low forward speeds has been reported. Inclusion of these effects has a profound impact on the noise predictions at higher cruise Mach numbers. Experimental verification of these effects at high speeds is required.

F. Propagation Modifiers

During cruise, the high speed flow around the airplane gives rise to aerodynamic pressure fields, possible shock waves and wakes from the trailing edges. Hence, the atmosphere in the vicinity of the airframe through which the acoustic waves travel to reach the airplane surface is not a homogeneous medium. These non-homogeneities can cause scattering and refraction of the acoustic waves and thus modify the predicted incident noise field. These effects are much more important during cruise in the near field than at takeoff conditions in the far field, where much aero-acoustics activity has been focused.

A detail study of the influence of these aerodynamic propagation modifiers on the acoustic field is needed e.g., the acoustic transmission through high speed wakes. The study needs to be both of a theoretical and experimental nature.

G. Transonic Acoustic Facility

Many of the problem areas recommended for further study require some kind of experimental verification at forward speeds corresponding to subsonic cruise conditions. Noise measurements on airplanes cover total noise (contributions from all moving sources), including the individual source transformation and propagation modifications. To isolate and study individual noise sources with their forward speed effects could probably best be done in a transonic acoustic facility.

Existing acoustic facilities which currently provide forward speed simulation are low speed, to approximately 400 ft./sec. Data acquired under these low speed conditions requires extensive velocity extrapolation.

Therefore the feasibility of developing a transonic acoustic wind tunnel facility should be considered. Such a facility must have a low self noise environment at Mach number up to 0.8 whether the noise originates from the tunnel drive or from the walls. For example the walls might require laminar flow control to reduce radiated turbulent boundary layer noise. Further, the working section should be anechoic. Such a high speed low noise environment, besides being applicable to the solution of LFC cruise noise problems, could also be used to investigate other aeroacoustical problems such as the near-field cruise noise of an advanced propeller.

3. Methods Update

As improved data prediction methods become available, (for example as a result of these recommendations, or through ANOPP noise prediction improvements or through other studies) they

should be incorporated into the Cruise Noise Prediction Methods Manual.

4. Methods Application

The cruise spectral directivity noise contours over LFC candidate configurations (wing mounted and tail mounted propulsion systems) will be so different to those which exist statically that they need to be determined. This should be done at discrete frequencies and for one third octave band center frequencies. This requires multiple point use of the prediction methods since they are only applicable to noise at a point.

It is desirable that for a few critical locations, based on the contours desired above, that reference cruise noise spectra be established. As more information becomes available and as the Cruise Noise Prediction Methods Manual is updated so the reference spectra should also be updated, and made available to interested parties. The reference spectra could be included in the Methods Manual.

FIGURE NUMBER

4.2 RECOMMENDATIONS ON LFC/ACOUSTICS CRITERIA

ILLUSTRATION TITLE

Two approaches to LFC/Acoustic criteria have been discussed. One is semi-empirical and corresponds to an extension of that used on the X-21 by taking into account the directionality and spectrum of the sound field. The other approach is more fundamental and involves solving an inhomogeneous Orr-Sommerfeld equation in which the source terms are proportional to acoustically induced fluctuating vorticity. In each of the two approaches certain simplifying assumptions were made in order to keep track of the basic coupling mechanisms.

OBJECTIVE:

The main objective in this recommendation is to identify specific tasks that will help generalize and improve the LFC/Acoustic criteria in both approaches by removing some of the simplifying assumptions. These are discussed below. Tasks 1 and 2 relate to improving the semi-emprical critical SPL predictions. The remaining tasks are for improving the fundamental approach.

TASK 1

Although critical SPL spectra can and have been generated for arbitrary suction distribution, angle of incidence and chord locations, the SPL values are relative, and to convert such values to absolute SPL, a constant dB level which in effect defines a $(u_b/U_\infty)_{crit}$ must be added. In Section 3.4.5, on application example, by comparison with a measured critical SPL, the upper limit was deduced to be 130 dB. The validity of such an upper limit needs to be investigated, and this involves an experimental program using suitable airfoil surfaces and correspondingly suitable suction distribution. When such a test is carried out, a set of measurements with different sound directionality should be incorporated as a subtask. Northrop tests, with directionality limited to longitudinal and transverse directions, showed significant effect of directionality. No tests have been reported where the sound propagates upstream.

PAGE NUMBER

199

In computing the critical SPL for the Lockheed airfoil for a specified suction distribution, the amplification spectra were computed by solving the homogeneous Orr-Sommerfeld equation. In the more fundamental approach which was restricted to plane sound wave impinging on a semi-infinite flat plate, the inhomogeneous Orr-Sommerfeld equation was solved with results showing that the amplification rate was space modulated and somewhat different to that from the homogeneous solution. In this task, it is suggested that the flat plate inhomogeneous equation evaluation be extended to the airfoil case. The previously computed homogeneous solution can still be used to construct the Green's function needed in evaluating the integral equation. The results will not only modify the critical SPL spectra, but should also allow localization of the situations if present.

TASK 3

The analysis on the coupling of sound to boundary layer disturbances has been developed so far for discrete frequency sound on flow over a semi-infinite rigid flat plate. It is known from measurements that the critical SPL is higher for broad band sound compared to a pure tone. Before attempting to simulate broad band sound, it is suggested that the semi-infinite rigid flat plate calculation be extended to include two and three pure tones with the same and varying phases.

TASK 4

Under this task it is proposed that the sound scattered by one and a distribution of slots be studied with a view to evaluating the acousto-hydrodynamic coupling. Finite differences are expected from the coupling with the incident plane wave, one of which is that the amplitude of the scattered sound field delays as the distance from the slot increases, unlike the constant amplitude of the incident sound. Another difference is due to discrete phase lag among the fluctuating vorticity sources at each of the slots. Contribution to the surface integrals from the flat plate will not be zero as in the case of rigid flat plate. A length scale proportional to the slot spacing is expected to be a parameter.

APPENDIX A

The Fluctuating Vorticity Field of a Sound Wave in a Non-Uniform Flow

The non-uniform mean flow considered is a uni-directional flow (in x direction) transversely sheared (in y direction). Such a flow approximates that over a flat plate or a jet issuing out of a nozzle, since the transverse components are normally much smaller than that along the main stream.

The convected acoustic wave equation governing the sound field is given by (Reference 3-20)

$$\nabla^2 P - \frac{1}{c^2}\frac{D^2P}{Dt^2} + 2\bar{\rho}\,\frac{\partial U}{\partial y}\,\frac{\partial v}{\partial x} = 0 \qquad \text{A-1}$$

Because the coefficients are not functions of the x and t independent variables, the solution can be written in the form,

$$P = F(y)\, e^{j(\omega t - k_x x)} \qquad \text{A-2}$$

where $F(y)$ takes the form of $e^{\pm jk_y y}$ in uniform unbounded flows (or in a homogeneous ambient medium). In the uniform part of bounded flows, $F(y)$ is made up of a combination of $e^{-jk_y y}$ and $Be^{+jk_y y}$, where B represents some form of reflection coefficient from the shear layer. Inside the shear layer, $F(y)$ is a continuous function of y and its distribution depends on the frequency of the sound wave and the mean flow profile, accounting for refraction effects.

The particle velocities associated with the acoustic pressure field as given by eq. (A2) is governed by the linearized momentum equations, namely

$$\frac{\partial u_a}{\partial t} + U\frac{\partial u_a}{\partial x} + v_a\frac{dU}{dy} = -\frac{1}{\bar{\rho}}\frac{dP}{\partial x} \qquad \text{A-3}$$

and

$$\frac{\partial v_a}{\partial t} + U \frac{\partial v_a}{\partial x} = - \frac{1}{\bar{\rho}} \frac{\partial P}{\partial y} \qquad \text{A-4}$$

in which the viscous terms have been left out as was done also for eq. (A-1).

An expression for v_a and u_a can be obtained by substituting eq. (A-2) in equations (A-4) and (A-3) and may be written in the form

$$\bar{\rho} c \, v_a = - \frac{1}{jk(1-MK)} \frac{\partial P}{\partial y} \qquad \text{A-5}$$

and

$$\bar{\rho} c \, u_a = - \frac{1}{jk(1-MK)} \frac{\partial P}{\partial x} - \frac{1}{k^2(1-MK)^2} \frac{dM}{dy} \frac{\partial P}{\partial y} \qquad \text{A-6}$$

where $M = U(y)/c$ and $k = \omega/c$, $K = (k_x/k)$

The fluctuating vorticity attached to the sound field may be defined by

$$\Omega_a = \frac{1}{2}\left(\frac{\partial v_a}{\partial x} - \frac{\partial u_a}{\partial y}\right) \qquad \text{A-7}$$

and may be evaluated by substituting eq. (A-5) and A-6).

In the special case of uniform mean flow, M is a constant, so that $\partial M/\partial y = 0$ and the last term of eq. (A-6) vanishes. If then eq. (A-5) and (A-6) are substituted in (A-7), one obtains

$$\bar{\Omega}_a = 0 \qquad \text{A-8}$$

for sound propagating in a uniform mean flow, or in a homogeneous ambient medium.

In the case of a transversely sheared mean flow, it can be shown that

$$\Omega_a = \frac{1}{2\bar{\rho}c}\left[\frac{K^2}{(1-MK)^2}\frac{\partial M}{\partial y}P(x,y,w) + \frac{1}{k^2}\frac{\partial}{\partial y}\left\{\frac{1}{(1-MK)^2}\frac{\partial M}{\partial y}\frac{\partial P}{\partial y}\right\}\right] \qquad \text{A-9}$$

Further simplification to eq. (A-9) can be made by carrying out the differentiation of the last term, and using a reduced form of eq. A-1 after substituting eq. A-2. If this is done, it can be shown that eq. (A-9) reduces to

$$\Omega_a = \frac{1}{2\bar{\rho}c}E(y,K,k)\quad \exp\,(j\omega t - k_x x) \qquad \text{A-10}$$

where

$$E(y,K,k) = \left\{\frac{2K^2}{(1-MK)^2} - 1\right\}\frac{\partial M}{\partial y}F(y) + \frac{1}{k^2(1-MK)^2}\frac{\partial^2 M}{\partial y^2}\frac{\partial F}{\partial y} \qquad \text{A-11}$$

or

$$E(\eta,K,k) = \left[\left\{\frac{2K^2}{(1-MK)^2} - 1\right\}\frac{\partial M}{\partial \eta}F(\eta) + \frac{1}{(k\delta)^2(1-MK)^2}\frac{\partial^2 M}{\partial \eta}\frac{\partial F}{\partial \eta}\right]\frac{1}{\delta(x)}$$

Thus the fluctuating vorticity attached to the sound field has the same axial phase dependence as the sound field, as it should, but its transverse distribution is a function of the frequency k, directionality of the sound

field through the term $K = k_x/k$, the sound pressure distribution $F(y)$, across the boundary layer and the first and second transverse derivatives of the mean flow $\partial M/\partial y$ and $\partial^2 M/dy^2$.

This fluctuating vorticity attached to the sound field vanishes outside the boundary even when the sound field is still present.

APPENDIX B

Perturbation and linearization of the vorticity transport equation, and the acoustically induced sources of the inhomogeneous Orr-Sommerfeld equation.

The acoustic perturbation of the vorticity transport equation involves expanding the relevant variables of the equation in terms of the steady state values and the fluctuating components. Recognizing that acoustic and boundary layer disturbances propagate with different speeds, the corresponding fluctuating velocity vectors denoted by the $\underset{\sim}{w}_a$ and $\underset{\sim}{w}_b$ whose components along the main stream are respectively u_a and u_b, and those transverse to main stream are denoted as v_a and v_b, respectively.

The components of the mean velocity along x and y are denoted by $U(x,y)$ and $V(x,y)$ and are assumed functions of x and y in the initial derivation. Thus

$$U_{(x,y,t)} = \bar{U}(x,y) + u_b(x,y,t) + u_a(x,y,t) \qquad \text{B-1}$$

$$V(x,y,t) = \bar{V}(x,y) + v_b(x,y,t) + v_a(x,y,t) \qquad \text{B-2}$$

where u_b and v_b are x and y components of the particle velocity associated with boundary layer disturbances and are governed by the linearized vorticity transport equation; and u_a and v_a are x and y components of the particle velocity associated with the acoustic field and are governed by the convected acoustic wave equation.

The vorticity vector, curl Ω, which reduces to the one component about the z axis for 2-dimensional flow becomes

$$\Omega_z = \frac{1}{2}\left(\frac{\partial V}{\partial x} - \frac{\partial U}{\partial y}\right) \qquad \text{B-3}$$

and can be expanded into a mean quantity $\bar{\Omega}$, and two fluctuating quantities Ω_b and Ω_a associated respectively with the boundary layer disturbance and the acoustic field. Thus

$$\Omega_z = \bar{\Omega} + \Omega_b + \Omega_a \qquad \text{B-4}$$

where

$$\bar{\Omega} = \frac{1}{2}\left(\frac{\partial \bar{V}}{\partial x} - \frac{\partial \bar{U}}{\partial y}\right)$$

$$\Omega_b = \frac{1}{2}\left(\frac{\partial v_b}{\partial x} - \frac{\partial u_b}{\partial y}\right) \qquad \text{B-5}$$

and

$$\Omega_a = \frac{1}{2}\left(\frac{\partial v_a}{\partial x} - \frac{\partial u_a}{\partial y}\right)$$

The vorticity transport equation representing the conservation of vorticity, states that the local time rate of change is balanced by convective transport (corresponding to accumulation) and dissipation by viscous effects and may be written in the form,

$$\frac{\partial \Omega}{\partial t} + \frac{\partial}{\partial x}(U\Omega) + \frac{\partial}{\partial y}(V\Omega) - \nu\nabla^2\Omega = 0 \qquad \text{B-6}$$

Equations B-1, B-2 and B-4 may be substituted in the above equation. In view of the fact that the sound field is assumed known (even if acoustic scattering in the form of diffraction, reflection and refraction have to be evaluated), the terms with subscript "a" can be transferred to the right of the equality sign. If this is done after linearizing eq. B-6 one obtains

$$\frac{\bar{D}}{Dt}\Omega_b + u_b\frac{\partial\bar{\Omega}}{\partial x} + v_b\frac{\partial\bar{\Omega}}{\partial y} - \nu\nabla^2\Omega_b = -\frac{\partial}{\partial t}\Omega_a + \text{div}\,(\underset{\sim}{w}_a\bar{\Omega}) - \nu\nabla^2\Omega_a \qquad \text{B-7}$$

where $\underset{\sim}{w}_a$ is the acoustic particle velocity and whose x and y components are u_a and v_a.

In obtaining the above equation, the divergence of the mean flow field and of the velocity field associated with the boundary layer disturbance have been taken to be zero.

Although equation B-7 shows the linearized vorticity transport equation as forced by the sound field, it is not in a suitable form for obtaining a solution due to the mixed variables Ω_b, u_b and v_b. In terms of a stream function ψ defined by

$$u_b = \partial\psi/dy,\ v_b = -\partial\psi/\partial x \quad \text{and} \quad 2\Omega_b = -\nabla^2\psi$$

equation B-7 becomes

$$\nu\nabla^4\psi - \frac{\bar{D}}{Dt}\nabla^2\psi + \frac{2\partial\psi}{\partial y}\frac{\partial\bar{\Omega}}{\partial x} - \frac{2\partial\psi}{\partial x}\frac{\partial\bar{\Omega}}{\partial y} = 2Q_a\,(\Omega_a, \underset{\sim}{w}_a, \bar{\Omega}) \qquad \text{B-8}$$

where $\underset{\sim}{w}_a$ is the acoustic particle velocity vector whose x and y components

are u_a and v_a respectively.

$$Q_a\ (\Omega_a, \underset{\sim}{w}_a, \bar{\Omega}) = \{\frac{\partial}{\partial t}\ \Omega_a + \text{div}\ (\underset{\sim}{w}_a \bar{\Omega}) - \nu\nabla^2\Omega_a\} \qquad \text{B-9}$$

Ω_a is defined in appendix A.

For flow over a flat plate, if the usual approximation that $\bar{V}(x,y) = 0$ and $\bar{U}$ = function of y only, then equation B-8 reduces to

$$\nabla^4\psi - \frac{1}{\nu}\frac{\bar{D}}{Dt}\nabla^2\psi - \frac{1}{\nu}\frac{\partial\psi}{\partial x}\frac{\partial^2 U}{dy^2} = -\frac{2}{\nu}Q_a(\Omega_a, \underset{\sim}{w}_a, \bar{\Omega}, x, y, t) \qquad \text{B-10}$$

and is the *inhomogeneous* Orr-Sommerfeld equation.

The source terms are linearly proportional to the sound field and represent a volume distribution of acoustically induced fluctuating vorticity of multipole orders. The first term represents a *time rate* of change of fluctuating vorticity, the second term is the *divergence of the vorticity flux* induced by the particle velocity associated with the sound fields, and the third term represents the dissipation of the fluctuating vorticity attached to the sound field.

APPENDIX C

Evaluation of the integral

$$\psi_1(x,\eta,\omega_s) = 2 \int\int \delta(x_s)^4 \{j\frac{\omega_s}{\nu} - \nabla_s^2\} \; \Omega_a(x_s,\eta_s,\omega_s) \; g(x,x_s,\eta,\eta_s,\omega_s) dx_s \; d\eta_s \qquad C\text{-}1$$

where $\Omega_a = \frac{1}{2} E(\eta_s,K,\omega_s) \; e^{-jk_x x_s}$ (see Appendix A) C-2

and $E(\eta_s,K,\omega_s)$ is a function of the sound pressure level and its distribution across the boundary layer.

$g(x,x_s,\eta,\eta_s,\omega_s)$ corresponds to the temporal Fourier transform of the response of the boundary layer at an arbitrary (x,η) due to a time harmonic point localized source at (x_s,η_s), similar to that from a vibrating ribbon, and may be written in the form,

$$g(x,x_s,\eta,\eta_s,\omega_s) = \bar{g}(\eta_s) \; \phi(\eta) \; e^{-j\beta(x-x_s)} \qquad C\text{-}3$$

where β is the spatial eigen-value of the homogeneous Orr-Sommerfeld corresponding to the most amplifying (or least damped) wave; $\phi(\eta)$ is the corresponding eigenfunction; and $\bar{g}(\eta_s)$ is the receptivity and describes the effectiveness of excitation as a function of the transverse location of the point source.

Because the boundary layer thickness in most cases of interest changes with distance along the free-stream direction, eq. (C-3) is better expressed in the form,

$$g\ (x,x_s,\eta,\eta_s,\omega_s) = \bar{g}(\eta_s)\ \phi(\eta)\ \exp - j \int_{x_s}^{x} \beta(x\ )\ dx \qquad C\text{-}4$$

Thus eq. (C-1), after some rearrangements may be written in form,

$$\psi(x,\eta,\omega_s) = \delta(x)\ \phi(\eta)\ \frac{F}{\rho c}\ j\left(\frac{\omega\delta}{U_\infty}\right)\left(\frac{U\delta}{\nu}\right) \iint B(x_s,\eta_s)\ \bar{g}(\eta_s)\ dx_s\ d\eta_s \qquad C\text{-}5$$

where $\delta = \delta(x)$, F is the SPL at the rigid surface and is twice the SPL of the incident wave,

$$B(x_s,\eta_s) = \left[\left\{\frac{\delta(x_s)}{\delta(x)}\right\}^3\left\{1 - j\ \omega_s\tau\left(\frac{kx}{k}\right)^2\right\} + j\ \frac{\omega_s\tau}{(k\delta)^2}\frac{d^2}{d\eta_s{}^2}\right]\left[\left\{\frac{2K^2}{(1-MK)^2}-1\right\}\frac{\partial M}{\partial \eta_s}\right]$$

$$x\ \exp - j\left\{k_s x_s + \int_{x_s}^{x} \beta(x\ )\ dx\right\} \qquad C\text{-}6$$

In obtaining equation C-5, a low frequency approximation of Equation III-C-2 has been used. In Equation C-6, $\omega_s\tau$ = 0.75 of the viscous relaxation time = $0.75\ \frac{\omega_s \nu}{c^2}$, and at low frequencies $\omega_s\tau << 1$, so that only the first term inside the first square brackett need to be retained, unless $k\delta << \omega_s\tau$, in which case the third term must also be retained.

Assuming that $\omega_s\tau << k\delta(x)$ (not valid close to leading edge), Equation C-5 becomes

$$\psi_1(x,\eta,\omega_s) = \delta(x)\ \phi(\eta)\ \frac{F}{\rho c}\ k\delta\ \frac{R_\delta}{M_\infty}\ e^{j\pi/2}\ \bar{D}_1(\theta_i,M_\infty)\ A_1(x,x_o,\omega_s) \qquad C\text{-}7$$

where

$$A_1(x,x_o,\omega_s) = \int_{x_o}^{x} \left[\left\{\frac{\delta(x_s)}{\delta(x)}\right\}^3 \exp -j\left\{k_x x_s + \int_{x_s}^{x} \beta(x) \, dx\right\}\right] dx_s \qquad C\text{-}8$$

and

$$D_1(\theta_i,M_\infty) = \int_0^1 \left\{\frac{2K^2}{(1-MK)^2} - 1\right\} \frac{dM}{d\eta_s} \bar{g}(\eta_s) \, d\eta_s \qquad C\text{-}9$$

As mentioned earlier, $\bar{g}(\eta_s)$ describes the effectiveness of boundary layer disturbance excitation by a vibrating ribbon as a function of location across the boundary layer; and details of its variation does not appear to be available either theoretically or experimentally. If it is treated as a constant say $\bar{g}_o$, then Equation C-9 reduces to

$$\bar{D}_1(\theta_i,M_\infty) = 2 \, \bar{g}_o \left\{\frac{K}{1-MK} - \frac{M}{2}\right\}_0^{\eta=1}$$

and since

$$K = \frac{k_x}{k} = \frac{\cos \theta_i}{1 + M_\infty \cos \theta_i}$$

one obtains,

$$\bar{D}_1 (\theta_i,M_\infty) = \bar{g}_o \, M_\infty \left\{\frac{2 \cos^2 \theta_i}{1 + M_\infty \cos \theta} - 1\right\} \qquad C\text{-}10$$

Thus Equation C-7 becomes

$$\psi_1(x,\eta,\omega_s) = \delta(x) \, \phi(\eta) \, \frac{F}{\bar{\rho}c} \, k\delta \, R_\delta \, e^{j\pi/2} \, \bar{g}_o \left\{\frac{2 \cos^2 \theta_i}{1 + M_\infty \cos \theta_i} - 1\right\} A_1(x,x_o,\omega_s) \qquad C\text{-}11$$

where $A_1(x,x_o,\omega_s)$ is given by Equation C-8 and must be computed numerically due to the variation of $\beta(x)$ with x.

APPENDIX D

Evaluation of the integral

$$\psi_2(x,\eta,\omega_s) = \frac{2}{\nu}\iint \text{div}\,(\underset{\sim}{w}_a\bar{\Omega})\;\delta(x_s^4)\;g\;(x,x_s,\eta,\eta_s,\omega_s)\;dx_s\;d\eta_s \qquad \text{D-1}$$

The above integral may be rewritten in the form,

$$\psi_2(x,\eta,\omega_s) = -\frac{2}{\nu}\iint (\underset{\sim}{w}_a\bar{\Omega})\cdot \text{grad}_s\,\{g\delta(x_s^4)\}\,dx_s\,d\eta_s$$

$$+\frac{2}{\nu}\iint \text{div}\,\{g\;\delta(x_s^4)\;\underset{\sim}{w}_a\bar{\Omega}\}\,dx_s\,d\eta_s \qquad \text{D-2}$$

In the above form, the variables of g have been omitted for convenience of writing, but g is still a function of x, x_s, η, η_s, and ω_s. The last integral in eq. D-2 can be replaced by a surface integral, and let this be denoted by ψ_{22} and let the first integral of equation D-2 which is a volume integral be denoted by ψ_{21}. Then eq. D-2 may be rewritten in the form

$$\psi_2\,(x,\eta,\omega_s) = \psi_{21}\,(x,\eta,\omega_s) + \psi_{22}(x,\eta,\omega_s) \qquad \text{D-3}$$

where

$$\psi_{21}\,(x,\eta,o_s) = -\frac{2}{\nu}\iint (\underset{\sim}{w}_a\bar{\Omega})\cdot \text{grad}_s\,\{g\;\delta(x_s^4)\}\,dx_s\,d\eta_s \qquad \text{D-4}$$

and

$$\psi_{22}\,(x,\eta,\omega_s) = \frac{2}{\nu}\int_s \{g\;\delta(x_s^4)\;\;\underset{\sim}{w}_a\bar{\Omega}\}_\eta\,dS_\eta \qquad \text{D-5}$$

where the subscript n denotes normal to surface S_n.

Evaluation of $\psi_{21}(x,\eta,\omega_s)$

From eq. D-4, ψ_{21} may be expanded to

$$\psi_{21}\ (x,\eta,\ \omega_s) = -\frac{2}{\nu}\iint [u_a\bar{\Omega}\ \frac{\partial}{\partial x_s}\ \{g\ \delta(x_s^4)\} + v_a\bar{\Omega}\ \frac{\partial}{\partial n_s}\ \{g\ \delta(x_s^3)\}\ dx_s\ d\eta_s \qquad \text{D-6}$$

where u_a and v_a are the acoustic particle velocities along and transverse to the mean flow direction respectively. As discussed in the main text,and appendix F, for acoustic frequencies $k << 1$, the variation of the sound field across the boundary layer is negligible. This results in the neglect of the second term of eq. D-6.

In appendix C it was suggested that $g(x,x_s,\eta,\eta_s,\omega_s)$ could be approximated by

$$g\ (x,x_s,\eta,\eta_s,\omega_s) = \bar{g}_o\ \phi(\eta)\ \exp -j \int_{x_s}^{x} \beta(x_s)dx_s \qquad \text{D-7}$$

From appendix A, u_a can be approximated to

$$u_a\ (x_s,\eta_s,\omega_s) = \frac{K}{1-MK}\ \frac{F(\eta_s)}{\bar{\rho}c}\ \exp -j\ (k_x x_s) \qquad \text{D-8}$$

where

$$K = \frac{k_x}{k} = \frac{\cos \theta_i}{1 + M_\infty \cos \theta_i} \qquad \text{D-9}$$

$$F(\eta) = F_o$$

and F_o is the constant sound pressure level in the boundary layer in the low freq. limit and is equal to twice the incident S.P.L.

After substituting for g and u_a from eqs. D-7 and D-8, eq. D-6 may be rearranged in the form,

$$\psi_{21}\ (x,\eta,\omega_s) = \delta(x)\ \phi(\eta)\ \bar{g}_o\ \frac{F_o}{\rho c}\ R_\delta\ D_2\ (\theta i, M_\infty)\ A_{21}\ (x,x_o,\omega_s) \qquad \text{D-10}$$

where $R_\delta = U_\infty\ \delta(x)/\gamma$

$$A_{21}\ (x,x_o,\omega_s) = \int_{x_o}^{x} \left| \left\{ \frac{\delta(x_s)}{\delta(x)} \right\} \left\{ \frac{4d\ \delta(x_s)}{dx_s} + j\beta(x_s)\delta(x_s)\ e^{-jk_x x_s - \int_{x_s}^{x} \beta(x_s)dx_s} \right\} \right| dx_s \qquad \text{D-11}$$

and must be integrated numerically due to the variation of $\beta(x_s)$ with x_s and

$$D_2\ (\theta_i, M_\infty) = \frac{1}{M_\infty} \int_o^1 \frac{K}{1-MK} \frac{dM}{d\eta_s}\ d\eta_s = \left| \log_n\ (1 + M_\infty \cos\ \theta) \right| / M_\infty \qquad \text{D-12}$$

Evaluation of surface integral ψ_{22} of eq. D-5

$$\psi_{22}\ (x,\eta,\omega) = \text{surface} \int \left\{ \frac{2}{\nu}\ g\ \delta(x_s^4)\ \underset{\sim}{w}_a \bar{\Omega} \right\}_n\ dS_n \qquad \text{D-13}$$

where the integration is carried out along the surface bounding the source region as shown in sketch:

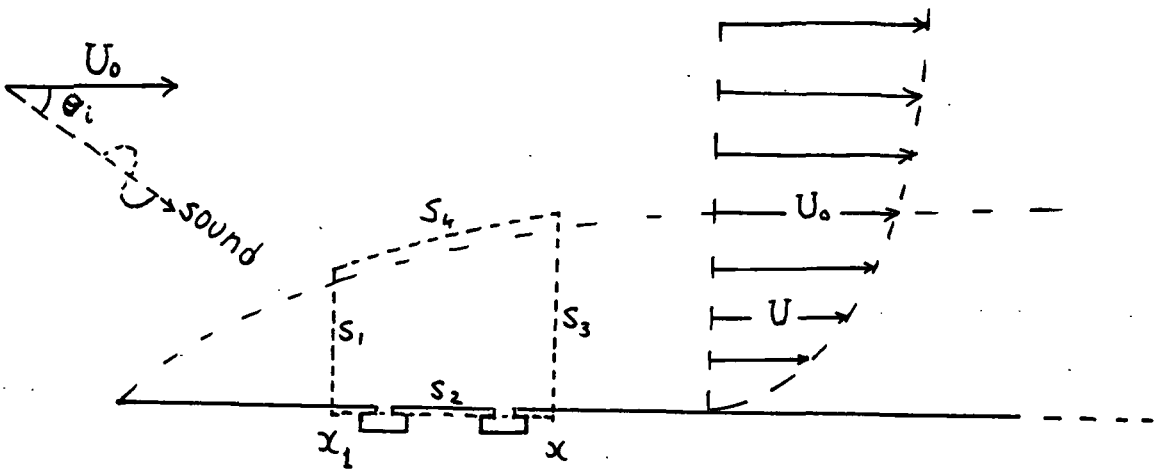

Figure D-1. Sketch shows control volume and surfaces in the evaluation of ψ_{21} and ψ_{22}.

It is required to evaluate the contributions to ψ_{22} of the normal components of $(g\ \delta(x_s^4)\ \underset{\sim}{w}_a\ \bar{\Omega})$ to the surfaces S_1, S_2, S_3 and S_4 circumscribing the source region between x_1 and x, where x_1 is arbitrary and x is one of of the coordinates of the field point (x,n) where the boundary layer disturbance is to be evaluated. There is no contribution from surface S_4 because $\bar{\Omega}$ is identically zero there since the surface is outside the boundary layer. On surface S_2, the normal component of $g\ \delta(x_s^2)\ \underset{\sim}{w}_a\ \bar{\Omega}$ is zero because v_a, the relevant component of $\underset{\sim}{w}_a$ is zero as a result of the rigid surface condition. If surface S_2 contained one or a distribution of slots, then v_a at the slot surfaces would not have been zero and a finite contribution to ψ_{22} would have resulted from these slots. Limiting the study to rigid flat plates, the only contributions to ψ_{22} are from surfaces S_1 and S_2 and may now be written in the form,

$$\psi_{22}(x,\eta,\omega_s) = \frac{c}{\nu}\left[\int_0^1 \left\{g\,\delta^3(x)\;u_a(x,\eta,\omega_s)\frac{dM}{d\eta_s}\right\}_x d\eta_s - \int_0^1 \left\{g\,\delta^3(x)\;u_a(x,\eta,\omega_s)\;\frac{dM}{d\eta_s}\right\}_{x_1} d\eta_s\right]$$

If the approximate forms for g and u_a of equations (D7) and (D8) are used, $\psi_{22}(x,\eta,\omega_s)$ may be rewritten in the form

$$\psi_{22}(x,\eta,\omega_s) = \delta(x)\;\phi(\eta)\;\bar{g}_o\;R_\delta\;\frac{F_o}{\bar{\rho}c}\;D_2(\theta_i,M_\infty)\;A_{22}(x,x_1,\omega_s) \qquad (D14)$$

where

$$A_{22}(x,x_1,\omega_s) = \left[\delta(x)\;e^{-ijk_x x - j\int_{x_0}^{x}\beta(x_s)dx_s} - \frac{\delta^3(x_1)}{\delta(x)}\,e^{jk_x x_1 - j\int_{x_0}^{x_1}\beta(x_s)dx_s}\right] \qquad (D15)$$

and $\quad D_2 = [\mathrm{Log}_n\;(1 + M_\infty \cos\theta_i)]\;/M_\infty$

Thus equation (D3), the solution to the surface integral of equation (D1) may now be written by combining equations (D10) and (D14) in the form,

$$\psi_2(x,\eta,\omega_s) = \delta(x)\;\phi(\eta)\;\frac{F_o}{\bar{\rho}c}\;\bar{g}_o\;R_\delta\;D_2(\theta_i,M_\infty)\;A_2(x,x_0,\omega_s) \qquad (D16)$$

where

$$A_2(x,x_0,\omega_s) = A_{21}(x,x_0,\omega_s) + A_{22}(x,x_0,\omega_s) \qquad (D17)$$

A_{21} and A_{22} defined in equations (D11) and (D15) are evaluated numerically and discussed in the main text.

APPENDIX E

EVALUATION OF THE SOUND FIELD INSIDE THE BOUNDARY OF A FLAT PLATE DUE TO AN INCIDENT PLANE WAVE, AND THE ASSOCIATED FLUCTUATING VORTICITY FLUX.

The convected acoustic wave equation governing the sound field in a unidirectional transversely sheared mean flow field is given by (Reference 3-20)

$$\nabla^2 P - \frac{1}{c^2} \frac{D^2 P}{Dt^2} + 2\bar{\rho} \frac{dU}{dy} \frac{dv}{dx} = 0 \qquad \text{E-1}$$

A plane wave is considered in the freestream incident at an θ_i to the freestream direction as shown in Figure 3-14. A part of this wave is reflected off from the upper surface of the shear layer and a part is refracted into the shear layer. The refracted portion of the wave upon reaching the rigid flat plate surface at the bottom of the shear layer is reflected back into the shear layer and will emerge at the upper surface of the shear as a "bottom" reflected wave. Since the mean flow is non-uniform, the reflection and refraction process can be physically visualized as a continous process as sketched in Figure 3-14. Sound waves propagating upstream are subjected to similar convective, refractive and reflective scattering and in addition zones of "relative silence" can be expected except for diffraction.

In evaluating the sound field inside the boundary layer, the above mentioned scattering effects (convection, refraction, reflection and diffraction) must be taken into account. An elegant method is to solve the

governing equation (E-1) numerically in the boundary layer and imposing the following boundary conditions: On the rigid flat plate the normal component of the acoustic particle velocity must vanish which is equivalent to $\partial P/dy = 0$; on the upper surface of the boundary layer, the acoustic pressure field and the normal displacement must be continous and therefore may be equated to the sum of the prescribed incident wave and a reflected wave of yet undetermined amplitude, which together are solutions of equation E-1 without the shear term.

In the uniform region of the mean flow, the pair of solutions satisfying equation E-1 are

$$P_2(x,y,\omega) = \left\{P_i\, e^{+j\,k_y\,y} + P_r\, e^{-j\,k_y\,y}\right\}\; e^{-j\,k_x\,x + j\omega t} \qquad \text{E-2}$$

where subscript 2 refers to external (to boundary layer)

i refers to incident plane wave

r refers to reflected plane wave

Then $$\frac{\partial P_2}{\partial y} = jk_y \{P_i e^{jk_y y} - P_r e^{-jk_y y}\}\; e^{-jk_x x + j\omega t} \qquad \text{E-3}$$

It can be easily shown that

$$k_x = k \cos\theta_i/\{1 + M_\infty \cos\theta_i\} \qquad \text{E-4}$$

$$k_y = k \sin\theta_i/\{1 + M_\infty \cos\theta_i\}$$

Inside the boundary layer, the solution of equation E-1 may be written in the form

$$P_I(x,y,\omega) = H(y)\ e^{-j\,k_x x + j\omega t} \qquad \text{E-5}$$

where $H(y)$ is the numerical solution of the following differential equation,

$$\begin{Bmatrix} H \\ H' \end{Bmatrix}' = \begin{bmatrix} 0 & 1 \\ a & b \end{bmatrix} \begin{Bmatrix} H \\ H' \end{Bmatrix} \qquad \text{E-6}$$

and the dash refers to derivative with respect to y; a and b are functions of the acoustic frequency parameter $k\delta$, the local Mach number which is a function of the mean velocity profile, the freestream Mach number and the directionality of the incident wave; more explicitly,

$$a(y,k\delta,M_\infty,\theta_i) = -(k\delta)^2[(1-MK)^2-K^2] \qquad \text{E-7}$$

$$b(y,k\delta,M_\infty,\theta_i) = \frac{-2K}{(1-MK)}\ \frac{dM}{dy}$$

$$\text{and } K = k_x/k = \cos\theta_i/\{1 + M_\infty \cos\theta_i\} \qquad \text{E-9}$$

Equation (E-6) has been evaluated numerically to provide the amplitude variation of the sound field inside the boundary layer and is shown in figures E-1 through E-3 for different non-dimensional frequencies $k\delta$ and angles of incidences θ_i. The amplitude distribution in the absence of mean flow (influenced only by reflection) is also shown to contrast the refractive effects. For the case of 180° incidence and higher non-dimensional frequencies, the rapid fall off in amplitude from the outer edge of the shear layer is noticeable and corresponds to the zone of "relative silence". For all angles

at low frequencies, it may be noted that the sound pressure level deviates very little from unity, implying little refraction.

The transverse distribution of the fluctuating vorticity flux induced by the sound field, second term of equation 3-10 of main text, has been evaluated using the acoustic field in the boundary layer and the mean transverse velocity gradients and is shown in figure E-4 through E-6 for different angles of incidence θ_i and non-dimensional acoustic frequencies $k\delta$. In the high frequency case, the variation of the vorticity distribution with angle θ_i is quite noticeable. At lower frequencies, the acoustically induced fluctuating vorticity flux is proportional to $k\delta$ and its distribution is shaped more by the mean shear distribution than the sound pressure distribution, except at high angles of incidence. Figure E-7 shows the acoustically induced fluctuating vorticity at the rigid plate surface as a function of frequency parameter for different angles of incidence. For the case of 180°, above a critical frequency the fall in the acoustically induced fluctuating vorticity flux is due to the reduced penetration of the sound inside the boundary layer.

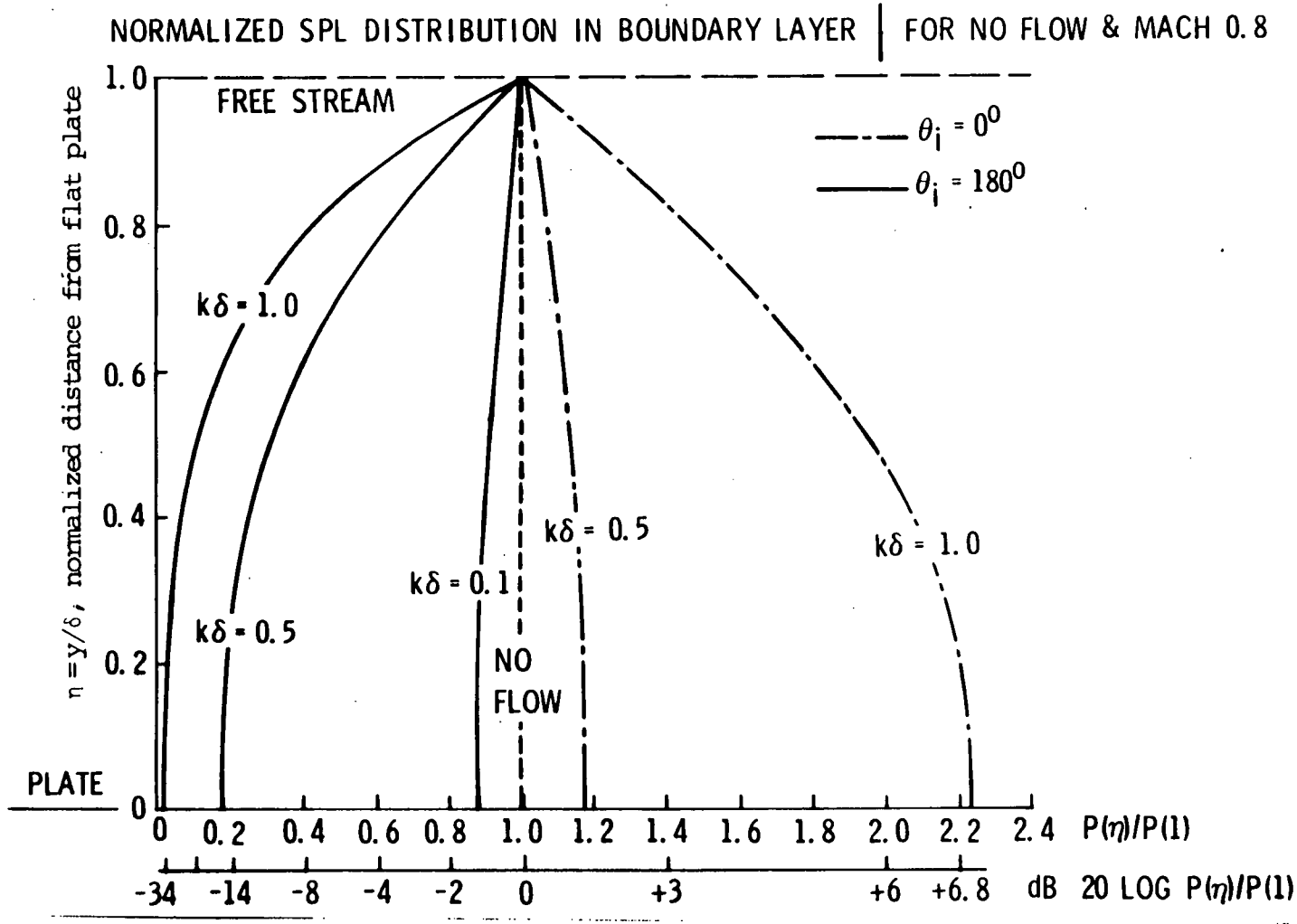

Figure E-1. Normalized SPL distribution in boundary layer of a rigid flat plate. Parameters are angle of incidence θ_i, frequency parameter $k\delta$ and Mach numbers = 0.8 and 0.0.

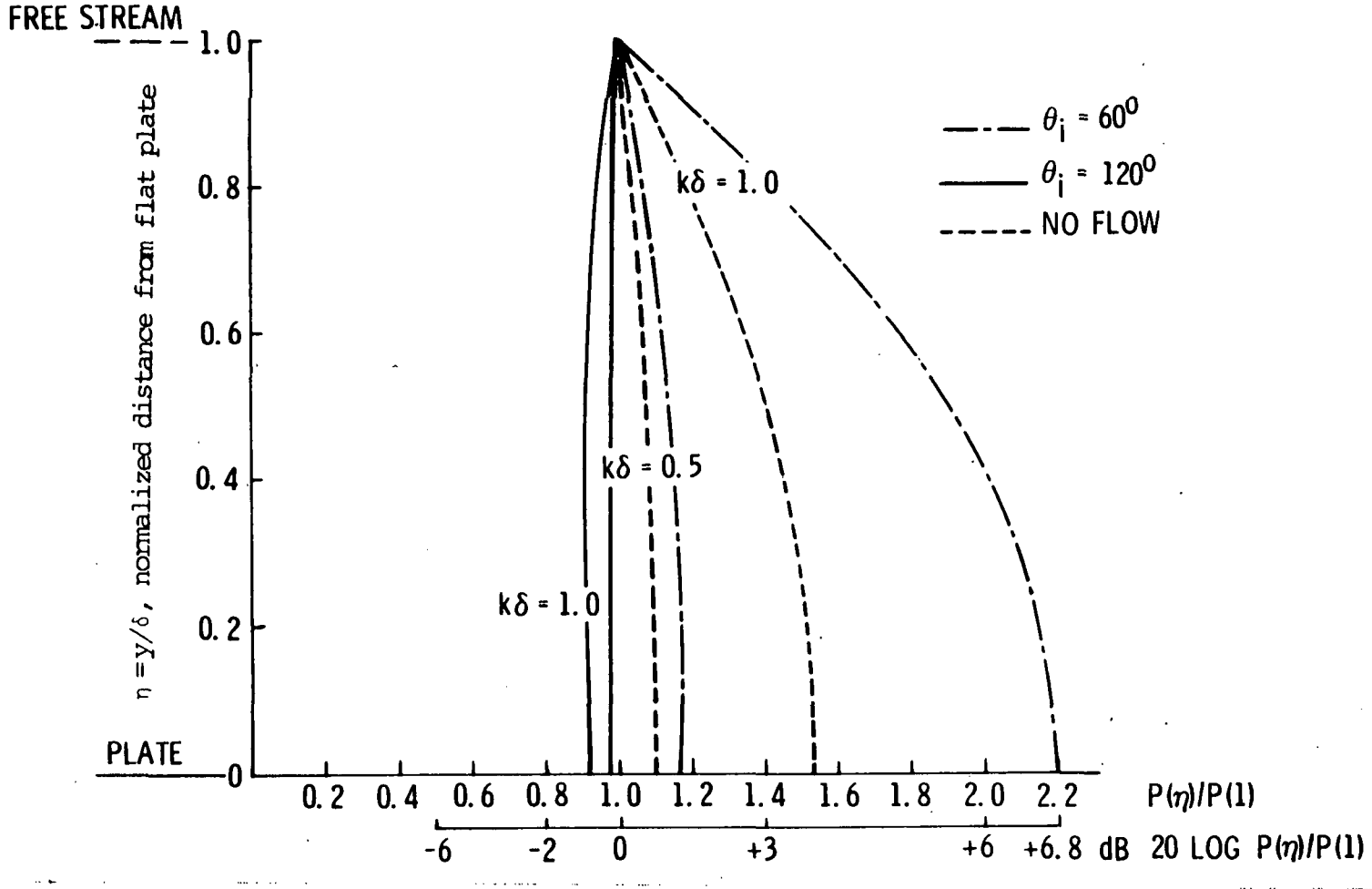

Figure E-2. Normalized SPL distribution in boundary layer of a rigid flat plate. Parameters are angle of incidence θ_i, frequency parameter $k\delta$ and Mach numbers = 0.8 and 0.0.

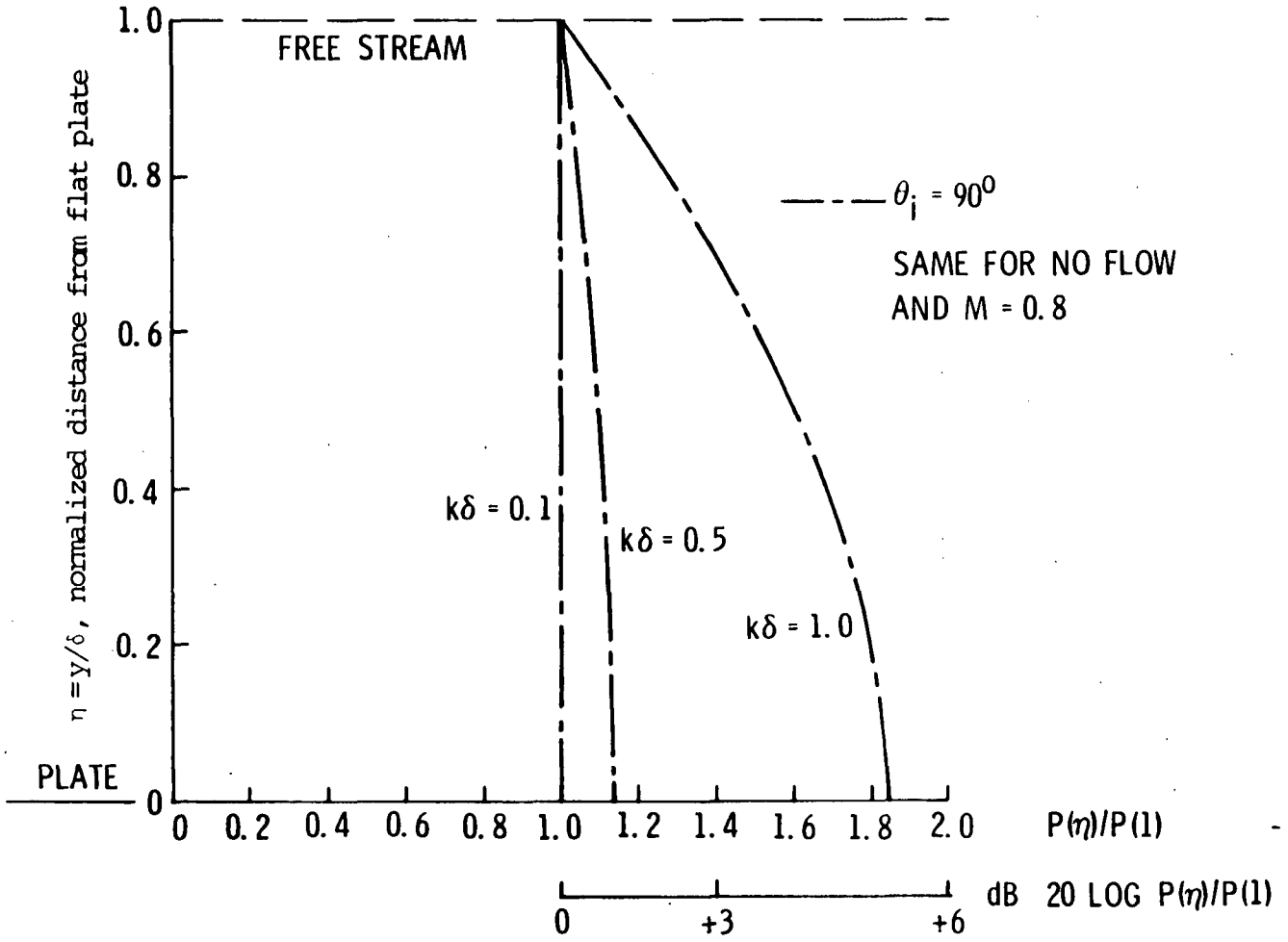

Figure E-3. Normalized SPL distribution in boundary layer of a rigid flat plate. Parameters are angle of incidence θ_i, frequency parameter kδ and Mach numbers = 0.8 and 0.0.

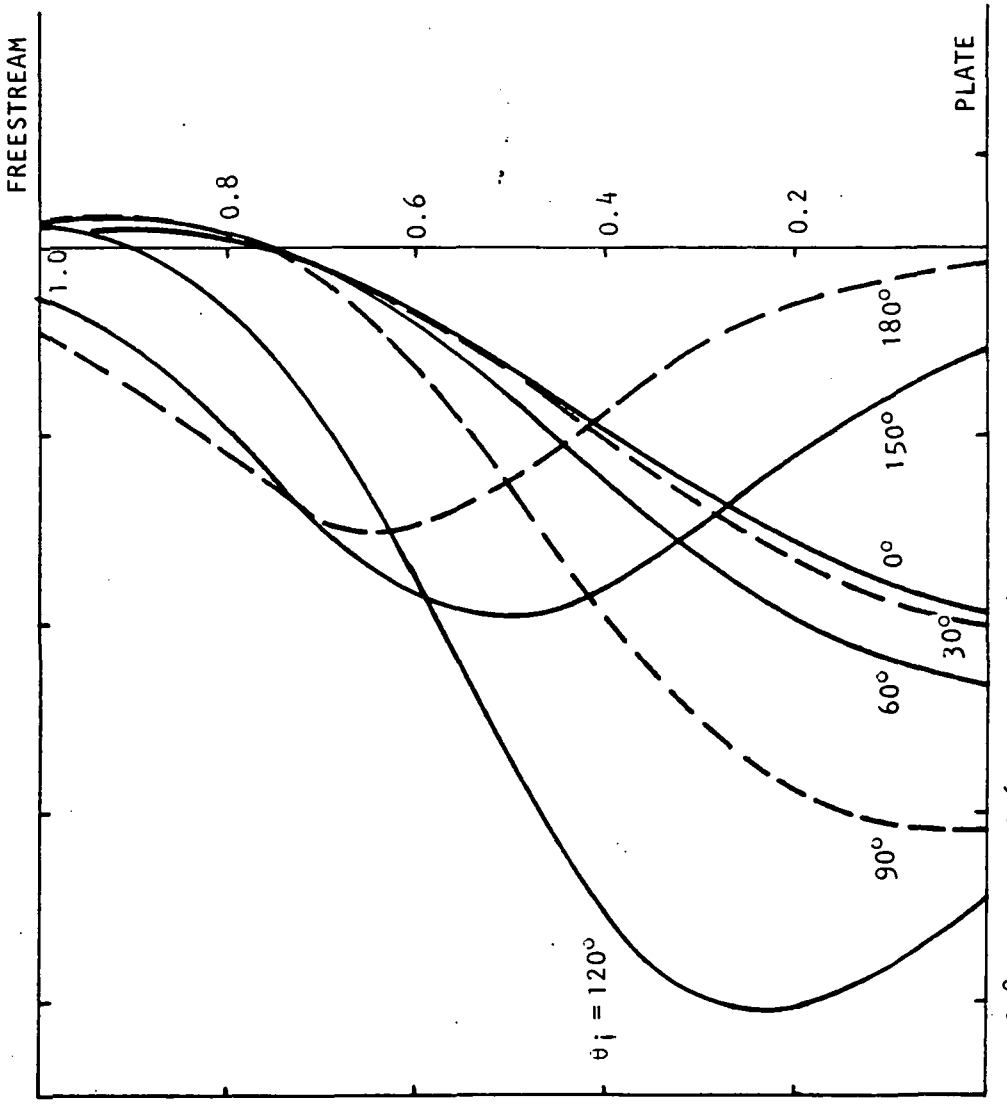

Figure E-4. Acoustically Induced Fluctuating Vorticity Distribution, $Q(\eta)$, Across Shear Layer for Different Angles of Incidence.
$k\delta$ = Nondimensional Frequency = 1.0
M_O = Freestream Mach Number = 0.8

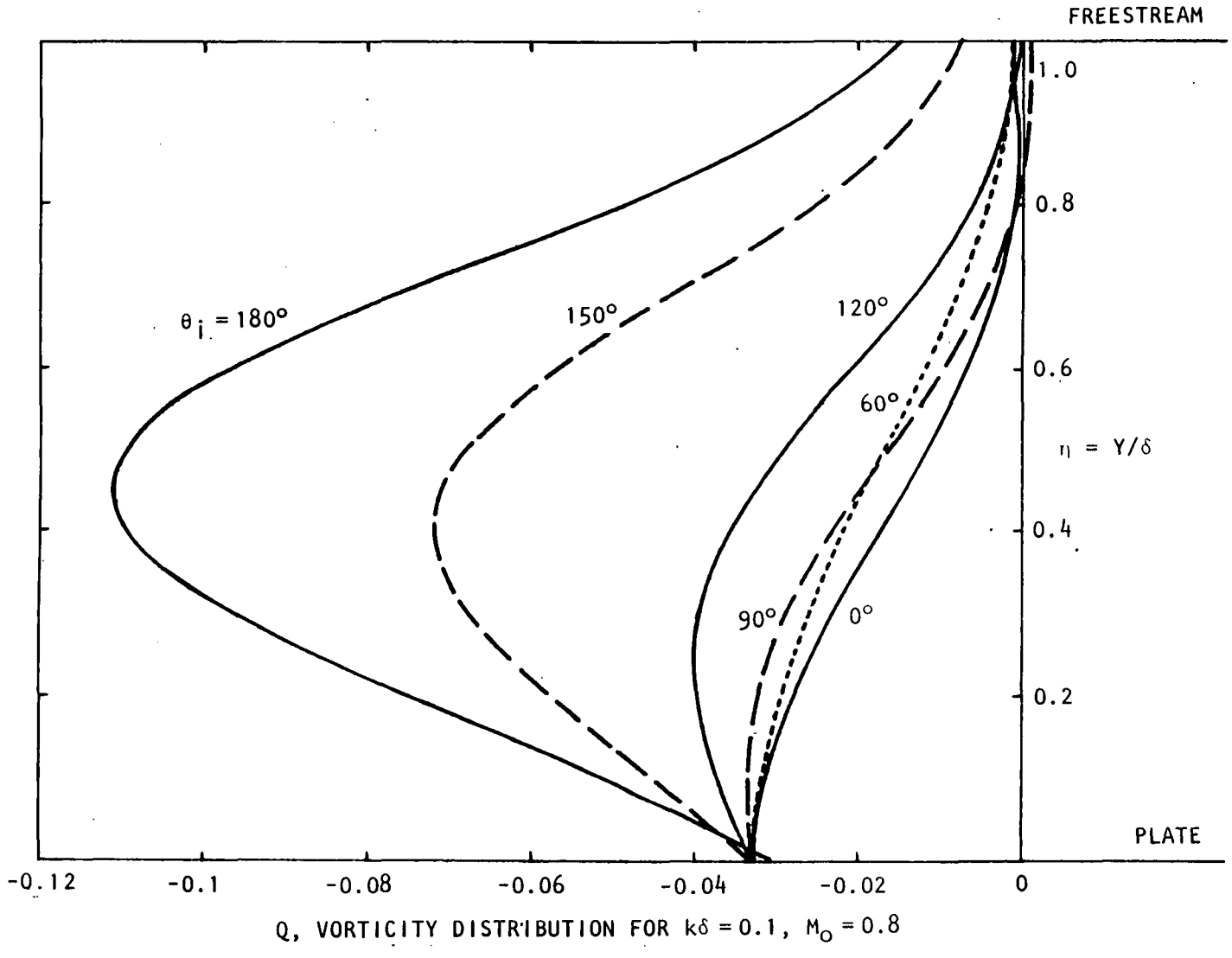

Figure E-5. Acoustically Induced Fluctuating Vorticity Distribution, $Q(\eta)$, Across Shear Layer for Different Angles of Incidence.
$k\delta$ = Nondimensional Frequency = 0.1
M_o = Freestream Mach Number = 0.8

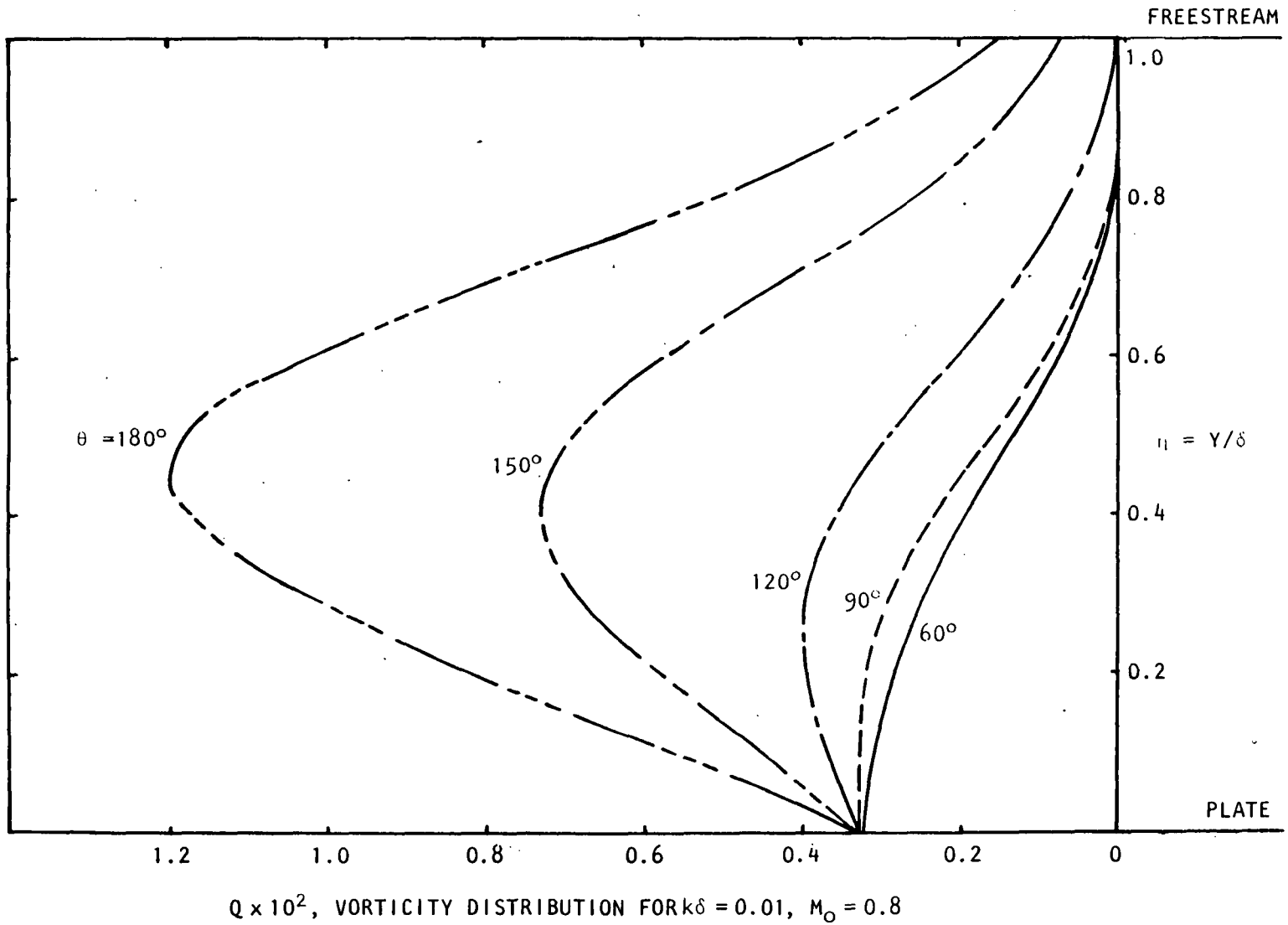

Figure E-6. Acoustically Induced Fluctuating Vorticity Distribution, $Q(\eta)$, Across Shear Layer for Different Angles of Incidence.
$k\delta$ = Nondimensional Frequency = 0.01
M_o = Freestream Mach Number = 0.8

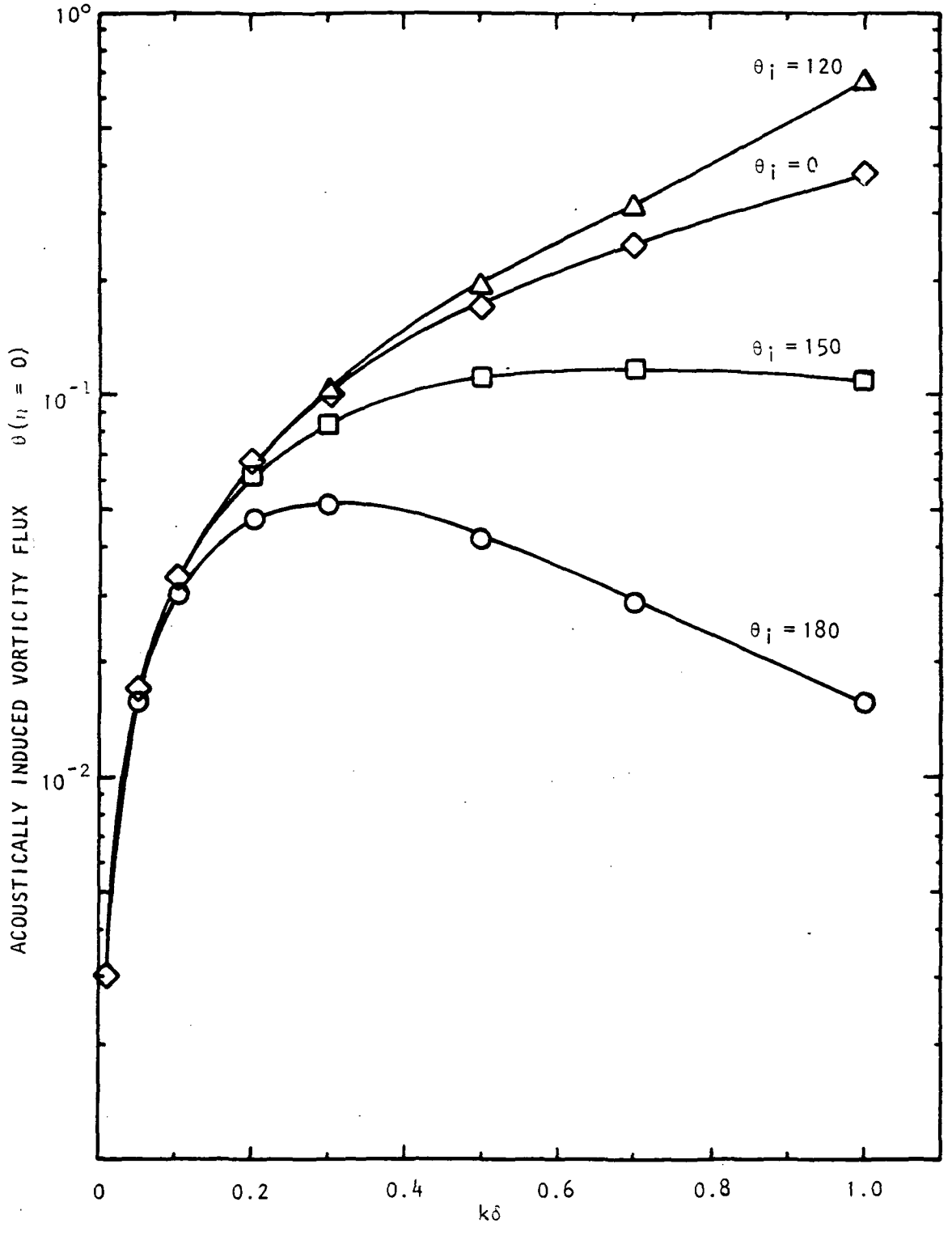

Figure E-7. Acoustically Induced Fluctuating Vorticity at Plate Surface, Q(0) As a Function of Nondimensional Frequency kδ, for Different Angles of Incidence, and $M_o = 0.8$

LIST OF SYMBOLS FOR SECTION 2

A	area
b	span
c	speed of sound
C	airfoil chord
D	diameter
dB	decibels, ref. 0.0002 dynes/cm^2
f	circular frequency
H	mean duct height
h	aircraft height
Hz	cycles per second
I	acoustic intensity
k	acoustic wavenumber, ω/c
L	effective duct length
M	Mach number
n	exponent
N	number of engines
OASPL	overall sound pressure level
P	acoustic pressure
PNL	perceived noise level
q	1/2 ρV^2, dynamic pressure
R	Reynolds number
r	Distance
S	number of inlet splitter rings
S_n	Strouhal numbers
V	Velocity
v	turbulent velocity
W	acoustic power
w	slot width
x, y, z	rectangular coordinates
Z	acoustic characteristic impedance

α	atmospheric absorption coefficient
Δ	increment
δ	boundary layer thickness
δ^*	boundary layer displacement thickness
λ	acoustic wavelength
ν	kinematic viscosity
ξ	angle
ρ	density
ϕ	angle from the inlet
ω	radian frequency

SUBSCRIPTS

A	aircraft
C	cruise condition
CE	convective effect
d	duct
DE	dynamic effect
i	element
J	jet
k	constant
m	maximum value
o	design condition
p	peak value
R	relative
SD	surface dipole
TOT	total
VQ	volume quadrupole

SUPERSCRIPTS

'	transformed coordinate

LIST OF SYMBOLS FOR SECTION 3

$A(x,x_o,\omega_s)$	x-dependent part of boundary layer velocity fluctuation
c	adiabatic speed of sound
$D(\theta i,M_\infty)$ $D_1(\theta i,M_\infty)$ $D_2(\theta i,M_\infty)$	factors expressing effects of sound directionality on boundary layer fluctuation.
D/D_t	substantial derivative = $\partial/\partial t + U\partial/\partial x$
dB	decibel
F	non-dimensional frequency parameter instability calculation = $\omega\nu/U_\infty^2$
$F(\eta)$	acoustic pressure distribution across boundary layer
* $g(\eta)$	Green's function
* $\bar{g}$	amplitude of Green's function, corresponds to receptivity of boundary layer fluctuation to a localized point source excitation
j	square root of (-1)
k, k_x, k_y	acoustic wave vector and its x and y components
$K = k_x/k$	non-dimensional x-component acoustic wave vector
LFC	laminar flow control
$L(\ )$	Orr-Sommerfeld operator

M_∞	free-stream Mach number
M	local Mach number
$\bar{P}_o$	steady state pressure at sea level
$\bar{P}$	steady state pressure at arbitrary altitude
P	acoustic pressure field
P_{ref}	standard reference acoustic pressure = 20×10^{-6} N/m^2
P_i	amplitude of incident sound pressure field
P_r	amplitude of reflected sound pressure field
P_w	amplitude of sound pressure field at rigid wall of flatplate
Q	source term of the inhomogeneous Orr-Sommerfeld eq.
Q_a	acoustically induced fluctuating vorticity source
$\bar{Q}$	$= \boxed{2Q_a/\nu}$
R_x	Reynolds number based on x coordinate
R_δ	Reynolds number based on boundary layer displacement thickness
SPL	sound pressure level
SPL_{crit}	critical sound pressure level (above which transition is induced)
TS	Tollmien-Schlichting

t	time variable
U_∞	free-stream mean velocity
U	local mean velocity
U', U''	first and second transverse derivatives of U
u'	x-component of total fluctuating velocity
u_a	x-component of acoustic velocity
u_b	x-component of boundary layer fluctuating velocity
V_{wall}	steady state suction velocity at wall
v_a	y-component of acoustic velocity
$\underset{\sim}{w}_a$	acoustic particle velocity vector
x, y	Cartesian coordinates, x along plate, y is transverse to plate
x_o, x_{ref}	reference location
x_s, y_s	Cartesian coordinate defining source location
β, α	real and imaginary parts of eigen value of the homogeneous Orr-Sommerfeld equation, define wave-length and amplification rate of boundary layer disturbances
δ	boundary layer displacement thickness
∇^2	2-D Laplacian
γ, γ_o	ratio of specific heats at arbitrary altitude and at standard reference pressure (sea-level) and temperature, respectively

η	non-dimensional transverse coordinate = (y/δ)
η_s	non-dimensional transverse coordinate defining source
ν	kinematic viscosity
ψ	stream function
$\phi(\eta)$	η or y dependent part of stream function
ω	angular frequency
ω_s	angular frequency of source
Ω_z	z-component total vorticity
$\bar{\Omega}$	z-component of mean vorticity
Ω_b	z-component of fluctuating vorticity associated with boundary layer distance
Ω_a	z-component of fluctuating vorticity associated with the acoustic field
$\bar{\rho}$	mean density
$\bar{\rho}_{wall}$	mean density at wall
τ	viscous relaxation time
θ_i	angle of incidence of the sound field with respect to flow direction

FIGURE NUMBER

REFERENCES FOR SECTIONS 1 AND 2

ILLUSTRATION TITLE

1-1. X-21A Engineering Section: Final Report on LFC Aircraft Design Data - Laminar Flow Control Demonstration Program. Northrop Corporation. NOR67-136, June 1967.

1-2. Sturgeon, R. F.; et al: Study of the Application of Advanced Technologies to Laminar Flow Systems for Subsonic Transports. Lockheed-Georgia Co. NASA CR-133949, May 1976.

2-1. Franken, P. A.; Kerwin, E. M.; et al.: Methods of Flight Vehicle Noise Prediction. WADC TR 58-343, Volume I, October 1958.

2-2. Eldred, K.; Roberts, W. and White, P.: Structural Vibrations in Space Vehicles. WADC TR 61-62, December 1961.

2-3. Ungar, E. E., et al.: A Guide for Predicting the Aural Detectibility of Aircraft. AFFDL-TR-71-22, March 1972.

2-4. Ungar, et al.: A Guide for Predicting the Vibrations of Fighter Aircraft in the Preliminary Design Stages. AFFDL-TR-71-63, April 1973.

2-5. Sutherland, L. C. and Brown, D.: Prediction Methods for Near Field Noise Environments of VTOL Aircraft. AFFDL-TR-71-180, May 1972.

2-6. Rudder, F. F., Jr. and Plumblee, H. E., Jr.: Sonic Fatigue Design Guide for Military Aircraft. AFFDL-TR-74-112, May 1975.

2-7. Ungar, E. E., et al.: A guide for Estimation of Aeroacoustic Loads on Flight Vehicle Surfaces. AFFDL-TR-76-91, Vol. I and II, February 1977.

2-8. Dunn, D. G. and Peart, N.A.: Aircraft Noise Source and Contour Estimation. NASA CR-114649, July 1973.

2-9. Reddy, N. N., et al.: V/STOL Aircraft Noise Prediction. FAARD-75-125, June 1975.

2-10. Magliozzi, B.: V/STOL Rotary Propulsion System Noise Prediction and Reduction. FAA-RD-76-49, two volumes, May 1976.

2-11. Rathe, E. J.: Note on Two Common Problems of Sound Propagation. J. Sound Vib. (1969) 10 (3), 472-479.

2-12. Ahuja, K. K.; Tester, B. J.; and Tanna, H. K.: Calculation of Far-Field Jet Noise Spectra from Near-Field Measurements Using True Source Location. AIAA 78-1153, 1978.

2-13. Siler, W.: Near and Far-Fields in a Marine Environment, J. Acous. Soc. Am., 46 (2) (Part 2) 1969.

2-14. Lighthill, M. J.: Sound Generated Aerodynamically, Proc. Roy. Soc. A 267A, pages 147-181, 1962.

2-15. Smith, M. J. T. and House, M. E.: Internally Generated Noise from Gas Turbine Engines, Measurement and Prediction. ASME Trans., Vol. 89, No. 1, Jan. 1967, pp. 117-190.

2-16. Burdsall, E. A. and Urban, R. H.: Fan-Compressor Noise: Prediction, Research and Reduction Studies. Pratt and Whitney Aircraft FAA-RD-71-73, 1971.

2-17. Benzakein, M. J., et al.: Fan/Compressor Noise Research. General Electric Co. FAA-RD-71-85, 1971.
Vol. I - Detailed Discussion, AD-740513
Vol. II - Detailed Discussion, AD-740514
Vol. III - Compilation of Test Data, AD-740515
Vol. IV - Compilation of Test Data, AD-740516

2-18. Aircraft Engine Noise Reduction. NASA SP-311, 1972.

2-19. Heidmann, M. F. and Feiler, C. E.: Noise Comparisons from Full-Scale Fan Tests at NASA Lewis Research Center. AIAA Paper 73-1017, Oct. 1973.

2-20. Feiler, C. E. and Conrad, E. W.: Noise from Turbomachinery. AIAA Paper 73-815, Aug. 1973.

2-21. Heidmann, M. F.: Interim Prediction Method for Fan and Compressor Source Noise. NASA TM X-71763, June 1975.

2-22. Smith, M. J. T. and Bushell, K. W.: Turbine Noise - Its Significance in the Civil Aircraft Noise Problem. ASME Paper 69-WA/GT-12, Nov. 1969.

2-23. Matthews, D. C.; Nagel, R. T. and Kester, J. D.: Review of Theory and Methods for Turbine Noise Prediction. AIAA Paper 75-540, March 1975.

2-24. Kazin, S. B. and Matta, R. K.: Turbine Noise Generation, Reduction, and Prediction. AIAA Paper 75-449, March 1975.

2-25. Krejsa, E. A. and Valerino, M. F.: Interim Prediction Method for Turbine Noise. NASA TM X-73566, November 1976.

2-26. Matta, R. K.; Sandusky, G. T. and Doyle, V. L.: GE Core Engine Noise Investigation - Low Emission Engines. General Electric Company. FAA-RD-77-4, February 1977.

2-27. Ho, P. Y., and Tedrick, R. N., Combustion Noise Prediction Techniques for Small Gas Turbine Engines, Inter-Noise 1972, International Conference on Noise Control Engineering, Proc., Washington, D. C., October 4-6, 1972, pp. 507-512.

2-28. Motsinger, R., Prediction of Engine Combustor Noise and Correlation with T64 Engine Low Frequency Noise, R72AEG313, General Electric Co., 1972.

REFERENCES (Continued)

2-29. Grande, E.: Core Engine Noise, AIAA Paper 73-1026, Oct. 1973.

2-30. Gerend, R. P. Kumasaka, H. A., and Roundhill, J. P.: Core Engine Noise, AIAA Paper 73-1027, Oct. 1973.

2-31. Huff, R. G., Clark, B. J., and Dorsch, R. G.: Interim Prediction Method for Low Frequency Core Engine Noise, NASA TM X-71627, Nov. 1974.

2-32. Strahle, W. C.: A Review of Combustion Generated Noise, AIAA Paper 73-1023, Oct. 1973.

2-33. Mathews, D. C., Rekos, N. F., and Nagel, R. T.: Combustion Noise Investigation, FAA-RD-77-3, Pratt and Whitney Aircraft, Feb. 1977.

2-34. Kazin, S. B., Matta, R. K., and Emmerling, J. J.: Core Engine Noise Control Program, FAA-RD-74-125, Vol. III, Supplement I, General Electric Company, March 1976.

2-35. Plumblee, H. E., et al.: Near Field Noise Analysis of Aircraft Propulsion Systems with Emphasis on Prediction Techniques for Jets. AFFDL-TR-67-43, Aug. 1967.

2-36. Thomson, A. G. R.: Acoustic Fatigue Design Data. Part I, NATO AGARD-AG-162-Part I, May 1972.

2-37. Cockburn, J. A. and Jolly, A. C.: Structural-Acoustic Response, Noise Transmission Losses and Interior Noise Levels of an Aircraft Fuselage Excited by Random Pressure Fields. AFFDL-TR-68-2, Aug. 1968.

2-38. Hermes, P. H. and Smith, D. L.: Measurement and Analysis of the J57-P21 Noise Field. AFFDL-TR-66-147, Wright-Patterson Air Force Base, Ohio, Nov. 1966.

2-39. Benzakein, M. J.; Chen, C. Y.; and Knott, P. R.: A Computational Technique for Jet Aerodynamic Noise. AIAA Paper 71-583, June 1971.

2-40. Chen, C. Y.; Knott, P. R.; and Benzakein, M. J.: Analytical Near Field Acoustic Model Formulations. Chap. III, Supersonic Jet Noise, AFAPL-TR-72-52, Aug. 1972.

2-41. Chen, C. Y.: Calculations of Far-Field and Near-Field Jet Noise. AIAA Paper 75-93, Jan. 1975.

2-42. Maestrello, L. and McDaid, E.: Near-Field Characteristics of a High Subsonic Jet. AIAA Paper 71-155, Jan. 1971.

2-43. Stone, J. R.: Interim Prediction Method for Jet Noise. NASA TMX-71618, 1974.

2-44. Pennock, A. P.; Swift, G.; and Marbert, J. A.: Externally Blown Flap Noise Reduction, NASA CR-134675, February 1975.

REFERENCES (Continued)

2-45. Plumblee, H. E. Ed.: A Study of the Effects of Forward Velocity on Turbulent Jet Mixing Noise. NASA CR-2702, July 1976.

2-46. Harper-Bourne, M. and Fisher, M. J.: The Noise from Shock Waves in Supersonic Jets. AGARD CP 131, Paper 11, September 1973.

2-47. Tanna, H. K.; Dean, P. D.; Burrin, R. H.: The Generation and Radiation of Supersonic Jet Noise, Vol. IV - Shock-Associated Noise Data. Air Force Aero Propulsion Laboratory, Technical Report AFAPL-TR-76-65, 1976.

2-48. Tester, B. J., Morris, P. J., Lau, J. C. and Tanna, H. K.: The Generation, Radiation and Prediction of Supersonic Jet Noise, AFAPL-TR-78-85, 1978.

2-49. Bryce, W. D. and Pinker, R. A.: The Noise from Unheated Supersonic Jets in Simulated Flight, AIAA 4th Aeroacoustic Conference, Paper No. 77-1327, October 1977.

2-50. Ahuja, K. K., Tester, B. J., and Tanna, H. K.: The Free Jet as a Simulator of Forward Velocity Effects on Jet Noise, NASA CR 3056, 1978.

2-51. Powell, A.: On the Mechanism of Choked Jet Noise. Proc. Phys. Soc. B. Vol. 66, pp. 1029-1056, 1953.

2-52. Powell, A.: On the Noise Emanating from a Two-Dimensional Jet Above the Critical Pressure. The Aeronautical Quarterly, Vol. IV, February 1953, pp. 103-122.

2-53. Powell, A.: The Reduction of Choked Jet Noise. Proc. Phys. Soc., London, 67B, pp 313-327, 1954.

2-54. Howlett, D. P.: Model and Full Scale Investigations of Shock Cell Noise. ARC (U.K.) 28, 563, December 1960.

2-55. Hay, J. A. and Rose, E. G.: In-Flight Shock Cell Noise. J. Sound Vib., 11 (4) pp 411-420, April 1970.

2-56. Hay, J. A.: Shock Cell Noise, Aircraft Measurement. J. Sound Vib., 17 (4), pp 509-516, August 1971.

2-57. Carmichael, R. F. and Pelke, D. E.: In-Flight Noise Measurements Performed on the X-21A Laminar Flow Aircraft, NOR64-81, 1964.

2-58. Westley, R. and Woolley, J. H.: An Investigation of the Near Noise Fields of a Choked Axi-Symmetric Air Jet, pp. 147-167, Aerodynamic Noise (Ed. H. S. Ribner), University of Toronto Press, 1969.

2-59. Westley, R. Wooley, J. H.: The Near Field Sound Pressures of a Choked Jet During a Screech Cycle. Aircraft Engine Noise and Sonic Boom, Chapter 23, AGARD CP 42, May 1969.

REFERENCES (Continued)

2-60. Reid, W. B. and Hadfield, C. M.: Flight Investigation of Shock Cell Noise on a Trident Aircraft; Part 2, Analysis of Noise Measurements. Aero. Dept. Note 5945/WBR/CMM/121, December 1967, Hawker Siddeley Aviation Ltd., Hatfield, England.

2-61. Hamilton Standard: Prop-Fan and Gearbox Near Field Noise Predictions, SP15A77, October 1977.

2-62. Lockheed-Georgia Co. Report No. LG72ER0011, Experimental STOL Transport Research Airplane, Vol. II, Propulsion and Noise, 1972.

2-63. Kazin, S. B., and Pass, J. E.: NASA/GE Quiet Engine 'C' Acoustic Test Results, NASA CR121176, April 1974.

2-64. Klujber, F.: Results of an Experimental Program for the Development of Sonic Inlets for Turbofan Engines, AIAA Paper No. 73-222, January 1973.

2-65. Savkar, S. D. and Kazin, S. B.: Some Aspects of Fan Noise Suppression Using High Mach Number Inlets, J. Aircraft, May 1975.

2-66. Sharland, I. J.: Sources of Noise in Axial Flow Fans. J. Sound Vib., Vol. 1, No. 3, pgs. 302-322, 1964.

2-67. Hayden, R. E.: Fundamental Aspects of Noise Reduction from Powered Lift Devices, SAE 730376, April 1973.

2-68. Hayden, R. E., Fox, H. L., Chanaud, R. C.: Some Factors Influencing Radiation of Sound from Flow Interaction with Edges of Finite Surfaces. NASA CR-145073, 1976.

2-69. Military Specification, Airplane Strength and Rigidity Flight Loads, MIL-A-00861A (USAF), March 1971.

2-70. Press, H. and Steiner, R.: An Approach to the Problem of Estimating Severe and Repeated Gust Loads for Missile Operation, NACA TN 4332, September 1958.

2-71. Phillips, O. M., Proc. R. Soc. Lond., A 234, 327-335, 1956.

2-72. Tam, C. K. W.: Intensity, Spectrum, and Directivity of Turbulent Boundary Layer Noise, J. Acoust. Soc. Am., 57 (1) January 1975.

2-73. Powell, A.: On the Aerodynamic Noise of a Rigid Flat Plate Moving at Zero Incidence, J. Acoust. Soc. Am., 31 (12) December 1959.

2-74. Powell, A.: Aerodynamic Noise and the Plane Boundary, J. Acoust. Soc. Am. 37 (4), August 1960.

2-75. Meecham, W. C.: Surface and Volume Sound from Boundary Layers, J. Acoust. Soc. Am., 37 (3), March 1965.

REFERENCES (Continued)

2-76. Maestrello, L.: Radiation from and Panel Response to a Supersonic Turbulent Boundary Layer, J. Sound Vib. 1969, 10 (2) 261-295.

2-77. Meecham, W. C.: Theory of Airframe Noise, J. Acoust. Soc. Am., 57 (6), June 1975.

2-78. Fink, M. R.: Airframe Noise Prediction Method, FAA-RD-77-29, March 1977.

2-79. Hardin, J. C.: Airframe Self-Noise - Four Years of Research, AGARD Lecture Series No. 80 on Aerodynamic Noise, Jan. 1977.

2-80. Hubbard, H. H.: Some Experiments Related to the Noise from Boundary Layers, J. Acoust. Soc. Am. 29 (3) 331-334, March 1957.

2-81. Wilson, L. N.: Experimental Investigation of the Noise Generated by the Turbulent Flow Around a Rotating Cylinder, J. Acoust. Soc. Am., 32 (10) October 1960. This is an abridged version of University of Toronto Institute of Aerophysics UTIA Rept. 57 (1959).

2-82. Cole, J. N., Eldred, K. M., et al: Noise Radiation from Jet Aircraft in Flight, J. Acoust. Soc. Am., 28, 804(A), 1956.

2-83. Cole, John N. and Kyrazis, Demos T.: A Method for Determining the Radiation Characteristics of Aircraft in Flight, J. Acoust. Soc. Am., 28:804(A), 1956.

2-84. Eldred, K. M. et al: In-Flight Noise Measurements on F94-C Aircraft, NOR-60-284, September 1960.

2-85. Rooney, T. R., Carmichael, R. F. and Eldred, K. M.: Investigation of Noise with Respect to the LFC, NB-66 Aircraft, Norair Report NOR-61-10, 1961.

2-86. X-21A Engineering Section: Laminar Flow Control Demonstration, Program Final Report, Northrop Corporation, NOR 61-141, April 1964.

2-87. X-21A Engineering Section: Final Report on LFC Aircraft Design Data-Laminar Flow Control Demonstration Program, Northrop Corporation, NOR 67-136, June 1967.

2-88. Ffowcs Williams, J. and Hall, L. H.: Aerodynamic Sound Generation by Turbulent Flow in the Vicinity of a Scattering Half Plane, J. Fluid Mechanics, Vol. 40, Part 4, March 1970, pp 657-670.

2-89. Hardin, J. C., Fratello, D. J., Hayden, R. E., Kadman, Y., and Africk, S.: Prediction of Airframe Noise, NASA TN D-7821, February 1975.

2-90. Fink, M. R.: Noise Component Method for Airframe Noise, AIAA Paper 77-1271, October 1977.

REFERENCES (Continued)

2-91. Brown, W. H. and Reddy, N. N.: Near-Field Pressures in the Wake of a Static Upper Surface Blown Configuration, Lockheed-Georgia Report LG77ER0104, May 1977.

2-92. Fink, M. R.: Prediction of Airfoil Tone Frequencies, J. Aircraft, January 1975, Vol. 12, No. 2.

2-93. Fethney, P.: An Experimental Study of Airframe Self-Noise, RAE Tech. Memo, Aero 1623, Feb. 1975.

2-94. Vaidya, P. G. and Dean, P. D.: State of the Art of Duct Acoustics. AIAA 4th Aeroacoustics Conference, Paper No. 77-1279, October 1977.

2-95. Kinsler, L. E. and Frey, A. R.: Fundamentals of Acoustics. John Wiley and Sons, Inc. 1950.

2-96. Morse, P. M. and Ingard, K. O.: Theoretical Acoustics. McGraw-Hill Book Company, 1968.

2-97. Beranek, L. L. Ed: Noise and Vibration Control; Chapter Sixteen Noise of Gas Flows. MGraw-Hill Book Company, 1971.

2-98. Ingard, U. and Singhai, V. K.: Flow Excitation and Coupling of Acoustic Modes of a Side Branch Cavity in a Duct. J. Acoust. Soc. Am., 60(5), November 1976.

2-99. Bacon, J. W.; Pfenninger, W.; and Moore, C. R.: Investigations of a 30 Degree Swept and a 17-Foot Chord Straight Suction Wing in the Presence of Internal Sound, External Sound and Mechanical Vibrations. Summary of LBLC Research, Vol. I, ASD-TDR-63-554, 1964.

2-100. Carlson, J. C. and Bacon, J. W.: Influence of Acoustical Disturbances in the Suction Ducting System on the LFC Characteristics of a 33° Swept Suction Wing. Northop Report NOR-65-232, 1965.

2-101. Carlson, J. C.: Investigation of the Laminar Flow Control Characteristics of a 33° Swept Suction Wing at High Reynolds Numbers in the NASA Ames 12-Foot Pressure Wind Tunnel in August 1965. Northrop Report NOR-66-58, January 1966.

2-102. Carmichael, R. F. and Finwall, P. E.: Analysis of the Results of the Laboratory Duct Model Test for the X-21A Laminar Flow Aircraft. NOR-65-303, November 1965.

2-103. Lekoudis, S. G.: Stability of Boundary Layers over Permeable Surfaces, AIAA Paper 78-203, January 1978.

2-104. Pfenninger, W.; Bacon, J.; and Goldsmith, J.: Flow Disturbances Induced by Low-Drag Boundary Layer Suction Through Slots. The Physics of Fluids Supplement, 1967.

2-105. Von Glahn, U. and Goodykoontz, J.: Forward Velocity Effects on Jet Noise with Dominant Internal Noise Sources. NASA TMX 71438, 1973.

2-106. Standard Values of Atmospheric Absorption as a Function of Temperature and humidity for Use in Evaluating Aircraft Flyover Noise. Aerospace Recommended Practice, ARP 866, Society of Automotive Engineers, April 1970.

2-107. Bass, H. E. and Shields, F. D.: A Study of Atmospheric Absorption of High Frequency Noise and Application to Fractional-Octave Bands. University of Mississippi, NASA Contract NAS3-19431, June 1976.

2-108. Mangiarotty, R. A., and Turner, B. A.: Wave Radiation Doppler Effect Correction for Motion of a Source, Observer and the Surrounding Medium", J. Sound Vib., (1967) 6 (1) pp 110-116.

2-109. Oestreicher, H. L.: The Effect of Motion on the Acoustic Radiation of a Sound Source. CADO Technical Digest, 16(9) 1951.

2-110. Blankenship, G. L.; Low, J. K. C.; Watkins, J. A. and Merriman, J.E.: Effect of Forward Motion on Engine Noise. NASA CR-134954, October 1977.

2-111. Blankenship, G. L.: Effect of Forward Motion on Turbomachinery Noise. AIAA 4th Aeroacoustics Conference, Paper No. 77-1346, October 1977.

2-112. Low, J. K. C.: Effect of Forward Motion on Jet and Core Noise. AIAA 4th Aeroacoustics Conference, Paper No. 77-1330, 1977.

2-113. Stone, J. R.: Flight Effects on Exhaust Noise for Turbojet and Turbofan Engines - Comparison of Experimental Data with Prediction. NASA TMX-73552, 1976.

2-114. Rawlins, A. D.: The Engine-Over-The-Wing Noise Problem, J. Sound Vib., 1977, 50 (4) pp 553-569.

2-115. DC-9 Flight Demonstration with Refanned JT8D Engines - Final Report, Volume IV, Flyover Noise, NASA CR-134860, Douglas Aircraft Company, 1975.

2-116. Rudd, M. J.: Note on the Scattering of Sound in Jets and the Wind, J. Sound Vib., 1973, 26(4), pp 551-560.

2-117. Beranek, L. L., Ed: Noise Reduction, McGraw-Hill, p. 193, 1960.

2-118. Maekawa, Z.: Noise Reduction by Screens. Applied Acoustics, Vol. 1, pp. 157-173, 1968.

2-119. Anderson, G. S. and Kurze, U. J.: Sound Attenuation by Barriers. Applied Acoustics, Vol. 4, pp 35-53, 1971.

REFERENCES (Continued)

2-120. Hellstrom, G.: Noise Shielding Aircraft Configurations, A Comparison Between Predicted and Experimental Results. ICAS Paper No. 74-58, 1974.

2-121. Dunn, D. G., et al.: Aircraft Configuration Noise Reduction. FAA-RD-76-76-1, Vol. 1, June 1976.

REFERENCES FOR SECTION 3

3-1. Schlichting, H.: Boundary Layer Theory. 1968, McGraw-Hill Book, Co.

3-2. Bacon, J. W.; Pfenninger, W.; and Moore, C. R.: Summary of LFC Research. ASD-TDR-63-554.

3-3. Carmichael, R. F.: LFC Demonstration Program. 1964, Final Report, NOR 61-141, chap. 11.

3-4. Pfenninger, W. and Reed, V. D.: Laminar Flow and Research Experiments. July 1966, Astronautic and Aeronautics, p. 44.

3-5. Schubauer, G. B. and Skramstad, H. K.: Laminar Boundary Layer Oscillations and Transition on a Flat Plate. 1948, NACA Rep. 909.

3-6. Tollmien, W.: General Instability Criterion of Laminar Velocity Distributions. 1936, NACA TM 792.

3-7. Berger, S. A. and Aroesty, S.: e^9: Stability Theory and Boundary Layer Transition. 1977, Ad-A038908 or R1898-ARPA.

3-8. Klebanoff, P. S. and Tidstrom, K. D.: Evolution of Amplified Waves Leading to Transition in a Boundary Layer with Zero Pressure Gradient. 1959, NASA TN D-195.

3-9. Wells, Jr., C. S.: Effects of Freestream Turbulence on Boundary Layer Transition. 1967, AIAA Journal, Vol. 5(1), p. 172.

3-10. Spangler, J. G. and Wells, Jr., C. S.: Effects of Freestream Disturbances on Boundary Layer Transition. 1968, AIAA Journal, Vol. 6(3), p. 543.

3-11. Freymuth, P.: On Transition in a Separated Boundary Layer. 1966, Journal Fluid Mechanics, Vol. 25(4).

3-12. Morkovin, M. V. and Paranjape, S. V.: On Acoustic Excitation of Sheer Layer. 1971, Z. Flugwiss. 19(8/9), p. 328.

3-13a. Pfizenmaier, E.: On the Structure of Velocity and Pressure Fluctuation in a Sound Influenced Free-Jet. 1974. Colloguium on Coherent Structures of Turbulence. Also DLR-Mit-74-25.

3-13b. Bechert, D. and Pfizenmaier, E.: On Wave-Like Pertubations in a Free Jet Travelling Fastener than the Mean Flow in the Jet. 1975. Journal of Fluid Mechanics, Vol. 72(2), p. 341.

3-14. Shapiro, P. J.: The Influence of Sound Upon Laminar Boundary Layer Instability. 1977, Report No. 83458-83560-1, Acoustics and Vibration Lab, MIT.

3-15. Schliz, W.: Experimentelle Untersuchungen Zur Akustichen Beeinflussungen Der Stromungrenzchicht in Luft. 1965/66, Acustica, Vol. 16, p. 208.

REFERENCES (Continued)

3-16. Mechel, F. and Schliz, W.: Undersuchungen Zur Akustichen Beeinflussung Der Stromungsgrenzschicht in Luft. 964 Acustica, Vol. 14, p. 325.

3-17. Lockheed-Georgia Company: Study of the Application of Advanced Technologies to Laminar Flow Control Systems for Subsonic Transports. 1976, NASA CR-133949, p. 305.

3-18. Nayfeh, A. H. and Elhady, N. M.: An Evaluation of Suction Through Porous Strips for Laminar Flow Control. 1979, AIAA Paper 79-1494.

3-19. Mechel, F.; Mertens, P. and Schliz, W.: Research on Sound Propagation in Sound Absorbent Ducts with Superimposed Air Streams. 1963, AMRL-TDR-62-140 (IV).

3-20. Mungur, P.: On the Sensitivity of Shear Layers to Sound. 1977, AIAA paper no. 77-1369, presented at 4th Aero-Acoustics Conference in Atlanta, Ga.

3-21. Sarlic, W. S. and A. H. Nayfeh: Non-parallel Stability of Boundary Layers with Pressure Gradients and Suction. 1977, AGARD CP-224.

3-22. Thomas, A. S. W. and Lekoudis, S. G.: Sound and Tollmien-Schlichting Waves in a Blasius Boundary Layer. Physics of Fluids, November 1978.

3-23. Moore, C. J.: The Role of Shear-Layer Instability Waves in Jet Exhaust Noise. 1977, J. Fluid Mechanics, 80(2), p. 321.

3-24. Lee, B. H. K.: Some Measurements of Spatial Instability Waves in Round Jets. 1976. 1976, AIAA Journal, Vol. 14(3), p. 348.

3-25. Hussain, A.K.M.F. and Zaman, K.B.M.Q.: Effect of Acoustic Excitation on the Turbulent Structure of a Circular Jet. 1975, Proc. 3rd Interagency Symp. Trans. Noise, University of Utah, p. 314.

3-26. Crow, S. C. and Champagne, F. H.: Orderly Structure in Jet Turbulence. 1971, J. Fluid Mechanics, Vol. 48, p. 547.

3-27. Brown, W. Byron: Numerical Calculation of the Stability of X-Flow Profiles in Laminar Boundary Layers on a Rotating Disc and on a Swept-Back Wing and an Exact Calculation of the Stability of the Blasius Velocity Profile. 1959, Northrop Norair Report NAI-59-5 (BLC-117), AD 314541.

3-28. Pfenninger, W. and Bacon, J. W.: About the Development of Swept Laminar Suction Wings with Full-Chord Laminar Flow. 1961, Boundary Layer and Flow Control, edited by Lachmann, Pergamon Press. Vol. II.

REFERENCES (Continued)

3-29. Srokowski, A. and Orszag, S.: Mass Flow Requirements for LFC Wing Design. 1977, AIAA Paper No. 77-1222.

3-30. Mack, L.: Three Dimensional Effects in Boundary Layer Stability. 1978, Twelfth Symp. on Naval Hydrodynamics, Washington, D.C. June 5-9, 1978.

3-31. Nayfeh, A. H. and Padhye, A.: The Relation between Temporal and Spatial Stability in 3-D Flows. 1978, AIAA Paper No. 78-1126.

3-32. Lekoudis, S.: Stability of Three-Dimensional Compressible Boundary Layers Over Wings with Suction. 1979, AIAA Paper No. 79-0265, presented at 17th AIAA Aerospace Sciences Meeting.

1. Report No.	2. Government Accession No.	3. Recipient's Catalog No.
NASA CR-159104		

4. Title and Subtitle	5. Report Date
A STUDY OF THE PREDICTION OF CRUISE NOISE AND LAMINAR FLOW CONTROL NOISE CRITERIA FOR SUBSONIC AIR TRANSPORTS	August 1979
	6. Performing Organization Code
7. Author(s)	8. Performing Organization Report No.
G. Swift and P. Mungur	LG78ER0218
	10. Work Unit No.
9. Performing Organization Name and Address	11. Contract or Grant No.
Lockheed-Georgia Company Marietta, Georgia 30063	NAS1-14946
	13. Type of Report and Period Covered
12. Sponsoring Agency Name and Address	FINAL REPORT May 1977 - June 1978
National Aeronautics and Space Administration Washington, D. C. 20546	14. Sponsoring Agency Code

15. Supplementary Notes

Contract Monitor - D. L. Lansing, Jr., NASA, Langley Research Center
Hampton, Virginia 23665

Program Manager - J. S. Gibson, Lockheed-Georgia Company, Marietta, Georgia 30063

16. Abstract

General procedures for the prediction of component noise levels incident upon airframe surfaces during cruise are developed. Contributing noise sources are those associated with the propulsion system, the airframe and the laminar flow control (LFC) system. Transformation procedures from the best prediction base of each noise source to the transonic cruise condition are established. A companion volume, Near-Field Noise Prediction for Aircraft in Cruising Flight, NASA CR-159105 summarizes and defines the noise prediction methods resulting from this study. The methods have been organized as computational algorithms which may be converted into computer programs.

Two approaches to LFC/Acoustic criteria are developed. The first is a semi-empirical extension of the X-21 LFC/Acoustic criteria to include sensitivity to the spectrum and directionality of the sound field. In the second, the more fundamental problem of how sound excites boundary layer disturbances is analyzed by deriving and solving an inhomogeneous Orr-Sommerfeld equation in which the source terms are proportional to the production and dissipation of sound induced fluctuating vorticity. Numerical solutions are obtained and compared with corresponding measurements.

Recommendations are made to improve and validate both the cruise noise prediction methods and the LFC/Acoustic criteria.

17. Key Words (Suggested by Author(s))	18. Distribution Statement
Aircraft, Laminar Flow Control, Aircraft Noise, Laminar Boundary Layers, Near-Field Noise, Vorticity, Flight Effects, Orr-Sommerfeld, Amplification, Propulsion Noise, Tollmien-Schlicting, Airframe Noise, Cross-Flow, Transition, Transformations, Critical Sound Pressure Level	Unlimited 245

19. Security Classif. (of this report)	20. Security Classif. (of this page)	21. No. of Pages	22. Price*
UNCLASSIFIED	UNCLASSIFIED	245	

* For sale by the National Technical Information Service, Springfield, Virginia 22161